

**Functional characterization of the three *Caenorhabditis elegans* orthologs of the human Parkinson's disease-associated gene *PARK9/ATP13A2***



**Dissertation**  
**an der Fakultät für Biologie der**  
**Ludwig-Maximilians-Universität München**

Vorgelegt von  
Jeffrey Zielich  
München, 21. August 2018

---

1. Gutachter:	PD. Dr. Eric John Lambie
2. Gutachter:	Prof. Dr. Marc Bramkamp
Tag der Abgabe:	21.08.2018
Tag der mündlichen Prüfung:	03.12.2018

---



## Eidesstattliche Erklärung

### **Erklärung:**

Diese Dissertation wurde im Sinne von § 13 der Prüfungs- und Studienordnung des Promotionsstudiengangs Life Science Munich von PD Dr. Eric John Lambie betreut. Ich erkläre hiermit, dass die Dissertation weder ganz noch in wesentlichen Teilen einer anderen Prüfungskommission vorgelegt worden ist und dass ich mich nicht anderweitig einer Doktorprüfung ohne Erfolg unterzogen habe.

### **Eidesstattliche Erklärung:**

Ich versichere hiermit an Eides statt, dass die vorgelegte Dissertation von mir selbständig und ohne unerlaubte Hilfe angefertigt wurde.

München, 21. August 2018

---

Jeffrey Zielich

## Table of Contents

<b>Declaration of Contribution .....</b>	<b>e</b>
<b>List of Publications .....</b>	<b>g</b>
<b>Abbreviations .....</b>	<b>h</b>
<b>1 Abstract.....</b>	<b>1</b>
<b>2 General Introduction .....</b>	<b>4</b>
<b>2.1 <i>Caenorhabditis elegans</i> as a model .....</b>	<b>4</b>
<b>2.2 Development of the hermaphrodite gonad of <i>C. elegans</i> .....</b>	<b>4</b>
<b>2.3 Distal tip cell migration .....</b>	<b>6</b>
<b>2.4 Soma-germline interaction .....</b>	<b>8</b>
<b>2.5 GON-2.....</b>	<b>8</b>
<b>2.6 CATP-6 .....</b>	<b>10</b>
<b>2.7 P5B ATPases .....</b>	<b>11</b>
<b>2.8 The Post-Albers transport cycle of the SERCA pump .....</b>	<b>11</b>
<b>2.9 The P5 subfamily .....</b>	<b>15</b>
<b>2.10 P5B ATPases in vertebrate clades.....</b>	<b>15</b>
<b>2.11 P5B ATPases and human disease.....</b>	<b>16</b>
<b>2.12 Subcellular localization .....</b>	<b>17</b>
<b>2.13 Subcellular phenotypes .....</b>	<b>18</b>
<b>2.13.1 Synuclein.....</b>	<b>18</b>
<b>2.13.2 Autophagic and lysosomal dysfunction .....</b>	<b>19</b>
<b>2.13.3 Mitochondria.....</b>	<b>20</b>
<b>2.13.4 Intracellular trafficking .....</b>	<b>20</b>

## Table of Contents

<b>2.14</b>	<b>The transport substrate of P5B ATPases .....</b>	<b>21</b>
2.14.1	Zinc.....	21
2.14.2	Manganese .....	22
2.14.3	Calcium .....	22
2.14.4	Magnesium .....	22
2.14.5	Polyamines .....	23
2.14.6	Regulation via lipid interaction .....	24
<b>2.15</b>	<b>Objectives .....</b>	<b>24</b>
<b>Chapter 1</b> .....	<b>Overlapping expression patterns and functions of three paralogous P5B ATPases in <i>Caenorhabditis elegans</i></b>	<b>26</b>
	Published: March 16, 2018. PLoS ONE 13: e0194451	
<b>Chapter 2</b> .....	<b>Redundant functions of three paralogous <i>Caenorhabditis elegans</i> P5B ATPases during gonadogenesis</b>	<b>62</b>
	Unpublished manuscript	
<b>Chapter 3</b> .....	<b>Novel Alleles of <i>gon-2</i>, a <i>C. elegans</i> Ortholog of Mammalian TRPM6 and TRPM7, Obtained by Genetic Reversion Screens</b>	<b>94</b>
	Published: November 25, 2015. PLoS ONE 10: e0143445	
<b>3</b>	<b>General Discussion.....</b>	<b>111</b>
3.1	Phylogenetic analysis of paralogous P5B ATPases .....	111
3.2	Spatial and temporal expression patterns of <i>C. elegans</i> P5B ATPases .....	112
3.3	Subcellular localization of P5B ATPases.....	113
3.4	The transport substrate(s) of P5B ATPases .....	114
3.5	P5B ATPase expression in the <i>C. elegans</i> reproductive system .....	115

## Table of Contents

<b>3.6</b>	<b>Overlapping functions of <i>catp-5</i>, <i>catp-6</i> and <i>catp-7</i> in fertility .....</b>	<b>116</b>
3.6.1	Redundancy of <i>catp-5</i> and <i>catp-6</i> .....	116
3.6.2	Redundancy of <i>catp-6</i> and <i>catp-7</i> .....	117
3.6.3	An integrated model for the functions of the <i>C. elegans</i> P5Bs within the hermaphrodite gonad.....	118
<b>3.7</b>	<b>Vulva development and DTC migration defects .....</b>	<b>119</b>
3.7.1	Vulva development defects in P5B mutants suggest possible impairment of Wnt signaling .....	119
3.7.2	Distal tip cell migration defects in nematode P5B mutants indicate perturbation of integrin function and Wnt signaling.....	120
3.7.3	Integrated model for DTC migration and vulva development defects .....	122
<b>3.8</b>	<b>Common functions of <i>catp-6</i> and <i>catp-7</i> in the somatic gonad precursors.....</b>	<b>125</b>
<b>3.9</b>	<b>GON-2 the TRPM6, TRPM7 ortholog .....</b>	<b>127</b>
<b>4</b>	<b>References.....</b>	<b>130</b>
<b>Acknowledgment.....</b>		<b>I</b>
<b>Appendices.....</b>		<b>II</b>
<b>Establishment of a CRISPR/Cas9-based strategy for inducible protein dimerization .....</b>		<b>III</b>
Published: April 17, 2018. microPublication: Biology		
<b>Rapamycin-induced protein dimerization as a tool for <i>C. elegans</i> research.....</b>		<b>IX</b>
Published: March 20, 2018. microPublication: Biology		
<b>Jeffrey Zielich CV .....</b>		<b>XIV</b>

## Declaration of Contribution

In this dissertation, I present the results of my doctoral research, which I conducted from November 2014 to July 2018 in the lab of PD Dr. Eric John Lambie. The results are presented in three chapters. Chapter 1 and Chapter 3 have been published in PLoS ONE, while Chapter 2 is an unpublished manuscript. All of the work in these three chapters is the result of collaborations with other scientists.

### Chapter 1:

**Zielich J.**, Tzima E., Schröder E. A., Jemel F., Conradt B., Lambie E. J., 2018 Overlapping expression patterns and functions of three paralogous P5B ATPases in *Caenorhabditis elegans* (M-H Lee, Ed.). PLoS ONE **13**: e0194451.

In chapter 1, I and Eric J. Lambie conceived the study, the experimental design and the methodology with inputs from Barbara Conradt. I constructed all but one of the CRISPR/Cas9 engineered strains (including the required molecular cloning), performed most of the crosses and maintained the strains. I performed most of the molecular cloning to generate fluorescent protein tagged transgenes. I performed microscopy and FRAP analysis. I collected the data to estimate the average brood sizes and growth rates for mutant animals. I analyzed all data including statistical and phylogenetic analysis. I prepared all figures and wrote the manuscript together with Eric J. Lambie. Eric J. Lambie, Barbara Conradt and I read and approved the final manuscript.

## Declaration of Contribution

### Chapter 2:

**Zielich J.**, Conradt B., Lambie E. J. Redundant functions of three paralogous *Caenorhabditis elegans* P5B ATPases during gonadogenesis. (Unpublished manuscript)

In chapter 2, I and Eric J. Lambie conceived the study, the experimental design and the methodology with inputs from Barbara Conradt. I constructed all universal MosSCI engineered strains (including the required molecular cloning), performed the crosses and maintained the strains. I performed the molecular cloning to generate chimeric proteins and most of the cloning to generate the fluorescent protein tagged transgenes including the cloning to generate catalytic inactive versions of the transgenes for rescue experiments. I performed all rescue experiments and microscopy. I analyzed all data including statistical analysis. I prepared all figures and wrote the manuscript together with Eric J. Lambie. A paper containing this chapter is in preparation.

### Chapter 3:

Lambie E. J., Bruce R. D., **Zielich J.**, Yuen S. N., 2015 Novel Alleles of *gon-2*, a *C. elegans* Ortholog of Mammalian TRPM6 and TRPM7, Obtained by Genetic Reversion Screens. (S-Z Xu, Ed.). PLoS ONE **10**: e0143445.

In Chapter 3, Eric J. Lambie, Robert D. Bruce, III, Sonia N. Yuen and I conceived the study and the experimental design. I crossed, maintained and scored the phenotypes of segregants from homozygous and heterozygous animals, and analyzed this data. Eric J. Lambie wrote the manuscript. Eric J. Lambie and I read and approved the final manuscript.

---

Jeffrey Zielich

---

PD Dr. Eric J. Lambie

## List of Publications

Zielich, J., Tzima, E., Schröder, E.A., Jemel, F., Conradt, B., Lambie, E.J., 2018 Overlapping expression patterns and functions of three paralogous P5B ATPases in *Caenorhabditis elegans*. **PLoS ONE 13, e0194451. doi:10.1371/journal.pone.0194451**

Lambie, E.J., Bruce, R.D., Zielich, J., Yuen, S.N., 2015 Novel Alleles of *gon-2*, a *C. elegans* Ortholog of Mammalian TRPM6 and TRPM7, Obtained by Genetic Reversion Screens. **PLoS ONE 10, e0143445. doi:10.1371/journal.pone.0143445**

### Method Publications:

Zielich J., Mangal S., Zanin E., Lambie E. J., 2018 Establishment of a CRISPR/Cas9-based strategy for inducible protein dimerization. **microPublication: Biology. Dataset. doi:10.17912/W2208R**

Mangal, S., Zielich, J., Lambie, E.J., Zanin, E., 2018 Rapamycin-induced protein dimerization as a tool for *C. elegans* research. **microPublication: Biology. Dataset. doi:10.17912/W2BH3H**

### Submitted for publication:

Herzig, V., Nixon, S., Salim, A., Verma, S., Abongwa, M., Zielich, J., Rios, L.R., Bais, S., Greenberg, R., Chubanov, V., Lambie, E.J., Capon, R., Robertson, A., Kotze, A.C., King, G.F., Discovery and characterization of a spider-venom polyamine with selective toxicity against the human filarial parasite *Brugia malayi* and other nematodes.

## Abbreviations

°C	Degrees Celsius
A	Adenine
aa	Amino-acid
AAK1	AP2 associated kinase 1
ABC	ATP-binding cassette
AC	Anchor cell
ASD	Autism spectrum disorder
C	Cytosine
CHO	Chinese hamster ovary
DFMO	$\alpha$ -difluoromethylornithine
DNA	Deoxyribonucleic acid
DTCs	Distal tip cells
E	Glutamic acid
EGF	Epidermal growth factor
Egl	Egg-laying defective
ER	Endoplasmic reticulum
Evl	Everted vulva
F	F <sub>0</sub>
FB-MOs	Fibrous body-membranous organelles
FRAP	Fluorescence Recovery after Photobleaching
G	Guanine
g	Gram
GBL	Gonadal basal lamina
gf	Gain-of-function
GFP	Green fluorescent protein
GOI	Gene of interest
Gon	Gonadless
Gro	Slow growth
h	Hours
HeLa	Henrietta Lacks
HHD	Hailey Hailey disease
HSP	Hereditary spastic paraplegia
KRS	Kufor-Rakeb syndrome
lf	Loss-of-function
min	Minutes
ml	Milliliter
ML	Maximum likelihood
mM	Millimolar
mRNA	Messenger RNA



## Abbreviations

Muv	Multivulva
MVBs	Multi-vesicular bodies
NCL	Neuronal ceroid lipofuscinoses
nmol	Nanomol
OAVS	Oculo auriculo vertebral spectrum
PA	Phosphatidic acid
PCR	Polymerase chain reaction
PD	Parkinson's disease
PI(3,5)P2	Phosphatidylinositol(3,5)bisphosphate
PI3K	Phosphoinositide 3-kinase
Pvl	Protruding vulva
RNA	Ribonucleic acid
RNAi	RNA interference
s	Seconds
SERCA	Sarcoplasmic/endoplasmic reticulum Ca <sup>2+</sup> pump
SLI	Specific language impairment
SNP	Single nucleotide polymorphism
Ste	Sterile
Sys	Symmetrical sisters
SYT11	Synaptotagmin 11
T	Thymine (DNA)
T	Threonine (amino acid)
TRPM	Transient receptor potential melastatin
Unc	Uncoordinated; sluggish
V	Vacuolar
VPCs	Vulval precursor cells
VU	Ventral uterine precursor
Vul	Vulvaless
wt	Wild type
$\mu$ l	Microliter
$\mu$ mol	Micromol

# 1 Abstract

P-type ATPases are an ancient family of transmembrane proteins that are found in genomes of eukaryotes as well as prokaryotes. These transporters use the energy derived from hydrolysis of ATP to actively transport substrates from one side of a lipid bilayer to the other. Missense-mutations in ATP13A2, one of the four human P5B ATPases, lead to early-onset Parkinson's disease (Kufor-Rakeb Syndrome). The genome of the model nematode *Caenorhabditis elegans* encodes three P5B ATPases: CATP-5, CATP-6 and CATP-7. This dissertation aims to provide a basic characterization of all three paralogous P5B ATPases of *C. elegans* with regard to expression, function and phenotypic analysis of deficient animals. In addition, this dissertation describes novel revertant mutations of *gon-2(lf)*, a genetic interactor of CATP-6.

The phylogenetic analysis presented in Chapter 1 suggests that the paralogous P5B ATPases of *C. elegans* evolved from a common ancestral protein after the origin of the *Caenorhabditis* clade. The sequence alignment of all three *C. elegans* P5B ATPases shows a high degree of similarity in the M4 transmembrane domain, which is thought to be the putative substrate interaction region. Therefore, CATP-5, CATP-6 and CATP-7 are likely to have the same substrate specificity and thus fulfill the same transport function.

In addition, Chapter 1 provides a detailed characterization of all three *C. elegans* P5B ATPases with regard to spatiotemporal expression pattern and subcellular localization in living animals, by using state-of-the-art CRISPR/Cas9 mediated recombination. Although each nematode P5B ATPase has a unique expression pattern, there is significant spatiotemporal overlap. In some tissues, each protein localizes to a different subcellular compartments e.g. early endosomes vs. plasma membrane. Whereas in other tissues they localize to the same compartment, e.g. the plasma membrane. Unlike its human ortholog, ATP13A2, CATP-6 does not localize to lysosomes.

## Abstract

By using CRISPR/Cas9 to generate a KO allele of CATP-7, it became possible to construct and analyze double and triple mutant strains involving *catp-5(0)*, *catp-6(0)* and *catp-7(dx189)*. The double mutants, *catp-6(0); catp-5(0)* and *catp-7(dx189) catp-6(0)* exhibit synthetic defects in germline proliferation and are often sterile. In *catp-7(dx189) catp-6(0); catp-5(0)* triple mutants, this synthetic sterility is strongly enhanced, and none of the animals produce progeny.

Chapter 2 describes the results of transgene complementation tests to rescue the corresponding phenotypes. The ability of each protein to undergo autophosphorylation is crucial in order to rescue the various mutant phenotypes, including the reestablishment of norspermidine sensitivity. CATP-6 and CATP-7 are redundantly required for the development of the somatic gonadal tissues, since expression of either gene product in somatic cells is sufficient to rescue sterility of *catp-7(dx189) catp-6(0)* double mutants. CATP-5 and CATP-6 are redundantly required for germline proliferation; the sterile phenotype of *catp-6(0); catp-5(0)* double mutants can be rescued by germline expression of either protein. Artificial sheath cell specific expression of CATP-5 can also bypass the requirement for CATP-6 in *catp-6(0); catp-5(0)* double mutants; this suggests that the putative transport substrate can probably be transferred from the somatic sheath cells to the germline via gap junctions. In addition, overexpression of CATP-7::GFP can substitute for CATP-6 in the genetic background of *gon-2(lf); catp-6(lf); gem-1(gf)*. Therefore, all three nematode P5B ATPases can probably perform the same function(s), but in different tissues and/or subcellular compartments.

Chapter 3 describes 10 revertant mutations of *gon-2(lf)* that affect 9 different residues within GON-2. Nine of the revertant mutations of *gon-2(lf)* are located in the N-terminal cytosolic domain and 1 mutation is located in the C-terminal cytosolic domain. Chapter 3 also describes a single *gon-2* mutant allele that reverts the Mg<sup>2+</sup>-hypersensitive phenotype of *gtl-2(0)* mutant animals. This mutation is located in the cytosolic C-terminal TRP-domain. Six

## Abstract

representative revertant mutations of *gon-2(lf)* were tested via scoring the phenotypes of segregants from homozygous and heterozygous animals. The suppression of the Gon phenotype by the 6 revertant mutations ranges from 85% (*dx99*) to 100% (*dx146*).

## 2 General Introduction

### 2.1 *Caenorhabditis elegans* as a model

The nematode *Caenorhabditis elegans* is an important model organism for genetic and molecular studies (Brenner 1974). *C. elegans* is easy to manipulate by traditional forward genetics approaches, by RNA interference (RNAi) and state-of-the-art genome editing systems like CRISPR/Cas9 (Brenner 1974; Fire *et al.* 1998; Chen *et al.* 2013; Dickinson and Goldstein 2016). *C. elegans* stocks can be maintained as self-fertile hermaphrodites (karyotype XX), which simplifies the accumulation of genetically identical animals for research. Males (karyotype XO) can also be generated, and these enable the construction of new genetic combinations (Brenner 1974). Because of its transparency and the invariant, fully mapped somatic cell lineage (959 cells in hermaphrodites and 1031 in males), *C. elegans* is a great tool to study developmental processes via live cell imaging (Sulston and Horvitz 1977; Kimble and Hirsh 1979; Sulston *et al.* 1983; Sulston 1988).

The reproductive tissue (gonad) of the adult *C. elegans* hermaphrodite is a symmetrical organ comprising one anterior and one posterior gonad arm, each containing both somatic cells and germ cells (Hirsh *et al.* 1976; Kimble and Hirsh 1979) (male gonad morphology and development are significantly different and will not be discussed here). The adult stage somatic gonad comprises five general tissues: distal tip cells (DTCs), gonadal sheath, spermatheca, spermatheca-uterine valve and uterus (Hirsh *et al.* 1976; Kimble and Hirsh 1979) (Fig 1). The entire gonad is covered by the gonadal basal lamina (GBL) (Hall *et al.* 1999).

### 2.2 Development of the hermaphrodite gonad of *C. elegans*

The development of the hermaphrodite gonad involves the regulation of cellular phenomena that are typical of organogenesis in all metazoans: patterned specification of cell fate, cell

## General Introduction

differentiation, cell migration, cell polarity, cell shape changes, and stem-cell proliferation (Miskowski *et al.* 2001). At the beginning of the L1 stage, the gonad primordium consists of four blast cells: Z1, Z2, Z3 and Z4 (Fig 1) (Sulston and Horvitz 1977). The two blast cells at the anterior and posterior ends, Z1 and Z4 are the precursors of the somatic gonad and are derived from the MS embryonic founder cell (Sulston and Horvitz 1977; Sulston *et al.* 1983). The other two blast cells, Z2 and Z3 are the germ line precursors, and are derived from the P4 embryonic blastomere (Sulston *et al.* 1983).

In hermaphrodites, Z1 and Z4 begin dividing midway through L1 stage (Kimble and Hirsh 1979). By the L2 stage, each cell has generated 6 descendants (in total 12 cells, anterior and posterior symmetric, Fig 1) (Kimble and Hirsh 1979). During L2, the 12 descendants do not divide, but they do grow and undergo positional changes (Kimble and Hirsh 1979). Two descendant cells, Z1.aa and Z4.pp remain at the distal tips of the primordium, and assume the DTC fate (Kimble and Hirsh 1979; Kimble and White 1981). The other 10 cells move into the center of the gonad, thereby excluding the germ cells (the descendants of Z2 and Z3) from the center and separating them into two pools (Kimble and Hirsh 1979). The germ cells approximately quadruple in number during the L2 stage, thus separating the migrating DTCs from the other somatic gonadal cells and elongating the gonadal primordium (Kimble and Hirsh 1979; Nishiwaki 1999).

Late during the L2 stage, either Z1.ppp or Z4.aaa migrates into the median plane of the developing gonad and becomes the anchor cell (AC), whereas the other cell assumes a ventral uterine precursor (VU) fate (Sulston and Horvitz 1977; Kimble and Hirsh 1979; Kimble 1981). The AC does not differentiate any further until the formation of the vulva and is critical for later vulva induction (Sulston and Horvitz 1977; Kimble and Hirsh 1979; Kimble 1981). During vulva morphogenesis, the AC fuses with the uterine-seam cell, resulting in a physical

connection of the vulva and the uterine lumen (Newman *et al.* 1996; Estes and Hanna-Rose 2009).

Both cells, Z1.ppp and Z4.aaa, have equal potential to become the AC cell and the decision is mediated by a stochastic alteration in expression levels of the Delta/Serrate-like Notch ligand LAG-2 and the Notch receptor LIN-12 (Seydoux and Greenwald 1989; Park *et al.* 2013). Before fate specification of Z1.ppp and Z4.aaa, each cell expresses LAG-2 and LIN-12 in equal amounts (Seydoux and Greenwald 1989; Wilkinson *et al.* 1994; Park *et al.* 2013). Subsequently, Notch signaling mediated inhibition leads to exclusive expression of LAG-2 in the AC and exclusive expression of LIN-12 in the VU (Wilkinson *et al.* 1994; Park *et al.* 2013).

The other nine somatic precursors give rise to all of the other 140 cells of the adult hermaphrodite somatic gonad via a predictable pattern of cell divisions during the L3 and L4 stages (Kimble and Hirsh 1979). The germ cells proliferate throughout the larval stages, but remain connected via thin cytoplasmic bridges and continue to be syncytial into the adult stage (Hirsh *et al.* 1976).

### **2.3 Distal tip cell migration**

DTC migration can be classified into 3 phases (Fig 1, reviewed by (Ming-Ching Wong 2012)). In the first phase, midway through L2, Z1.aa and Z4.pp begin migrating away from the midbody towards the anterior and posterior, respectively (Kimble and White 1981; Nishiwaki 1999). This migration follows along the ventral basement membrane, which overlies the ventral muscles (Ming-Ching Wong 2012). During the L3 stage the second phase starts; the DTCs make two turns: one 90° turn away from the ventral basement membrane towards the dorsal side and, once the dorsal side is reached, another 90° turn back towards the midbody (Nishiwaki 1999). The third phase takes place during the L4 stage, when the DTCs migrate towards the midbody along the basement membrane that overlies the dorsal muscles (Ming-Ching Wong 2012). Once the DTCs reach their final positions, dorsal of the vulva, cessation of migration

occurs (Kimble and Hirsh 1979; Kimble and White 1981; Nishiwaki 1999; Ming-Ching Wong 2012).

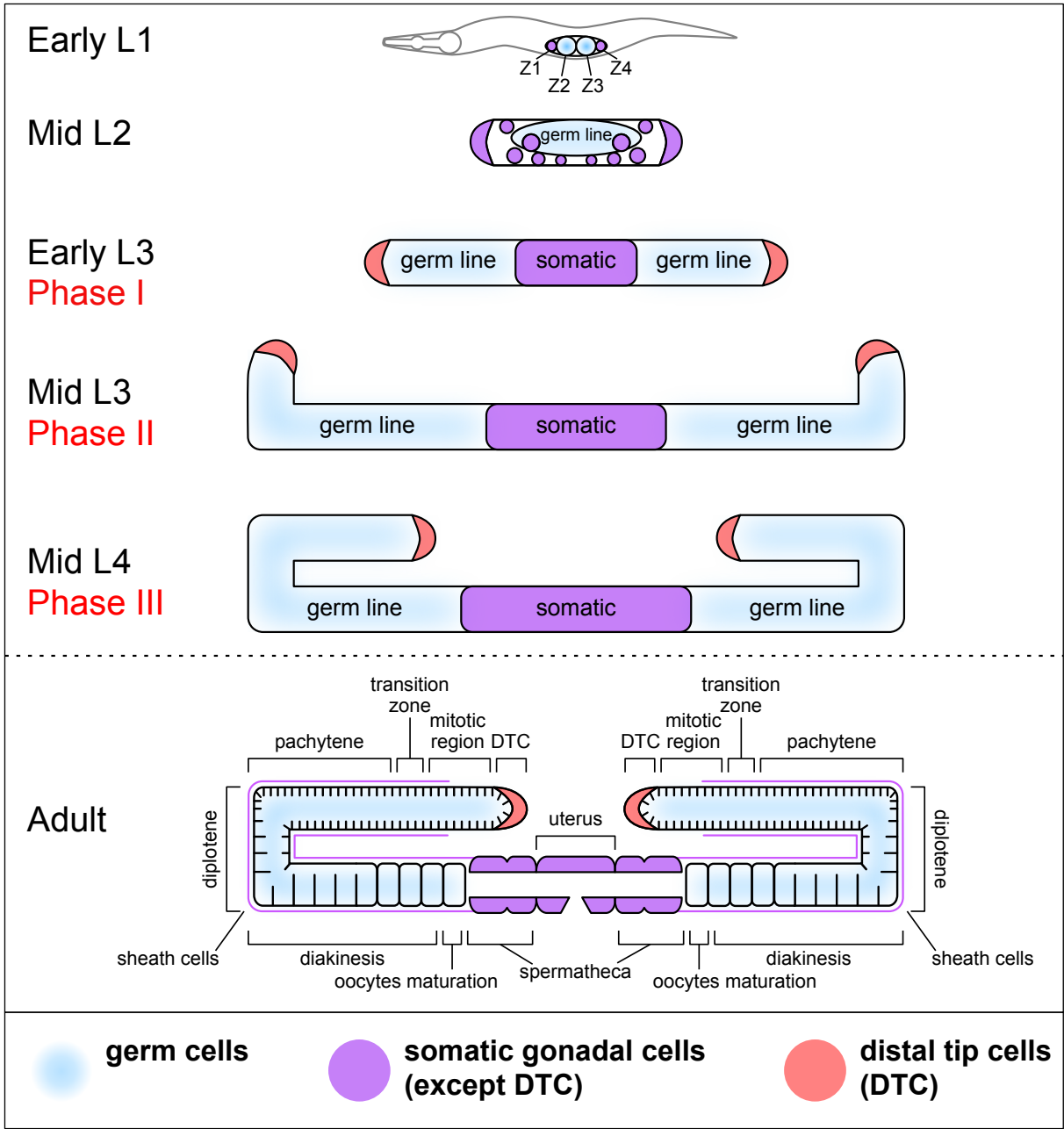


**Fig 1: Gonad development in the *C. elegans* hermaphrodite.** Schematic overview of gonad development in the different larval stages: L1-L4 and adult stage. Phase I-III (red): Distal tip cell migration phases. Blue gradient: Germ line. Purple: Somatic gonad (except distal tip cells). Salmon-pink: Distal tip cells. Inspired by (Kimble and White 1981; Miskowski *et al.* 2001; Itoh *et al.* 2005).



## 2.4 Soma-germline interaction

The DTCs are crucial for germline proliferation during larval development (Kimble and White 1981), and are physiologically connected to the germ line via numerous gap junctions (Starich *et al.* 2014). Furthermore, in both larval and adult stage animals, the DTCs express the membrane-bound Delta/Serrate-like signaling protein, LAG-2, thereby promoting the mitotic proliferation of the neighboring germ cells, which express the Notch-family receptor GLP-1 (Austin and Kimble 1987; Priess *et al.* 1987; Austin and Kimble 1989; Henderson *et al.* 1994; Berry *et al.* 1997).

Within each gonad arm, the germ line is surrounded by five pairs of very thin gonadal sheath cells (Fig 1) (Hirsh *et al.* 1976; Kimble and Hirsh 1979). The sheath cells are physiologically connected to the pachytene, diplotene and diakinesis stage germ cells via numerous gap junctions (McCarter *et al.* 1997; Hall *et al.* 1999; Starich *et al.* 2014). Laser ablation of the precursors of the sheath cells results in impaired germline proliferation and also prevents germ cells from progressing meiotically beyond the pachytene stage (McCarter *et al.* 1997). Exit from pachytene is mediated by the MAP kinase signaling cascade, and oocytes subsequently remain arrested in diakinesis until fertilization (Ward and Carrel 1979; Church *et al.* 1995).

The proximal sheath cells are fenestrated by small pores that enable yolk protein uptake into oocytes (Hall *et al.* 1999). Moreover, proximal sheath cells are smooth-muscle-like cells that contract and mediate ovulation into the spermatheca (McCarter *et al.* 1997; Rose *et al.* 1997; McCarter *et al.* 1999).

## 2.5 GON-2

Multiple mutant alleles of *gon-2* I were identified as critical for gonad development (Sun and Lambie 1997). The thermosensitive allele, *gon-2(q388)*, is a strong loss-of-function allele, henceforth called *gon-2(lf)* (Sun and Lambie 1997). *gon-2(lf)* mutant animals shifted to

restrictive temperature (23.5°C) show severe gonadogenesis defects; in some animals, none of the gonadal precursor cells undergo any postembryonic divisions (Sun and Lambie 1997). Affected adult animals are classified as Gonadless (Gon), because they lack somatic gonad tissue and, consequently, have very few germ cells (Kimble and Hirsh 1979; Kimble and White 1981; Sun and Lambie 1997). Furthermore, due to the absence of an AC the induction of the vulva does not take place (Sun and Lambie 1997). In less penetrant cases, the development of the somatic gonad is delayed and incomplete, leading to abnormal morphology of the gonad and the vulva (Sun and Lambie 1997). However, the orientation of gonadal cell division axes and cell fates per se do not seem to be affected (Sun and Lambie 1997).

GON-2 encodes a member of the TRPM (Transient Receptor Potential Melastatin) cation channel family (West *et al.* 2001). TRPM proteins are found in all metazoans, and belong to the TRP superfamily (Ramsey *et al.* 2006). In contrast to other known ion channels, the mammalian TRPM2, TRPM6 and TRPM7 proteins each contain an enzymatic domain (Ramsey *et al.* 2006). TRPM2 contains a nudix hydrolase domain and TRPM6 and TRPM7 contain a kinase domain (Yamaguchi *et al.* 2001; Perraud *et al.* 2001; Ryazanova *et al.* 2004). GON-2 is one of three *C. elegans* proteins (along with GTL-1 and GTL-2) that shows similarity to human TRPM6 and TRPM7; however, the nematode proteins lack the kinase domain (Harteneck *et al.* 2000; West *et al.* 2001; Teramoto *et al.* 2005).

Human TRPM6 is expressed in the intestine, kidney and lung whereas TRPM7 is expressed ubiquitously (Schlingmann *et al.* 2002; Groenestege *et al.* 2006). It has been shown that TRPM6 requires assembly with TRPM7 to form heterotetrameric complexes that have channel function (Chubanov *et al.* 2004). These channels are important for both cellular and organismal Mg<sup>2+</sup> homeostasis (Schlingmann *et al.* 2002; Chubanov *et al.* 2004; Groenestege *et al.* 2006; Schlingmann *et al.* 2007).

GON-2 and GTL-1 are both expressed in *C. elegans* intestinal cells and are required for  $Mg^{2+}$  and  $Ca^{2+}$  uptake (Teramoto *et al.* 2005; Xing *et al.* 2008). GTL-2 is expressed in the excretory cell (functional equivalent to the kidney) and the hypodermal syncytium and mediates the clearance of excess  $Mg^{2+}$  from the pseudocoelom (Nelson and Riddle 1984; Buechner *et al.* 1999; Teramoto *et al.* 2010; Stawicki *et al.* 2011). In contrast to GTL-1, GON-2 activity is highly sensitive to free intracellular  $Mg^{2+}$ , and is fully inhibited at  $\leq 1$  mM (Teramoto *et al.* 2010).

GON-2 probably functions in Z1 and Z4, although it has not been possible to ascertain its subcellular localization in the gonad precursors; however, since GON-2::GFP localizes to the plasma membrane of intestinal cells (Teramoto *et al.* 2005), it is likely that GON-2 localizes to the plasma membrane of Z1 and Z4, where it could mediate  $Mg^{2+}$  uptake to promote cell proliferation (Wolf *et al.* 2008; Kemp *et al.* 2009).

## 2.6 CATP-6

Mutations in *catp-6* IV were identified in a forward genetic screen based on their ability to prevent the gain-of-function allele *gem-1(dx66)* X (henceforth called *gem-1(gf)*), from suppressing *gon-2(lf)* (Lambie *et al.* 2013). *gem-1* encodes a member of the SLC16A/monocarboxylate transporter protein family (Kemp *et al.* 2009). In Z1 and Z4, GEM-1::GFP is localized predominantly to the plasma membrane, whereas CATP-6::GFP localizes to small cytoplasmic vesicles adjacent to the plasma membrane (Kemp *et al.* 2009; Lambie *et al.* 2013). The data suggest that CATP-6 acts upstream of GEM-1, since overexpression of GEM-1 can bypass the requirement for CATP-6 activity (Kemp *et al.* 2009; Lambie *et al.* 2013). *catp-6* encodes one of three paralogous nematode P5B ATPases (Lambie *et al.* 2013). The other two paralogous genes are *catp-5* and *catp-7* (Heinick *et al.* 2010; Lambie *et al.* 2013). Analysis of the nematode P5B ATPases is the main objective of this dissertation.

## 2.7 P5B ATPases

P-type ATPases are a diverse and ancient family of transmembrane proteins that are found in the genomes of both eukaryotes and prokaryotes (Møller *et al.* 1996). These molecular pumps use the energy derived from hydrolysis of ATP to actively transport substrates against their electrochemical gradient from one side of a membrane to the other (Møller *et al.* 1996; Bublitz *et al.* 2011). P-type (phosphorylated) are distinct from other ATPase transporters, such as the F-type ( $F_0F_1$ ), V-type (Vacuolar) and ABC-type (ATP-binding cassette) (Pedersen and Carafoli 1986; Higgins 1992). The members of the P-type ATPases family have four well-defined types of structural domains: the actuator domain (A), the nucleotide binding domain (N), the phosphorylation domain (P) and the transmembrane domain (M) (Bublitz *et al.* 2010; Møller *et al.* 2010).

These structural domains contain multiple signature motifs, including the highly conserved cytoplasmic DKTGT motif within the P-domain (Møller *et al.* 1996; Palmgren and Nissen 2011). This motif enables the P-type ATPases to form a phosphorylated enzyme intermediate during the Post-Albers transport cycle, a series of conformational changes that are dependent on the sequential autophosphorylation and dephosphorylation of the initial aspartic acid residue (D) (Post 1969; Walderhaug *et al.* 1985; Møller *et al.* 1996; Albers 2003; Toyoshima and Inesi 2004).

## 2.8 The Post-Albers transport cycle of the SERCA pump

The Post-Albers transport cycle has been well studied in the case of transporters such as the sarcoplasmic/endoplasmic reticulum  $Ca^{2+}$  pump (SERCA) (Toyoshima *et al.* 2000; Toyoshima and Inesi 2004) and the  $Na^+/K^+$ -ATPase (Morth *et al.* 2007; 2011). During this cycle, a series of conformational changes of the four structural domains occurs. Each structural domain contains at least one signature motif that is critical for binding to the transport substrate, binding ATP and its associated  $Mg^{2+}$ , autophosphorylation or dephosphorylation. In order to prevent a back

flow of transport substrates, P-type ATPases transiently open and close only towards one side of the membrane at a time (Jardetzky 1966; Bublitz *et al.* 2011). Although this section describes the Post-Albers transport cycle in forward direction, the transport cycle can run in opposite direction under favorable conditions *in vitro* (Lancaster 2004).

The first step of the transport cycle is called the E1 state. Using the SERCA pump as an example, when the transporter enters this state, it opens toward the cytosol, releasing 2-3 H<sup>+</sup> from the substrate binding pocket and exposing a high-affinity Ca<sup>2+</sup>-binding site (Post 1969; Albers 2003; Toyoshima and Inesi 2004; Bublitz *et al.* 2011). Ca<sup>2+</sup> binds to the two binding sites in the binding pocket formed by transmembrane segments M4, M5, M6 plus M8 (Toyoshima *et al.* 2000; Møller *et al.* 2010).

In the E1 state, multiple signature motifs enable the enzyme to interact with ATP and its associated Mg<sup>2+</sup>, ultimately leading to autophosphorylation of the transporter. The lysine residue (K) at the beginning of the signature motif KG(A/S)PE within the N-domain is critical for binding to the 6-amino group of the adenine ring of ATP (Clausen *et al.* 2003; Sørensen *et al.* 2010; Møller *et al.* 2010). Within the P-domain, the signature motifs TGDN and GDGxND are crucial for the interaction with the Mg<sup>2+</sup> ion complexed with ATP (Palmgren and Nissen 2011). The aspartic acid residue (D) at the beginning of the DKTGT motif acts as an acceptor and enables the transporter to form an acyl-phosphate bond with the γ-phosphoryl group of ATP through an S<sub>N</sub>2 type nucleophilic substitution mechanism (Bastide *et al.* 1973; Champeil 1996; Sørensen 2004). The phosphorylation reaction is enabled by the close proximity of the negatively charged γ-phosphoryl group of ATP to the aspartic acid residue (D) within the DKTGT motif (Møller *et al.* 1996; Sørensen 2004; Møller *et al.* 2010). Subsequently after phosphorylation, the enzyme closes towards the cytosol leading to the E1P state (Toyoshima and Inesi 2004).

## General Introduction

The E1P state is ADP-sensitive, thus the phosphoryl group can be retransferred to ADP in the reverse reaction (Kühlbrandt 2004; Toustrup-Jensen *et al.* 2009; Yamasaki *et al.* 2010). The transition from E1P to E2P state is the slowest phase of the catalytic cycle due to multiple conformational changes of the transporter and therefore this is the rate-limiting step (Kühlbrandt 2004; Palmgren and Nissen 2011). The A-domain rotates by 110°, which moves the signature motif TGE in close proximity to the autophosphorylation site (Kühlbrandt 2004; Toyoshima and Inesi 2004). This prevents retransfer of the phosphoryl group to ADP, and promotes dissociation of ADP, leading to the E2P state which is ADP-insensitive (Kühlbrandt 2004; Toyoshima and Inesi 2004; Bublitz *et al.* 2011).

During the transition from E1P to E2P, the P-domain tilts, which decreases the affinity of the P-domain-attached transmembrane segments (M4 and M5) for Ca<sup>2+</sup> and results in opening of the substrate binding pocket towards the extracytosolic compartment (Kühlbrandt 2004; Olesen 2004; Bublitz *et al.* 2011). Ca<sup>2+</sup> is then released and 2-3 H<sup>+</sup> bind to the binding pocket (Toyoshima *et al.* 2000; Toyoshima and Inesi 2004).

The E2P-E2 transition is initiated when the threonine residue (T) and the glutamic acid residue (E) of the TGE motif interact with a water molecule (Olesen 2004), probably competing for the hydrogen bonds of the Mg<sup>2+</sup> ion near the phosphorylation site (Kühlbrandt 2004). The glutamic acid residue (E) of the TGE motif then detracts a proton from the water molecule, which subsequently attacks the phosphoryl group leading to enzyme dephosphorylation (Olesen 2004). Mg<sup>2+</sup> and the phosphoryl group then dissociate, which leads to the E2 state (Kühlbrandt 2004).

In the E2 state, the position of the A-domain remains almost unchanged due to its interaction with the P- and the N-domain (Kühlbrandt 2004). At the end of the cycle, new ATP binds and the transporter opens again towards the cytosol; this pulls the domains back into the

positions of the E1 state, thereby releasing the bound 2-3  $H^+$  and starting the cycle again (Kühlbrandt 2004; Toyoshima and Inesi 2004; Lancaster 2004).

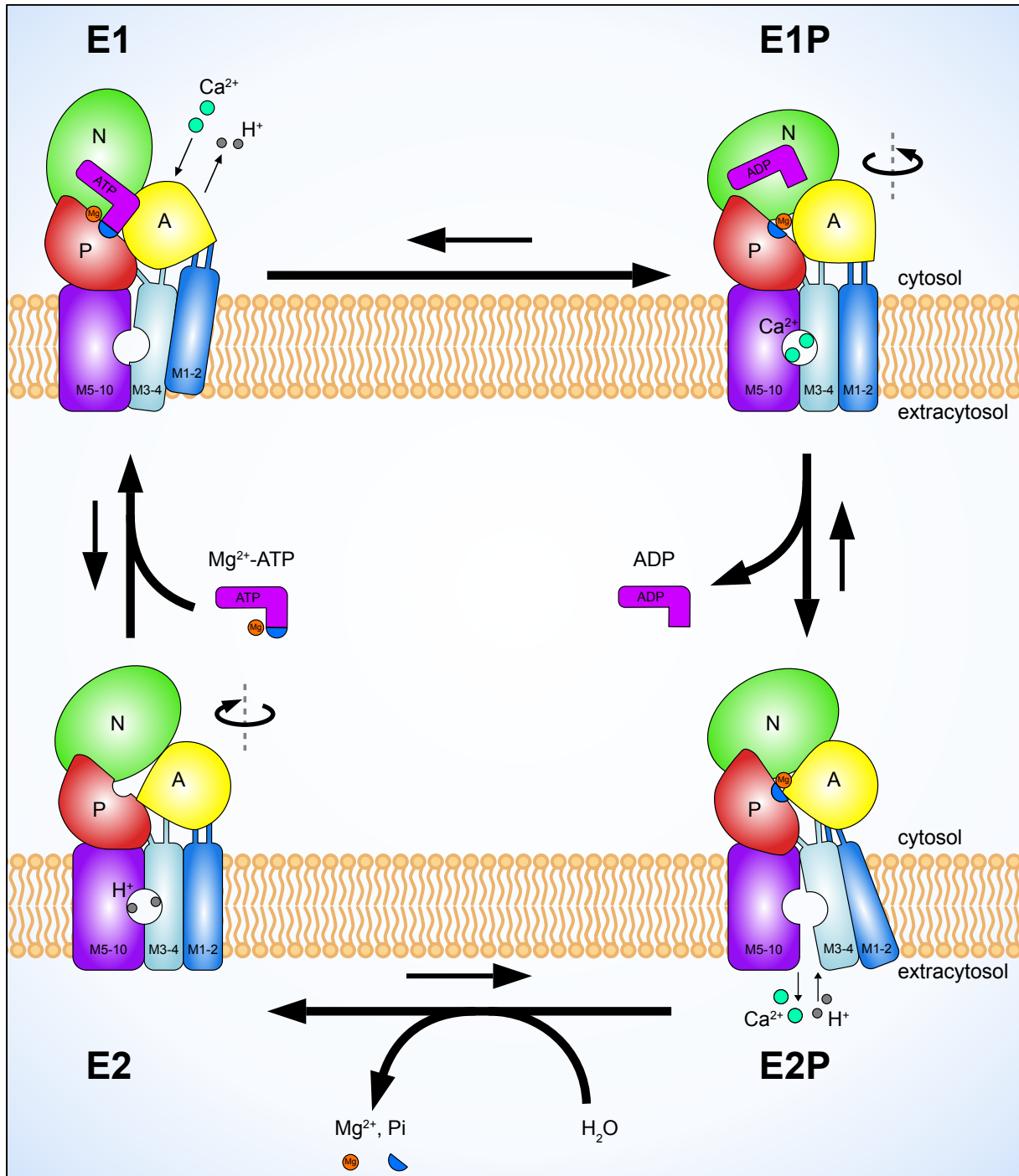


**Fig 2: The Post-Albers transport cycle of the SERCA pump.** E1 state. E1P state. E2P state. E2 state. Under favorable conditions, the transport cycle can run in opposite direction. Inspired by (Kühlbrandt 2004; Lancaster 2004; Bublitz *et al.* 2011).

## 2.9 The P5 subfamily

The P-type ATPases can be grouped into 5 subfamilies, P1-P5 (Axelsen and Palmgren 1998). The cellular functions and substrate specificities are well studied for most of the members of the P1-P4 subfamilies, including the antiporter Na<sup>+</sup>/K<sup>+</sup>-ATPase (Morth *et al.* 2007), and SERCA pump (Toyoshima *et al.* 2000). The members of the P1-P3 subfamilies transport either ions or heavy metals, whereas P4 ATPases are phospholipid flippases (Kühlbrandt 2004; Palmgren and Nissen 2011; Bublitz *et al.* 2011; van Veen *et al.* 2014).

Members of the P5 subfamily are characterized by the presence of a PPxxPxx motif within the putative substrate-interaction region of transmembrane segment M4 and have been further classified into subgroups A and B (Møller *et al.* 2008; Sørensen *et al.* 2010). In P5A ATPases, the putative substrate-interaction motif is PP(D/E)xPx<sub>2</sub>E (Møller *et al.* 2008; Sørensen *et al.* 2010), whereas in P5B ATPases it is PP(A/V)xPAx (Møller *et al.* 2008; Sørensen *et al.* 2010), suggesting that the two subgroups have different substrate specificities (Møller *et al.* 2008; Sørensen *et al.* 2010). However, specific substrates have not been definitively determined for either the P5A or P5B subgroups (Møller *et al.* 2008; Bublitz *et al.* 2010; 2011; van Veen *et al.* 2014; Sørensen *et al.* 2018). Since the focus of this dissertation is on the P5B ATPases, the P5A subgroup will not be discussed further.

## 2.10 P5B ATPases in vertebrate clades

The human genome encodes four paralogous P5B ATPases (Sørensen *et al.* 2018). A recent phylogenetic analysis revealed that several distinct P5B ATPase diversification events occurred (Sørensen *et al.* 2018). The diversification within vertebrate evolution seems to be independent from the diversification events within the Protostomia clade (Sørensen *et al.* 2018). ATP13A2-like proteins appear to be the most basal form; these proteins show a higher degree of similarity to the P5B ATPases from the Protostomia clade than do the ATP13A3-like proteins (Sørensen *et al.* 2018). ATP13A3-like proteins are only found in the Deuterostomia clade (Sørensen *et al.*



2018). Within the Ambulacraria clade distinct diversification events occurred, and the multiple paralogs group to the ATP13A3-like cluster (Sørensen *et al.* 2018). Although in some ray-finned fish (Actinopterygii) genomes there are more than two P5B ATPases present, these protein sequences only group to either ATP13A2 or ATP13A3-like clusters, suggesting that in the Actinopterygii clade only two types of P5B ATPases exist and that independent diversification events occurred within particular species, e.g. *Salmo salar* (which has four paralogs) (Sørensen *et al.* 2018). Three types of P5B ATPases are present in lobe-finned fish (Sarcopterygii), as well as in amphibians, and four types can be found in the Amniota clade (reptiles, birds and mammals) namely ATP13A2, ATP13A3, ATP13A4 and ATP13A5 (Sørensen *et al.* 2018).

### 2.11 P5B ATPases and human disease

Sequence alterations involving each of the four human P5Bs have been found to be associated with one or more diseases. Two single nucleotide polymorphisms (SNPs) in *atp13a5* were found in a family with 3 Hailey Hailey disease (HHD) patients, but not in 2 non-affected family members (van Beek *et al.* 2015). In contrast, the 2 non-affected family members showed another homozygous SNP that was detected as heterozygous in all 3 affected family members, suggesting that an accumulation of SNPs in *atp13a5* might be required to cause HHD (van Beek *et al.* 2015).

ATP13A4 is expressed in fetal brain tissue, and mutations in *atp13a4* have been associated with autism spectrum disorder (ASD) (Kwasnicka-Crawford *et al.* 2005; Vallipuram and Grenville 2010; Biamino *et al.* 2016). It was speculated that ATP13A3 has a role in cellular aging and tumor suppression (Habtemichael and Kovacs 2002). Recently, it was proposed that high ATP13A3 expression along with low to moderate Cav-1 expression could be used as a biomarker for  $\alpha$ -difluoromethylornithine (DFMO) based therapies in pancreatic cancers (Madan *et al.* 2016). Moreover, a 25-year-old male with oculo auriculo vertebral spectrum

(OAVS) showed a 723 kb microduplication on chromosome 3q29 covering the locus of ATP13A3 along with other genes (Guida *et al.* 2015).

Mutations in ATP13A2 also known as PARK9, have been found to be associated with the autosomal recessive Kufor-Rakeb syndrome (KRS), a form of early onset Parkinson's disease (PD) displaying nigro-striatal dopaminergic degradation, pallido-pyramidal neurodegeneration and dementia (Al-Din *et al.* 1994; Hampshire *et al.* 2001; Ramirez *et al.* 2006). On the other hand, mutations in ATP13A2 were also found in a family that suffers from neuronal ceroid lipofuscinoses (NCL), an inherited disease that affects the brain and the retina (Bras *et al.* 2012). NCL is characterized by the accumulation of autofluorescent lipopigments in the lysosome (Bras *et al.* 2012). In line with human NCL, tibetan terriers that suffer from NCL carried a homozygous SNP in ATP13A2 leading to a protein that lacks 69 aa due to skipping of exon 16 (Wöhlke *et al.* 2011). Recently, homozygous mutations in ATP13A2 have been linked to another neurodegenerative disorder, hereditary spastic paraplegia (HSP) (Estrada-Cuzcano *et al.* 2017).

### 2.12 Subcellular localization

Given the known importance of P5B ATPases for human diseases the question concerning the exact cellular function arises. One step towards answering this question is to unambiguously identify the subcellular localization of P5B ATPases.

In human tissue culture cells, ectopically expressed ATP13A2 localizes to lysosomes, early and late endosomes/multi-vesicular bodies (MVBs) as well as recycling endosomes, which is in line with its role in NCL (Ramirez *et al.* 2006; Kong *et al.* 2014; Holemans *et al.* 2015; Sørensen *et al.* 2018). Interestingly, N- or C-terminally GFP-tagged ATP13A2 (live cell imaging) as well as catalytically inactive ATP13A2(D508N) and wild type (wt) ATP13A2 (immunocytochemistry) were found to localize to the same subcellular compartments, indicating that neither the GFP-tag nor the transport activity has an impact on the localization

(Sørensen *et al.* 2018). In the same study, ATP13A3 was shown to localize to recycling endosomes, late endosomes and lysosomes, similar to ATP13A2 (Sørensen *et al.* 2018).

Vallipuram *et al.* (2010) used immunocytochemistry to stain for ectopically expressed ATP13A4 and detected association with the endoplasmic reticulum (ER) in COS-7 cells. In contrast, by staining for endogenous ATP13A4 in HeLa (Henrietta Lacks) cells, association with early and late endosomes was detected (Sørensen *et al.* 2018). The authors observed a similar pattern by using GFP-tagged ATP13A4 (Sørensen *et al.* 2018). So far, it has not been possible to unambiguously determine the subcellular localization of ATP13A5 (Sørensen *et al.* 2018).

### **2.13 Subcellular phenotypes**

Neurodegeneration can be induced through malfunction of variable cellular processes. In line with the critical role of ATP13A2 in neurodegenerative disorders and its subcellular localization in the endolysosomal pathway, loss-of-function mutations of ATP13A2 and related P5B ATPases were shown to result in diverse cellular impairments, ranging from protein aggregation to mitochondrial dysfunction.

#### **2.13.1 Synuclein**

The accumulation of  $\alpha$ -synuclein in Lewy-bodies is a major hallmark of PD (Polymeropoulos *et al.* 1997). Multiple studies link ATP13A2 function to the reduction of  $\alpha$ -synuclein aggregates. Overexpression of ATP13A2 in cultured cells causes reduced intracellular  $\alpha$ -synuclein levels, but increased  $\alpha$ -synuclein levels in exosomes (Kong *et al.* 2014).

ATP13A2 deficient mice showed increased sensitivity towards the toxic effects of overexpressed human  $\alpha$ -synuclein, displaying enhanced age-related sensorimotor deficits (Dirr *et al.* 2018). Another recent study showed that ATP13A2 deficient mice display an increased sensitivity towards  $Mn^{2+}$ , concomitant with increased  $\alpha$ -synuclein aggregates in the ventral

midbrain (Fleming *et al.* 2018). In *C. elegans*, CATP-6 RNAi increased  $\alpha$ -synuclein induced dopaminergic neurodegeneration (Gitler *et al.* 2009).

On the other hand Kett *et al.* (2015) reported that elimination of ATP13A2 activity in mice leads to age-related motor dysfunctions that were independent of  $\alpha$ -synuclein aggregation (Kett *et al.* 2015). Recently, another ATP13A2 deficient mice model was analyzed, again without detecting any abnormal levels of  $\alpha$ -synuclein (Rayaprolu *et al.* 2018).

### **2.13.2 Autophagic and lysosomal dysfunction**

Impaired function of the autophagy pathway has been strongly associated with PD (Lynch-Day *et al.* 2012). Several studies suggest that ATP13A2 is critical for proper lysosomal function and/or the autophagy pathway.

RNAi against ATP13A2 was found to cause impaired lysosomal degradation capacity (Usenovic *et al.* 2012b). Usenovic *et al.* (2012b) suggested that loss-of-ATP13A2-induced lysosomal dysfunction leads to impaired lysosomal clearance of autophagic vesicles. ATP13A2 and another PD-linked gene, synaptotagmin 11 (SYT11), were shown to act in the same pathway regulating autophagy (Bento *et al.* 2016). Bento *et al.* (2016) suggested that steady-state ATP13A2 blocks MYCBP2-induced ubiquitination thereby stabilizing SYT11 which is critical for lysosomal function and autophagosomal clearance. On the other hand, Demirsoy *et al.* (2017) found that overexpression of wild type ATP13A2, catalytically inactive ATP13A2(D508N), or the N-terminus of ATP13A2 reduced intracellular accumulation of ubiquitinated proteins in cells exposed to the proteasome inhibitor Bortezomib. These authors suggested that this effect is caused by increased cargo export through nanovesicles such as exosomes, rather than by autophagic degradation.

### 2.13.3 Mitochondria

Mitochondrial dysfunction is strongly associated with PD (Winklhofer and Haass 2010). Loss-of-function mutations in Parkin (PARK2) and PINK1 (PARK6) have been found in patients suffering from juvenile and early-onset PD (Matsumine *et al.* 1997; Kitada *et al.* 1998; Valente *et al.* 2001; Pickrell and Youle 2015). Both proteins function in mitochondrial quality control (Pickrell and Youle 2015).

With regard to ATP13A2, KRS patient fibroblasts showed increased mitochondrial fragmentation concomitant with increased mitochondrial DNA levels, decreased ATP synthesis, and increased oxygen consumption (Grünewald *et al.* 2012). Ectopic expression of wt ATP13A2 could rescue the observed phenotypes (Grünewald *et al.* 2012). Grünewald *et al.* (2012) proposed that ATP13A2 contributes to the maintenance of healthy mitochondria. In line with this, patient loss-of-function mutations in ATP13A2 caused impaired mitochondrial function, as evidenced by decreased levels in ATP production and reduction of mitochondrial membrane potential (Park *et al.* 2014). Furthermore, overexpression of ATP13A2 protected against Zn<sup>2+</sup> stress-induced mitochondrial fragmentation and cell death (Park *et al.* 2014).

### 2.13.4 Intracellular trafficking

A yeast two-hybrid screen revealed 43 ATP13A2 interactors, of which eight act in vesicular trafficking (Usenovic *et al.* 2012a). Kett *et al.* (2015) reported protein trafficking defects, endolysosomal abnormalities and accumulation of ubiquitinated protein aggregates in the brain of ATP13A2 deficient mice. In these mice cathepsin D maturation and trafficking to the lysosome was found to be defective, but these observations were independent of general lysosomal dysfunction (Kett *et al.* 2015). In contrast to Dehay *et al.* (2012), Kett *et al.* (2015) did not observe any perturbation of lysosomal pH in ATP13A2 deficient mice cells. Rinaldi *et al.* (2015) observed that ectopic expression of ATP13A2 rescued Fe<sup>3+</sup> stress-induced actin

cytoskeleton remodeling, which the authors suggested to be the reason for vesicle trafficking defects and impaired lysosome degradation pathway in CHO (Chinese hamster ovary) cells.

### **2.14 The transport substrate of P5B ATPases**

Identification of the transport substrate is a critical step towards understanding the cellular function of P5B ATPases. Since the putative substrate-interaction region M4 of the human P5B ATPases is highly conserved, it is likely that all P5Bs transport the same substrate (Møller *et al.* 2008; Sørensen *et al.* 2018). Although experimental support has been provided for several different candidate substrates, so far none of these candidates has been unambiguously determined to be the direct transport substrate of P5B ATPases (Holemans *et al.* 2015; Sørensen *et al.* 2018).

#### **2.14.1 Zinc**

Zn<sup>2+</sup> has been suggested as a P5B candidate transport substrate in several recent papers. Fibroblasts isolated from patients with loss of ATP13A2 function showed an increased sensitivity to high extracellular Zn<sup>2+</sup> concentrations (Tsunemi and Krainc 2014), and overexpression of ATP13A2 in cultured cells causes resistance towards the toxic effects of Zn<sup>2+</sup> (Kong *et al.* 2014). Kong *et al.* (2014) proposed a model in which the modulation of Zn<sup>2+</sup> levels in MVBs regulates the biogenesis of exosomes containing  $\alpha$ -synuclein, therefore protecting the cell against  $\alpha$ -synuclein aggregates.

Additionally, patient loss-of-function mutations in ATP13A2 caused impaired Zn<sup>2+</sup> homeostasis, but also altered the expression of Zn<sup>2+</sup> transporters, suggesting a compensatory effect (Park *et al.* 2014). In *Saccharomyces cerevisiae*, P5B ATPase (YPK9) activity was found to confer resistance to toxic levels of Zn<sup>2+</sup> (Kong *et al.* 2014).

### 2.14.2 Manganese

Schmidt *et al.* (2009) reported that YPK9 localizes to the vacuole and suggested the transporter to be involved in sequestering  $Mn^{2+}$  (plus  $Cd^{2+}$ ,  $Ni^{2+}$  and  $Se^{2+}$ ), since depletion of YPK9 causes increased sensitivity to these ions. Therefore, YPK9 might protect against the toxic oxidative stress effects of  $Mn^{2+}$  (plus  $Cd^{2+}$ ,  $Ni^{2+}$  and  $Se^{2+}$ ) in the cytosol (Schmidt *et al.* 2009). Consequently,  $Mn^{2+}$  has also been suggested as a candidate transport substrate. In humans,  $Mn^{2+}$  overexposure humans leads to a progressive disorder called manganism, with symptoms that are similar to those of PD (Crossgrove and Zheng 2004). ATP13A2 was shown to be upregulated upon  $Mn^{2+}$  stress in mammalian cell culture (Tan *et al.* 2011). Interestingly, overexpression of ATP13A2 protected these cells from  $Mn^{2+}$  induced cell death (Tan *et al.* 2011).

Since yeast YPK9 and human ATP13A2 are potentially involved in uptake and/or homeostasis of  $Mn^{2+}$ , Gitler *et al.* (2009) suggested that CATP-6 could play a similar role, by protecting against neurotoxic effects of  $Mn^{2+}$  and  $\alpha$ -synuclein aggregation (Schmidt *et al.* 2009; Tan *et al.* 2011).

### 2.14.3 Calcium

It has also been suggested that P5B ATPases might mediate  $Ca^{2+}$  transport. Ramonet *et al.* (2012) found that RNAi of ATP13A2 leads to reduced intracellular calcium levels in cortical neurons. Furthermore, the overexpression of ATP13A4 in COS-7 cells caused an increase in cellular  $Ca^{2+}$  levels, whereas overexpression of the catalytically inactive ATP13A4(D646E) protein found in patients with ASD did not cause such an increase (Vallipuram and Grenville 2010).

### 2.14.4 Magnesium

As mentioned above, CATP-6 interacts genetically with regulators of  $Mg^{2+}$  homeostasis within the somatic gonad precursors of *C. elegans* (Lambie *et al.* 2013). In line with this, the amoebal

P5B-ATPase, Kil2 of *Dictyostelium discoideum* is a candidate  $Mg^{2+}$  pump, since it is essential for  $Mg^{2+}$  dependent killing of ingested *Klebsiella pneumoniae* (Lelong *et al.* 2011).

### 2.14.5 Polyamines

P5B ATPases have also been suggested as candidate polyamine transporters. The first evidence of this was provided by Heinick *et al.* (2010), who characterized the *C. elegans catp-5* gene. These investigators found that CATP-5 localizes to the apical face of the intestinal cells and its inactivation confers to resistance toxic levels of norspermidine. Moreover, *catp-5(0)* causes a synthetic slow growth phenotype when combined with mutations that impair polyamine synthesis (Heinick *et al.* 2010). Therefore, the most parsimonious explanation is that CATP-5 imports polyamines into the intestinal cells.

There is also evidence that mammalian P5Bs might act as polyamine transporters. Expression of ATP13A2 in CHO cells caused increased sensitivity against the toxic polyamine paraquat and 2-fold increase of cellular spermidine (de Tezanos Pinto *et al.* 2012; La Hera *et al.* 2013). Expression of ATP13A2 was shown to protect against  $Fe^{3+}$  induced cell damage, whereas catalytically inactive ATP13A2(D508N) was ineffective (Rinaldi *et al.* 2015). Rinaldi *et al.* (2015) proposed that polyamines might be the transport substrate of ATP13A2 and that polyamines such as spermidine could protect against iron-induced oxidative damage within lysosomes that fuse with autophagosomes.

Recently, the human paralog ATP13A3 was also suggested to be involved in polyamine transport since ATP13A3 expression is highly upregulated upon blocking of polyamine synthesis via DFMO in human pancreas-liver carcinoma cells (Madan *et al.* 2016). In line with this, cell viability was reduced upon ATP13A3 RNAi after treatment with DFMO and supplementation of spermidine (Madan *et al.* 2016).



### 2.14.6 Regulation via lipid interaction

In at least some cases, P5B ATPase activity is regulated by interaction with phospholipids within the lipid bilayer of cellular membranes. Recently, it was shown that the N-terminal hydrophobic helix, Ma, of ATP13A2, ATP13A and ATP13A4 associates with the membrane such that both the N- and the C-terminus are facing the cytosol (Holemans *et al.* 2015; Sørensen *et al.* 2018). Holemans *et al.* (2015) suggested that Ma acts like a molecular switch that is able to activate the catalytic cycle upon interaction with phosphatidic acid (PA) and phosphatidylinositol(3,5)bisphosphate (PI(3,5)P2) in the lipid bilayer. Martin *et al.* (2016) confirmed that ectopically expressed ATP13A2 protects against the toxic effects of  $Zn^{2+}$ ,  $Mn^{2+}$  and  $Fe^{3+}$ , but the authors did not find any evidence that  $Zn^{2+}$ ,  $Mn^{2+}$  nor  $Fe^{3+}$  is the direct transport substrate of ATP13A2. Furthermore, ATP13A2 was also found to confer protection against the mitochondrial complex I inhibitor, rotenone (Martin *et al.* 2016). Interestingly, the protective effect against  $Zn^{2+}$ ,  $Mn^{2+}$ ,  $Fe^{3+}$  and rotenone was found to rely on the binding to PA and PI(3,5)P2 (Martin *et al.* 2016).

### 2.15 Objectives

Although proper P5B ATPase function is known to be essential for human health, little is known about the functions of these transporters during development. This dissertation aims to provide a basic characterization of the roles of P5B ATPases in animal development, using the nematode *C. elegans* as a model system.

In Chapter 1, I performed a phylogenetic analysis of the three *C. elegans* paralogs in comparison with closely related species from the Caenorhabditis clade and also more distantly related nematodes. It is most likely that the paralogous P5B ATPases in *C. elegans* evolved from a common ancestral protein after the origin of the Caenorhabditis clade. The protein alignment of all three *C. elegans* P5B ATPases shows a high degree of similarity, particularly in the M4 transmembrane domain, which is the putative substrate interaction region. This

suggests that CATP-5, CATP-6 and CATP-7 could have the same substrate specificity and therefore fulfill the same function. Moreover, I used CRISPR/Cas9 to characterize the *C. elegans* P5B ATPases with regard to spatiotemporal expression pattern and subcellular localization in living animals. I further show that the three paralogs have overlapping functions in the development of the reproductive system, since I observed synthetic sterility in *catp-6(0)*; *catp-5(0)* and *catp-7(dx189) catp-6(0)* double mutants.

In Chapter 2, I performed transformation rescue assays in order to examine the basis for the observed sterility phenotypes. I found evidence that CATP-6 and CATP-7 are redundantly required for the development of the somatic gonadal tissues, since expression of either gene product in somatic cells is sufficient to rescue sterility. CATP-5 and CATP-6 are redundantly required for germline proliferation, since sterility can be rescued by germline expression of either protein. As further evidence of overlapping function, I found that CATP-5 can substitute for CATP-6 in the sheath cells and that overexpression of CATP-7::GFP can substitute for CATP-6 in the genetic background of *gon-2(lf)*; *catp-6(lf)*; *gem-1(gf)*. Moreover, I can show that the catalytic function is critical in order to rescue various P5B ATPase phenotypes in *C. elegans*, including the reestablishment of sensitivity to toxic polyamines.

In Chapter 3, we describe 10 revertant mutations of *gon-2(lf)* (*gon-2(q388)*) that affect 9 different residues within GON-2, and a single *gon-2* mutant allele that reverts the  $Mg^{2+}$ -hypersensitive phenotype of *gtl-2(0)* mutant animals. I tested 6 representative revertant mutations of *gon-2(lf)* via scoring the phenotypes of segregants from homozygous as well as heterozygous animals.

# Chapter 1

---

## **Overlapping expression patterns and functions of three paralogous P5B ATPases in *Caenorhabditis elegans***

Jeffrey Zielich, Elena Tzima, Eva Ayla Schröder, Faten Jemel, Barbara Conradt, Eric J. Lambie

**Published: March 16, 2018. PLoS ONE 13: e0194451**

---

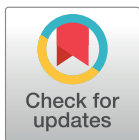
## RESEARCH ARTICLE

# Overlapping expression patterns and functions of three paralogous P5B ATPases in *Caenorhabditis elegans*

Jeffrey Zielich<sup>1</sup>, Elena Tzima<sup>1</sup>, Eva Ayla Schröder<sup>1</sup>, Faten Jemel<sup>1</sup>, Barbara Conradt<sup>1,2</sup>, Eric J. Lambie<sup>1\*</sup>

**1** Department of Cell and Developmental Biology, Ludwig Maximilian University, Planegg-Martinsried, Munich, Germany, **2** Center for Integrated Protein Science Munich, Ludwig Maximilian University, Munich, Germany

\* [lambie@bio.lmu.de](mailto:lambie@bio.lmu.de)



## Abstract

P5B ATPases are present in the genomes of diverse unicellular and multicellular eukaryotes, indicating that they have an ancient origin, and that they are important for cellular fitness. Inactivation of ATP13A2, one of the four human P5B ATPases, leads to early-onset Parkinson's disease (Kufor-Rakeb Syndrome). The presence of an invariant PPALP motif within the putative substrate interaction pocket of transmembrane segment M4 suggests that all P5B ATPases might have similar transport specificity; however, the identity of the transport substrate(s) remains unknown. Nematodes of the genus *Caenorhabditis* possess three paralogous P5B ATPase genes, *catp-5*, *catp-6* and *catp-7*, which probably originated from a single ancestral gene around the time of origin of the *Caenorhabditid* clade. By using CRISPR/Cas9, we have systematically investigated the expression patterns, subcellular localization and biological functions of each of the P5B ATPases of *C. elegans*. We find that each gene has a unique expression pattern, and that some tissues express more than one P5B. In some tissues where their expression patterns overlap, different P5Bs are targeted to different subcellular compartments (e.g., early endosomes vs. plasma membrane), whereas in other tissues they localize to the same compartment (plasma membrane). We observed lysosomal co-localization between CATP-6::GFP and LMP-1::RFP in transgenic animals; however, this was an artifact of the tagged LMP-1 protein, since anti-LMP-1 antibody staining of native protein revealed that LMP-1 and CATP-6::GFP occupy different compartments. The nematode P5Bs are at least partially redundant, since we observed synthetic sterility in *catp-5(0)*; *catp-6(0)* and *catp-6(0)* *catp-7(0)* double mutants. The double mutants exhibit defects in distal tip cell migration that resemble those of *ina-1* (alpha integrin ortholog) and *vab-3* (Pax6 ortholog) mutants, suggesting that the nematode P5Bs are required for *ina-1* and/or *vab-3* function. This is potentially a conserved regulatory interaction, since mammalian ATP13A2, alpha integrin and Pax6 are all required for proper dopaminergic neuron function.

## OPEN ACCESS

**Citation:** Zielich J, Tzima E, Schröder EA, Jemel F, Conradt B, Lambie EJ (2018) Overlapping expression patterns and functions of three paralogous P5B ATPases in *Caenorhabditis elegans*. PLoS ONE 13(3): e0194451. <https://doi.org/10.1371/journal.pone.0194451>

**Editor:** Myon-Hee Lee, East Carolina University, UNITED STATES

**Received:** December 14, 2017

**Accepted:** March 2, 2018

**Published:** March 16, 2018

**Copyright:** © 2018 Zielich et al. This is an open access article distributed under the terms of the [Creative Commons Attribution License](https://creativecommons.org/licenses/by/4.0/), which permits unrestricted use, distribution, and reproduction in any medium, provided the original author and source are credited.

**Data Availability Statement:** All relevant data are within the paper and its Supporting Information files.

**Funding:** Part of the funding for this work was provided by the Deutsche Forschungsgemeinschaft (<http://www.dfg.de/en/>) via grant number LA 3380/2-1 to Eric Lambie. Additional funding was provided by the Center for Integrated Protein Science Munich (<http://www.cipsm.de/>) to Barbara Conradt. The funders had no role in study design, data collection and analysis,

decision to publish, or preparation of the manuscript.

**Competing interests:** The authors have declared that no competing interests exist.

## Introduction

P-type ATPases are an ancient family of transmembrane proteins that use the energy derived from hydrolysis of ATP to actively transport substrates across membranes [1]. These transporters have four types of structural domains (Fig 1, Fig 2B): the actuator domain (A), the nucleotide binding domain (N), the phosphorylation domain (P) and the transmembrane domain (M) [2]. The signature characteristic of P-type ATPases is the highly conserved cytoplasmic DKTGT motif (P-domain, Fig 1) [1], which is autophosphorylated on aspartate during the catalytic cycle [3]. The P-type ATPases can be grouped into 5 subfamilies, P1-P5 [4]. The cellular functions and substrate specificities have been defined for one or more representatives of each of the P1-P4 subfamilies; however, specific substrates have not been definitively determined for either of the P5 subgroups, P5A and P5B [2,5–7]. In this study, we focus on the P5B P-type ATPases, which have a putative substrate interaction motif of PPALP within transmembrane segment M4 [7,8].

The *C. elegans* genome encodes three P5B ATPases: CATP-5, CATP-6 and CATP-7. These proteins have a high degree of similarity, particularly in the M4 transmembrane domain (Fig 1, Fig 2D), which is thought to be critical for coordinating substrate in the binding pocket formed by M4, M5, M6, M8 and M9 [10] (Fig 1, Fig 2B). This suggests that CATP-5, CATP-6 and CATP-7 could have the same substrate specificity and therefore fulfill the same biochemical functions, but in different tissues and/or subcellular compartments.

CATP-5::GFP has been shown to localize to the apical/surface of the intestinal cells and is required for the efficient uptake of polyamines from the gut lumen [11]. We previously showed that CATP-6 localizes to vesicular structures in multiple cell types, and that it acts to promote the function of the SLC16A transporter, GEM-1 [12]. No characterization of *catp-7* has yet been reported in the literature. In this study, we use CRISPR/Cas9 to characterize all three *C. elegans* P5B P-type ATPases with regard to spatiotemporal expression pattern, subcellular localization and biological function in living animals.

## Material and methods

### Strains and genetics

All strains were maintained at 23.5°C on nematode growth medium (NGM) plates with *E. coli* strain AMA1004 [13] as food source. Bristol N2 was used as the wild-type (wt) strain [14]. Some of the mutations and genome modifications were obtained from the *Caenorhabditis* Genetics Center at the University of Minnesota (CGC, Minneapolis, MN, USA), the National Bioresource Project (University of Tokyo, Japan), and the laboratory of Dr. Barth Grant (Rutgers University, NJ, USA). The following alleles were used in this study: *xnIs459[yfp::ral-1a + unc-119(+)]* III [15], *catp-6(ok3473)* IV, *catp-7(tm4438)* IV [16], *catp-7(dx189[delta 1492 bp Ma-M3 + gfp + loxP])* IV, *catp-6(dx183[catp-6::gfp::3xFlag + loxP])* IV, *catp-6(dx179[catp-6::degron::mKate2::3xFlag + loxP])* IV, *catp-7(dx185[gfp::catp-7 + loxP])* IV, *catp-7(dx191[mcherry::catp-7 + loxP])* IV, *catp-7(dx193[gfp::catp-7 + loxP])* IV, *ltIs44(P<sub>pie-1</sub>mCherry::ph<sup>PLCδ</sup>)* V [17], *catp-5(dx187[gfp::catp-5 + loxP])* X, *catp-5(tm4481)* X [16], *bgIs312[pes-6::gfp]* [18], *xnIs484[mCherry::sec-10 + unc-119(+)]* [15], *pwIs1039[p<sub>snx-1</sub>citrine::hgrs-1<sub>unc-54</sub> UTR-cb-unc-119]*, *pwIs1175[p<sub>snx-1</sub>tgn-38::gfp<sub>unc-54</sub> UTR-cb-unc-119]*; *unc-119(ed3)*, *pwIs1176[p<sub>snx-1</sub>ss-gfp-cd4-hcimp<sub>unc-54</sub> UTR-cb-unc-119]*; *unc-119(ed3)* [19].

### Protein sequence alignment

Alignments were performed by using CLC Main Workbench 8.0 (Qiagen Bioinformatics). Parameters were kept as default (gap open cost: 10, gap extension cost: 1, end gap cost: as any



**Fig 1. *C. elegans* P5B sequence alignment.** Protein sequence alignment of *C. elegans* P5B ATPases in comparison with Human ATP13A2. Blue: Putative membrane associated domain Ma [9] and putative transmembrane domains M1–M10 (TMHMM v1.6). Yellow: A (actuator) domain. Red: P (phosphorylation) domain. Green: N (nucleotide binding) domain [8]. Orange: Putative kink in Ma through conserved glycine. Pink: Putative lipid binding site. Purple: P-type ATPase motifs [9]. Green triangle: Fluorescent protein insertion site via CRISPR/Cas9. Dashed grey boxes: *catp-5(tm4481)*, *catp-6(ok3473)* and *catp-7(tm4438)* respectively. Dotted grey box: *catp-7(dx189)* CRISPR/Cas9 mediated deletion.

<https://doi.org/10.1371/journal.pone.0194451.g001>

other). Transmembrane domains were predicted by using TMHMM 1.6 CLC Main Workbench Plugin. Domains and motifs were identified according to the literature [8,9].

### Core sequence alignment

Core sequences were identified according to [7]. Alignments were performed by using CLC Main Workbench 7.7.2 (Qiagen Bioinformatics). Parameters were kept as default (gap open cost: 10, gap extension cost: 1, end gap cost: as any other).

### Phylogenetic analysis

Sequences were obtained by using pblastp suite <https://blast.ncbi.nlm.nih.gov/Blast.cgi> or directly from <http://flybase.org> and <http://www.wormbase.org>. Alignment was performed by using the alignment tool of CLC Main Workbench 7.9.1 (Qiagen Bioinformatics). Parameters were kept as default (gap open cost: 10, gap extension cost: 1, end gap cost: as any other). We tested for the appropriate model by using MEGA6.06 [20]. A Maximum Likelihood tree was constructed via PhyML3.2 [21] by using the model LG+G ([22], gamma shape parameter: 0.628) and Bootstrap branch support (100 replicates). The final tree was modified by using CLC Main Workbench 7.9.1 (Qiagen Bioinformatics) and Affinity Designer 1.6.0 (Serif).

### Molecular biology

Standard methods for DNA amplification, analysis and manipulation were used. PCR products were amplified by using Phusion® High-Fidelity DNA Polymerase (New England Biolabs), according to the manufacturer's protocol. DNA sequences were obtained by Sanger sequencing.

### Plasmid construction

***P<sub>catp-5</sub>catp-5::gfp<sub>let-858</sub>* and *P<sub>pdp-12</sub>catp-5::gfp<sub>let-858</sub>*.** We amplified the coding sequence of *catp-5a* from the fosmid WRM0614C\_D10 together with 4100 bp 5' of exon 1 as a putative promoter. Sequence ends: 5' ttgtctgtgacaacaacagg and 3' agactatagagagcaaatgt (plus homology to *gfp* and backbone). We fused the coding sequence of *gfp* and the sequence of *let-858* 3'UTR in frame to the 3' end of *catp-5a* by using Gibson cloning (backbone: pGEM-7Zf(+)) [23]. We exchanged *P<sub>catp-5</sub>* with the putative *pdp-12* promoter [24] (amplified from wt genomic DNA, 3591 bp) via Gibson cloning. Sequence ends: 5' ctgaagcttagcctcttcac and 3' ctctgaaatagggttaaagc (plus homology to *catp-5a* and backbone)

***P<sub>catp-6</sub>catp-6::mKate2<sub>let-858</sub>*.** We amplified the coding sequence of *catp-6a* from the fosmid WRM067B\_F08 together with 1135 bp 5' of exon1 as a putative promoter. Sequence ends: 5' gccacaataaataataata and 3' aaaagctgaacgcacttac (plus homology to *mKate2* and backbone). We fused the coding sequence of *mKate2* and the sequence of *let-858* 3'UTR in frame to the 3' end of *catp-6a* by using Gibson cloning (backbone: pGEM-7Zf(+)). We used the aa sequence GASGASGAS as a flexible linker between CATP-6 and mKate2.

***P<sub>catp-7</sub>catp-7::gfp<sub>let-858</sub>*.** We amplified the coding sequence of *catp-7a* from the fosmid WRM0640A\_C09 together with 2377 bp 5' of exon1 as a putative promoter. Sequence ends: 5' ttactttacgggggtgaccct and 3' gtcagaggcggaaaggtgct (plus homology to *gfp* and backbone). We

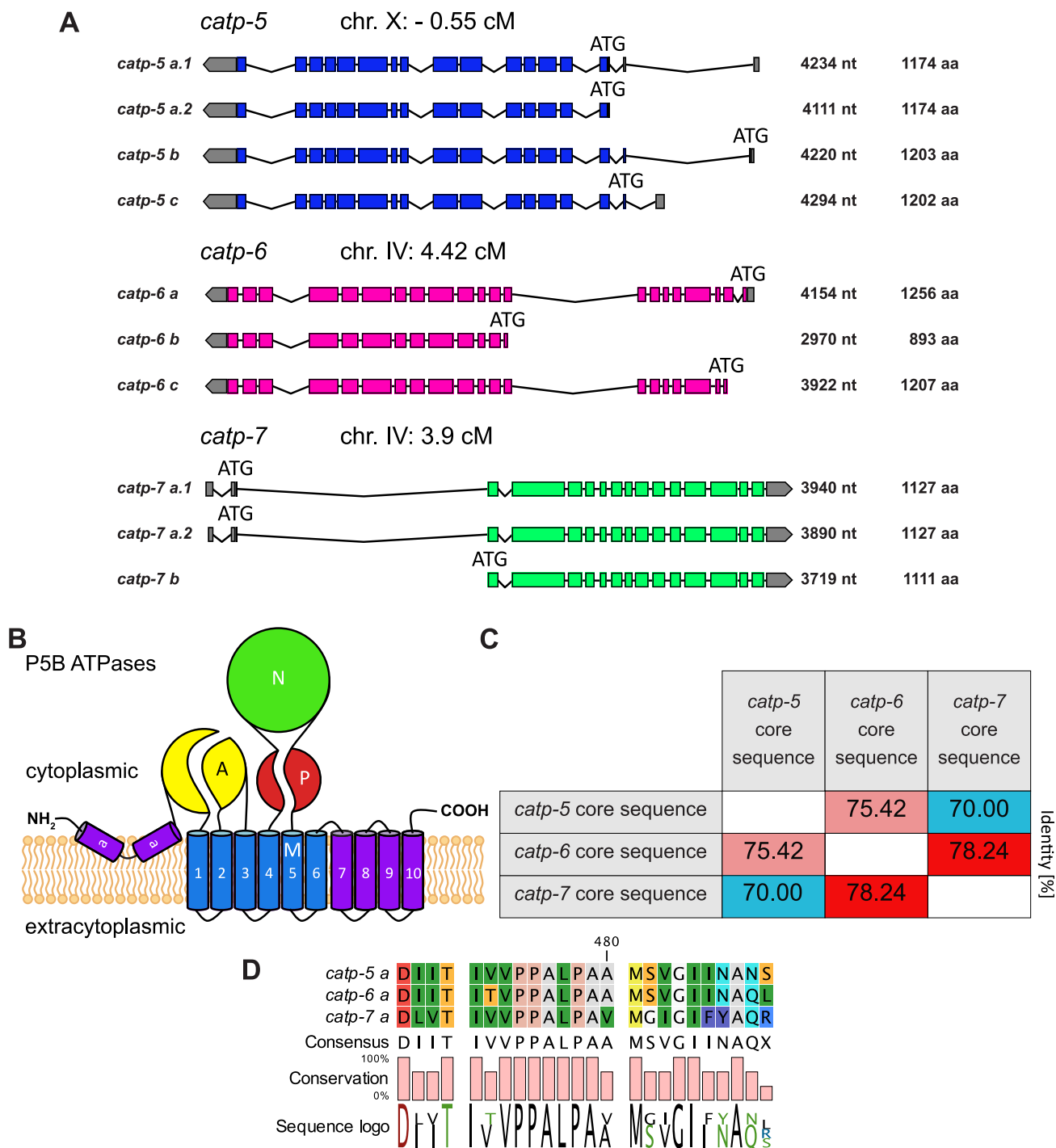


**Fig 2. Paralogous P5B ATPases of *C. elegans*.** (A) Genomic locations including transcripts, transcript length (in nucleotides, nt) and protein length (in amino acids, aa) of *catp-5*, *catp-6* and *catp-7* (WormBase WS262). (B) Schematic of the general structure of P5B ATPases. The A (actuator) domain, the P (phosphorylation) domain, the N (nucleotide binding) domain and the M (transmembrane M1–M10) domain plus the additional membrane associated (Ma) domain are indicated [9]. (C) Similarity matrix of CATP-5, CATP-6 and CATP-7 core sequences. The core sequences consists of 239 aa, according to [7]. (D) Comparison of the amino acid sequences of M4.

<https://doi.org/10.1371/journal.pone.0194451.g002>



fused the coding sequence of *gfp* and the sequence of *let-858* 3'UTR in frame to the 3' end of *catp-7a* by using Gibson cloning (backbone: pGEM-7Zf(+)). We used the aa sequence GPGGP as a flexible linker between CATP-7 and GFP.

***P<sub>sth-1</sub>lmp-1::rfp<sub>unc-54</sub>*, *P<sub>sth-1</sub>rfp::rab-5<sub>unc-54</sub>* and *P<sub>sth-1</sub>rfp::rab-11<sub>unc-54</sub>*.** The coding sequences of *lmp-1* (Sequence ends: 5' atggtgtctaaggcggaaga 3' aactggggcacaactaat), *rab-5* (5' atggccgcccgaacgcagg 3' taaataagaattccaactga) and *rab-11* (5' atgggtctctgtgacgatga 3' agcagtg ttgatccataa) were amplified from wt genomic DNA (added homology to *Tagrffp* [25], *unc-54* 3' UTR or *P<sub>sth-1</sub>*). We fused the putative *sth-1* promoter (*P<sub>sth-1</sub>* 1230 bp: 5' gaagctgaatgcgatgtctt 3' tctttttgtgtagagcaac) [26] plus the coding sequence of *rfp* in frame to the 5' end (or *rfp* to the 3' end of *lmp-1*) and the sequence of *unc-54* 3'UTR to the 3' end of *rab-5* and *rab-11* by using Gibson cloning.

***P<sub>rgs-1</sub>lmp-1::rfp<sub>unc-54</sub>*.** We amplified the putative *rgs-1* promoter (2393 bp, Sequence ends: 5' agtaattggcgtaagtttc 3' ctgcgacgtgttgcgcag) [27] from wt genomic DNA with primers that provide homology to *lmp-1* for *in vivo* recombination with *lmp-1::rfp<sub>unc-54</sub>*.

### CRISPR/Cas9 mediated genome modifications

All sgRNAs were designed by using either the online sgRNA design tool <http://crispr.cos.uni-heidelberg.de/index.html> [28] or <http://www.e-crisp.org/E-CRISP/> [29]. sgRNA expression plasmids were cloned by using pRB1017 following the protocol of [30]. The sgRNAs were expressed under the control of a PU6 promoter. In order to obtain large genome modifications we used two different drug-selection based methods, as recommended [31,32]. We used the following injection-mix concentrations for the self-excising cassette (SEC) drug selection method [32]: pDD162 (*P<sub>eft-3</sub>*Cas9 expression plasmid) at 50 ng/μl, sgRNA plasmid (based on pRB1017) at 50 ng/μl, SEC repair template at 10 ng/μl (based on pDD282 and pDD285), L3790 (*P<sub>myo-2gfp</sub>*, Fire Lab 1995 Vector Kit) at 7 ng/μl. We used the following injection-mix concentrations for the dual marker selection cassette (DMSC) method [31]: *P<sub>eft-3</sub>::Cas9\_SV40-NLS::tbb-2\_UTR* (*P<sub>eft-3</sub>*Cas9 expression plasmid) at 50 ng/μl, sgRNA plasmid (based on pRB1017) at 100 ng/μl, DMSC repair template at 50 ng/μl (based on loxP\_*myo-2\_neoR\_GFP\_intron*), pCFJ90 at 2.5 ng/μl (*P<sub>myo-2mcherry</sub>*), pCFJ104 at 5ng/μl (*P<sub>myo-3mcherry</sub>*). Detailed procedures and a list of all primers used for repair template construction will be provided upon request. All genome modifications were performed in a wild type N2 background, unless stated otherwise.

***catp-5(dx187[gfp::catp-5 + loxP]) X.*** We targeted exon 1 of *catp-5a* by using sgRNA(*catp-5#2*): ctctcgcttcataatttctgtgg (underlined PAM). DMSC *gfp*-fusion repair template was constructed according to [31]. The PAM was mutated silently from tgg to tgc. The coding sequence of *gfp* + *loxP* was inserted into the genome 3' of the following sequence: acaatccatcgacaaaatt and 5' of the sequence: aagcgagagaaagacaatcc.

***catp-6(dx183[catp-6:gfp::3xFlag + loxP]) IV and catp-6(dx179[catp-6::degron::mKate2::3xFlag + loxP]) IV.*** We targeted the last exon of *catp-6a* by using sgRNA(*catp-6#14*): gttccgaaaggctgtgaggagg (underlined PAM). SEC *gfp*-fusion repair template was constructed according to [32]. The PAM was mutated from agg to aaa which changes proline 1239 to a phenylalanine (CATP-6a(P1239F)); this residue is not evolutionarily conserved. The coding sequence of *gfp::3xFlag* + *loxP* and a sequence that encodes a short flexible linker (ggagcatcgg-gagcctcaggagcatcg, GASGASGAS) was inserted into the genome 3' of the following sequence: aaaagcttgaacgcacttac and 5' of the sequence: aatcacttgttttagattt.

The *degron::mKate2* fusion was obtained by following the same procedure. But in addition we introduced the coding sequence of a *degron* motif [33] into the repair template, 5' of the coding sequence of *mKate2* and flanked by two flexible aa linkers of the same sequence (GASGASGAS).

***catp-7(dx185[gfp::catp-7 + loxP]) IV and catp-7(dx191[mcherry::catp-7 + loxP]) IV.*** We targeted exon 2 of *catp-7a* by using the sgRNA(catp-7#12): catgaggaggcggatgggg (underlined PAM). DMSC *gfp*-fusion and *mcherry*-fusion repair template were constructed according to [31]. The PAM was mutated silently from ggg to gcg. The coding sequence of either *gfp* + *loxP* or *mcherry* + *loxP* was inserted into the genome 3' of the following sequence: gatcg-tatgggcctggcgg and 5' of the sequence: tctgccgtccaagaattc.

***catp-6(dx179[catp-6::degron::mKate2::3xFlag + loxP]) catp-7(dx193[gfp::catp-7 + loxP]) IV.*** We targeted exon 2 of *catp-7a* in the genetic background of *catp-6(dx179[catp-6::degron::mKate2::3xFlag + loxP]) IV*, by using sgRNA(catp-7#12): catgaggaggcggatgggg (underlined PAM). *gfp* + *loxP* integration was obtained as described in the previous section.

***catp-6(ok3473) catp-7(dx189[delta 1492 bp Ma-M3 + gfp + loxP]) IV.*** We targeted exon 2 of *catp-7a* in the background of *catp-6(ok3473)* by using the following sgRNAs: sgRNA(catp-7#12): catgaggaggcggatgggg and sgRNA(catp-7#2): cgttcaccttttctaccgtggg (underlined PAM). The PAM of the first sgRNA was mutated silently from ggg to gcg. DMSC *gfp*-fusion repair template was constructed according to [31] by using homology tails that omit 1492 bp between exon 2 and exon 5. After recombination with the genome, 1492 bp between exon 2 and exon 5 were excised and *gfp* + *loxP* was inserted into the genome 3' of the following sequence: cgaccgcctccacccatcc. And 5' of the sequence: cgtgggagttcaattggaaa. The integration led to a frameshift 3' of *gfp*. Worms were propagated as heterozygotes (*catp-6(ok3473) catp-7(dx189)/nT1[qIs51]* (IV;V)).

### Immunochemistry

Worms were dissected in M9 to release gonadal tissues. Gonads were transferred to polylysine-D-coated slides and covered with coverslips [34]. The slides were frozen on dry-ice cooled steel plates. Coverslips were removed after 10 min, slides were fixed for 10 min in -20°C methanol and thereafter transferred to -20°C acetone for 10 min. Slides were incubated in AbA + 1% Triton X-100 (PBS + 0.05% Tween-20 + 0.5% BSA + 1% Triton X-100) for 20 min [35]. Afterwards, samples were blocked for 30 min in BLOCK (PBS + 2% BSA + 2% powdered milk (Sigma) + 0.05% Tween-20). Slides were then washed for 5 min in PBST (PBS + 0.1% Tween-20). Primary antibodies were diluted 1:10 (anti-LMP-1 and anti-RME-1 [35]) and 1:500 (anti-GFP, ab290, Abcam) in BLOCK and used for incubation overnight. Next, slides were washed for 10 min in PBST. Secondary antibodies were diluted 1:500 in BLOCK and used for 1h incubation (IgG Alexa 594 anti mouse and Alexa 488 anti rabbit). Slides were washed for 5 min in PBST, then transferred to PBS for an additional 5 min. Gonads were mounted with VECTA-SHIELD Antifade Mounting Medium with DAPI (Vector Laboratories) and sealed with nail polish. A Leica TCS SP5 II confocal microscope was used for imaging.

### Imaging

Animals were mounted on 4% agarose pads for confocal, DIC and epifluorescence microscopy. Whole worms were immobilized with 10 mM levamisole and/or 1 mM sodium azide. Animals were imaged by using either Leica TCS SP5 II confocal microscope (Leica Application Suite LAS software) or Zeiss Axioskop 2 and MetaMorph software (Molecular Devices). Image processing was performed in Fiji/imageJ 2.0.0 [36], brightness and contrast was adjusted either in Fiji/imageJ 2.0.0 or Affinity Designer 1.6.0 (Serif).

### Fluorescence Recovery after Photobleaching (FRAP)

A Leica TCS SP5 II confocal microscope was used for imaging and photobleaching. We performed photobleaching for 1 min (laser intensity change from 6% to 80% and back) of an ROI

in the excretory cell of L4 transgenic animals of the genotype: *catp-5(tm4481) + P<sub>pgp-12</sub>catp-5::gfp<sub>let-858</sub> + rol-6(su1006), bgIs312[pes-6::gfp], xnlIs459[yfp::ral-1a + unc-119(+)] III and xnlIs484[mCherry::sec-10 + unc-119(+)]*. Fluorescence recovery over time was measured via Fiji/imageJ 2.0.0 [36]. In order to compensate for any movement, we averaged 4–10 pixel of unbleached areas left and right to the ROI and used these measurements to normalize according to [37]. Statistical analysis was performed by using RStudio Version 1.0.143 (<https://www.rstudio.com>). Shapiro-Wilk test in combination with graphical analysis was used to test for normality. Equality of variance was tested via Levene's test. We used an ANOVA (command: aov) and subsequent Tukey post-hoc test.

### Co-localization

**Head neurons:** Animals were immobilized with 1 mM sodium azide. Animals were mounted on 4% agarose pads. **Spermatheca:** Gonads were dissected in L-15/FBS medium [38] with 20 gauge hypodermic needles and mounted without any agar pad directly on microscope slides. Leica TCS SP5 II confocal microscope was used for imaging.

### Brood size estimation

Triplicates of 10 L4 animals for each genotype were transferred to freshly seeded NGM plates (at 20°C). To obtain the complete progeny of all 10 animals per triplicate, worms were transferred to new seeded NGM plates twice a day (morning and afternoon). Once the progeny on a plate reached young adult stage the plates were shifted to 10°C. After six days, the complete progeny were washed off with MPEG (M9 plus 0.05% polyethylene glycol 8000 (PEG)) thereafter frozen at -80°C. Water plus PEG (0.05%) was added to a volume of 30 ml. After shaking, 3 ml of worm suspension was taken to count the average brood size of 1 animal. Statistical analysis was performed by using RStudio Version 1.0.143 (<https://www.rstudio.com>). Shapiro-Wilk test in combination with graphical analysis was used to test for normality. Equality of variance was tested via Levene's test. We used an ANOVA (command: aov) and subsequent Tukey post-hoc test.

### Growth rate estimation

Triplicates of 10 adult animals for each genotype were transferred to freshly seeded NGM plates (at 20°C). All 10 animals were removed after exactly 1 h. 48 h later, the progeny were scored according their developmental stage. The progeny of all 3 replicates were pooled for analysis. Statistical analysis was performed by using RStudio Version 1.0.143 (<https://www.rstudio.com>). We used Fisher's exact test and subsequent Holm's correction for multiple comparison (command: pairwiseNominalIndependence).

## Results

### *C. elegans* P5B isoforms and sequence similarity

According to WormBase (WS262), the *catp-5* locus gives rise to four mRNAs, which differ only in their 5' end regions (Fig 2A). The *catp-5a.1* and *catp-5a.2* transcripts both encode the same protein isoform, CATP-5a (1174 aa). *catp-5b* encodes CATP-5b (1203 aa) and *catp-5c* encodes CATP-5c (1202 aa). All three isoforms display the typical P5B ATPase structure: One membrane associated segment (Ma) [9], ten transmembrane segments (M1-M10), an actuator domain formed by two cytoplasmic loops (between Ma-M1 and M2-M3), plus a nucleotide binding domain and a phosphorylation domain located in the large cytoplasmic loop (M4-M5, Fig 1, Fig 2B).

The *catp-6* locus produces three different mRNAs (WS262), each with a different 5' end region and encoding a distinct protein isoform. *catp-6a* and *catp-6c* encode isoforms that display the typical P5B ATPase structure (CATP-6a, 1256 aa, and CATP-6c 1207 aa). However, the isoform encoded by *catp-6b* is only 893 aa in length and lacks residues N-terminal to M3. We do not know whether CATP-6b is expressed and/or functionally significant in vivo; however, the RNA seq data summarized on WormBase (WS262), suggest that *catp-6b* is not a highly-abundant transcript.

The *catp-7* locus gives rise to three different mRNAs (WS262), each with a different 5' end region. *catp-7a.1* and *catp-7a.2* each encode CATP-7a, 1127 aa. *catp-7b* encodes CATP-7b, 1111 aa. CATP-7a and CATP-7b both include all of the canonical P-type ATPase domains.

We compared the core amino acid sequences of *C. elegans* CATP-5, CATP-6 and CATP-7 according to [7]. Based on this, we found that CATP-6 is slightly more similar to CATP-7 than it is to CATP-5 (78.24% vs 75.42% identity) (Fig 2C), whereas CATP-5 and CATP-7 are the least similar, sharing 70.0% identity.

### Phylogenetic analysis of paralogous P5B ATPases

We obtained orthologous P5B ATPase aa sequences of five additional *Caenorhabditis* species (*C. japonica*, *C. brenneri*, *C. briggsae*, *C. latens* and *C. remanei*), more distant nematode species (*Pristionchus pacificus*, *Onchocerca flexuosa* and *Trichinella spiralis*) and *Drosophila melanogaster* as an outgroup from <http://www.wormbase.org>, <http://www.flybase.org> and from <https://www.ncbi.nlm.nih.gov>. Since, the genomes of these species are thought to be fully sequenced [39–42], it is very likely that we have included all paralogous P5B ATPases for each species. We constructed a Maximum Likelihood tree by using the model LG+G [22] (Fig 3). We found that each *Caenorhabditis* species, except *C. brenneri*, has one CATP-5-like, one CATP-6-like and one CATP-7-like P5B ATPase. The CATP-6-like and CATP-7-like paralogs are more similar to each other than they are to the CATP-5-like paralogs, suggesting that *catp-6* and *catp-7* originated from the most recent gene duplication event. Although the genome of *Pristionchus pacificus* also codes for three paralogous P5B ATPases, these do not group with the paralogous P5B ATPases of the *Caenorhabditis* clade. The genomes of more distantly related nematodes, such as *Onchocerca flexuosa* and *Trichinella spiralis*, encode only a sole P5B ATPase.

### CATP-5 expression pattern

In previous studies, the spatiotemporal expression patterns of CATP-5 and CATP-6 were characterized by the expression of tagged proteins using extrachromosomal arrays [11,12]. In the current study, we sought to verify and extend these findings by using both extrachromosomal arrays and by tagging the endogenous loci using CRISPR/Cas9.

In order to generate a tagged version of CATP-5 for use on extrachromosomal arrays, we fused the coding sequence of *gfp* to the 3' end of the *catp-5* coding sequence, and drove expression using the putative *catp-5* promoter (4.1 kb upstream of *catp-5a.1*). Consistent with the report of Heinick et al. [11], we found that CATP-5::GFP is expressed in the intestinal cells, where it localizes to the apical brush border (Fig 4A.5), and the excretory cell, where it appears to be distributed throughout the cytosol (Fig 4A.2,3). In addition, we observed CATP-5::GFP expression in the spermatheca (localized to the apical face, see below) and amphid sensory neurons (localized to the sensilla) (Fig 4A.1).

Since the presence of a C-terminal GFP tag could potentially interfere with proper subcellular localization, we used CRISPR/Cas9-mediated recombination to tag the endogenous CATP-5 protein at the N-terminus of CATP-5a (Fig 1) [31]. We refer to the protein encoded by the tagged locus (*catp-5(dx187[gfp::catp-5 + loxP]) X*), as native GFP::CATP-5. The expression

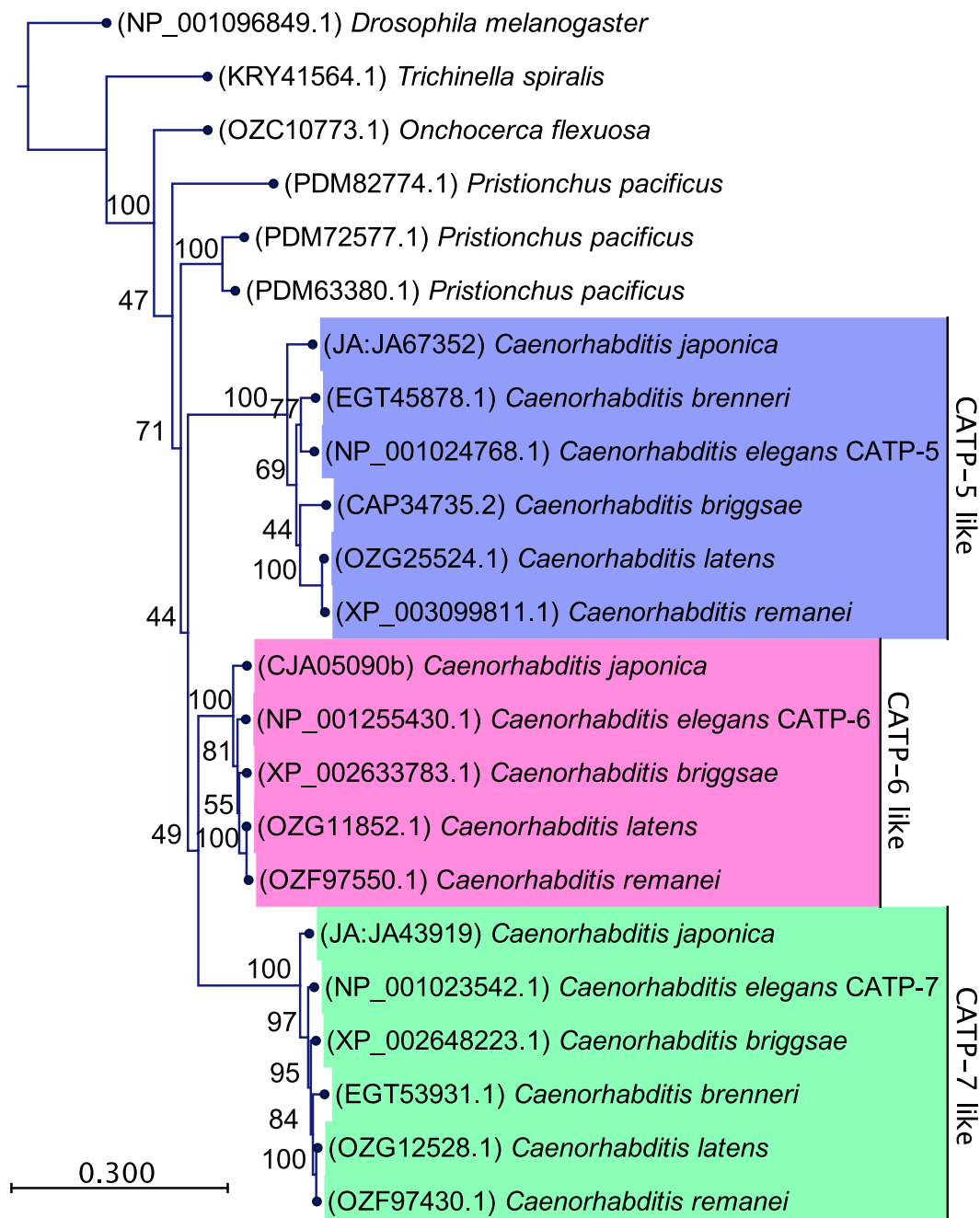


**Fig 3. Phylogenetic analysis of paralogous P5B ATPases.** Maximum Likelihood tree of 9 nematode species (including 6 *Caenorhabditis* species) and *Drosophila melanogaster* as an outgroup. Statistical model: LG+G. Bootstrap values for each node are indicated (100 replicates).

<https://doi.org/10.1371/journal.pone.0194451.g003>

pattern of native GFP::CATP-5 is nearly identical to that of CATP-5::GFP. However, we also detected expression on the plasma membrane of the distal tip cells (DTC) (Fig 4A.4) and on the plasma membrane of pachytene-stage germ cells (see below). We also generated a native



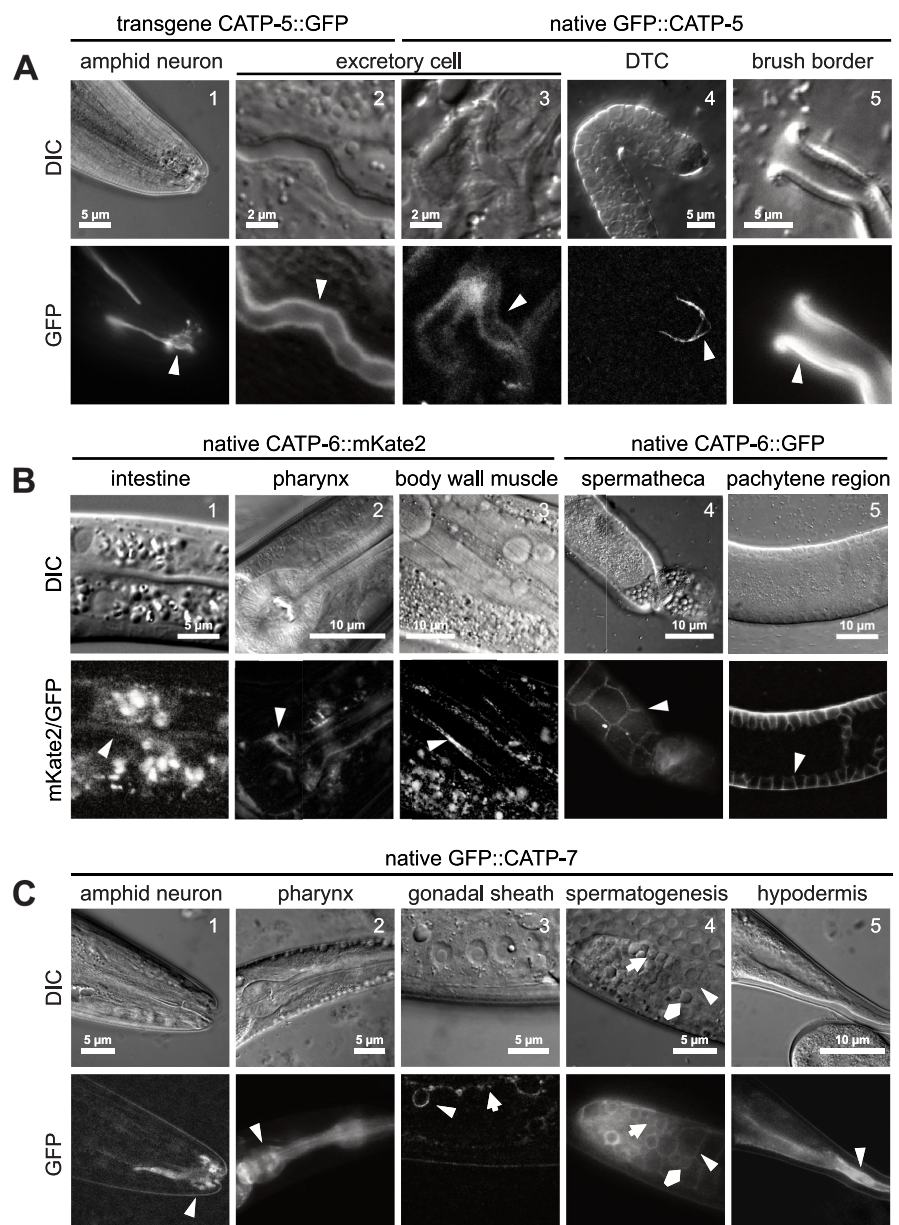


**Fig 4. Tissue-specific expression patterns of CATP-5, CATP-6 and CATP-7.** Transgene CATP-X::FP indicates expression from an extrachromosomal array. Native CATP-X::FP indicates CRISPR/Cas9 tagged endogenous locus. (A) Representative tissues in which CATP-5 is expressed. Ex [*P<sub>catp-5</sub>catp-5::gfp::rol-6(d)*] and *catp-5(dx187[gfp::catp-5 + loxP])* X. (B) Representative tissues in which CATP-6 is expressed. *catp-6(dx183[catp-6::gfp::3xFlag + loxP])* IV and *catp-6(dx179[catp-6::degtron::mKate2::3xFlag + loxP])* IV. (C) Representative tissues in which CATP-7 is expressed. *catp-7(dx185[gfp::catp-7 + loxP])* IV. Arrowheads indicate fluorescence signal (B1 and B3 GFP panels contain extensive autofluorescence signal from intestine). (C.3) Arrowhead: Sheath cell with an engulfed an apoptotic germ cell. Arrow: Sheath cell. (C.4) Arrowhead: Spermatocyte. Arrow: Spermatid. Pentagon: Residual body. (C.5) Arrowhead: Hyp10.

<https://doi.org/10.1371/journal.pone.0194451.g004>

*catp-5* allele in which *gfp* is inserted at the N-terminus of CATP-5c; however, we did not observe any GFP signal in these animals.

### CATP-6 expression pattern

To create a red fluorescent protein tagged version of CATP-6 for use on extrachromosomal arrays, we fused the coding sequence for mKate2 to the 3' end of the *catp-6* coding sequence, with expression driven by the putative *catp-6* promoter (1135 bp 5' of exon 1 of *catp-6a*). The expression pattern of this transgene was essentially identical to that of the *gfp*-modified version of fosmid WRM067B\_F08 used in our previous study [12]. However, we did observe that the signal from CATP-6::mKate was more finely resolved than that of CATP-6::GFP.

To obtain tagged native versions of CATP-6, we used CRISPR/Cas9 to produce two different tagged versions of *catp-6*, each with a fluorescent protein (FP) fused to the end of the coding sequence (Fig 1) [32]. One allele (*catp-6(dx183[catp-6::gfp::3xFlag + loxP])* IV) utilized GFP, whereas the other (*catp-6(dx179[catp-6::degron::mKate2::3xFlag + loxP])* IV) utilized mKate2 tag preceded by a degron motif [33]. (The degron segment is not functional in this genetic background). The expression patterns of the native FP-fusions are very similar to those observed using extrachromosomal transgenes. CATP-6::FP is expressed in a punctate pattern in many neurons in the head and tail, all body wall muscles, the posterior gut, the spermatheca, the DTC and the pharyngeal cells (Fig 4B and below). CATP-6::FP is also expressed in the gonadal sheath cells, where it appears to be closely associated with the plasma membrane and is not punctate (see below). Notably, native CATP-6::FP is strongly expressed in the germ line within the mitotic region, the transition zone and the pachytene region (Fig 4B.5 and below), and appears to localize to the plasma membrane.

### CATP-7 expression

To construct a tagged version of CATP-7 for use on extrachromosomal arrays, we inserted *gfp* at the 3' end of the *catp-7* coding sequence, with expression driven by the putative *catp-7* promoter (2377 bp 5' of exon1 of *catp-7a*). To tag the native locus, we inserted the coding sequence of either *gfp* or *mcherry* into the second exon of isoform *catp-7a* via CRISPR/Cas9 (*catp-7(dx185[gfp::catp-7 + loxP])* IV and *catp-7(dx191[mcherry::catp-7 + loxP])* IV), Fig 1, [31]). The expression and localization of the native N-terminal fusion GFP::CATP-7 closely resemble those of the C-terminally tagged extrachromosomal transgene. Native GFP::CATP-7 is expressed closely associated with the plasma membrane of the amphid sensory neurons (localized to the sensilla), the gonadal sheath cells, the spermatheca, the hypodermis and the excretory cell (Fig 4C and below). GFP::CATP-7 is expressed in most pharyngeal cells, where it localizes to the plasma membrane, plus internal membranous tubules (Fig 4C.2). GFP::CATP-7 is also expressed in the intestine, where it is associated with tubular structures in the basolateral domain and with vesicles in the apical domain immediately below the microvilli (see below; basolateral not shown). GFP::CATP-7 is strongly expressed in spermatocytes and spermatids (Fig 4C.4 and below). In the case of mCherry::CATP-7, we observed that the tagged protein was expressed and localized as for GFP::CATP-7, but it also accumulated in large aggregates within the cytosol (see below). This is most likely due to multimerization of mCherry, since this has been reported by others [43].

The CRISPR/Cas9-mediated single *fp*-fusion strains were not backcrossed after they were generated, but they did not show any obvious differences compared to wt N2. We estimated the average brood size for each single *gfp*-fusion strain in comparison with wt N2 (Table 1). There is no statistical difference detectable when the brood size of each CRISPR engineered strain is compared to N2. But the brood size of native *catp-6::gfp* differs from the brood size of

**Table 1. Estimated average brood size.** Mean of 3 replicates. SEM = Standard error of the mean. Group letter: Groups that share the same letter (ab) do not statistically differ from each other. Groups with different letters are significantly different from each other (a, b and c). ANOVA, Tukey post-hoc test. Adj. *p*-value threshold < 0.05.

Genotype	Mean	SEM [±]	Group letter <i>p</i> -value < 0.05
N2	317	5	ab
<i>catp-5(tm4481)</i> X	303	10	ab
<i>catp-6(ok3473)</i> IV	95	7.3	c
<i>catp-7(tm4438)</i> IV	295	9.9	ab
<i>catp-5(dx187[gfp::catp-5 + loxP])</i> X	281	10.6	b
<i>catp-6(dx183[catp-6::gfp::3xFlag + loxP])</i> IV	370	41.8	a
<i>catp-7(dx185[gfp::catp-7 + loxP])</i> IV	351	11.9	ab
<i>catp-6(dx179[catp-6::degtron::mKate2::3xFlag + loxP])</i> IV; <i>catp-5(dx187[gfp::catp-5 + loxP])</i> X	314	5.7	ab
<i>catp-6(dx179[catp-6::degtron::mKate2::3xFlag + loxP])</i> <i>catp-7(dx193[gfp::catp-7 + loxP])</i> IV	299	5.5	ab

<https://doi.org/10.1371/journal.pone.0194451.t001>

native *gfp::catp-5* (Table 1, group b and a, ANOVA, Tukey post-hoc test, adj. *p*-value = 0.02327153).

Additionally, we estimated the growth rate of the progeny (1 h layoff) from 30 worms (Table 2). 48 h after the layoff, 98–100% of the progeny of the single *fp*-fusion strain had reached the L4 stage, which is comparable to wt N2.

## P5B subcellular localization in selected tissues

**P5B expression in intestinal cells.** CATP-5 and CATP-7 are both expressed in the intestine. Native GFP::CATP-5 and transgene CATP-5::GFP localize to the apical brush border of the intestinal cells (Fig 4A, Fig 5A). Native GFP::CATP-7 and transgene CATP-7::GFP localize to small vesicles immediately beneath the apical brush border (Fig 5A). We also observed that both GFP::CATP-7 and CATP-6::GFP localize to tubular structures in the basolateral domain of the intestinal cells. In first stage larvae, native GFP::CATP-7 and native CATP-6::mKate2 localize to the apical brush border of the intestinal cells (Fig 4B, Fig 5B).

**P5B expression in the excretory cell.** CATP-7::GFP is clearly localized to the basolateral membrane of the excretory cell, since the GFP signal is not in close proximity to the lumen of

**Table 2. Estimated growth rate.** The progeny (1 h layoff) from 30 worms for each genotype were scored after 48 h according to their developmental stage. L3 = Larval stage 3. L4 = Larval stage 4. Both presented as percentage. n = Total number of scored worms. Groups that share the same letter (x) do not statistically differ from each other. Groups with different letters are significantly different from each other (x and y). Fisher's exact test. Adj. *p*-value threshold < 0.05.

Genotype	L3 [%]	L4 [%]	n	Group letter <i>p</i> -value < 0.05
N2	1	99	233	x
<i>catp-5(tm4481)</i> X	1	99	276	x
<i>catp-6(ok3473)</i> IV	38	63	40	y
<i>catp-7(tm4438)</i> IV	1	99	278	x
<i>catp-5(dx187[gfp::catp-5 + loxP])</i> X	1	99	314	x
<i>catp-6(dx183[catp-6::gfp::3xFlag + loxP])</i> IV	0	100	219	x
<i>catp-7(dx185[gfp::catp-7 + loxP])</i> IV	2	98	224	x
<i>catp-6(dx179[catp-6::degtron::mKate2::3xFlag + loxP])</i> IV; <i>catp-5(dx187[gfp::catp-5 + loxP])</i> X	1	99	283	x
<i>catp-6(dx179[catp-6::degtron::mKate2::3xFlag + loxP])</i> <i>catp-7(dx193[gfp::catp-7 + loxP])</i> IV	0	100	201	x

<https://doi.org/10.1371/journal.pone.0194451.t002>



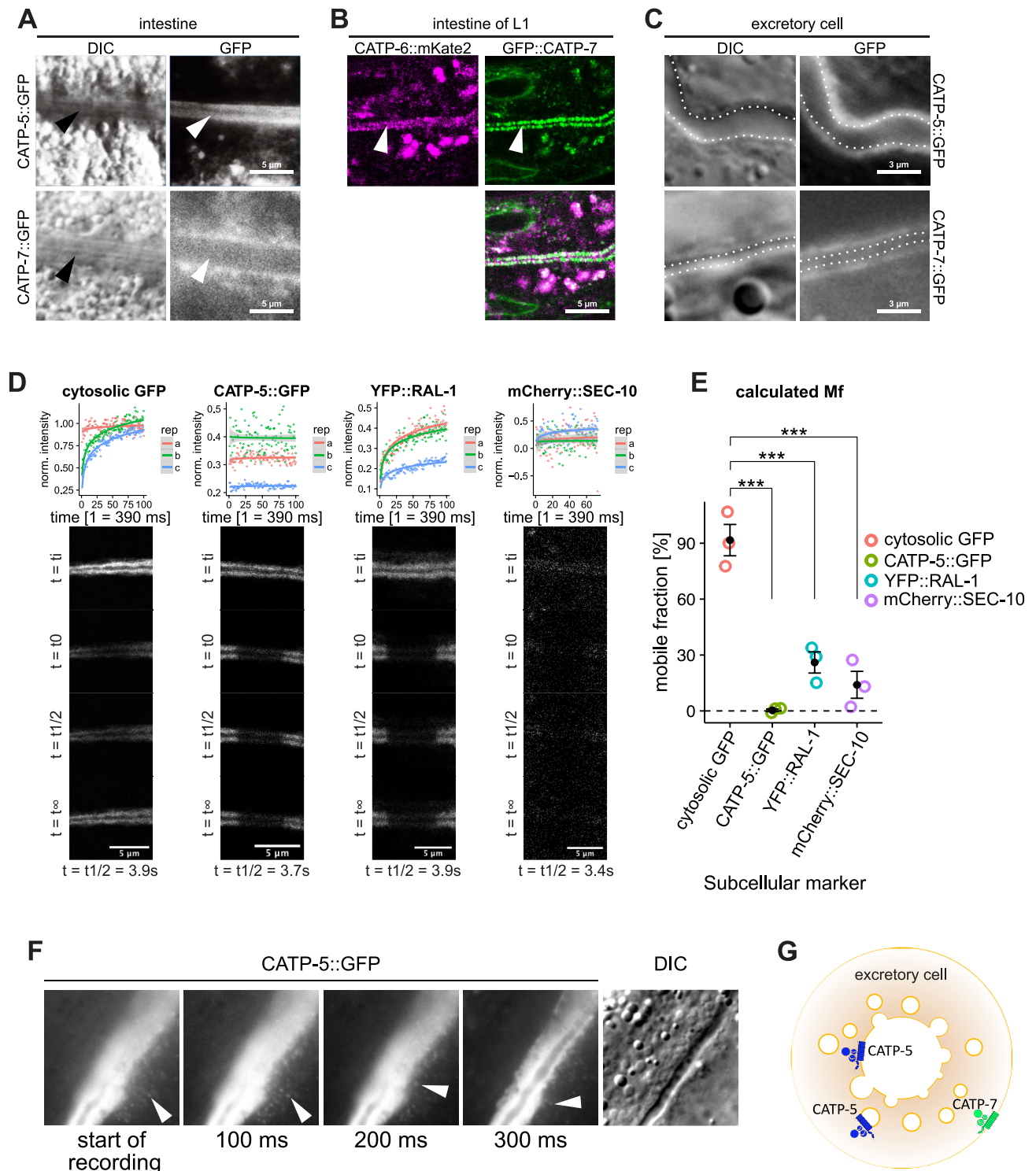


**Fig 5. P5B expression in intestinal cells and the excretory cell.** (A) Expression of transgene CATP-5::GFP vs. transgene CATP-7::GFP in intestinal cells. *Ex* [*P*<sub>catp-5</sub>*catp-5::gfp;rol-6(d)*] and *Ex* [*P*<sub>catp-7</sub>*catp-7::gfp;rol-6(d)*]. Arrowheads indicate apical brush border. (B) Expression of native CATP-6::mKate2 vs. native GFP::CATP-7 in intestinal cells of L1. *catp-6(dx183[catp-6::gfp::3xFlag + loxP])* IV and *catp-6(dx179[catp-6::degrom::mKate2::3xFlag + loxP])* IV. (C) Expression of transgene CATP-

5::GFP vs. transgene CATP-5::GFP in the excretory cell. Ex [*P<sub>catp-5</sub>catp-5::gfp;rol-6(d)*] and Ex [*P<sub>catp-7</sub>catp-7::gfp;rol-6(d)*] (D) FRAP experiment (60 s bleaching) of transgene CATP-5::GFP vs. cytosolic GFP, YFP::RAL-1 and mCherry::SEC-10. *catp-5(tm4481)*; Ex [*P<sub>pgp-12</sub>catp-5::gfp;rol-6(d)*], *bglIs312[pes-6::gfp]*, *xnIs459[yfp::ral-1a + unc-119(+)]* III and *xnIs484[mCherry::sec-10 + unc-119(+)]*. (E) Calculated mobile fraction (Mf) of FRAP experiment. ANOVA, Tukey post-hoc test, adj. *p*-value: \*\*\*  $\leq 0.001$ . (F) CATP-5::GFP positive vesicles (arrowheads) escape from ruptured excretory cell. (G) Schematic overview of CATP-5::GFP and CATP-7::GFP localization in the excretory cell.

<https://doi.org/10.1371/journal.pone.0194451.g005>

the excretory canal on DIC (Fig 5C and 5G). On the other hand, CATP-5::GFP signal appears distributed throughout the cytosol of the excretory cell. We wondered whether this localization might be an artifact due to soluble GFP derived from the transgene (e.g., via proteolytic cleavage, or cryptic promoter usage). To test this hypothesis, we performed a Fluorescence Recovery after Photobleaching (FRAP) experiment [37]. We photobleached FP-tagged proteins in the excretory cell and measured the signal-recovery over time, normalized to an unbleached area of the cell (Fig 5D). We tested CATP-5::GFP<sup>excretory</sup> specifically expressed in the excretory cell of *catp-5* mutant animals (*catp-5(tm4481)* + *P<sub>pgp-12</sub>catp-5::gfp* + *rol-6(su1006)*) and cytosolic GFP (*bglIs312[pes-6::gfp]*) [18], plus two membrane-associated controls: YFP::RAL-1 (*xnIs459[yfp::ral-1a]*, marker for cytosolic vesicles) and mCherry::SEC-10 (*xnIs484[mCherry::sec-10]*, marker for the luminal membrane [15]). To quantitate mobility, we calculated the mobile fraction (Mf) of each FP-fusion (Fig 5E).

As expected, cytosolic GFP shows a calculated Mf of 92% (Fig 5E). Whereas CATP-5::GFP<sup>excretory</sup> displays a Mf of only 0.33%, which is highly significantly different from cytosolic GFP (ANOVA, Tukey post-hoc test, adj. *p*-value = 0.0000307). Thus, it is very unlikely that the signal we observe is coming from cytosolic GFP in the excretory cell for transgene *catp-5::gfp<sup>excretory</sup>*.

The cytosolic vesicle-associated control YFP::RAL1 shows a Mf of 26% and the luminal membrane control SEC10::mCherry shows a Mf of 14%. Both Mf values are significantly different from the Mf value of cytosolic GFP (Fig 5E, ANOVA, Tukey post-hoc test, adj. *p*-value = 0.0003369 and adj. *p*-value = 0.0001015 respectively). But there is no statistical differences detectable between the Mfs of: CATP-5::GFP<sup>excretory</sup> vs. YFP::RAL1, CATP-5::GFP<sup>excretory</sup> vs. mCherry::SEC-10 nor YFP::RAL1 vs. mCherry::SEC-10.

During one imaging experiment, we serendipitously ruptured the basolateral membrane of the excretory cell and could thus observe consequences of cytoplasmic leakage into the extracellular fluid. In this case, we observed that CATP-5::GFP escaped from the cell in the form of small GFP-positive punctae, consistent with vesicular localization (Fig 5F). In addition, as cytosolic signal became depleted, it became possible to see that some of the CATP-5::GFP was tightly associated with the luminal membrane. We were able to reproduce the observation of persistent luminal association of CATP-5::GFP in two other experiments in which we used pressure on the coverglass to rupture the worm and sever the excretory canal.

**Subcellular localization of CATP-6 in neurons and pharynx.** In order to determine the subcellular compartment to which CATP-6 localizes, we imaged CATP-6::FP in relation to various compartment markers in head neurons via confocal microscopy.

When we expressed the lysosomal marker, LMP-1::RFP in neurons using the *rgs-1* promoter, we found strong colocalization with CATP-6::GFP. However, LMP-1::RFP and CATP-6::GFP both localized to the plasma membrane in these cells (Fig 6A). Evidently, overexpression of LMP-1 and/or the presence of the C-terminal RFP tag leads to inappropriate localization of both LMP-1 and CATP-6. As an alternative approach, we performed immunocytochemistry by staining for native CATP-6::GFP (anti-GFP) and endogenous LMP-1 (anti-LMP-1, Fig 6B and 6C). With this method, we did not observe strong colocalization of LMP-1 and CATP-6::GFP, either within neurons or in pharyngeal cells (Fig 6B and 6C).

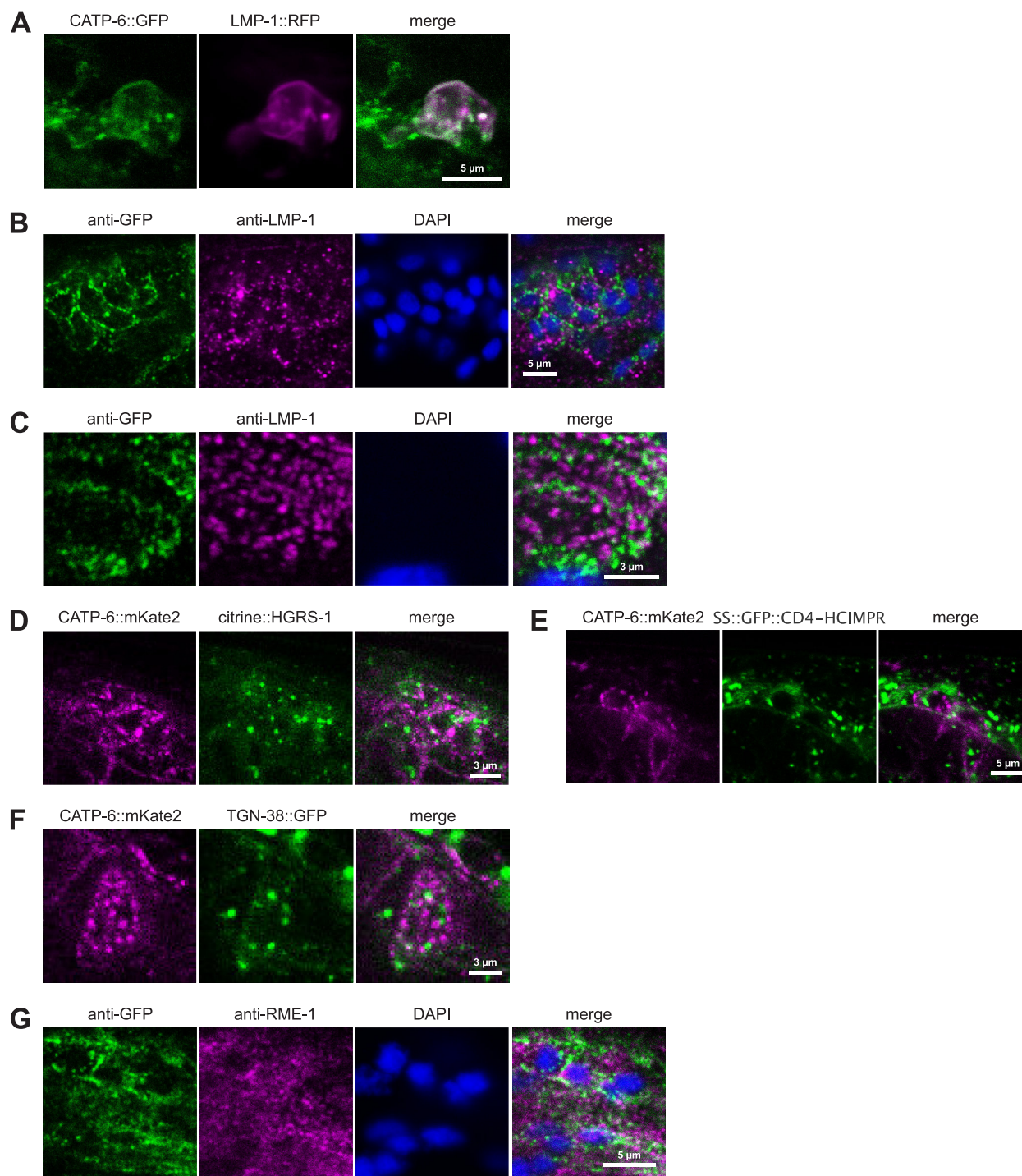


**Fig 6. Subcellular localization of CATP-6 in neurons and pharynx.** (A) Co-localization of native CATP-6::GFP vs. LMP-1::RFP in living neurons. *catp-6(dx183[catp-6::gfp::3xHag + loxP])* IV, *Ex [P<sub>catp-6</sub>catp-6::gfp::P<sub>th-1</sub>lmp-1::rfp::rol-6(d)]*. (B-C) Immunostaining of native CATP-6::GFP vs. native LMP-1 in neurons and pharyngeal bulb. *catp-6(dx183[catp-6::gfp::3xFlag + loxP])* IV. (D-F) Co-localization of native CATP-6::mKate2 vs. citrine::HGRS1, SS::GFP::CD4-HCIMP, and TGN-38::GFP in living neurons. *catp-6(dx179[catp-6::degron::mKate2::3xFlag + loxP])* IV, *pwIS1039[p<sub>snx-1</sub>citrine::hgrs-1<sub>unc-54</sub> UTR-cb-unc-119]*, *pwIS1176[p<sub>snx-1</sub>ss::gfp-cd4-hcimp<sub>unc-54</sub> UTR-cb-unc-119]*; *unc-119(ed3)* and *pwIS1175[p<sub>snx-1</sub>lgn-38::gfp<sub>unc-54</sub> UTR-cb-unc-119]*; *unc-119(ed3)*. (G) Immunostaining of native CATP-6::GFP vs. native RME-1 in neurons. *catp-6(dx183[catp-6::gfp::3xFlag + loxP])* IV.

<https://doi.org/10.1371/journal.pone.0194451.g006>



We used transgenic strains generated by Norris et al. [19] to test whether CATP-6::FP colocalizes with either of two endosomal markers, citrine::HGRS-1 or SS::GFP::CD4-HCIMPR. Although each of these markers exhibits a punctate subcellular localization pattern, they are clearly distinct from CATP-6::mKate2 (Fig 6D and 6E). We also examined the trans-Golgi marker, TGN-38::GFP [19], and found that although it does exhibit a punctate subcellular localization, this is also distinct from CATP-6::mKate2 (Fig 6F).

As a marker for recycling endosomes we used immunostaining to assess colocalization of native CATP-6::GFP and RME-1 in neurons (Fig 6G). Again, although the pattern of RME-1 appears punctate, it is largely distinct from that of CATP-6::GFP.

**Subcellular localization of CATP-6 in the spermatheca.** In the spermathecal epithelial cells, CATP-6::FP localizes to cytoplasmic punctae that probably correspond to membranous vesicles near the basolateral plasma membrane. We analyzed native CATP-6::GFP in combination with transgene CATP-6::GFP (*gfp* modified fosmid WRM067B\_F08 to increase GFP signal) in relation to RFP-labeled compartment markers expressed in the spermatheca (using the *sth-1* promoter [26]).

In living spermathecal cells, CATP-6::GFP strongly colocalizes with LMP-1::RFP expressed from a transgene (Fig 7A). However, the CATP-6::GFP positive vesicles are much larger than usual, so we suspected that the colocalization might be an artifact. Therefore, we used immunostaining to assess colocalization of native CATP-6::GFP and LMP-1 within the spermatheca (Fig 7B). In these preparations, the LMP-1 and CATP-6::GFP localization patterns are clearly different. LMP-1 is not associated with the basolateral cell membranes and the CATP-6 positive vesicles are relatively normal in size and shape.

In the case of RFP::RAB-5 we observed overlap with CATP-6::GFP in proximity to the plasma membrane of basolateral cell-cell junctions. This is consistent with the expected localization of RAB-5 to early endosomes (Fig 7C). The localization pattern of RFP::RAB-11 (expected to label recycling endosomes), is largely distinct from that of CATP-6::GFP (Fig 7D). We used immunostaining to assess colocalization of native CATP-6::GFP and RME-1 as a second marker for recycling endosomes within the spermatheca (Fig 7E). Again, the pattern of RME-1 is largely distinct from that of CATP-6::GFP.

## Overlapping expression patterns in developing reproductive tissues

All three paralogous P5B ATPases are expressed in the spermathecal epithelial cells. In order to directly compare their localization patterns, we constructed strains in which different pairs of proteins are tagged. Since the *catp-6* and *catp-7* loci are very tightly linked on chromosome IV, it was not possible to obtain a homozygous double-labeled strain by meiotic recombination. Therefore, we used CRISPR/Cas9 to generate a strain that expresses both native CATP-6::mKate2 and native GFP::CATP-7. The strain was not backcrossed but did not show any obvious difference compared to wt N2. We estimated the average brood size of this strain (Table 1) plus the growth rate of the progeny (1 h layoff) (Table 2) and did not observe any difference compared to wt N2. In double-tagged animals, it is clear that the localization patterns of the two proteins within the spermathecal cells are distinct: CATP-6::mKate2 localizes to punctae in the basolateral domain, whereas GFP::CATP-7 localizes to the lateral and luminal cell borders, as well as to spermatids (Fig 8A).

By intercrossing, we obtained a strain that expresses both native CATP-6::mKate2 and native GFP::CATP-5 (Fig 8C). This double-tagged strain did not differ from wt N2 in terms of brood size or growth rate (Table 1, Table 2). Native GFP::CATP-5 is expressed in a pattern qualitatively similar to that of native GFP::CATP-7, localizing to the apical lateral and luminal borders of the spermatheca (compare Fig 8A to Fig 8C), but GFP::CATP-5 is not detectable in

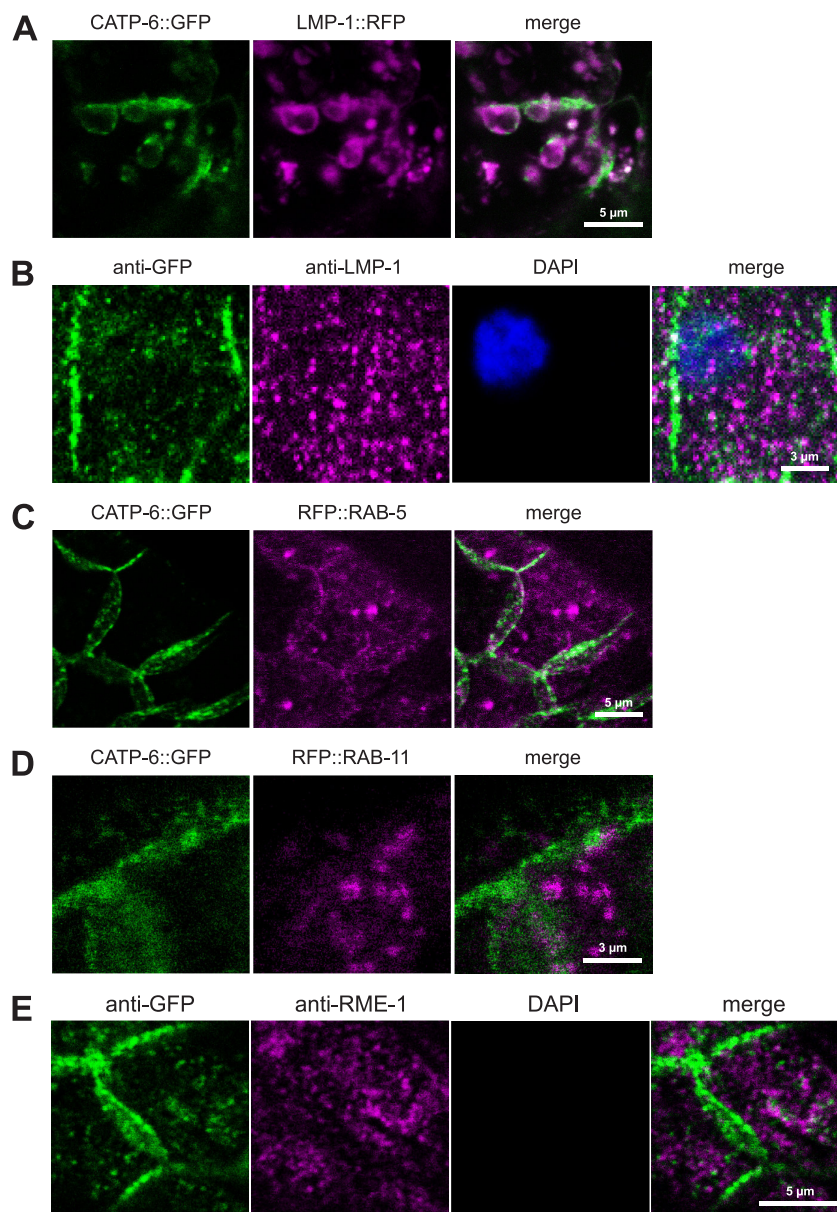


**Fig 7. Subcellular localization of CATP-6 in the spermatheca.** (A) Co-localization of native CATP-6::GFP vs. LMP-1::RFP in living spermatheca. *catp-6(dx183[catp-6::gfp::3xFlag + loxP]) IV, Ex [P<sub>catp-6</sub>catp-6::gfp;P<sub>sth-1</sub>lmp-1::rfp;rol-6(d)]*. (B) Immunostaining of native CATP-6::GFP vs. native LMP-1 in the spermatheca. *catp-6(dx183[catp-6::gfp::3xFlag + loxP]) IV*. (C-D) Co-localization of native CATP-6::GFP vs. RFP::RAB-5 and RFP::RAB-11 in living spermatheca. *catp-6(dx183[catp-6::gfp::3xFlag + loxP]) IV, Ex [P<sub>catp-6</sub>catp-6::gfp;P<sub>sth-1</sub>rfp::rab-5;rol-6(d)]* or *Ex [P<sub>catp-6</sub>catp-6::gfp;P<sub>sth-1</sub>rfp::rab-11;rol-6(d)]*. (E) Immunostaining of native CATP-6::GFP vs. native RME-1 in the spermatheca. *catp-6(dx183[catp-6::gfp::3xFlag + loxP]) IV*.

<https://doi.org/10.1371/journal.pone.0194451.g007>

spermatids. We obtained a strain that expresses both native mCherry::CATP-7 and native GFP::CATP-5 via crossing of the single *fp*-tagged strains (Fig 8B). Membrane-associated mCherry::CATP-7 signal localizes to the same lateral and luminal borders as GFP::CATP-5,

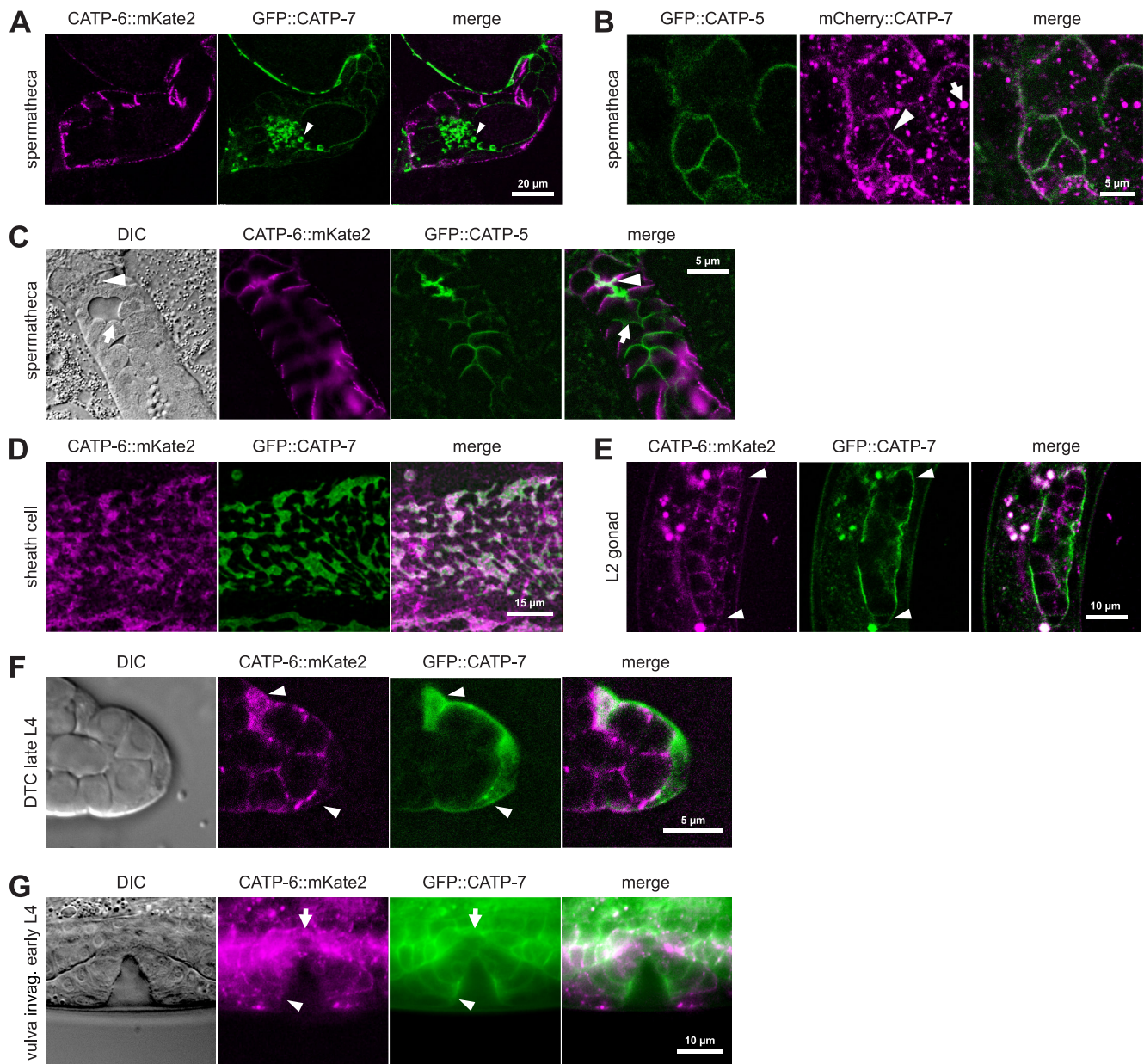


**Fig 8. Overlapping expression patterns in developing reproductive tissues.** (A) Native CATP-6::mKate2 vs. native GFP::CATP-7 in living spermatheca. *catp-6(dx179[catp-6::degtron::mKate2::3xFlag + loxP]) catp-7(dx193[gfp::catp-7 + loxP])* IV. (B) Native GFP::CATP-5 vs. native mCherry::CATP-7 in living spermatheca. *catp-7(dx191[mcherry::catp-7 + loxP])* IV; *catp-5(dx187[gfp::catp-5 + loxP])* X. Arrowhead: Membrane bound mCherry signal. Arrow: mCherry aggregates. (C) Native CATP-6::mKate2 vs. native GFP::CATP-5 in living spermatheca. *catp-6(dx179[catp-6::degtron::mKate2::3xFlag + loxP])* IV; *catp-5(dx187[gfp::catp-5 + loxP])* X. Arrowhead: Apical luminal membrane. Arrow: Apical lateral borders. (D-G) Native CATP-6::mKate2 vs. native GFP::CATP-7 in living sheath cell (adult) and developing gonad (L2), DTC (late L4) and vulva morphogenesis (early L4). *catp-6(dx179[catp-6::degtron::mKate2::3xFlag + loxP]) catp-7(dx193[gfp::catp-7 + loxP])* IV. Arrowheads: (E and F): DTCs. Note: the DTCs extend long processes to cover nearby germ cells, even in early larvae (G): Colocalization of CATP-6::mKate2 and GFP in central somatic gonad (arrowhead).

<https://doi.org/10.1371/journal.pone.0194451.g008>

confirming that both CATP-5 and CATP-7 localize to the same subcellular compartment in the spermatheca (Fig 8B).



In the gonadal sheath cells, native GFP::CATP-7 localizes to large, raft-like patches on the plasma membrane, where it colocalizes with native CATP-6::mKate2 (Fig 8D). Moreover, we observe areas of the sheath cell that are positive for native CATP-6::mKate2, but not for native GFP::CATP-7 (Fig 8D). In favorable cross-section images, we were able to observe that native GFP::CATP-7 and native CATP-6::mKate2 are present on both the outer (pseudocoelom-facing) inner (germline-facing) plasma membrane surfaces of the sheath cell (see below).

Native GFP::CATP-7, as well as CATP-6::mKate2 are expressed in the DTCs of early stage gonads (L2, Fig 8E). CATP-6::mKate2 is also expressed in larval germ cells, exhibiting a punctate localization pattern, consistent with endosomal localization. Native GFP::CATP-7 and native CATP-6::mKate2 are also both expressed in the DTCs of L4 animals, although the CATP-6 expression is comparatively weak (Fig 8F). As in other tissues, GFP::CATP-7 and GFP::CATP-5 localization to the plasma membrane appears fairly smooth/continuous, whereas CATP-6::mKate2 appears punctate, consistent with endosomal localization (Fig 4A.4, Fig 8E and 8F).

In addition to somatic gonad cells, native GFP::CATP-7 and CATP-6::mKate2 are both strongly expressed in the developing vulva (Fig 8G). Again, GFP::CATP-7 appears continuously associated with the plasma membrane, whereas CATP-6::mKate2 localization is punctate.

### Overlapping expression in the germ line

Native CATP-6::FP is strongly expressed in the adult germ line, and colocalizes with the plasma membrane marker *ltIs44(P<sub>pie-1</sub>mCherry::ph<sup>PLCδ</sup>)* within the mitotic, transition, and pachytene regions (Fig 9B). CATP-6::mKate2 is also associated with the plasma membrane of diakinesis-stage oocytes (Fig 9F). In L4 stage hermaphrodites, CATP-6::mKate2 localizes to vesicles in the rachis between the spermatocytes during spermatogenesis (Fig 9A and 9C). We also detect a weak cytoplasmic signal for CATP-6::mKate2 in spermatids (Fig 9E). Native GFP::CATP-7 is not expressed in the mitotic, transition or pachytene regions of the adult hermaphrodite germ line; however, it is strongly associated with the plasma membrane of spermatocytes and residual bodies in L4 larvae and young adults (Fig 9A and 9C, Fig 4C.4). In spermatids, GFP-CATP-7 localizes to punctae that probably correspond to fibrous body-membranous organelles (FB-MOs [44], Fig 9E). Native GFP::CATP-5 is expressed very weakly in the mitotic, transition and pachytene region of the germ line and also localizes to the plasma membrane (Fig 9D).

### Phenotypic analysis of single, double and triple null mutants

All three paralogous P5B ATPases are strongly expressed in the germ line and the somatic gonadal tissues (Fig 10A). Since the gonadal sheath cells and distal tip cell are known to be physiologically coupled to the germ line ([45,46], Fig 10A and 10B), we considered it likely that the P5Bs would have essential functions during gonad development and germline proliferation. To test this hypothesis, we obtained and/or generated single, double and triple null mutant strains for *catp-5*, *catp-6* and *catp-7*.

The single null mutants are all homozygous viable and fertile. *catp-5(tm4481)* is a 705 bp deletion that removes the coding sequences for 235 aa of M3 and M4 including the putative substrate binding site, the phosphorylation site (P domain) within the large intracellular loop, plus half of the N domain and also results in a frameshift (Fig 1). *catp-5(0)* animals have an overtly wt phenotype, as expected [11], with brood size and growth rate similar to those of wt N2 (Table 1, Table 2).

*catp-6(ok3473)* is a deletion of 934 bp that removes the coding sequences for 281 aa of M5, M6 and M7, including half of the P domain and one Mg<sup>2+</sup> coordination motive (GDGAND),

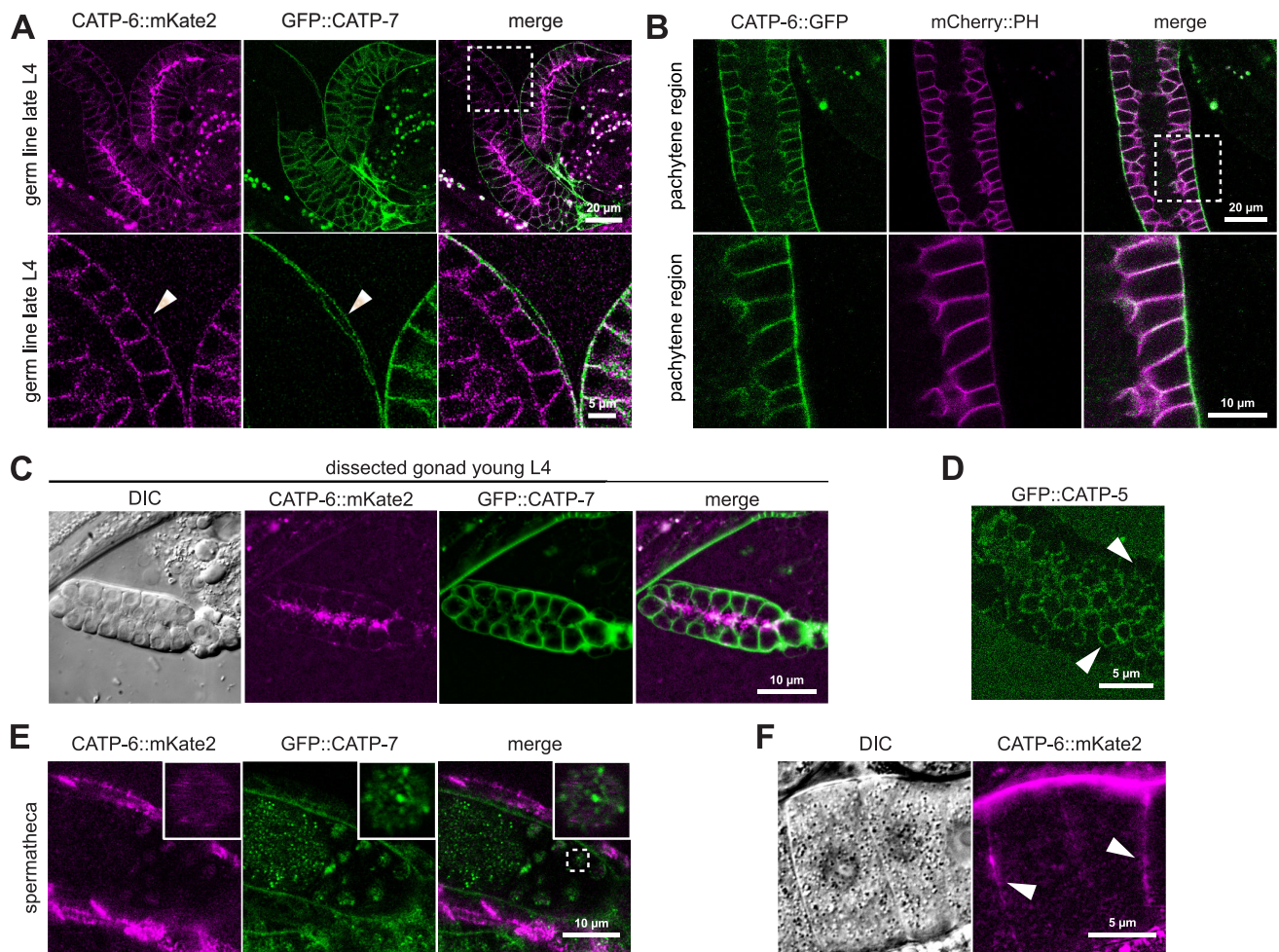


**Fig 9. Overlapping expression in the germ line.** (A, C and E) Native CATP-6::mKate2 vs. native GFP::CATP-7 in germ line during spermatogenesis (L4, A and C) and in spermatheca of young adults (E). *catp-6(dx179[catp-6::degtron::mKate2::3xFlag + loxP]) catp-7(dx193[gfp::catp-7 + loxP])* IV. (B) Co-localization of native CATP-6 vs. mCherry PH. *catp-6(dx183[catp-6::gfp::3xFlag + loxP]) IV; ltl44(P<sub>pie-1</sub>,mCherry::ph<sup>PLCδ</sup>)* V. (D) Native GFP::CATP-5 in pachytene region of adults. *catp-5(dx187[gfp::catp-5 + loxP])* X. (F) Native CATP-6::mKate2 localizes to the plasma membrane of diakinesis stage oocytes (arrowhead); cytoplasmic signal is autofluorescence. *catp-6(dx179[catp-6::degtron::mKate2::3xFlag + loxP])*.

<https://doi.org/10.1371/journal.pone.0194451.g009>

followed by a frameshift (Fig 1). *catp-6(0)* mutants are Egl (egg-laying defective), Unc (uncoordinated; sluggish) and Gro (slow growth). *catp-6(0)* mutants present a highly significant smaller brood size when compared to N2 (Table 1, group c, ANOVA, Tukey post-hoc test, adj. *p*-value = 0.000000416). Only 63% of the progeny of *catp-6(0)* animals reached L4 stage after 48 h, which is highly significant different to wt N2 (Table 2, group y, Fisher's exact test, adj. *p*-value = 0.0000000000705).

*catp-7(tm4438)* is a deletion of 1222 bp (plus 6 bp insertion) that removes the coding sequence for 384 aa and therefore most of the large cytoplasmic loop between the N domain (ATP binding site) and the P domain (Mg<sup>2+</sup> coordination motive TGDN), but does not result in a frame shift (Fig 1). *catp-7(0)* single mutants are overtly wt, with brood size and growth rate the same as wt N2 (Table 1, Table 2).



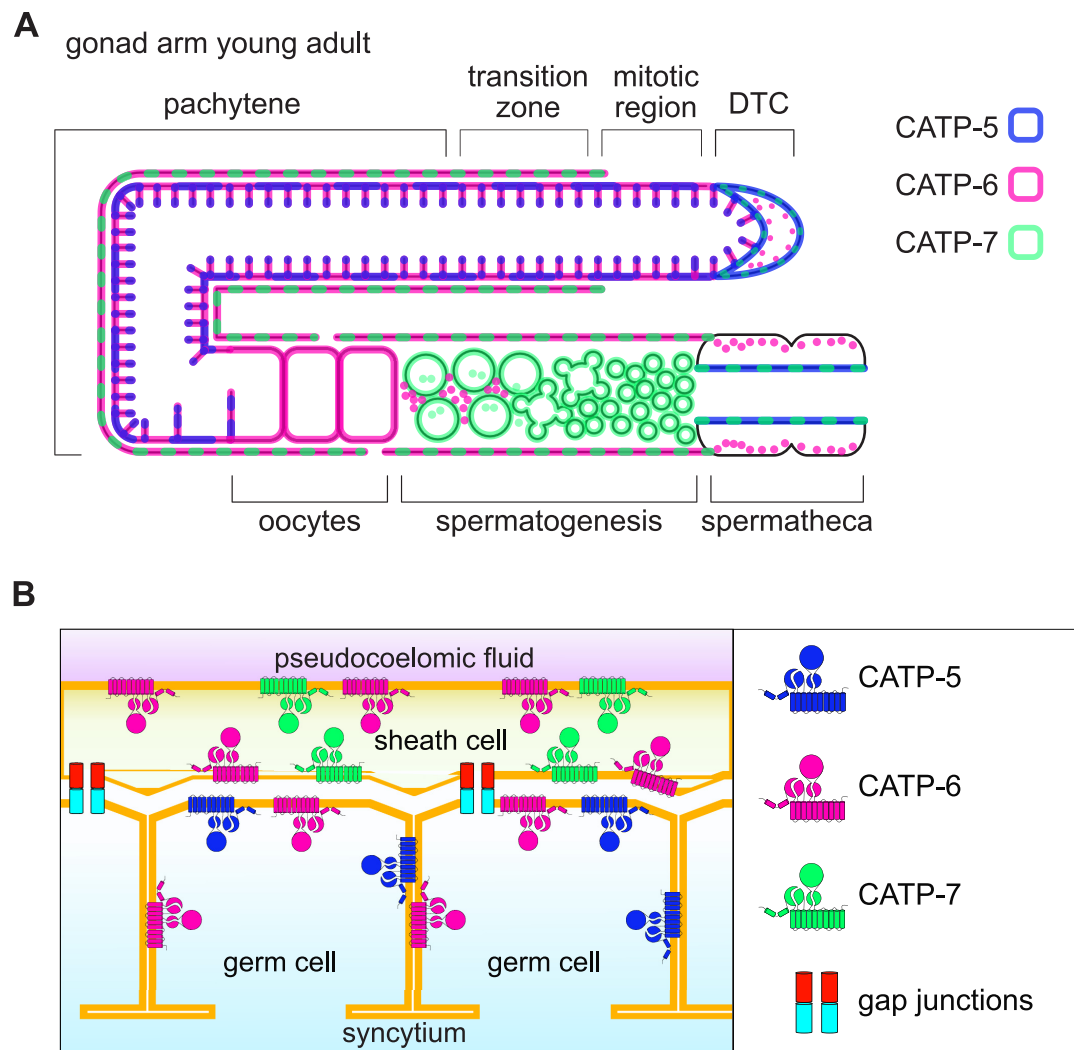


**Fig 10. Schematic overview of P5B ATPase expression in somatic gonad and germ line.** (A) CATP-5, CATP-6 and CATP-7 expression in somatic gonad and germ line in a young adult hermaphrodite. Most of the ovary is contiguously covered by somatic sheath cells; however, there this coverage ceases prior to the distal tip cell. In addition, the proximal sheath cells are perforated by "sheath pores" 100–200 nm in diameter, allowing contact between oocytes that have pinched off the syncytium and the pseudocoelomic fluid [46]. Dashed lines: 2 paralogs expressed in the same subcellular compartment. (B) Schematic of P5B localization in the distal oviduct (pachytene) region of the gonad.

<https://doi.org/10.1371/journal.pone.0194451.g010>

*catp-7(0); catp-5(0)* double mutants appear very similar to wild type. Mid L4, young adults and 1 day old adults do not have any obvious phenotype in terms of somatic gonad development or germline proliferation.

*catp-6(0); catp-5(0)* double mutants are nearly completely sterile (Ste). Therefore, these worms were obtained from a balanced strain heterozygous for *catp-6(0)* (*catp-6(ok3473)/nT1[qIs51]* (IV;V); *catp-5(tm4481)*). Among the double mutant progeny obtained from this strain, we found that most (Fig 11E, 92%; n = 153) were sterile; these animals acquired a Pvl phenotype (Protruding vulva) as they aged (Fig 11A and 11E). The remaining fraction (8%) of the double mutants were fertile (Fig 11E) and appeared essentially wild type. However, nearly all of the progeny of these worms (99% (n = 112) were sterile (Fig 11E). Since the sterile

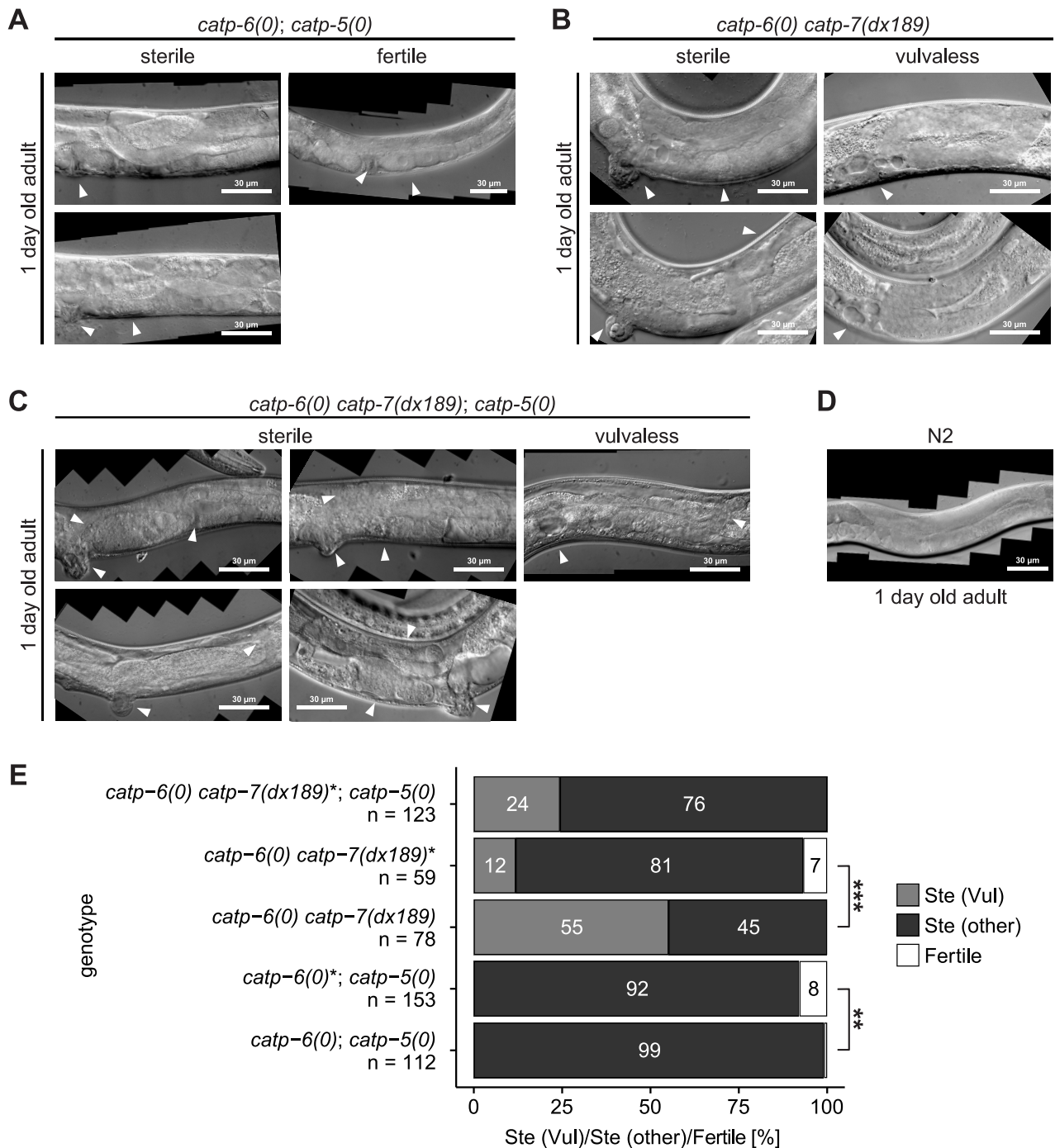


**Fig 11. Phenotypic analysis of single, double and triple null mutants.** (A-C) 1 day old adult gonad of: *catp-6(0); catp-5(0)* double mutants (*catp-6(ok3473)* IV; *catp-5(tm4481)* X), *catp-6(0) catp-7(dx189)* double mutants (*catp-6(ok3473) catp-7(dx189[delta 1492 bp Ma-M3 + gfp + loxP]* IV) and *catp-6(0) catp-7(dx189); catp-5(0)* triple mutants (*catp-6(ok3473) catp-7(dx189[delta 1492 bp Ma-M3 + gfp + loxP]* IV; *catp-5(tm4481)* X). (D) 1 day old adult gonad of wt N2. (E) Quantification of phenotypic segregants. (Ste (Vul)): Sterile Vulvaless; Ste (other): Sterile Evl, Pvl or Muv. Fertile: Able to produce progeny (normal vulva). Asterisk indicates that animals were obtained from a hermaphrodite heterozygous for the mutant chromosome. Fisher's exact test and subsequent Holm's correction for multiple comparison, adj. *p*-value: \*\*  $\leq 0.01$ , \*\*\*  $\leq 0.001$ .

<https://doi.org/10.1371/journal.pone.0194451.g011>

phenotype is more severe when the progeny are derived from a hermaphrodite homozygous for *catp-6(0)*, this suggests that *catp-6(+)* probably provides maternal rescue (Fisher's exact test, adj. *p*-value = 0.00896; paternal rescue is also possible, but this is less likely). Young adult *catp-6(0); catp-5(0)* animals have a fully developed gonad, but the number of germ cells is smaller than in wild type (S1 Fig). These animals possessed both sperm and oocytes at this stage (S1 Fig). Mid to late L4-stage *catp-6(0); catp-5(0)* animals showed no obvious phenotype in terms of DTC migration (S1 Fig).

As one-day-old adults, *catp-6(0); catp-5(0)* animals are obviously different from wt N2. The DTCs inappropriately continue to migrate, leading to abnormal gonad arm positions (Fig 11A). Although pachytene exit was not blocked, the growth of late stage oocytes was impaired and, unlike wild type worms, the first ovulation had not yet taken place (Fig 11A). A small fraction of the *catp-6(0); catp-5(0)* animals are fertile (1%), but these have a greatly reduced brood size, ranging from 1 to 19 progeny (Fig 11A and 11E).

*catp-6* and *catp-7* are separated by only 0.52 cM on chromosome IV, and we were not successful in obtaining the *catp-6(0) catp-7(0)* double mutant by meiotic recombination. Therefore, we used CRISPR/Cas9 to generate a null allele of *catp-7* in the background of *catp-6(0)*. We exchanged 1492 bp between exon 2 and exon 5 of isoform *catp-7a* with the coding sequence of *gfp*. The deletion removes the coding sequences for Ma to M3, the A domain (dephosphorylation motif TGE) and results in a subsequent frameshift (*catp-7(dx189)*, Fig 1). Therefore, *catp-7(dx189)* is not able to encode a functional transporter protein. Since we found that *catp-6(0) catp-7(dx189)* animals are usually sterile (Ste); the double mutant chromosome was maintained over a balancer (*catp-6(ok3473) catp-7(dx189)/ nT1[qIs51]* (IV;V)).

Homozygous *catp-6(0) catp-7(dx189)* worms that are derived from a heterozygous hermaphrodite display a high fraction of sterility (81% *n* = 59). These animals also typically exhibit abnormal vulva phenotypes, including Pvl, Evl (everted vulva) and Muv (Multivulva). Furthermore, 12% (*n* = 59) of *catp-6(0) catp-7(dx189)* were Vul (vulvaless). Homozygous *catp-6(0) catp-7(dx189)* worms derived from a homozygous hermaphrodite, are more severely affected: 55% (*n* = 78) are Vul (Ste (Vul)) and 100% (*n* = 78) are sterile (Ste (other), Fig 11E). This suggests that *catp-6(+)* and/or *catp-7(+)* probably confer maternal rescue of these gonadal defects (Fisher's exact test, adj. *p*-value = 0.000000108).

Mid to late L4 *catp-6(0) catp-7(dx189)* worms exhibit a delay in DTC migration when compared to wt L4 of the same stage (S2 Fig), probably due to reduced germline proliferation. Young adult *catp-6(0) catp-7(dx189)* animals often show a fully reflexed gonad (S2 Fig). However, in contrast to wild type, no gametogenesis has yet taken place in the proximal arm (S2 Fig). Roughly half of analyzed gonads exhibit a DTC migration defect by omitting the second turn towards the midsection (S2 Fig and Fig 11B). 1 day old adult *catp-6(0) catp-7(dx189)* worms have often completed spermatogenesis, but oogenesis and ovulation are typically delayed (Fig 11B). The overall number of germ cells is usually much smaller than in wild type, suggesting a defect in germline proliferation.

We used DAPI staining of extruded gonads to determine whether gonadal sheath cells were still present in animals with defective germline proliferation. We were not able to unambiguously determine the exact number of sheath cell nuclei per gonad arm; however, we consistently observed multiple sheath cell nuclei (S3 Fig), thus indicating that the mutant phenotype does not result from a complete absence of gonadal sheath cells.

We obtained animals of genotype *catp-6(0) catp-7(dx189); catp-5(0)* from hermaphrodites of genotype *catp-6(ok3473) catp-7(dx189)/ nT1[qIs51]* (IV;V); *catp-5(tm4481)*. All of the *catp-6(0) catp-7(dx189); catp-5(0)* animals produced by this strain were sterile. Furthermore, 76% (*n* = 123) had an abnormal vulva phenotype—everted, protruding, or multivulva (Ste (other)) and 24% (*n* = 123) were Vul (Ste (Vul), Fig 11E and 11C).

Mid to late L4 *catp-6(0) catp-7(dx189); catp-5(0)* animals showed a strong delay in DTC migration when compared to wt from the same stage (S4 Fig). The number of germ cells is severely diminished, suggestive of a proliferation defect (S4 Fig).

Among 1 day old adult triple mutants, some were able to produce both sperm and oocytes, but the oocytes were relatively small and abnormal in appearance. These animals also occasionally exhibited abnormal distal germline proliferation (Fig 11C), and some also had proximal germline proliferation. Most of the animals displayed severe defects in DTC migration with multiple inappropriate turns and perpetual DTC migration. Vul animals often had a large cavity in the midsection, consistent with the formation of at least a partial uterus in the absence of a vulva (Fig 11C).

## Summary and discussion

### Spatial and temporal expression patterns

We find that the *C. elegans* P5B ATPases are expressed in a wide range of tissues. Within these tissues, they exhibit both dynamic and overlapping expression patterns. These are summarized in Table 3 and Fig 10A. Depending upon context, each of the P5Bs may localize either to internal membranous structures or to the plasma membrane. However, each protein has distinct targeting signals, e.g., CATP-5 and CATP-7 both localize to the apical plasma membrane in spermathecal epithelial cells, but in the excretory cell CATP-7 is on the basolateral plasma membrane, whereas CATP-5 localizes to vesicles and the apical/luminal membrane.

### Overlapping functions in reproductive tissues

Each of the single mutants, *catp-5(0)*, *catp-6(0)* and *catp-7(0)* is viable and fertile. However, we observed distinct synthetic sterile phenotypes in the *catp-6(0); catp-5(0)* and *catp-6(0) catp-7*

Table 3. Summary of expression and localization of nematode P5Bs.

	CATP-5	CATP-6	CATP-7
Intestine (L1)	Apical brush border plasma membrane	Apical brush border plasma membrane	Apical brush border plasma membrane
Intestine (adults)	Apical brush border plasma membrane	Basolateral and subapical tubular/vesicular	Basolateral and subapical tubular/vesicular
Pharyngeal muscle	Not detectable	Cortical vesicles	Plasma membrane. T-tubules(?)
Neurons	Apical plasma membrane (amphids)	Cortical vesicles	Apical plasma membrane (amphids)
Germ line (adults)	Plasma membrane in hermaphrodite distal and pachytene regions	Plasma membrane in hermaphrodite distal and pachytene regions	Not detectable
Germ line (spermatogenesis)	Not detectable	Vesicular in spermatocytes. Cytoplasmic in spermatids.	Plasma membrane in spermatocytes. FB-MOs in spermatids.
DTC	Plasma membrane	Cortical vesicles	Plasma membrane and vesicles
Developing vulva (L4)	Not detectable	Cortical vesicles	Plasma membrane
Central somatic gonad (early L4)	Not detectable	Cortical vesicles	Plasma membrane
Spermatheca	Apical plasma membrane	Basolateral cortical vesicles.	Apical plasma membrane
Z1 and Z4	Not detectable	Cortical vesicles	Plasma membrane and vesicles
Excretory cell (larvae and adults)	Vesicular, luminal membrane	Not detectable	Basolateral plasma membrane
Hypodermis (adults)	Not detectable	Not detectable	Plasma membrane
Gonadal sheath (adults)	Not detectable	Plasma membrane rafts and between rafts	Plasma membrane rafts

<https://doi.org/10.1371/journal.pone.0194451.t003>

(*dx189*) double mutants. We do not observe any mutant phenotypes in the CRISPR/Cas9 tagged strains (*catp-6::mKate2* IV, *gfp::catp-5* X, or *catp-6::mKate2 gfp::catp-7* IV double mutants (Table 1, Table 2)), therefore we conclude that the *fp*-tagged alleles are functional.

*catp-6(0); catp-5(0)* double mutants, have nearly normal somatic gonad development, but exhibit delayed germline proliferation and have very small brood sizes. Since both CATP-5 and CATP-6 are present on the plasma membrane of pachytene-stage germ cells, the simplest interpretation is that these two proteins function redundantly within this tissue to take up a common substrate from the extracellular fluid. However, CATP-6 is also expressed on the plasma membrane of the gonadal sheath cells, which are physiologically connected to the pachytene-stage germ line via numerous gap junctions [45]. Thus, the germ line should be able to obtain P5B transport substrates either by direct uptake or by transfer from the sheath cells (Fig 10B). Additional work will be necessary to resolve the basis for the sterility of the *catp-6(0); catp-5(0)* double mutant.

*catp-6(0) catp-7(dx189)* double mutants exhibit variably severe defects in somatic gonad development, with uterine, spermathecal and sheath cells under-represented or absent. Given the known importance of the sheath cells for germline proliferation, their absence would be sufficient to explain the sterile phenotype of *catp-6(0) catp-7(dx189)* double mutants. However, we observed impaired germline proliferation even in animals where multiple sheath cells were present, so it is possible that sheath cell function is defective in *catp-6(0) catp-7(dx189)* animals.

The basis for the vulvaless phenotype of *catp-6(0) catp-7(dx189)* animals is also currently unresolved. The anchor cell could be missing and/or it could be defective in its ability to produce the inductive LIN-3 signal [47,48]. Furthermore, since CATP-6::mKate2 and GFP::CATP-7 are both expressed in the developing vulval epithelial cells, it could be that the VPCs of double mutants are not competent to respond to LIN-3.

### Distal tip cell migration phenotype

Although distal tip cell (DTC) migration is normal in each of the P5B single mutants, double and triple mutants show characteristic defects in migration of the DTCs. The perpetual DTC migration defect observed in *catp-6(0); catp-5(0)* double mutants is very similar to that observed in *vab-3(lf)* mutants, in which the alpha integrin *ina-1* is not downregulated [49,50]. Furthermore, in *catp-6(0) catp-7(dx189)* double mutants, the DTCs frequently omit the second turn towards the center of the animal; this phenotype is very similar to that observed in mutants where either one of the integrin-associated proteins, SRC-1 or talin, is defective [51,52].

We speculate that *catp-5*, *catp-6* and *catp-7* function redundantly within the DTCs to allow correct localization and/or function of integrins and integrin-associated proteins. Given the known association between P5B ATPase function and Parkinsons disease, it may be significant that the human ortholog of *vab-3* is Pax6, which has been shown to be important for dopaminergic neuron survival [53]. Moreover, the expression of integrin  $\alpha 5\beta 1$  is crucial for dopaminergic neurite outgrowth to the striatal cell region [54]. Since  $\alpha 5\beta 1$  integrin is known to be a target of Pax6 [55], we speculate that this is a conserved regulatory interaction, and that P5B ATPases may act coordinately to regulate integrin function.

### P5B subcellular localization

Mammalian P5B ATPases have been reported to localize to lysosomes, late endosomes, multi-vesicular bodies, (ATP13A2; [9,56–58] and ER (ATP13A4, [59]). While there are hints that ATP13A3 may localize to the plasma membrane [60], this has not been definitively established. We find that each of the nematode P5Bs can localize to the plasma membrane in certain tissues

and stages of development. We observed that the CATP-6 localization pattern in spermathecal epithelial cells exhibits obvious similarity to that of the early endosomal marker RFP::RAB-5. Higher resolution imaging will be necessary to confirm that RAB-5 and CATP-6 colocalize at the level of individual vesicles. We did not observe substantial localization of CATP-6 to vesicular compartments marked by LMP-1 (lysosomes), RME-1 (recycling endosomes), RAB-11 (recycling endosomes), HGRS-1 (early endosomes), SS::GFP::CD4-HCIMPR (endosomes) or TGN-38 (trans-Golgi network). Therefore, we do not find strong evidence that the nematode P5Bs function primarily within lysosomes.

### P5B substrate specificity

Although the transport specificity of P5B ATPases has not been unambiguously determined, various candidates have been proposed based on biological evidence. In the yeast, *Saccharomyces cerevisiae*, loss of P5B (Ypk9) function results in hypersensitivity to  $Mn^{2+}$ , leading to the suggestion that Ypk9 detoxifies  $Mn^{2+}$  by pumping it into the vacuole. In the slime mold, *Dictyostelium discoideum*, loss of P5B (Kil2) function prevents  $Mg^{2+}$ -dependent killing of phagocytosed bacteria, leading to the suggestion that Kil2 pumps  $Mg^{2+}$  into the phagosome. In mammalian tissue culture cells, loss of ATP13A2 function results in overaccumulation of  $Zn^{2+}$ , suggesting that this P5B might play a role in  $Zn^{2+}$  homeostasis [57]. On the other hand, ATP13A3 has recently been implicated as a candidate polyamine transporter [60]. With regard to the nematode P5Bs, the data of Heinick et al. [11] strongly suggest that polyamines are transported from the gut lumen into the intestinal cells via CATP-5 expressed on the plasma membrane. If CATP-6 and CATP-7 have the same specificity as CATP-5, then this would provide a simple explanation for their functional overlap within the germ line and the somatic sheath cells. This would also suggest that the sheath cells and the germ line are unable to autonomously produce sufficient quantities of polyamines to enable normal development and function of the reproductive system. Furthermore, given our original identification of CATP-6 as an interactor of the GON-2  $Mg^{2+}$  channel, it is possible that the P5Bs function as antiporters, exchanging polyamines and  $Mg^{2+}$  between compartments.

### Supporting information

**S1 Fig. L4s and young adult *catp-6(0); catp-5(0)* double mutants.** *catp-6(ok3473) IV; catp-5(tm4481) X*. (EPS)

**S2 Fig. L4s and young adult *catp-6(0) catp-7(dx189)* double mutants.** *catp-6(ok3473) catp-7(dx189[delta 1492 bp Ma-M3 + gfp + loxP] IV*. (EPS)

**S3 Fig. DAPI staining of sheath cell nuclei of *catp-6(0) catp-7(dx189)* double mutants.** *catp-6(ok3473) catp-7(dx189[delta 1492 bp Ma-M3 + gfp + loxP] IV*. (EPS)

**S4 Fig. L4s and young adult *catp-6(0) catp-7(dx189); catp-5(0)* triple mutants.** *catp-6(ok3473) catp-7(dx189[delta 1492 bp Ma-M3 + gfp + loxP] IV; catp-5(tm4481) X*. (EPS)

### Acknowledgments

Special thanks to Laura Besora Casals, Hoang Son Luu and Sergi Masgrau Alsina for generating plasmids *P<sub>catp-6</sub>catp-6::mKate2<sub>let-858</sub>* and *P<sub>catp-7</sub>catp-7::gfp<sub>let-858</sub>*.



Some of the strains used in this study were provided by the CGC, which is funded by NIH Office of Research Infrastructure Programs (P40 OD010440), and the National BioResource Project (NBRP; <https://shigen.nig.ac.jp/c.elegans/>).

This work was supported by a grant to E.J.L (LA 3380/2-1) from the Deutsche Forschungsgemeinschaft. Funding to B.C. was provided by the Center for Integrated Protein Science Munich.

## Author Contributions

**Conceptualization:** Jeffrey Zielich, Barbara Conradt, Eric J. Lambie.

**Data curation:** Jeffrey Zielich.

**Formal analysis:** Jeffrey Zielich, Eric J. Lambie.

**Funding acquisition:** Barbara Conradt, Eric J. Lambie.

**Investigation:** Jeffrey Zielich, Elena Tzima, Eva Ayla Schröder, Faten Jemel, Eric J. Lambie.

**Methodology:** Jeffrey Zielich, Eric J. Lambie.

**Project administration:** Eric J. Lambie.

**Resources:** Eric J. Lambie.

**Supervision:** Eric J. Lambie.

**Validation:** Jeffrey Zielich, Eric J. Lambie.

**Visualization:** Jeffrey Zielich, Eric J. Lambie.

**Writing – original draft:** Jeffrey Zielich, Eric J. Lambie.

**Writing – review & editing:** Jeffrey Zielich, Barbara Conradt, Eric J. Lambie.

## References

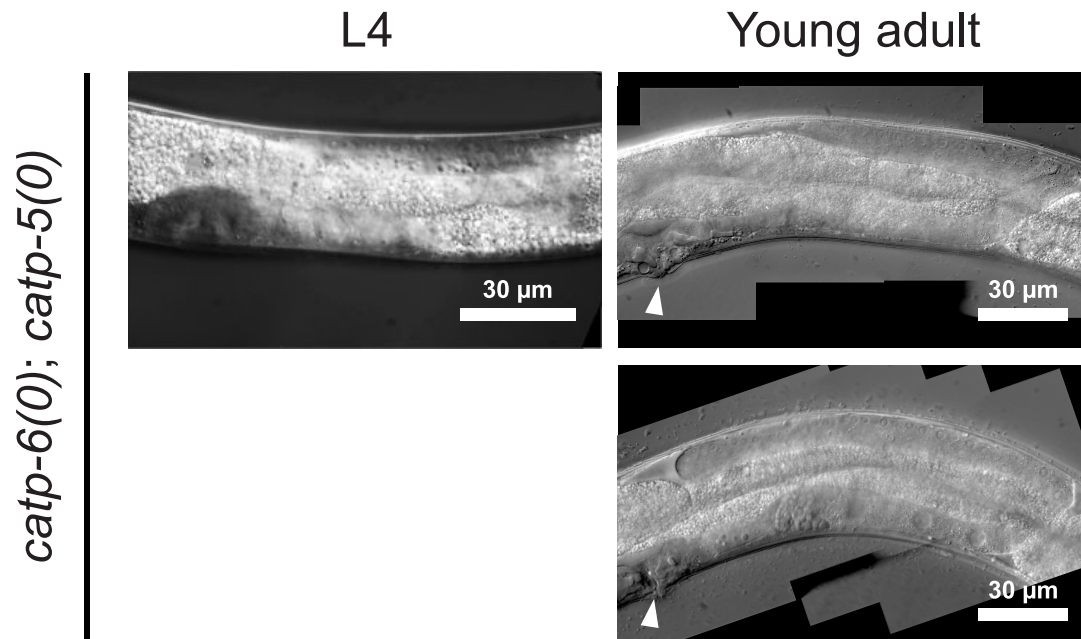
1. Møller JV, Juul B, le Maire M. Structural organization, ion transport, and energy transduction of P-type ATPases. *Biochim Biophys Acta*. 1996 May 6; 1286(1):1–51. PMID: [8634322](#)
2. Bublitz M, Poulsen H, Morth JP, Nissen P. In and out of the cation pumps: P-type ATPase structure revisited. *Curr Opin Struct Biol*. 2010 Jul 31; 20(4):431–9. <https://doi.org/10.1016/j.sbi.2010.06.007> PMID: [20634056](#)
3. Walderhaug MO, Post RL, Saccomani G, Leonard RT, Briskin DP. Structural relatedness of three ion-transport adenosine triphosphatases around their active sites of phosphorylation. *J Biol Chem*. 1985 Mar 25; 260(6):3852–9. PMID: [3156136](#)
4. Axelsen KB, Palmgren MG. Evolution of Substrate Specificities in the P-Type ATPase Superfamily. *J Mol Evol*. Springer-Verlag; 1998 Jan; 46(1):84–101. PMID: [9419228](#)
5. van Veen S, Sorensen DM, Holemans T, Holen HW, Palmgren MG, Vangheluwe P. Cellular function and pathological role of ATP13A2 and related P-type transport ATPases in Parkinson's disease and other neurological disorders. *Front Mol Neurosci*. Frontiers; 2014; 7.
6. Bublitz M, Morth JP, Nissen P. P-type ATPases at a glance. *Journal of Cell Science*. The Company of Biologists Ltd; 2011 Jul 31; 124(Pt 15):2515–9. <https://doi.org/10.1242/jcs.088716> PMID: [21768325](#)
7. Møller AB, Asp T, Holm PB, Palmgren MG. Phylogenetic analysis of P5 P-type ATPases, a eukaryotic lineage of secretory pathway pumps. *Mol Phylogenet Evol* [Internet]. 2008 Feb; 46(2):619–34. Available from: <http://linkinghub.elsevier.com/retrieve/pii/S105579030700382X> <https://doi.org/10.1016/j.ympev.2007.10.023> PMID: [18155930](#)
8. Sørensen DM, Buch-Pedersen MJ, Palmgren MG. Structural divergence between the two subgroups of P5 ATPases. *Biochim Biophys Acta*. 2010 Jun; 1797(6–7):846–55. <https://doi.org/10.1016/j.bbabi.2010.04.010> PMID: [20416272](#)
9. Holemans T, Sørensen DM, van Veen S, Martin S, Hermans D, Kemmer GC, et al. A lipid switch unlocks Parkinson's disease-associated ATP13A2. *Proc Natl Acad Sci USA*. 2015 Jul 21; 112(29):9040–5. <https://doi.org/10.1073/pnas.1508220112> PMID: [26134396](#)

10. Morth JP, Pedersen BP, Buch-Pedersen MJ, Andersen JP, Vilsen B, Palmgren MG, et al. A structural overview of the plasma membrane Na<sup>+</sup>, K<sup>+</sup>-ATPase and H<sup>+</sup>-ATPase ion pumps. *Nat Rev Mol Cell Biol*. Nature Publishing Group; 2011 Jan; 12(1):60–70. <https://doi.org/10.1038/nrm3031> PMID: 21179061
11. Heinick A, Urban K, Roth S, Spies D, Nunes F, Phanstiel O, et al. *Caenorhabditis elegans* P5B-type ATPase CATP-5 operates in polyamine transport and is crucial for norspermidine-mediated suppression of RNA interference. *FASEB J*. 2010 Jan 3; 24(1):206–17. <https://doi.org/10.1096/fj.09-135889> PMID: 19762559
12. Lambie EJ, Tieu PJ, Lebedeva N, Church DL, Conradt B. CATP-6, a *C. elegans* Ortholog of ATP13A2 PARK9, Positively Regulates GEM-1, an SLC16A Transporter. Ahmed S, editor. *PLoS ONE*. 2013 Oct 9; 8(10):e77202. <https://doi.org/10.1371/journal.pone.0077202> PMID: 24130856
13. Casadaban MJ, Martinez-Arias A, Shapira SK, Chou J. Beta-galactosidase gene fusions for analyzing gene expression in *escherichia coli* and yeast. *Meth Enzymol*. 1983; 100:293–308. PMID: 6312261
14. Brenner S. The genetics of *Caenorhabditis elegans*. *Genetics*. 1974 May; 77(1):71–94. PMID: 4366476
15. Armenti ST, Chan E, Nance J. Polarized exocyst-mediated vesicle fusion directs intracellular lumenogenesis within the *C. elegans* excretory cell. *Dev Biol*. NIH Public Access; 2014 Oct 1; 394(1):110–21. <https://doi.org/10.1016/j.ydbio.2014.07.019> PMID: 25102190
16. Consortium TCEDM. Large-Scale Screening for Targeted Knockouts in the *Caenorhabditis elegans* Genome. G3#58; Genes|Genomes|Genetics. G3: Genes, Genomes, Genetics; 2012 Nov 1; 2(11):1415–25.
17. Audhya A, Hyndman F, McLeod IX, Maddox AS, Yates JR, Desai A, et al. A complex containing the Sm protein CAR-1 and the RNA helicase CGH-1 is required for embryonic cytokinesis in *Caenorhabditis elegans*. *J Cell Biol*. Rockefeller University Press; 2005 Oct 24; 171(2):267–79. <https://doi.org/10.1083/jcb.200506124> PMID: 16247027
18. Joyce PI, Satija R, Chen M, Kuwabara PE. The Atypical Calpains: Evolutionary Analyses and Roles in *Caenorhabditis elegans* Cellular Degeneration. Chisholm AD, editor. *PLoS Genet*. Public Library of Science; 2012 Mar 29; 8(3):e1002602. <https://doi.org/10.1371/journal.pgen.1002602> PMID: 22479198
19. Norris A, Tammineni P, Wang S, Gerdes J, Murr A, Kwan KY, et al. SNX-1 and RME-8 oppose the assembly of HGRS-1/ESCRT-0 degradative microdomains on endosomes. *Proc Natl Acad Sci USA*. 2017 Jan 17; 114(3):E307–16. <https://doi.org/10.1073/pnas.1612730114> PMID: 28053230
20. Tamura K, Stecher G, Peterson D, Filipski A, Kumar S. MEGA6: Molecular Evolutionary Genetics Analysis version 6.0. *Mol Biol Evol*. 2013 Dec; 30(12):2725–9. <https://doi.org/10.1093/molbev/mst197> PMID: 24132122
21. Guindon S, Dufayard J-F, Lefort V, Anisimova M, Hordijk W, Gascuel O. New algorithms and methods to estimate maximum-likelihood phylogenies: assessing the performance of PhyML 3.0. *Syst Biol*. 2010 May; 59(3):307–21. <https://doi.org/10.1093/sysbio/syq010> PMID: 20525638
22. Le SQ, Gascuel O. An Improved General Amino Acid Replacement Matrix. *Mol Biol Evol*. Oxford University Press; 2008 Jul 1; 25(7):1307–20. <https://doi.org/10.1093/molbev/msn067> PMID: 18367465
23. Gibson DG, Young L, Chuang R-Y, Venter JC, Hutchison CA, Smith HO. Enzymatic assembly of DNA molecules up to several hundred kilobases. *Nature Methods*. Nature Publishing Group; 2009 May; 6(5):343–5. <https://doi.org/10.1038/nmeth.1318> PMID: 19363495
24. Zhao Z, Fang L, Chen N, Johnsen RC, Stein L, Baillie DL. Distinct regulatory elements mediate similar expression patterns in the excretory cell of *Caenorhabditis elegans*. *J Biol Chem*. American Society for Biochemistry and Molecular Biology; 2005 Nov 18; 280(46):38787–94. <https://doi.org/10.1074/jbc.M505701200> PMID: 16159881
25. Merzlyak EM, Goedhart J, Shcherbo D, Bulina ME, Shcheglov AS, Fradkov AF, et al. Bright monomeric red fluorescent protein with an extended fluorescence lifetime. *Nature Methods*. Nature Publishing Group; 2007 Jul; 4(7):555–7. <https://doi.org/10.1038/nmeth1062> PMID: 17572680
26. Bando T, Ikeda T, Kagawa H. The Homeoproteins MAB-18 and CEH-14 Insulate the Dauer Collagen Gene col-43 from Activation by the Adjacent Promoter of the Spermatheca Gene *sth-1* in *Caenorhabditis elegans*. *J Mol Biol*. 2005 Apr; 348(1):101–12. <https://doi.org/10.1016/j.jmb.2005.01.045> PMID: 15808856
27. Dong MQ, Chase D, Patikoglou GA, Koelle MR. Multiple RGS proteins alter neural G protein signaling to allow *C. elegans* to rapidly change behavior when fed. *Genes Dev*. Cold Spring Harbor Laboratory Press; 2000 Aug 15; 14(16):2003–14. PMID: 10950865
28. Stemmer M, Thumberger T, del Sol Keyer M, Wittbrodt J, Mateo JL. CCTop: An Intuitive, Flexible and Reliable CRISPR/Cas9 Target Prediction Tool. Maas S, editor. *PLoS ONE*. Public Library of Science; 2015 Apr 24; 10(4):e0124633. <https://doi.org/10.1371/journal.pone.0124633> PMID: 25909470
29. Heigwer F, Kerr G, Boutros M. E-CRISP: fast CRISPR target site identification. *Nature Methods*. Nature Research; 2014 Feb 1; 11(2):122–3. <https://doi.org/10.1038/nmeth.2812> PMID: 24481216

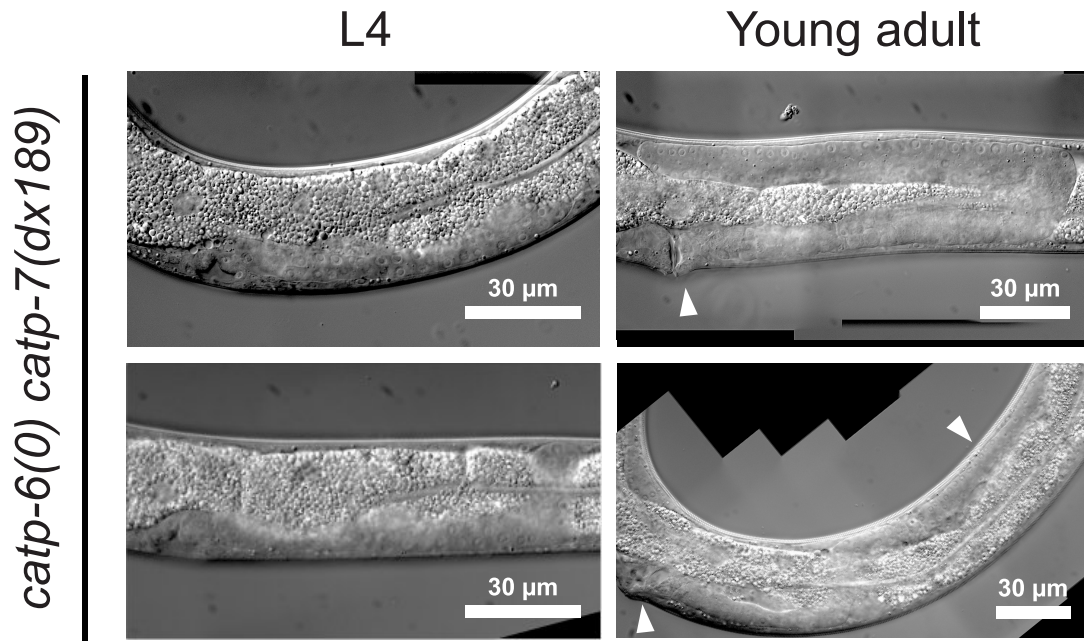


30. Arribere JA, Bell RT, Fu BXH, Artilles KL, Hartman PS, Fire AZ. Efficient marker-free recovery of custom genetic modifications with CRISPR/Cas9 in *Caenorhabditis elegans*. *Genetics*. 2014 Oct 31; 198(3):837–46. <https://doi.org/10.1534/genetics.114.169730> PMID: 25161212
31. Norris AD, Kim H-M, Colaiácovo MP, Calarco JA. Efficient Genome Editing in *Caenorhabditis elegans* with a Toolkit of Dual-Marker Selection Cassettes. *Genetics* [Internet]. *Genetics*; 2015 Oct 1; 201(2):449–58. Available from: <http://www.genetics.org/cgi/doi/10.1534/genetics.115.180679> <https://doi.org/10.1534/genetics.115.180679> PMID: 26232410
32. Dickinson DJ, Pani AM, Heppert JK, Higgins CD, Goldstein B. Streamlined Genome Engineering with a Self-Excising Drug Selection Cassette. *Genetics* [Internet]. 2015 Aug; 200(4):1035–49. Available from: <http://www.genetics.org/cgi/doi/10.1534/genetics.115.178335> <https://doi.org/10.1534/genetics.115.178335> PMID: 26044593
33. Zhang L, Ward JD, Cheng Z, Dernburg AF. The auxin-inducible degradation (AID) system enables versatile conditional protein depletion in *C. elegans*. *Development*. Oxford University Press for The Company of Biologists Limited; 2015 Dec 15; 142(24):4374–84. <https://doi.org/10.1242/dev.129635> PMID: 26552885
34. Mikeladze-Dvali T, Tobel von L, Strnad P, Knott G, Leonhardt H, Schermelleh L, et al. Analysis of centriole elimination during *C. elegans* oogenesis. *Development*. 2012 Apr 3; 139(9):1670–9. <https://doi.org/10.1242/dev.075440> PMID: 22492357
35. Hadwiger G, Dour S, Arur S, Fox P, Nonet ML. A monoclonal antibody toolkit for *C. elegans*. Hendricks M, editor. *PLoS ONE* [Internet]. 2010 Apr 13; 5(4):e10161. Available from: <http://dx.plos.org/10.1371/journal.pone.0010161> <https://doi.org/10.1371/journal.pone.0010161> PMID: 20405020
36. Schindelin J, Arganda-Carreras I, Frise E, Kaynig V, Longair M, Pietzsch T, et al. Fiji: an open-source platform for biological-image analysis. *Nature Methods*. Nature Research; 2012 Jul 1; 9(7):676–82. <https://doi.org/10.1038/nmeth.2019> PMID: 22743772
37. Day CA, Kraft LJ, Kang M, Kenworthy AK. Analysis of protein and lipid dynamics using confocal fluorescence recovery after photobleaching (FRAP). *Curr Protoc Cytom*. 2012 Oct; Chapter 2:Unit2.19.
38. Christensen M, Estevez A, Yin X, Fox R, Morrison R, McDonnell M, et al. A primary culture system for functional analysis of *C. elegans* neurons and muscle cells. *Neuron*. 2002 Feb 14; 33(4):503–14. PMID: 11856526
39. *C. elegans* Sequencing Consortium. Genome sequence of the nematode *C. elegans*: a platform for investigating biology. *Science*. 1998 Dec 11; 282(5396):2012–8. PMID: 9851916
40. Sternberg PW. Genome sequence of additional *Caenorhabditis* species: enhancing the utility of *C. elegans* as a model organism. [Internet]. genome.gov. 2003 [cited 2017 Dec 7]. Available from: [https://www.genome.gov/pages/research/sequencing/seqproposals/c\\_remaneiseq.pdf](https://www.genome.gov/pages/research/sequencing/seqproposals/c_remaneiseq.pdf)
41. Yook K, Harris TW, Bieri T, Cabunoc A, Chan J, Chen WJ, et al. WormBase 2012: more genomes, more data, new website. *Nucleic Acids Res*. Oxford University Press; 2012 Jan 1; 40(D1):D735–41.
42. Adams MD, Celniker SE, Holt RA, Evans CA, Gocayne JD, Amanatides PG, et al. The genome sequence of *Drosophila melanogaster*. *Science*. 2000 Mar 24; 287(5461):2185–95. PMID: 10731132
43. Melentijevic I, Toth ML, Arnold ML, Guasp RJ, Harinath G, Nguyen KC, et al. *C. elegans* neurons jettison protein aggregates and mitochondria under neurotoxic stress. *Nature Publishing Group*. 2017 Feb 16; 542(7641):367–71. <https://doi.org/10.1038/nature21362> PMID: 28178240
44. Ward S, Argon Y, Nelson GA. Sperm morphogenesis in wild-type and fertilization-defective mutants of *Caenorhabditis elegans*. *J Cell Biol*. The Rockefeller University Press; 1981 Oct; 91(1):26–44. PMID: 7298721
45. Starich TA, Hall DH, Greenstein D. Two Classes of Gap Junction Channels Mediate Soma-Germline Interactions Essential for Germline Proliferation and Gametogenesis in *Caenorhabditis elegans*. *Genetics*. 2014 Nov 7; 198(3):1127–53. <https://doi.org/10.1534/genetics.114.168815> PMID: 25195067
46. Hall DH, Winfrey VP, Blaeuer G, Hoffman LH, Furuta T, Rose KL, et al. Ultrastructural Features of the Adult Hermaphrodite Gonad of *Caenorhabditis elegans*: Relations between the Germ Line and Soma. *Dev Biol*. 1999 Aug; 212(1):101–23. <https://doi.org/10.1006/dbio.1999.9356> PMID: 10419689
47. Katz WS, Lesa GM, Yannoukakos D, Clandinin TR, Schlessinger J, Sternberg PW. A point mutation in the extracellular domain activates LET-23, the *Caenorhabditis elegans* epidermal growth factor receptor homolog. *Mol Cell Biol*. 1996 Feb; 16(2):529–37. PMID: 8552080
48. Katz WS, Hill RJ, Clandinin TR, Sternberg PW. Different levels of the *C. elegans* growth factor LIN-3 promote distinct vulval precursor fates. *Cell*. 1995 Jul 28; 82(2):297–307. PMID: 7628018
49. Nishiwaki K. Mutations affecting symmetrical migration of distal tip cells in *Caenorhabditis elegans*. *Genetics*. 1999 Jul; 152(3):985–97. PMID: 10388818
50. Meighan CM, Schwarzbauer JE. Control of *C. elegans* hermaphrodite gonad size and shape by vab-3/ Pax6-mediated regulation of integrin receptors. *Genes Dev*. Cold Spring Harbor Lab; 2007 Jul 1; 21(13):1615–20. <https://doi.org/10.1101/gad.1534807> PMID: 17606640

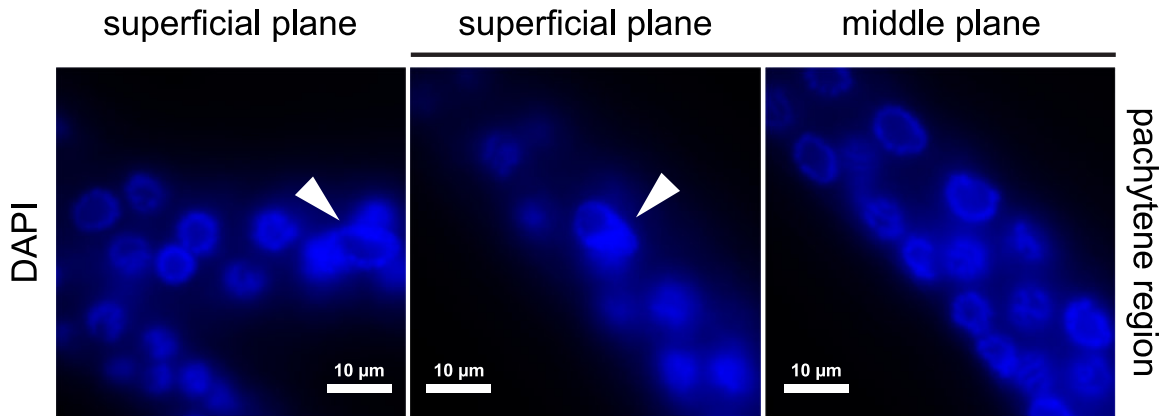
51. Cram EJ, Clark SG, Schwarzbauer JE. Talin loss-of-function uncovers roles in cell contractility and migration in *C. elegans*. *Journal of Cell Science*. 2003 Oct 1; 116(Pt 19):3871–8. <https://doi.org/10.1242/jcs.00705> PMID: 12915588
52. Itoh B, Hirose T, Takata N, Nishiwaki K, Koga M, Ohshima Y, et al. SRC-1, a non-receptor type of protein tyrosine kinase, controls the direction of cell and growth cone migration in *C. elegans*. *Development*. 2005 Dec; 132(23):5161–72. <https://doi.org/10.1242/dev.02103> PMID: 16251208
53. Thomas MG, Stone L, Allan P, Barker AR, White BR. PAX6 expression may be protective against dopaminergic cell loss in Parkinson's disease. *CNS & Neurological Disorders—Drug Targets*. 2016 Jan 31; 15(1):73–9.
54. Izumi Y, Wakita S, Kanbara C, Nakai T, Akaiki A, Kume T. Integrin  $\alpha 5 \beta 1$  expression on dopaminergic neurons is involved in dopaminergic neurite outgrowth on striatal neurons. *Sci Rep*. 2017 Feb 8; 7:42111. <https://doi.org/10.1038/srep42111> PMID: 28176845
55. Duncan MK, Kozmik Z, Cveklava K, Piatigorsky J, Cvekl A. Overexpression of PAX6(5a) in lens fiber cells results in cataract and upregulation of ( $\alpha$ )5( $\beta$ )1 integrin expression. *Journal of Cell Science*. 2000 Sep; 113 (Pt 18):3173–85.
56. Ramirez A, Heimbach A, Gründemann J, Stiller B, Hampshire D, Cid LP, et al. Hereditary parkinsonism with dementia is caused by mutations in ATP13A2, encoding a lysosomal type 5 P-type ATPase. *Nat Genet*. Nature Publishing Group; 2006 Oct 1; 38(10):1184–91. <https://doi.org/10.1038/ng1884> PMID: 16964263
57. Tsunemi T, Krainc D. Zn<sup>2+</sup> dyshomeostasis caused by loss of ATP13A2/PARK9 leads to lysosomal dysfunction and alpha-synuclein accumulation. *Hum Mol Genet*. 2014 May 8; 23(11):2791–801. <https://doi.org/10.1093/hmg/ddt572> PMID: 24334770
58. Kong SMY, Chan BKK, Park J-S, Hill KJ, Aitken JB, Cottle L, et al. Parkinson's disease-linked human PARK9/ATP13A2 maintains zinc homeostasis and promotes  $\alpha$ -Synuclein externalization via exosomes. *Hum Mol Genet*. 2014 Jun 1; 23(11):2816–33. <https://doi.org/10.1093/hmg/ddu099> PMID: 24603074
59. Vallipuram J, Grenville J. The E646D-ATP13A4 Mutation Associated with Autism Reveals a Defect in Calcium Regulation. *Cell Mol Neurobiol*. Springer US; 2010 Mar 1; 30(2):233–46. <https://doi.org/10.1007/s10571-009-9445-8> PMID: 19731010
60. Madan M, Patel A, Skruber K, Geerts D, Altomare DA, Iv OP. ATP13A3 and caveolin-1 as potential biomarkers for difluoromethylornithine-based therapies in pancreatic cancers. *Am J Cancer Res*. 2016; 6(6):1231–52. PMID: 27429841



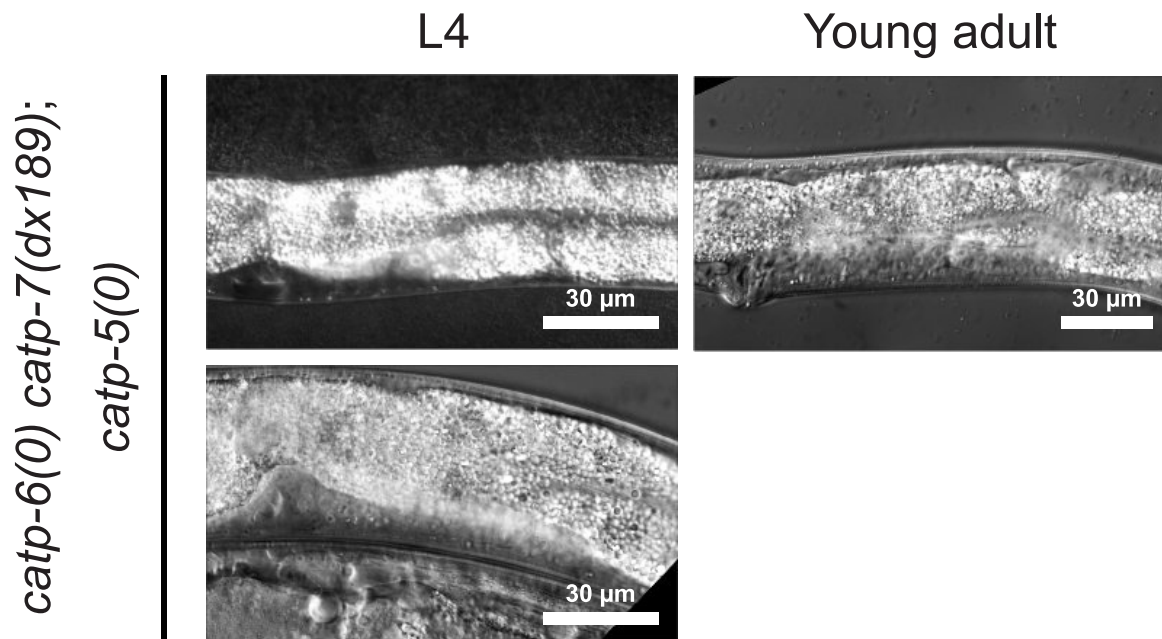
**S Fig 1: L4s and young adult *catp-6(0); catp-5(0)* double mutants. *catp-6(ok3473)* IV; *catp-5(tm4481)* X.**



**S Fig 2: L4s and young adult *catp-6(0) catp-7(dx189)* double mutants. *catp-6(ok3473) catp-7(dx189)[Δ 1492 bp Ma-M3 + gfp + loxP]* IV.**



**S Fig 3: DAPI staining of sheath cell nuclei of *catp-6(0) catp-7(dx189)* double mutants. *catp-6(ok3473) catp-7(dx189[Δ 1492 bp Ma-M3 + gfp + loxP])* IV.**



**S Fig 4:** L4s and young adult *catp-6(ok3473) catp-7(dx189); catp-5(tm4481)* triple mutants. *catp-6(ok3473) catp-7(dx189)[Δ 1492 bp Ma-M3 + gfp + loxP]* IV; *catp-5(tm4481)* X.

## Chapter 2

---

### **Redundant functions of three paralogous *Caenorhabditis elegans* P5B ATPases during gonadogenesis**

Jeffrey Zielich, Barbara Conradt, Eric J. Lambie

**Unpublished manuscript**

---

**Redundant functions of three paralogous *Caenorhabditis elegans***

**P5B ATPases during gonadogenesis**

**Jeffrey Zielich, Barbara Conradt and Eric J Lambie**

Author affiliation:

Department of Cell and Developmental Biology

Ludwig-Maximilians-University

Großhaderner Str. 2

82152 Planegg-Martinsried

Munich, Germany



## Abstract

P-type ATPases are an ancient family of transmembrane proteins that use the energy derived from hydrolysis of ATP to actively transport substrates across membranes. Inactivation of ATP13A2, one of the four human P5B ATPases, leads to early-onset Parkinson's disease (Kufor-Rakeb Syndrome). The presence of the invariant PP(A/V)xPAx motif within transmembrane segment M4 suggests that all P5B ATPases might recognize similar transport substrates. The genome of the model nematode *Caenorhabditis elegans* encodes three P5B ATPases: CATP-5, CATP-6 and CATP-7, which probably diversified from a single ancestral gene around the time of origin of the Caenorhabditid clade. Recently, we used CRISPR/Cas9 to independently tag the endogenous *catp-5*, *catp-6* and *catp-7* loci. We have also used CRISPR/Cas9 to generate a KO allele of CATP-7, enabling us to construct and analyze double and triple mutant strains. We found that CATP-6 and CATP-7 are redundantly required for the development of the somatic gonadal tissues, whereas CATP-5 and CATP-6 are redundantly required for germline proliferation. In this study, we show that the sterile phenotype of *catp-7(dx189) catp-6(0)* can be rescued by somatic expression of either CATP-6 or CATP-7. Furthermore, the ability of each protein to undergo autophosphorylation is crucial for function in this context, suggesting that they may act redundantly to transport a common substrate into somatic gonad cells. We find that the sterile phenotype of *catp-6(0); catp-5(0)* can be rescued by expressing either CATP-5 or CATP-6 in the germ line, consistent with the idea that these proteins act redundantly within this tissue. In addition, we find that the *catp-6(0); catp-5(0)* mutant phenotype can be rescued by expressing either CATP-5 or CATP-6 in the gonadal sheath cells, suggesting that the transport substrate could be transferred from the somatic cells to the germ line via gap junctions. We attempted to compare the functionalities of CATP-5 and CATP-6 through the use of chimeric proteins; however, these failed to localize properly, so they could not be assayed for function.

## Introduction

P-type ATPases are an ancient family of transmembrane proteins that actively transport substrates across membranes using energy derived from hydrolysis of ATP (Møller *et al.* 1996). P-type ATPases comprise four types of structural domains: The actuator domain (A), the nucleotide binding domain (N), the phosphorylation domain (P) and the transmembrane domain (M) (Bublitz *et al.* 2010). A highly conserved cytoplasmic DKTGT motif (P-domain) is one of the signature characteristics of this enzyme family (Møller *et al.* 1996). The aspartic acid residue at the beginning of this motif enables the enzyme to form a phosphorylated enzyme intermediate during the catalytic cycle (Walderhaug *et al.* 1985). The family of P-type ATPases can be grouped into 5 subfamilies, P1-P5 (Axelsen and Palmgren 1998). Members of the P5 subfamily are characterized by the presence of a PPxxPxx motif within the putative substrate-interaction region of transmembrane segment 4 (M4) and can be further classified into subgroups A and B (Møller *et al.* 2008). Specific substrates have not been definitively determined for either the P5A or P5B subgroups (Møller *et al.* 2008; Bublitz *et al.* 2010; 2011; van Veen *et al.* 2014; Sørensen *et al.* 2018). In this study, we focus on the P5B P-type ATPases, which possess the motif PP(A/V)xPAx within the putative substrate-interaction region (Møller *et al.* 2008; Sørensen *et al.* 2010).

Three paralogous P5B ATPases are encoded by the *C. elegans* genome: CATP-5, CATP-6 and CATP-7. Inactivation of *catp-5* confers resistance to toxic levels of norspermidine and also causes a synthetic slow growth phenotype when combined with mutations that impair polyamine synthesis (Heinick *et al.* 2010). Furthermore, CATP-5 localizes to the apical plasma membrane of intestinal cells, consistent with the idea that it mediates (or is indirectly required for) the uptake of dietary polyamines from the gut lumen.

Previously, we identified mutations in *catp-6* based on their ability to prevent *gem-1(gf)* mutations from suppressing *gon-2(lf)* (Table 1). *gem-1* encodes an SLC16A transporter protein

(Kemp *et al.* 2009) and *gon-2* encodes an ortholog of the mammalian TRPM6 and TRPM7 cation channels (Sun and Lambie 1997; Lambie *et al.* 2015). Our data suggest that CATP-6 acts upstream of GEM-1, since overexpression of GEM-1 can bypass the requirement for CATP-6 activity (Kemp *et al.* 2009; Lambie *et al.* 2013).

Recently we used CRISPR/Cas9 to characterize all three *C. elegans* P5B ATPases, CATP-5, CATP-6 and CATP-7, with regard to their spatiotemporal expression patterns and subcellular localization (Zielich *et al.* 2018). Our phylogenetic analysis suggests that *catp-5*, *catp-6* and *catp-7* originated from a single ancestral gene within the Caenorhabditid clade (Lambie *et al.* 2013; Zielich *et al.* 2018). The protein alignment of all three *C. elegans* P5B-ATPases shows a high degree of similarity, particularly in the M4 transmembrane domain, which is thought to be critical for substrate-interaction (Morth *et al.* 2011; Zielich *et al.* 2018). This suggests that CATP-5, CATP-6 and CATP-7 could have the same substrate specificity and therefore fulfill the same function, but in different tissues and/or subcellular compartments.

We further used CRISPR/Cas9 to generate a KO allele of *catp-7*, enabling us to construct and analyze double and triple mutant strains involving *catp-5(0)*, *catp-6(0)* and *catp-7(dx189)*. We found that CATP-6 and CATP-7 are redundantly required for the development of the somatic gonadal tissues, and that CATP-5 and CATP-6 act redundantly to promote germline proliferation. *catp-7(dx189) catp-6(0); catp-5(0)* triple mutants are even more severely affected, indicating that the three paralogues P5B ATPases have multiple overlapping roles during gonad development. In this study, we aim to identify the tissue specific requirements of CATP-5, CATP-6 and CATP-7. In addition, we aim to analyze to what extent the nematode P5B ATPases can be interchanged and whether their autophosphorylation is necessary for biological function.

## Material and Methods

### Strains and genetics

All strains were maintained at 23.5°C on nematode growth medium (NGM) plates with *E. coli* strain AMA1004 (Casadaban *et al.* 1983) as food source. Bristol N2 was used as the wild type (wt) strain. Mutations and genome modifications were obtained from the *Caenorhabditis* Genetics Center at the University of Minnesota (CGC, Minneapolis, MN, USA), the National Bioresource Project at University of Tokyo, or generated in our lab. The following alleles were used in this study: *dxSi1[P<sub>mex-5</sub>::catp-5::gfp]* II, *dxSi2[P<sub>mex-5</sub>::catp-6::gfp]* II, *catp-7(tm4438)* IV (Consortium 2012), *catp-7(dx189[Δ 1492 bp Ma-M3 + gfp + loxP])* IV, *catp-7(dx185[gfp::catp-7 + loxP])* IV, *catp-6(dx179[catp-6::degron::mKate2::3xFlag + loxP])* IV, (Zielich *et al.* 2018), *catp-6(ok3473)* IV, *catp-5(tm4481)* X (Consortium 2012).

### Molecular biology

Standard methods for DNA amplification, analysis and manipulation were used. PCR products were amplified by using Phusion® High-Fidelity DNA Polymerase (New England Biolabs), according to the manufacturer's protocol. DNA sequences were determined by Sanger sequencing.

### Plasmid construction

*P<sub>catp-5</sub>catp-5::gfp<sub>let-858</sub>* and *P<sub>catp-5</sub>catp-5(D474N)::gfp<sub>let-858</sub>*

*P<sub>catp-5</sub>catp-5(D474N)::gfp<sub>let-858</sub>* was obtained via site directed mutagenesis of *P<sub>catp-5</sub>catp-5::gfp<sub>let-858</sub>* (Zielich *et al.* 2018).

*P<sub>catp-6</sub>catp-6::mKate2<sub>let-858</sub>* and *P<sub>catp-6</sub>catp-6(D465N)::mKate2<sub>let-858</sub>*

*P<sub>catp-6</sub>catp-6(D465N)::mKate2<sub>let-858</sub>* was obtained via site directed mutagenesis of *P<sub>catp-6</sub>catp-6::mKate2<sub>let-858</sub>* (Zielich *et al.* 2018).

***P<sub>catp-7</sub>::gfp<sub>let-858</sub>* and *P<sub>catp-7(D497N)</sub>::gfp<sub>let-858</sub>***

*P<sub>catp-7(D497N)</sub>::gfp<sub>let-858</sub>* was obtained via site directed mutagenesis of *P<sub>catp-7</sub>::gfp<sub>let-858</sub>* (Zielich *et al.* 2018).

***P<sub>catp-5(Ma)</sub>::catp-6(M1-M10)::catp-5(C-term)::gfp<sub>let-858</sub>***

We amplified the N- and C-terminus of *catp-5a* fused to *gfp* including the plasmid backbone from *P<sub>catp-5</sub>::gfp<sub>let-858</sub>*. Sequence ends: 5' ttgaaaggtagctctagaa and 3' aattgggggtcagtgcctaaag (plus homology to *catp-6*). We amplified M1-M10 of *catp-6* from the fosmid WRM067B\_F08. Sequence ends: 5' ctgtatcttcgttatgga and 3' gtatcccagcaaaaagaaat (plus homology to *catp-5*). The PCR products were fused together via Gibson cloning (backbone: pGEM-7Zf(+)).

***P<sub>catp-5</sub>::catp-5(Ma)::catp-6(M1-M4)::catp-5(N&Pdomain)::catp-6(M5-M10)::catp-5(C-term)::gfp<sub>let-858</sub>***

We digested *P<sub>catp-5</sub>::catp-5(Ma)::catp-6(M1-M10)::catp-5(C-term)::gfp<sub>let-858</sub>* with *Bsu36I* and *HpaI* and removed the smaller fragment. We amplified the N- and P-domain of *catp-5* from *P<sub>catp-5</sub>::gfp<sub>let-858</sub>*. Sequence ends: 5' agaccctgttaagctatctg and 3' tgcgtgagcggcttaagag (plus homology to *catp-6* M4 and M5). The products were fused together via Gibson cloning (backbone: pGEM-7Zf(+)).

***P<sub>catp-5</sub>::catp-5(Ma)::catp-6(M1-M9<sub>1/2</sub>)::catp-5(M9<sub>1/2</sub>-M10)::gfp<sub>let-858</sub>***

We digested *P<sub>catp-5</sub>::catp-5(Ma)::catp-6(M1-M10)::catp-5(C-term)::gfp<sub>let-858</sub>* with *ClaI* and *PshAI* and removed the smaller fragment. We amplified M9<sub>1/2</sub> and the C-terminus of *catp-5* including a part of *gfp* from *P<sub>catp-5</sub>::gfp<sub>let-858</sub>*. Sequence ends: 5' gttgtgatttagatcaacat and 3' ctccagtgaagaattcttct (plus homology to *catp-6* M9<sub>1/2</sub> and *gfp*). The PCR products were fused together via Gibson cloning (backbone: pGEM-7Zf(+)).

### **Spermathecal expression of chimeric constructs**

Each of the chimeric constructs were digested with *Sall* or *StuI* to open the plasmid 5' of the first exon of *catp-5a*. We amplified the putative *sth-1* promoter (*P<sub>sth-1</sub>* 1230 bp: 5'

gaagctgaatgcgatgtctt 3' tcttttgtgctagagcaac) (Bando *et al.* 2005) from genomic DNA using primers that provide homology to *catp-5a* for *in vivo* recombination with the chimeric constructs (Kemp *et al.* 2007).

### Microinjection for rescue and expression experiments

We used standard microinjection methods to generate transgenic animals (Stinchcomb *et al.* 1985). Expression and rescue constructs were injected in concentrations ranging from 30 ng/μl to 50 ng/μl final concentration. When generating extrachromosomal arrays, we used the dominant Roller plasmid, pRF4 (*rol-6(su1006)*) (Mello *et al.* 1991), as co-injection marker at a concentration of 150 ng/μl.

#### *dxSi1(P<sub>mex-5</sub>catp-5::gfp)* and *dxSi2(P<sub>mex-5</sub>catp-6::gfp)*

We cloned *P<sub>mex-5</sub>catp-5::gfp* and *P<sub>mex-5</sub>catp-6::gfp* via Gibson cloning into the universal MosSCI integration vector pCFJ350 (Frøkjaer-Jensen *et al.* 2008). *P<sub>mex-5</sub>* was amplified from wt genomic DNA (Sequence ends: 5' aaatatcagtttttaaata and 3' ttgaatgttcagacagaga). We used the following injection-mix concentrations: pCFJ601 at 50 ng/μl (*P<sub>efr-3</sub>Mos1* transposase), pGH8 at 10 ng/μl (*P<sub>rab-3</sub>mCherry<sub>mex-54</sub>*), pCFJ90 at 2.5 ng/μl (*P<sub>myo-2</sub>mcherry*), pCFJ104 at 5ng/μl (*P<sub>myo-3</sub>mcherry*) (Frøkjaer-Jensen *et al.* 2008). DNA was injected into EG6699 for single-copy integration on chromosome II.

### Norspermidine sensitivity

We poured standard NGM plates containing 3 mM norspermidine (Sigma-Aldrich) with *E. coli* strain AMA1004 (Casadaban *et al.* 1983) as food source. We picked 1 transgenic animal (*P<sub>catp-5</sub>catp-5::gfp<sub>let-858</sub>* or *P<sub>catp-5</sub>catp-5(D474N)::gfp<sub>let-858</sub>, rol-6(su1006)*) on each plate (in triplicates), removed them after 1 day and counted the surviving/dead transgenic progeny 2 days later. Dead animals were scored as GFP positive non-responsive L1s on the plates and imaged by using Leica M205 A stereomicroscope (Leica Application Suite LAS software).

## Statistical analysis of rescue experiments

Statistical analysis was performed by using RStudio Version 1.0.143 (<https://www.rstudio.com>). We used Fisher's exact test and subsequent Holm's correction for multiple comparison (command: pairwiseNominalIndependence).

## Imaging

Animals were mounted on 4% agarose pads for DIC and epifluorescence microscopy. Whole worms were immobilized with 10 mM levamisole and/or 1 mM sodium azide. Gonads: Animals were dissected in L-15/FBS medium (Christensen *et al.* 2002) with 20 gauge hypodermic needles and mounted without any agar pad directly on microscope slides. Animals were imaged by using Zeiss Axioskop 2 and MetaMorph software (Molecular Devices). Image processing was performed in Fiji/imageJ 2.0.0 (Schindelin *et al.* 2012), brightness and contrast was adjusted either in Fiji/imageJ 2.0.0 or Affinity Designer 1.6.0 (Serif).

**Table 1: Used genotype with corresponding phenotypes.**

Genotype abbreviation	Genotype	Phenotype
<i>catp-5(0)</i>	<i>catp-5(tm4481)</i> X	wt
<i>catp-6(0)</i>	<i>catp-6(ok3473)</i> IV	Egl, Unc and Gro
<i>catp-6(lf)</i>	<i>catp-6(dx114)</i> IV	Egl, Unc and Gro
<i>catp-7(0)</i>	<i>catp-7(tm4438)</i> IV	wt
<i>catp-7(dx189) catp-6(0)</i>	<i>catp-7(dx189) catp-6(ok3473)</i> IV	Sterile, impaired somatic gonad development and germline proliferation
<i>catp-6(0); catp-5(0)</i>	<i>catp-6(ok3473)</i> IV; <i>catp-5(tm4481)</i> X	Sterile, impaired germline proliferation
<i>catp-7(dx189) catp-6(0); catp-5(0)</i>	<i>catp-7(dx189) catp-6(ok3473)</i> IV; <i>catp-5(tm4481)</i> X	Sterile, impaired somatic gonad development, impaired germline proliferation
<i>gem-1(gf)</i>	<i>gem-1(dx66)</i> X	wt
<i>gon-2(lf)</i>	<i>gon-2(q388)</i> I	Gonadless (at restrictive temperature 23.5°C)
<i>gon-2(lf); gem-1(gf)</i>	<i>gon-2(q388)</i> I; <i>gem-1(dx66)</i> X	Normal gonad development
<i>gon-2(lf); catp-6(lf); gem-1(gf)</i>	<i>gon-2(q388)</i> I; <i>catp-6(dx114)</i> IV; <i>gem-1(dx66)</i> X	Gonadless (at restrictive temperature 23.5°C)

## Results

In our recent study we showed that all three *C. elegans* P5B ATPases are expressed in a wide range of tissues (Zielich *et al.* 2018). Each paralog is expressed in the germ line and in multiple somatic gonadal tissues. Although each of the single mutants, *catp-5(0)*, *catp-6(0)* and *catp-7(0)* is viable and fertile, we observed distinct synthetic sterile phenotypes in the *catp-6(0); catp-5(0)* and *catp-7(dx189) catp-6(0)* double mutants (Table 1).

### **Rescue of *catp-7(dx189) catp-6(0)* sterility by transgene expression of *catp-6* and *catp-7***

*catp-7(dx189) catp-6(0)* double mutants are sterile and display variably severe defects in somatic gonad development (Zielich *et al.* 2018). The overall number of germ cells is much smaller than in wt, indicating a germline proliferation defect. Since *catp-6* and *catp-7* are expressed in both the somatic gonad and the germ line, the sterile phenotype of *catp-7(dx189) catp-6(0)* double mutants could result from redundant functioning of these genes in one or both tissues. To investigate this, we tested whether expression of either gene from an extrachromosomal array could rescue sterility. The expression of either CATP-6::mKate2 or CATP-7::GFP from an extrachromosomal array and under the control of its native promoter restores fertility to 99% of transgenic worms (Fig 3, n = 338 and n = 318 respectively; Fishers' exact test, adj. *p*-value = 5.74e-32 and adj. *p*-value = 2.67e-32 respectively). Since extrachromosomal arrays are typically not expressed in the germ line (Kelly *et al.* 1997), restoration of fertility suggests that somatic expression of either CATP-6::mKate2 or CATP-7::GFP is probably sufficient for function. Furthermore, we did not observe germline expression of either fusion protein among transgenic animals.



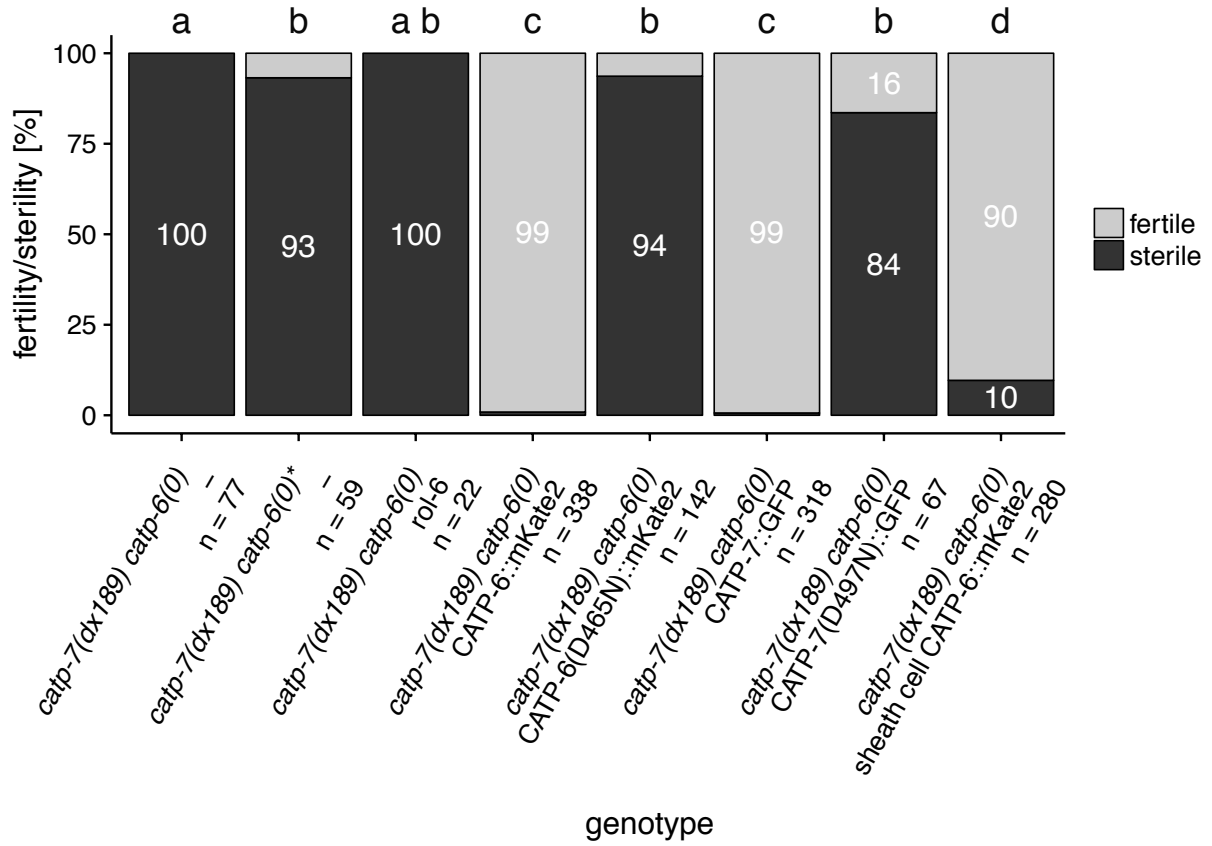


**Fig 3: Rescue of *catp-7(dx189) catp-6(0)* synthetic sterility.** Asterisk indicates that animals were obtained from a hermaphrodite heterozygous for the mutant chromosome, (*catp-7(dx189[delta 1492 bp Ma-M3 + gfp + loxP]) catp-6(ok3473) IV*). Rescue was performed via transgene expression from extra chromosomal arrays. *Ex [rol-6(d)]* as control. *Ex [P<sub>catp-6</sub>catp-6::mKate2; rol-6(d)]*, *Ex [P<sub>catp-6</sub>catp-6(D465N)::mKate2; rol-6(d)]*, *Ex [P<sub>catp-7</sub>catp-7::gfp; rol-6(d)]*, *Ex [P<sub>catp-7</sub>catp-7(D497N)::gfp; rol-6(d)]* and *Ex [P<sub>lim-7</sub>catp-6::mKate2;rol-6(d)]*. Groups that share the same letter do not statistically differ from each other. Groups with different letters are significantly different from each other. Fisher's exact test. Adj. *p*-value threshold < 0.05.

*catp-6* and *catp-7* are expressed in the gonadal sheath cell and in the distal tip cells (DTCs), both of which are important for germline proliferation (McCarter *et al.* 1997; Hall *et al.* 1999; Starich *et al.* 2014). However, defects in DTC signaling typically cause premature meiotic entry, rather than the type of general proliferation impairment seen in *catp-7(dx189) catp-6(0)* double mutants (Kimble and White 1981). Therefore, we tested whether sheath cell specific expression of *P<sub>lim-7</sub>catp-6::mKate2* from an extrachromosomal array could rescue sterility of the *catp-7(dx189) catp-6(0)* double mutants. As expected, the transgenic animals displayed CATP-6::mKate2 expression in the sheath cell (Zielich *et al.* 2018), but not in the

## Chapter 2

germ line (Fig 4A, S Fig 5A). We found that this array restored fertility to 90% of transgenic animals (Fig 3, n = 280; Fishers' exact test, adj.  $p$ -value = 6.07e-20). Although expression within the sheath cells is the most likely basis for rescue of the sterile phenotype, we did also observe expression of  $P_{lim-7}catp-6::mKate2$  in some head and tail neurons (Fig 4A) and occasional expression in the DTCs (data not shown).

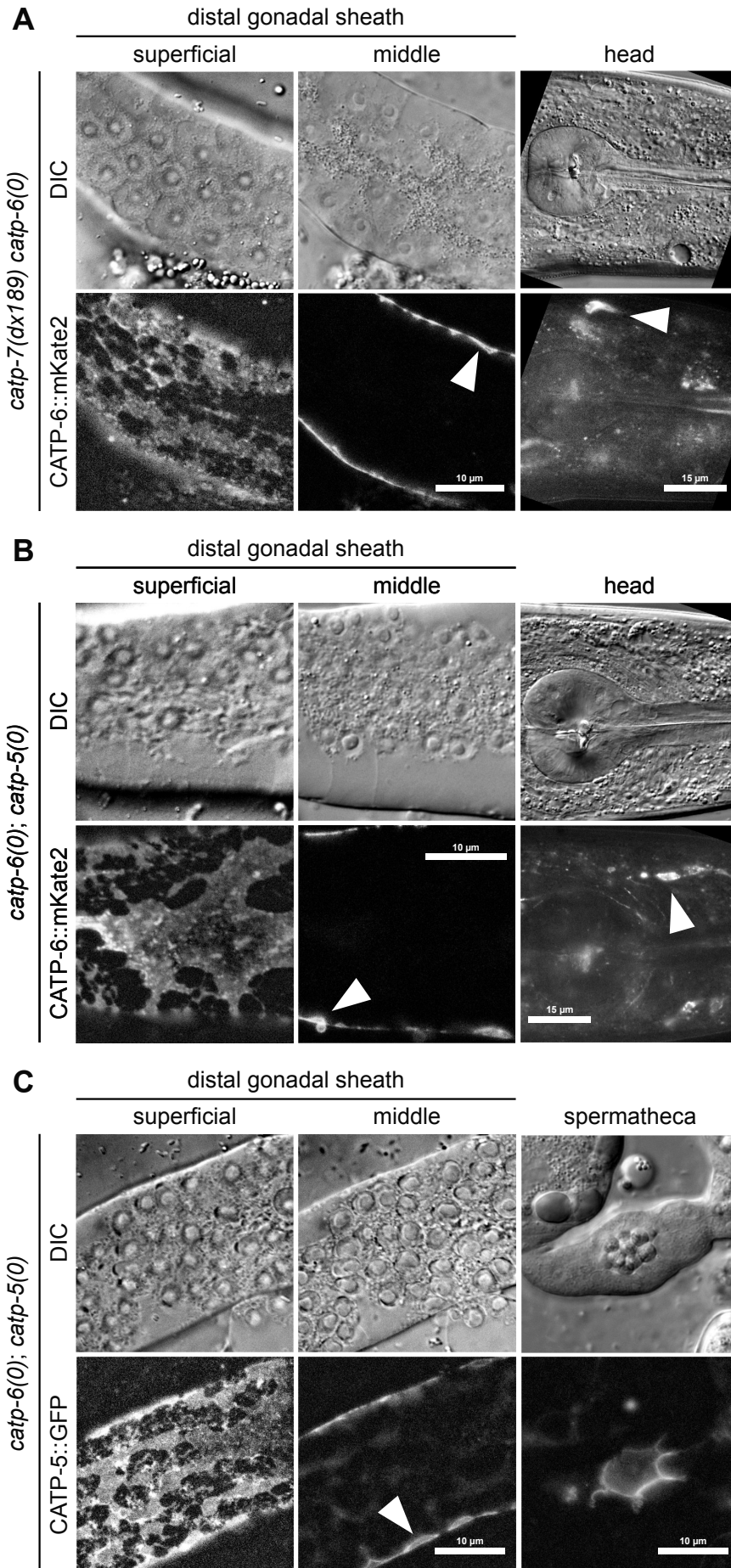


**Fig 4: Sheath cell specific expression of CATP-6::mKate2 and CATP-5::GFP.** Sheath cell specific expressed CATP-6::mKate2 (*Ex [P<sub>lim-7</sub>:catp-6::mKate2; rol-6(d)]*) rescues both double mutants ((A) *catp-7(dx189[delta 1492 bp Ma-M3 + gfp + loxP]) catp-6(ok3473)* IV and (B) *catp-6(ok3473)* IV; *catp-5(tm4481)* X). The transgene localizes to the plasma membrane of the sheath cells (superficial) in a similar pattern as reported for native CATP-6 (Zielich *et al.* 2018) but not to the plasma membrane of germ cells in the pachytene region (middle). In both cases expression in a minor fraction of neurons is detectable. (C) Sheath cell specific expressed CATP-5::GFP (*Ex [P<sub>lim-7</sub>:catp-5::gfp; rol-6(d)]*) rescues *catp-6(ok3473)* IV; *catp-5(tm4481)* X. CATP-5::GFP localizes to the plasma membrane of the sheath cells (superficial) a similar pattern as reported for native CATP-6 and native CATP-7 (Zielich *et al.* 2018) but not to the plasma membrane of germ cells in the pachytene region (middle). Occasionally expression is detectable in the apical domain of spermathecal cells. Arrowheads: Transgene is expressed on both faces of the sheath cell (middle(A-C)) and expression in neurons (head (A, B)).

### **Rescue of *gon-2(lf); catp-6(lf); gem-1(gf)* sterility by transgene expression of *catp-6* and *catp-7***

Previously, we found that *catp-6(0)* and *catp-6(dx114)* (a strong loss-of-function allele of *catp-6*, Table 1) block the ability of *gem-1(gf)* mutations to suppress *gon-2(lf)*. Transgene expression of *catp-6::gfp* under the control of its endogenous promoter, or targeted to the somatic gonad precursors Z1 and Z4 by the *ehn-3* promoter (but not by the pan-neuronal *unc-119* promoter), was able to restore the ability of *gem-1(gf)* mutations to suppress *gon-2(lf)* (Lambie *et al.* 2013). By examination of our CRISPR-tagged strains, we found that native CATP-6::mKate2 and native GFP::CATP-7 are both expressed in Z1 and Z4 (Fig 5). CATP-6::mKate2 appears punctate in Z1 and Z4, consistent with endosomal localization (Fig 5). GFP::CATP-7 appears more smooth, possibly CATP-7 localizes to the plasma membrane of Z1 and Z4 (Fig 5). Although the CATP-6::mKate2 and GFP::CATP-7 localization patterns are different, we do observe overlapping expression in some of the punctae (Fig 5).

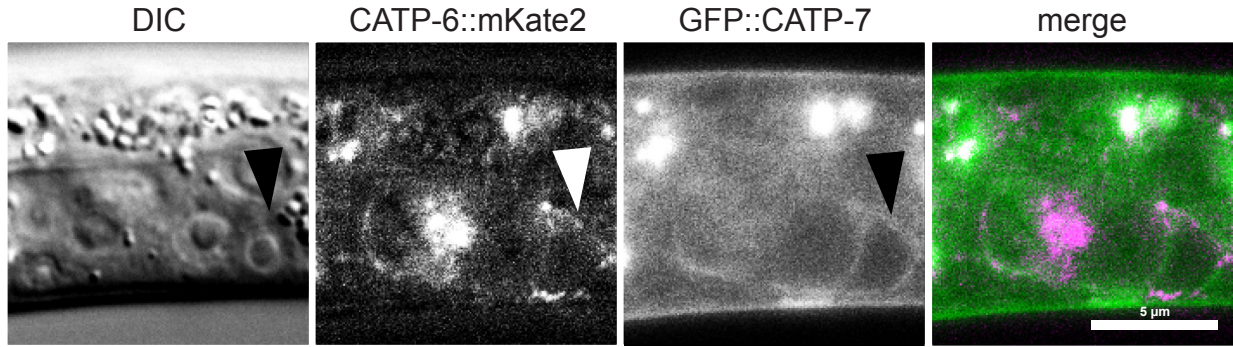


**Fig 5: Partially overlapping expression patterns of CATP-6 and CATP-7 in the somatic gonad precursors Z1 and Z4.** Native CATP-6::mKate2 vs. native GFP::CATP-7 in Z1 and Z4 of living L1. *catp-7(dx193[gfp::catp-7 + loxP]) catp-6(dx179[catp-6::degron::mKate2::3xFlag + loxP])* IV. Arrowheads: Somatic gonad precursor Z4.

We wondered whether overexpression of CATP-7 could reestablish the ability of *gem-1(gf)* to suppress *gon-2(lf)* in a *gon-2(lf); catp-6(lf); gem-1(gf)* mutant background. To test this hypothesis, we expressed CATP-7::GFP from an extrachromosomal array in a *gon-2(lf); catp-6(lf); gem-1(gf)* mutant background. We found that the majority of the transgenic animals (Fig 6, 64%,  $n = 363$ ; Fishers' exact test, adj.  $p$ -value =  $1.81e-32$ ) develop a gonad and are fertile. Control *gon-2(lf); catp-6(lf); gem-1(gf)* transgenic animals that lack overexpression of CATP-7::GFP (*rol-6(su1006)*) show fertility of only 8% (Fig 6,  $n = 62$ ).

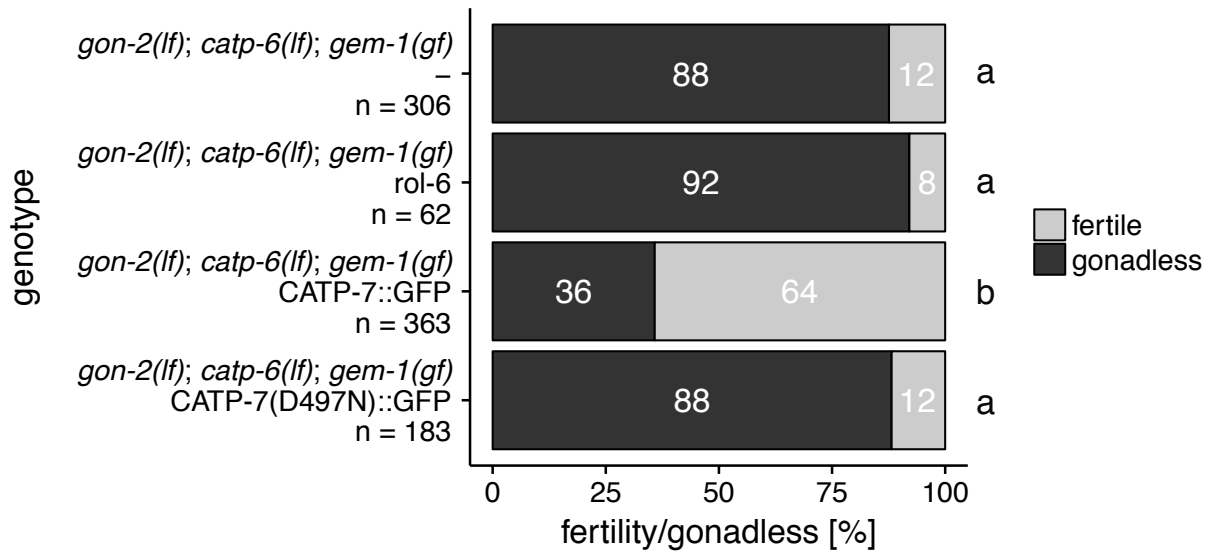


**Fig 6: wt CATP-7 can compensate for CATP-6 in a *gon-2(lf); catp-6(lf); gem-1(gf)* mutant background.** Rescue was performed via transgene expression from extra chromosomal arrays. *Ex [rol-6(d)]* as control. *Ex [P<sub>catp-7</sub>:catp-7::gfp; rol-6(d)]* and *Ex [P<sub>catp-7</sub>:catp-7(D497N)::gfp; rol-6(d)]*. Groups that share the same letter do not statistically differ from each other. Groups with different letters are significantly different from each other. Fisher's exact test. Adj. *p*-value threshold < 0.05.

### Rescue of *catp-6(0); catp-5(0)* sterility by transgene expression of *catp-5* and *catp-6*

*catp-6(0); catp-5(0)* double mutants show almost normal somatic gonad development, but germline proliferation is delayed and these animals have very small brood sizes. Since *catp-5* and *catp-6* are expressed in both the somatic gonad and the germ line, the sterile phenotype of *catp-6(0); catp-5(0)* double mutants could result from redundant requirements for the action of these genes in one or both tissues (Zielich *et al.* 2018). As above, we first tested whether expression of either gene from an extrachromosomal array could rescue sterility. In the case of *P<sub>catp-6</sub>:catp-6::mKate2*, we found that 99.7% of transgenic *catp-6(0); catp-5(0)* worms were fertile (Fig 7, n = 303; Fishers' exact test, adj. *p*-value = 2.01e-29). This suggests that *catp-6* function within somatic tissues is sufficient to promote germline proliferation. However, expression of CATP-5::GFP from an extrachromosomal array did not restore fertility (Fig 7, 18%, n = 126; Fishers' exact test, adj. *p*-value = 0.0504). This result is consistent with our observation that *catp-5* is normally expressed in the germ line, but not the gonadal sheath cells.

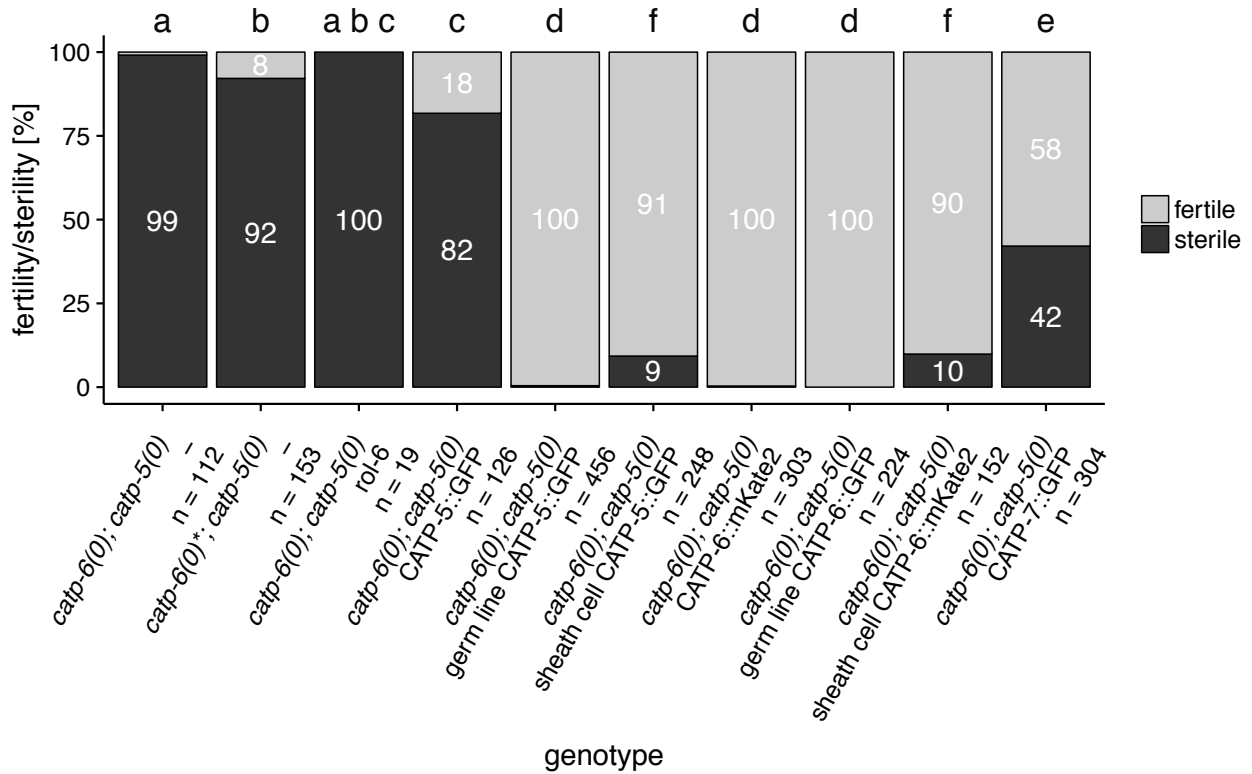


**Fig 7: Synthetic sterility rescue of *catp-6(0); catp-5(0)* double mutants (*catp-6(ok3473)* IV; *catp-5(tm4481)* X).** Asterisk indicates that animals were obtained from a hermaphrodite heterozygous for the mutant chromosome. Rescue was performed via transgene expression from extra chromosomal arrays or via single copy integration of the transgene (germ line). Extrachromosomal arrays: *Ex [rol-6(d)]* as control, *Ex [P<sub>catp-5</sub>.catp-5::gfp; rol-6(d)]*, *Ex [P<sub>lim</sub>.catp-5::gfp; rol-6(d)]*, *Ex [P<sub>catp-6</sub>.catp-6::mKate2; rol-6(d)]*, *Ex [P<sub>lim</sub>.catp-6::mKate2; rol-6(d)]* and *Ex [P<sub>catp-7</sub>.catp-7::gfp; rol-6(d)]*. Germ line specific expression via single copy integrations: *dxSi1[P<sub>mex-5</sub>::catp-5::gfp]* II and *dxSi2[P<sub>mex-5</sub>::catp-6::gfp]* II. Groups that share the same letter do not statistically differ from each other. Groups with different letters are significantly different from each other. Fisher's exact test. Adj. *p*-value threshold < 0.05.

In order to test whether germline expression of either CATP-5 or CATP-6 could restore fertility to the double mutant, we used MosSCI (Frøkjær-Jensen *et al.* 2014) to integrate single copies of *catp-5::gfp* and *catp-6::gfp* under the control of the germ line specific *mex-5* promoter. As expected based on the CRISPR/Cas9 tagged constructs (Zielich *et al.* 2018), CATP-5::GFP and CATP-6::GFP derived from the MosSCI insertions localize to the plasma membrane of germ cells (Fig 8). The gene products of *dxSi1(P<sub>mex-5</sub>.catp-5::gfp)* and *dxSi2(P<sub>mex-5</sub>.catp-6::gfp)* are expressed in germ cells in the mitotic region, transition zone, pachytene region, diplotene region and diakinesis-stage oocytes (Fig 8). In our previous study we detected CATP-

6::mKate2, but not CATP-5::GFP on the plasma membrane of oocytes. However, the expression level of native CATP-5::GFP was very low, and possibly below the threshold of detection in oocytes (Zielich *et al.* 2018).

The expression of either CATP-5::GFP or CATP-6::GFP within the germ line is sufficient to fully restore fertility (Fig 7, 99.5% and 100% respectively,  $n = 456$  and  $n = 224$ ; Fishers' exact test, adj.  $p$ -value =  $1.21e-31$  and adj.  $p$ -value =  $2.41e-28$  respectively). As expected, *catp-6(0); catp-5(0)* double mutants expressing either CATP-5::GFP or CATP-6::GFP in the germ line appeared Egl (egg-laying defective), Unc (uncoordinated; sluggish) and Gro (slow growth), similar to *catp-6(ok3473)* single mutants (Lambie *et al.* 2013; Zielich *et al.* 2018).

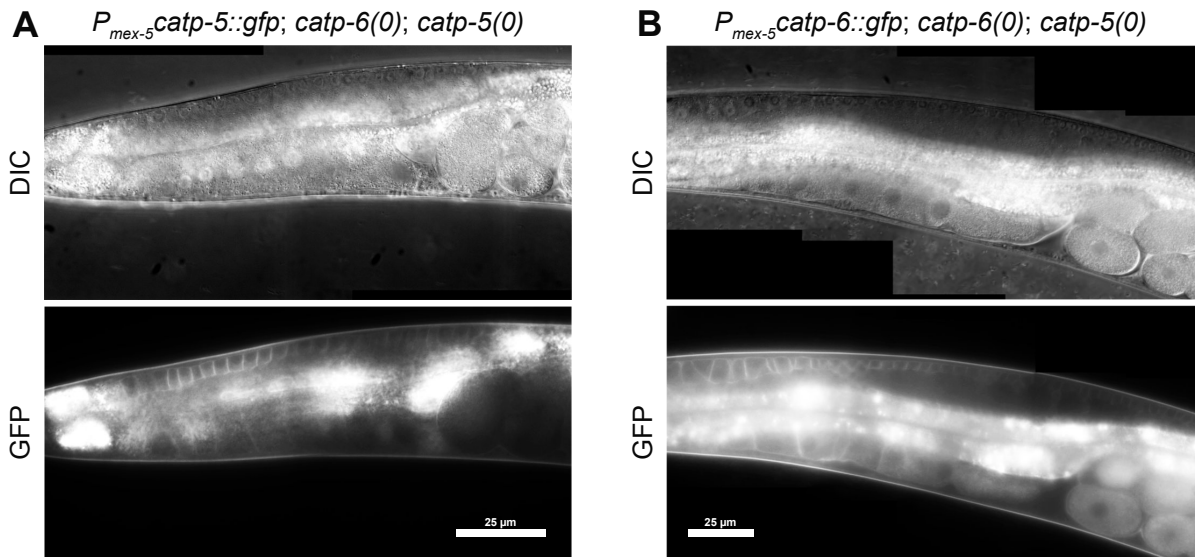


**Fig 8: Germ line specific expression of CATP-5::GFP and CATP-6::GFP rescues *catp-6(0); catp-5(0)* double mutants.** Germ line specific expression of single copy integrations: (A) *dxSi1[P<sub>mex-5</sub>::catp-5::gfp]* II and (B) *dxSi2[P<sub>mex-5</sub>::catp-6::gfp]* II in rescued *catp-6(ok3473)* IV; *catp-5(tm4481)* X double mutants.

Since the gonadal sheath cells are physiologically connected to the pachytene-stage germ line via numerous gap junctions (Starich *et al.* 2014), the germ line should be able to obtain P5B transport substrates either by direct uptake from the pseudocoelomic fluid or by transfer from the sheath cells. To test this, we used the sheath cell-specific promoter of the *lim-7* gene



to drive expression of *catp-6::mKate2*. We found that an extrachromosomal array carrying *P<sub>lim-6</sub>::catp-6::mKate2* was able to efficiently rescue the sterile phenotype of *catp-6(0); catp-5(0)* double mutants (Fig 7, 90%, n = 152; Fishers' exact test, adj. *p*-value = 4.14e-16). Again, we observed expression of the transgene in head and tail neurons (Fig 4B) and occasional expression in the DTCs of rescued animals. However, since native CATP-5 is expressed in the DTCs, and CATP-5::GFP expression from an extrachromosomal array does not rescue the sterility of *catp-6(0); catp-5(0)* animals, it is not likely that expression of *catp-6* within the DTC is either necessary or sufficient to restore fertility.

### **Sheath cell expression of CATP-5 can substitute for CATP-6 in *catp-6(0); catp-5(0)* mutants**

Next, we wondered whether ectopic expression of CATP-5::GFP within the sheath cells could compensate for the lack of CATP-6. We found that *catp-6(0); catp-5(0)* animals carrying an extrachromosomal array with *P<sub>lim-7</sub>::catp-5::gfp* were strongly rescued for fertility (Fig 7, 91%, n = 248; Fishers' exact test, adj. *p*-value = 1.48e-17). CATP-5::GFP localized to the plasma membrane of the sheath cells in a raft-like pattern comparable to seen for CATP-6::mKate2 and CATP-7::GFP (Fig 4A-B, Fig 10A), and we did not observe expression within the germ line (Fig 4C, S Fig 5). We observed occasional expression of the transgene in the spermatheca of rescued animals (Fig 4C), localizing to the apical face of spermathecal cells as reported for native GFP::CATP-5 (Zielich *et al.* 2018). However, since CATP-5::GFP expression from an extrachromosomal array (expressed in the spermatheca and DTCs) does not rescue the sterility of *catp-6(0); catp-5(0)* animals, it is not likely that spermathecal expression of *catp-5* is either necessary or sufficient to restore fertility.

### Rescue of *catp-7(dx189) catp-6(0); catp-5(0)* sterility by transgenic *catp-6*

The *catp-7(0); catp-5(0)* mutant has a nearly wild type phenotype. Therefore, we predicted that expression of CATP-6::mKate2 from an extrachromosomal array should be able to efficiently restore fertility to *catp-7(dx189) catp-6(0); catp-5(0)* animals. Indeed, the expression of CATP-6::mKate2 from an array almost fully restores fertility to the triple mutant (Fig 9, 97%,  $n = 115$ ; Fishers' exact test, adj.  $p$ -value =  $3.22e-12$ ).

### Overexpression of CATP-7 can for substitute CATP-6

Since native CATP-6 and CATP-7 are both expressed in the sheath cells (Zielich *et al.* 2018), we tested whether overexpression of CATP-7::GFP can compensate for the absence of CATP-6 in *catp-6(0); catp-5(0)* double mutants. Indeed,  $P_{catp-7::gfp}$  on an extrachromosomal array was able to restore fertility in 58% of the animals (Fig 7,  $n = 304$ ; Fishers' exact test, adj.  $p$ -value =  $2.28e-07$ ). However, expression of CATP-7::GFP from an array resulted in only weak restoration of fertility to *catp-7(dx189) catp-6(0); catp-5(0)* animals, which is not significantly different from the control (Fig 9, 19%,  $n = 26$ ; Fishers' exact test, adj.  $p$ -value = 0.352).

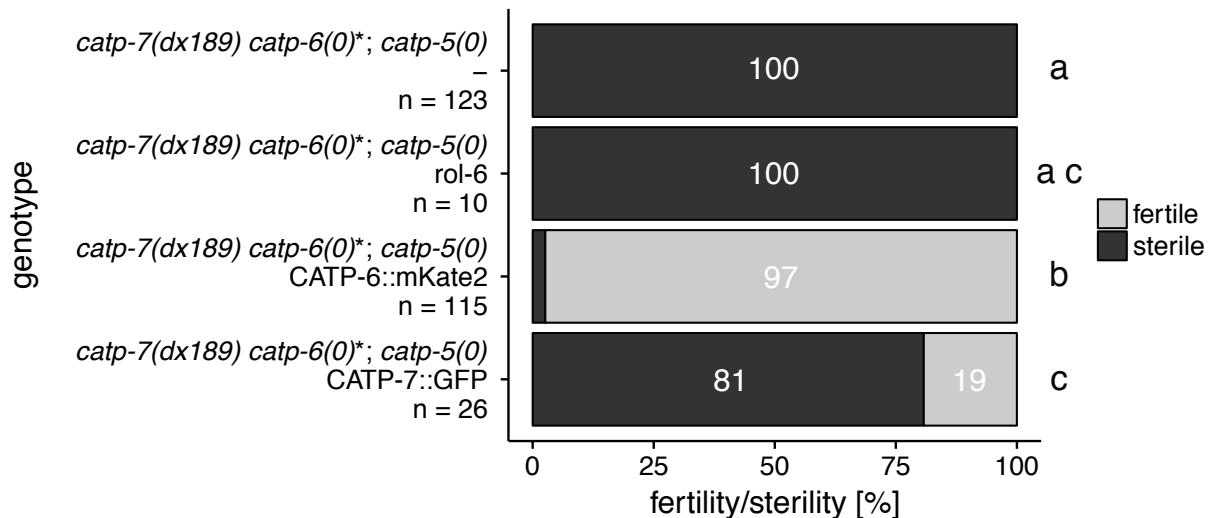


**Fig 9: Rescue of synthetic sterility of *catp-7(dx189) catp-6(0); catp-5(tm4481)* triple mutants (*catp-7(dx189)[delta 1492 bp Ma-M3 + gfp + loxP]* *catp-6(ok3473)* IV; *catp-5(tm4481)* X).** Asterisk indicates that animals were obtained from a hermaphrodite heterozygous for the mutant chromosome. Rescue was performed via transgene expression from extrachromosomal arrays. *Ex [rol-6(d)]* as control. *Ex [P<sub>catp-6</sub>catp-6::mKate2; rol-6(d)]* and *Ex [P<sub>catp-7</sub>catp-7::gfp; rol-6(d)]*. Groups that share the same letter

do not statistically differ from each other. Groups with different letters are significantly different from each other. Fisher's exact test. Adj. *p*-value threshold < 0.05.

### **Autophosphorylation is required for the functions of *catp-5*, *catp-6* and *catp-7***

Given their similarity to other P-type ATPases, the primary biological function of CATP-5, CATP-6 and CATP-7 is expected to be the transport of substrates across membranes. This process requires a series of conformational changes that are dependent on the sequential autophosphorylation and dephosphorylation of the transporter. Since the cognate residues are highly conserved, we were able to create versions of each gene that encode non-phosphorylatable proteins and test whether these could rescue the mutant phenotypes of representative single and double mutants. We found that catalytically inactive (non-phosphorylatable) mutant versions of CATP-6 (CATP-6(D465N)::mKate2) and CATP-7 (CATP-7(D497N)::GFP) showed only very weak rescue of the *catp-7(dx189) catp-6(0)* sterile phenotype, which was not statistically different compared to control transgenic *catp-7(dx189) catp-6(0)* animals (Fig 3, 6% and 16% respectively, n = 142 and n = 67; Fishers' exact test, adj. *p*-value = 0.665 and adj. *p*-value = 0.0731 respectively). Importantly, the subcellular localization of CATP-6(D465N)::mKate2 and CATP-7(D497N)::GFP resembles the subcellular localization of the wild type tagged proteins (Fig 10).

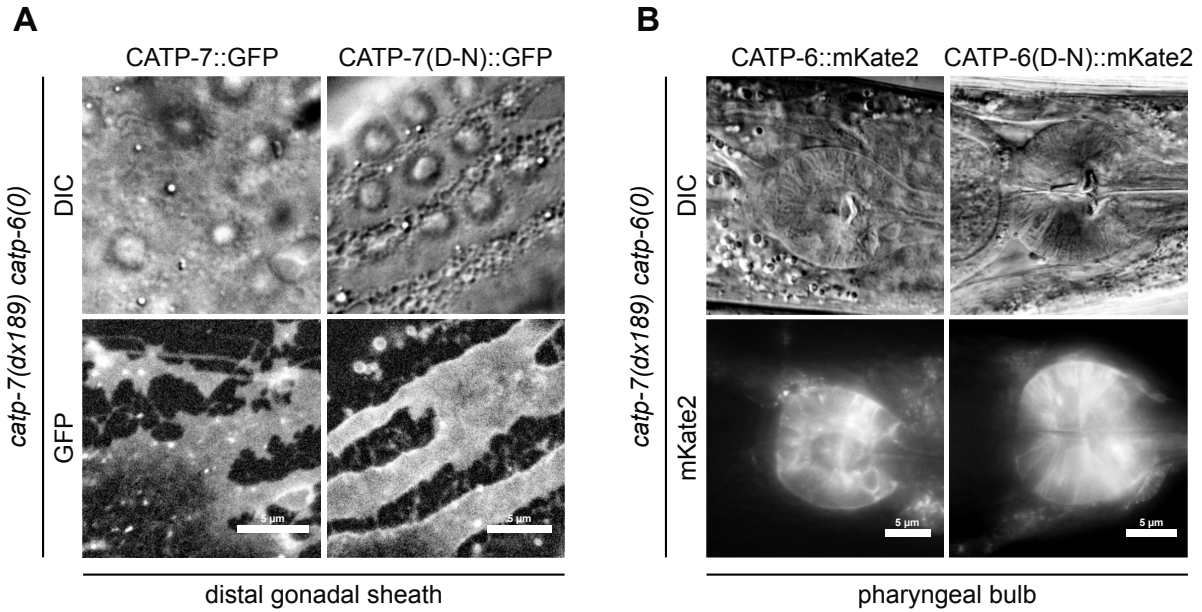


**Fig 10: Catalytic inactive CATP-6/CATP-7::FP displays the same expression pattern as wt CATP-6/CATP-7::FP.** (A) Sheath cell expression of *Ex [P<sub>catp-7</sub>:catp-7::gfp; rol-6(d)]* and *Ex [P<sub>catp-7</sub>:catp-7(D497N)::gfp; rol-6(d)]* in *catp-7(dx189) catp-6(0)* double mutants (*catp-7(dx189)[delta 1492 bp Ma-M3 + gfp + loxP]* *catp-6(ok3473)* IV). (B) Head expression of *Ex [P<sub>catp-6</sub>:catp-6::mKate2; rol-6(d)]* and *Ex [P<sub>catp-6</sub>:catp-6(D465N)::mKate2; rol-6(d)]* in *catp-7(dx189) catp-6(0)* double mutants.

Likewise, overexpression of catalytically inactive CATP-7(D497N)::GFP was not able to substitute for CATP-6 in restoring *gem-1(gf)* activity. We observed only weak rescue, which was not statistically different from control *gon-2(lf); catp-6(0); gem-1(gf)* transgenic animals (Fig 6, 12%,  $n = 183$ ; Fishers' exact test, adj.  $p$ -value = 0.356).

In the case of CATP-5, we expressed wt CATP-5::GFP and catalytically inactive CATP-5(D474N)::GFP in *catp-5(0)* mutant animals. We were able to detect strong GFP at the apical/luminal face of intestinal cells for both transgenic lines (Fig 11C and B). In order to assay for CATP-5 function, we tested whether the transgenic proteins could restore sensitivity to 3 mM norspermidine (Heinick *et al.* 2010). We found that animals that expressed CATP-5(D474N)::GFP remained resistant to norspermidine (99% viable,  $n = 106$ ), but animals expressing wt CATP-5::GFP were not able to survive (2% viable,  $n = 55$ , Fig 11A and B; Fishers' exact test, adj.  $p$ -value =  $1.12 \times 10^{-40}$ ).

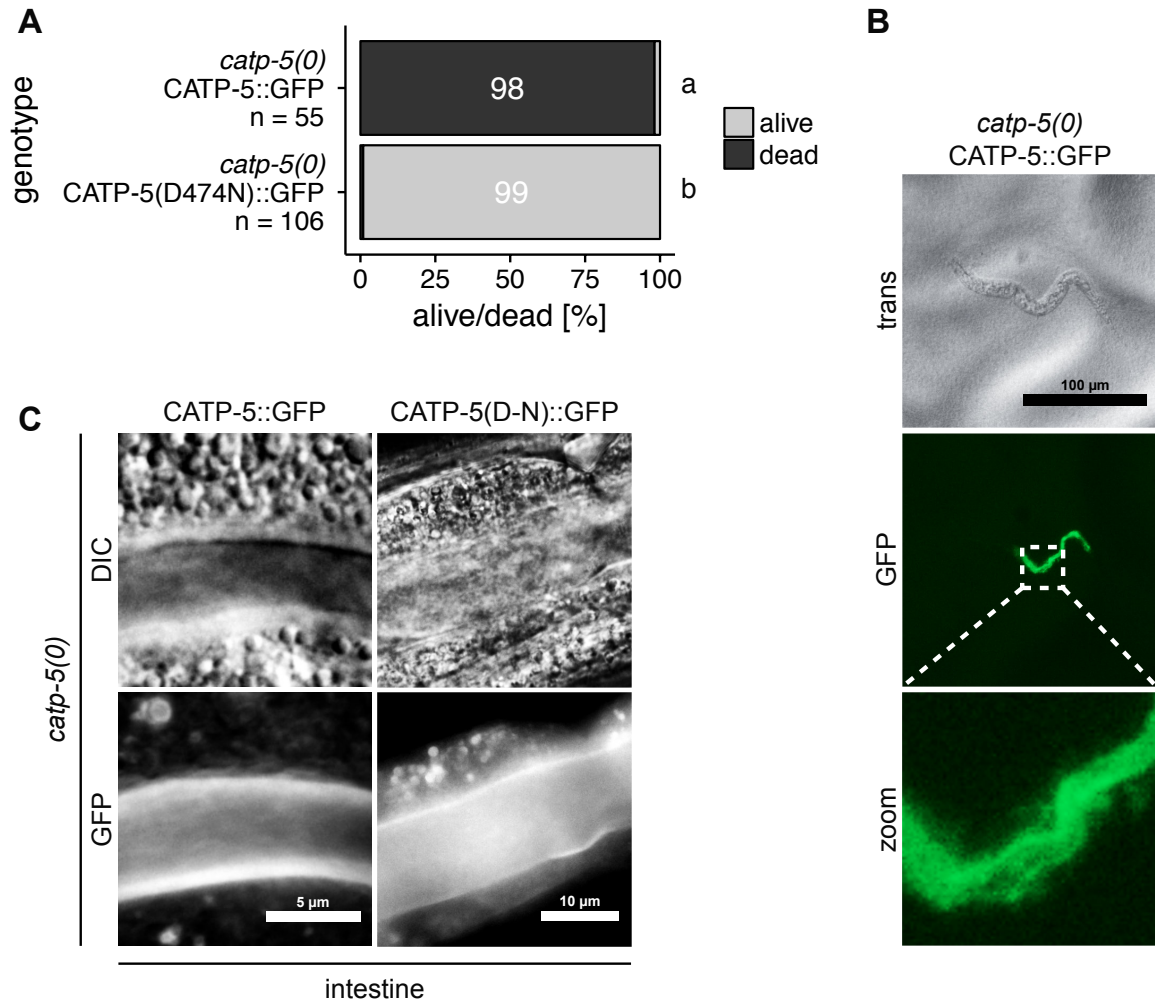


**Fig 11: Sensitivity towards toxic norspermidine requires catalytic active CATP-5.** (A) Expression of wt CATP-5::GFP (*Ex [P<sub>catp-5</sub>catp-5::gfp; rol-6(d)]*) restores norspermidine [3 mM on NGM plates] sensitivity in *catp-5(tm4481)* mutant animals whereas catalytic inactive CATP-5(D474N)::GFP (*Ex [P<sub>catp-5</sub>catp-5(D474N)::gfp; rol-6(d)]*) does not. Groups that share the same letter do not statistically differ from each other. Fisher's exact test. *p*-value threshold < 0.05. (B) GFP positive dead L1 (*catp-5(tm4481)*; *Ex [P<sub>catp-5</sub>catp-5::gfp; rol-6(d)]*) on NGM plates containing 3 mM norspermidine. (C) Both mutant and wild type GFP-tagged proteins localize to the apical brush border of intestinal cells.

### Subcellular localization of CATP-5/CATP-6 chimeric proteins

As an additional test of the interchangeability of CATP-5 and CATP-6, we sought to generate a version of CATP-6 that would localize to the apical surface of polarized epithelial cells. To this end we used domain swapping to attempt to relocalize the transporter activity of CATP-6. We generated 3 chimeric CATP-5/CATP-6 proteins fused to GFP (with the 5' and 3' flanking regions of *catp-5*). We considered it most likely that the key targeting signal(s) would be in the

N- and/or C-terminal cytoplasmic segments. Therefore, we created a construct that encodes a chimeric protein with the central portion of CATP-6 fused to the N- and C-termini of CATP-5 (Fig 12C). Since the apical targeting signal of CATP-5 could also be located in the large cytoplasmic segment between M4 and M5, which carries the N- and P-domains, we further modified CATP-6 by exchanging this region with the corresponding region of CATP-5 (Fig 12D). Next we created a chimeric protein which is a fusion of central part of CATP-6 (M1–M9<sub>1/2</sub>) and the N and C-terminal part of CATP-5 (Ma & M9<sub>1/2</sub>–M10) (Fig 12E). The fusion junction was situated in the middle of the M9 domain in order to eliminate a potential lysosomal targeting signal located in the M10 domain of CATP-6 (GYXXΦ\* (Kostich *et al.* 2000)).

We expressed each chimeric construct in *catp-5(0)* mutant animals so that we could assay for restoration of norspermidine sensitivity. Expression in the intestine and the excretory cell was driven by the *catp-5* promoter. In each case, we found that the chimeric proteins were highly expressed in the intestinal cells (Fig 12C.2–E.2) and the excretory cell (S Fig 6). However, none of the chimeric proteins localized to the apical face of intestinal cells (Fig 12C.2–E.2) as observed for CATP-5::GFP (Fig 11). As an additional test of the apico-basal targeting of the chimeric proteins, we expressed each in the polarized epithelial cells of the spermatheca (Fig 12C.1–E.1). Again, although the chimeric proteins appear to be associated with membranous compartments, (Fig 12C.1–E.1) they do not localize to the apical plasma membrane as observed for CATP-5::GFP (Fig 4C), and are possibly retained in the endoplasmic reticulum (ER).

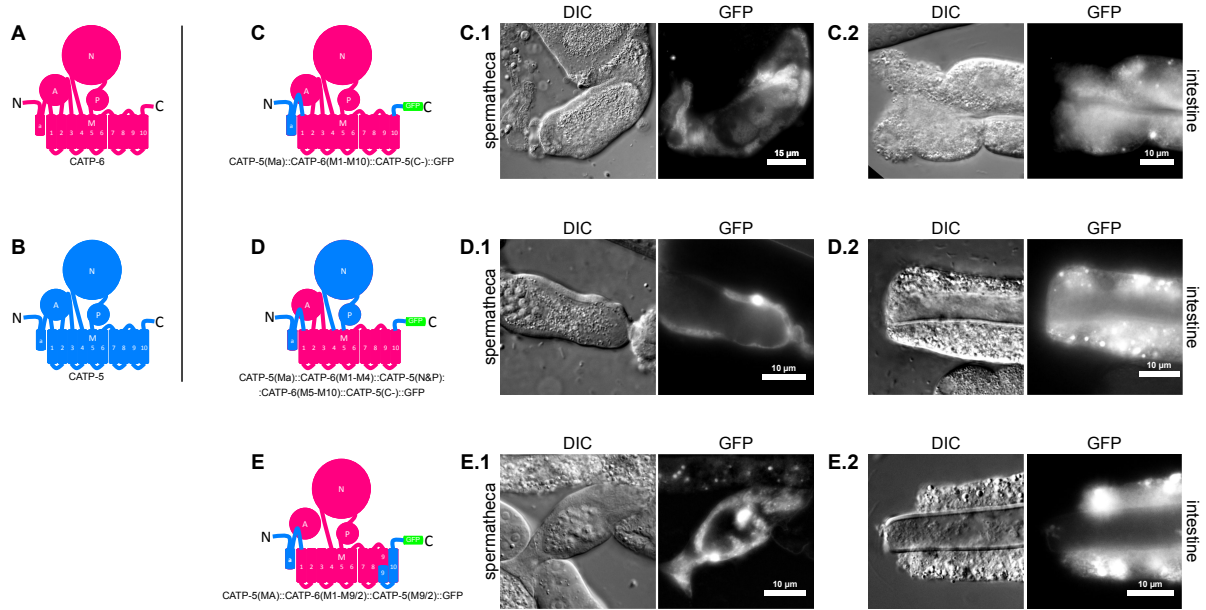


**Fig 12: Expression of chimeric fusion proteins of CATP-5 and CATP-6.** (A) Schematic protein structure of CATP-6. (B) Schematic protein structure of CATP-5. (C-E) Schematic protein structure of three distinct domain combinations of CATP-5 and CATP-6 fused to GFP. (C.1-E.1) Expression of chimeric fusion proteins in living spermatheca of *catp-5(tm4481)* mutant animals. Transgene expression from extra chromosomal arrays: (C.1) *Ex [P<sub>stb</sub>.catp-5(Ma)::catp-6(M1-M10)::catp-5(C-term)::gfp; rol-6(d)]*, (D.1) *Ex [P<sub>stb</sub>.catp-5(Ma)::catp-6(M1-M4)::catp-5(N&Pdomain)::catp-6(M5-M10)::catp-5(C-term)::gfp; rol-6(d)]*, (E.1) *Ex [P<sub>stb</sub>.catp-5(Ma)::catp-6(M1-M9<sub>1/2</sub>)::catp-5(M9<sub>1/2</sub>-M10)::gfp; rol-6(d)]*. (C.2-E.2) Expression of chimeric fusion proteins in cross sectioned living intestinal cells of *catp-5(tm4481)* mutant animals. Transgene expression from extra chromosomal arrays: (C.2) *Ex [P<sub>catp-5</sub>.catp-5(Ma)::catp-6(M1-M10)::catp-5(C-term)::gfp; rol-6(d)]*, (D.2) *Ex [P<sub>catp-5</sub>.catp-5(Ma)::catp-6(M1-M4)::catp-5(N&Pdomain)::catp-6(M5-M10)::catp-5(C-term)::gfp; rol-6(d)]*, (E.2) *Ex [P<sub>catp-5</sub>.catp-5(MA)::catp-6(M1-M9<sub>1/2</sub>)::catp-5(M9<sub>1/2</sub>-M10)::gfp; rol-6(d)]*.

## Discussion

### Common functions of *catp-6* and *catp-7* in the somatic gonad precursors

When we screened for mutations that block the ability of *gem-1(gf)* to suppress *gon-2(q388)*, we found multiple alleles *catp-6*, but no alleles of *catp-7* (Lambie *et al.* 2013). This suggests that *catp-6* is more important than *catp-7* for *gem-1* activity. In this study, we found that overexpression of *catp-7* is able to partially compensate for the absence of *catp-6* in a *gon-2(lf); catp-6(lf); gem-1(gf)* background. Since we can detect native CATP-7::GFP as well as native CATP-6::mKate2 expression in Z1 and Z4, we speculate that the key site of action for P5B ATPases in the somatic gonad precursors is the vesicular compartment to which CATP-6

localizes, and that when CATP-7 is overexpressed its concentration in this compartment increases via endocytosis and membrane trafficking.

How might the activities of CATP-6 and CATP-7 relate to those of GON-2 and GEM-1 within the gonad precursor cells? GON-2 is known to be permeable to both  $Mg^{2+}$  and  $Ca^{2+}$ , both of which are good candidates for promoting cell division (Berridge 1995; Sun and Lambie 1997; West *et al.* 2001; Teramoto *et al.* 2005; Rubin 2005; Xing *et al.* 2008; Wolf *et al.* 2008; Wolf and Trapani 2012; Humeau *et al.* 2018); however, the gonadogenesis defect of *gon-2(lf)* mutants can be partially suppressed by supplementation with  $Mg^{2+}$ , but not  $Ca^{2+}$  (Teramoto *et al.* 2005; Kemp *et al.* 2009; Teramoto *et al.* 2010). Although we have not demonstrated that GON-2 functions within the gonadal precursors themselves, this is the most parsimonious explanation for the mutant phenotype. Based on electrophysiological characterization of GON-2 activity within cultured intestinal cells, we know that GON-2 is strongly inhibited by physiological levels of free intracellular  $Mg^{2+}$  (Teramoto *et al.* 2005; Xing *et al.* 2008). With regard to GEM-1, we know that either a *gem-1(gf)* mutation or overexpression of wild type GEM-1 protein is sufficient to suppress *gon-2(lf)* (Kemp *et al.* 2009). Furthermore, *gem-1(gf)* can suppress *gon-2(0)*, suggesting that GEM-1 might promote (or directly mediate) cellular  $Mg^{2+}$  uptake in parallel to GON-2 (Kemp *et al.* 2009). Thus, considering only  $Mg^{2+}$  homeostasis, our data could be most simply explained by proposing that CATP-6 and CATP-7 promote (or directly mediate) transport of  $Mg^{2+}$  into a vesicular storage compartment, thus allowing the gonad precursors to build up their cellular stores of  $Mg^{2+}$  without inhibiting GON-2. CATP-6 and CATP-7 could also possibly mediate storage (and/or release, e.g., as antiporters) of other candidate transport substrates, such as  $Zn^{2+}$  or polyamines, since the actions of these molecules could synergize with those of cellular  $Mg^{2+}$  to promote cell divisions (Kihara and Snell 1957; Rowatt and Williams 1992; MacDonald 2000; Miller-Fleming *et al.* 2015).



### Overlapping functions of *catp-6* and *catp-7* in germline proliferation

In our previous study, we observed that *catp-7(dx189) catp-6(0)* double mutants exhibit synthetic defects in somatic gonad development, with spermathecal, sheath and uterine cells variably under-represented or absent (Zielich *et al.* 2018). Germline proliferation and gametogenesis are severely impaired even in animals where proximal and distal somatic gonadal tissues are present. This is consistent with the known dependency of the germline on interaction with the somatic gonad cells (McCarter *et al.* 1997; 1999; Starich *et al.* 2014). Since *catp-6* and *catp-7* are both expressed in the somatic gonad cells, the simplest explanation for these observations is that these two proteins function redundantly within these tissues. Here, we report that the *catp-7(dx189) catp-6(0)* sterile phenotype can be efficiently rescued by expression of either *catp-6::mKate2* or *catp-7::gfp* from an extrachromosomal array. This is consistent with a principal defect in somatic gonadal tissues, since expression from extrachromosomal arrays is usually silenced in the germ line. The sterile phenotype can also be rescued by driving expression of *catp-6::mKate2* using a promoter that is strongly expressed in the sheath cells, consistent with the idea that sheath cell dysfunction is a major contributor to the germline proliferation defect. Overall, our data support the idea that CATP-6 and CATP-7 can transport the same substrate(s) into the sheath cell cytoplasm. It is likely that CATP-6 and CATP-7 are functioning as transporters, rather than scaffolding proteins, since we found that catalytically inactive (autophosphorylation defective) versions of each protein fail to provide rescuing activity. The germline proliferation defect of *catp-7(dx189) catp-6(0)* animals could be due to a failure of the sheath cells to provide CATP-7/CATP-6 transport substrate to the germ line via gap junctions, or it could be due to a physiological defect of the sheath cells resulting from the absence of the activities of CATP-6 and CATP-7.

### **Overlapping functions of CATP-6 and CATP-5 in germline proliferation**

*catp-6(0); catp-5(0)* double mutants have nearly normal somatic gonad development, but germline proliferation is severely impaired. In this study, we found that germline proliferation can be rescued by targeted expression of *catp-6* within either the germ line or the gonadal sheath cells. In wt animals CATP-5 is expressed in the germ line, the DTCs and the spermatheca, but not in the sheath cells. Somatic expression of *catp-5* under the control of its native promoter (silenced in the germ line but expressed in DTCs and spermatheca) does not rescue sterility. However, expression of *catp-5* can rescue germline proliferation when targeted to either the germ line or to the sheath cells. Interestingly, overexpression of *catp-7* in the somatic gonad can also partially restore fertility to the *catp-6(0); catp-5(0)* double mutant. Therefore, it is likely that all three paralogous nematode P5B ATPases perform a common function within the gonad.

### **Integrated model for functions of CATP-5, CATP-6 and CATP-7 in the gonad**

We speculate that within the gonadal sheath cells, CATP-6 and CATP-7 function redundantly to accumulate transport substrate from the pseudocoelomic fluid. This substrate could then be transferred to the germ line via gap junctions. The germ line could also take up transport substrate directly from the pseudocoelomic fluid via CATP-5 and/or CATP-6. If all three proteins transport the same substrate(s), this raises the question of why native CATP-5 expression within the germ line is not sufficient to permit fertility in *catp-7(dx189) catp-6(0)* animals. However, the expression level of native CATP-5 within the germ line is very low, and probably not sufficient to mediate sufficient uptake of transport substrate. Notably, *catp-7(dx189) catp-6(0)* animals are not always sterile, whereas *catp-7(dx189) catp-6(0); catp-5(0)* animals are always sterile. Thus, CATP-5 does weakly compensate for the absence of CATP-6 and CATP-7 activity.

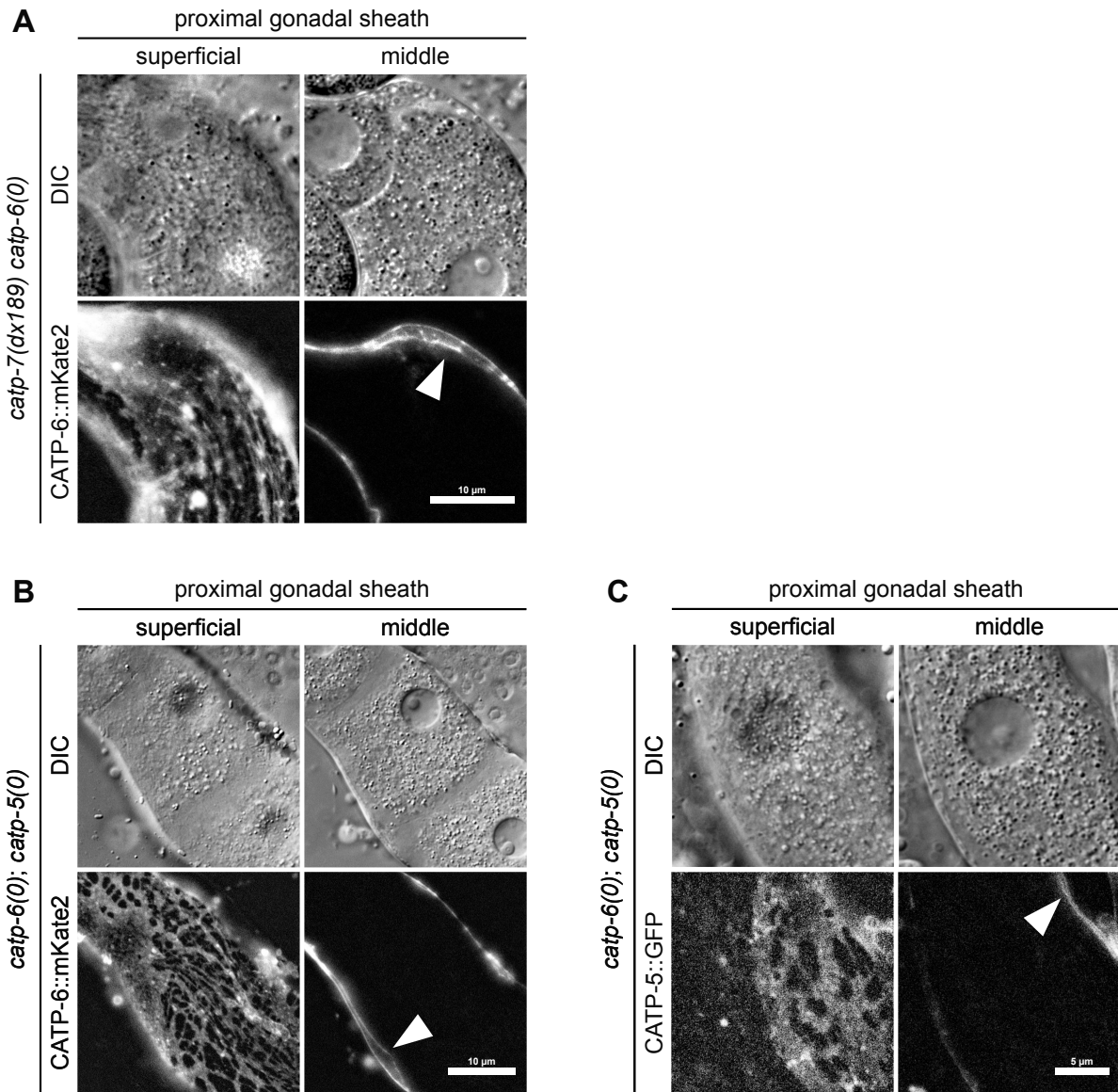
### **Polyamines as a candidate transport substrate**

In combination with the results of Heinick *et al.* (2010), our data suggest that one important function of the P5B transporters in *C. elegans* could be to supply polyamines to the germ line, primarily via a relay through the gonadal sheath cells. If this is correct, then it would indicate that the sheath cells and the germ line are unable to autonomously produce sufficient quantities of polyamines to enable normal development and function of the reproductive system. Additionally, our data suggest that the catalytic activity of CATP-5 is critical for reestablishing norspermidine sensitivity, consistent with a transport function rather than a scaffolding function such as that reported by Ruaud *et al.* (2007) for CATP-1.

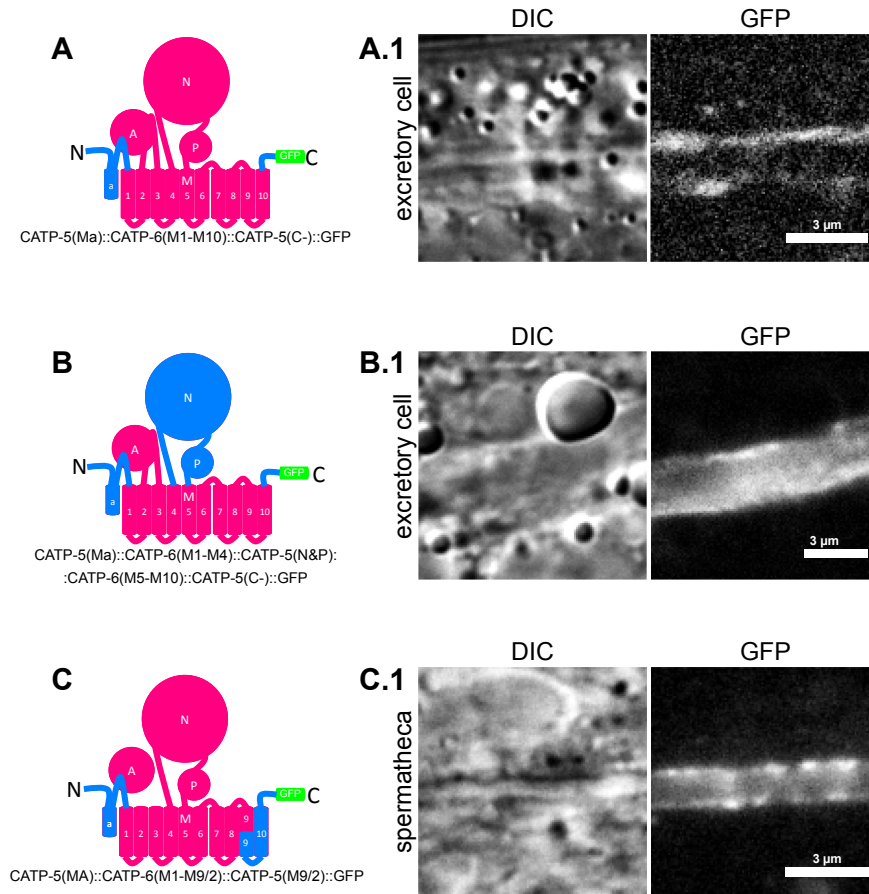
We attempted to determine whether the transport function of CATP-6 could substitute for that of CATP-5 in promoting polyamine uptake by the intestinal cells. However, the chimeric constructs that we tested were not targeted to the apical brush border, so we were not able to answer this question.

### **Acknowledgments**

Special thanks to Laura Besora Casals for generating plasmids  $P_{catp-6(D465N)::mKate2_{let-858}}$ . Some of the strains used in this study were provided by the CGC, which is funded by NIH Office of Research Infrastructure Programs (P40 OD010440), and the National BioResource Project (NBRP; <https://shigen.nig.ac.jp/c.elegans/>). This work was supported by a grant to E.J.L. (LA 3380/2-1) from the Deutsche Forschungsgemeinschaft. Additional funding was provided to B.C. by the Center for Integrated Protein Science Munich.



**S Fig 5: Proximal sheath cell expression of CATP-6::mKate2 and CATP-5::GFP.** Sheath cell specific expressed CATP-6::mKate2 (*Ex [P<sub>lim</sub>:catp-6::mKate2; rol-6(d)]*) rescues both double mutants ((A) *catp-7(dx189[delta 1492 bp Ma-M3 + gfp + loxP]) catp-6(ok3473)* IV and (B) *catp-6(ok3473)* IV; *catp-5(tm4481)* X). The transgene localizes to raft like structures on the plasma membrane of the sheath cells (superficial) as reported for native CATP-6 (Zielich *et al.* 2018) but not to the plasma membrane of diakinesis stage oocytes (middle). (C) Sheath cell specific expressed CATP-5::GFP (*Ex [P<sub>lim</sub>:catp-5::gfp; rol-6(d)]*) rescues *catp-6(ok3473)* IV; *catp-5(tm4481)* X. CATP-5::GFP localizes to raft like structures on the plasma membrane of the sheath cells (superficial) as reported for native CATP-6 and native CATP-7 (Zielich *et al.* 2018). Arrowheads: Transgene is expressed on both faces of the sheath cell (middle(A-C)).



**S Fig 6: Expression of chimeric fusion proteins of CATP-5 and CATP-6 in the excretory cell.** (A-C) Schematic protein structure of three distinct domain combinations of CATP-5 and CATP-6 fused to GFP. (A.1-C.1) Expression of chimeric fusion proteins in the excretory cell of *catp-5(tm4481)* mutant animals. Transgene expression from extra chromosomal arrays: (A.1) *Ex [P<sub>catp-5</sub>catp-5(Ma)::catp-6(M1-M10)::catp-5(C-term)::gfp; rol-6(d)]*, (B.1) *Ex [P<sub>catp-5</sub>catp-5(Ma)::catp-6(M1-M4)::catp-5(N&Pdomain)::catp-6(M5-M10)::catp-5(C-term)::gfp; rol-6(d)]*, (C.1) *Ex [P<sub>catp-5</sub>catp-5(MA)::catp-6(M1-M9<sub>1/2</sub>)::catp-5(M9<sub>1/2</sub>-M10)::gfp; rol-6(d)]*.



## Chapter 3

---

### **Novel Alleles of *gon-2*, a *C. elegans* Ortholog of Mammalian TRPM6 and TRPM7, Obtained by Genetic Reversion Screens**

Eric J. Lambie, Robert D. Bruce III, Jeffrey Zielich, Sonia N. Yuen

**Published: November 25, 2015. PLoS ONE 10: e0143445**

---

## RESEARCH ARTICLE

# Novel Alleles of *gon-2*, a *C. elegans* Ortholog of Mammalian TRPM6 and TRPM7, Obtained by Genetic Reversion Screens

Eric J. Lambie<sup>1\*</sup>, Robert D. Bruce, III<sup>2</sup>, Jeffrey Zielich<sup>1</sup>, Sonia N. Yuen<sup>3</sup>

**1** Department of Cell and Developmental Biology, Ludwig Maximilian University, Munich, Germany, **2** Dept. of Internal Medicine, Madigan Army Medical Center, Fort Lewis-McChord, Washington, United States of America, **3** Department of Otolaryngology, Boston Children's Hospital, Boston, Massachusetts, United States of America

\* [lambie@bio.lmu.de](mailto:lambie@bio.lmu.de)



## OPEN ACCESS

**Citation:** Lambie EJ, Bruce RD, III, Zielich J, Yuen SN (2015) Novel Alleles of *gon-2*, a *C. elegans* Ortholog of Mammalian TRPM6 and TRPM7, Obtained by Genetic Reversion Screens. PLoS ONE 10(11): e0143445. doi:10.1371/journal.pone.0143445

**Editor:** Shang-Zhong Xu, University of Hull, UNITED KINGDOM

**Received:** September 16, 2015

**Accepted:** November 4, 2015

**Published:** November 25, 2015

**Copyright:** This is an open access article, free of all copyright, and may be freely reproduced, distributed, transmitted, modified, built upon, or otherwise used by anyone for any lawful purpose. The work is made available under the [Creative Commons CC0](https://creativecommons.org/licenses/by/4.0/) public domain dedication.

**Data Availability Statement:** All relevant data are within the paper.

**Funding:** EJL was the recipient of National Institutes of Health grant R01GM49785. The funders had no role in study design, data collection and analysis, decision to publish, or preparation of the manuscript.

**Competing Interests:** The authors have declared that no competing interests exist.

## Abstract

TRP (Transient Receptor Potential) cation channels of the TRPM subfamily have been found to be critically important for the regulation of  $Mg^{2+}$  homeostasis in both protostomes (e.g., the nematode, *C. elegans*, and the insect, *D. melanogaster*) and deuterostomes (e.g., humans). Although significant progress has been made toward understanding how the activities of these channels are regulated, there are still major gaps in our understanding of the potential regulatory roles of extensive, evolutionarily conserved, regions of these proteins. The *C. elegans* genes, *gon-2*, *gtl-1* and *gtl-2*, encode paralogous TRP cation channel proteins that are similar in sequence and function to human TRPM6 and TRPM7. We isolated fourteen revertants of the missense mutant, *gon-2(q338)*, and these mutations affect nine different residues within GON-2. Since eight of the nine affected residues are situated within regions that have high similarity to human TRPM1,3,6 and 7, these mutations identify sections of these channels that are potentially critical for channel regulation. We also isolated a single mutant allele of *gon-2* during a screen for revertants of the  $Mg^{2+}$ -hypersensitive phenotype of *gtl-2(-)* mutants. This allele of *gon-2* converts a serine to phenylalanine within the highly conserved TRP domain, and is antimorphic against both *gon-2(+)* and *gtl-1(+)*. Interestingly, others have reported that mutation of the corresponding residue in TRPM7 to glutamate results in deregulated channel activity.

## Introduction

The TRP (Transient Receptor Potential) superfamily of eukaryotic cation channels comprises seven subfamilies: TRPA, TRPC, TRPM, TRPML, TRPN, TRPP and TRPV [1–3]. In all cases, channel activity is thought to result from the association of four subunits, each of which has six transmembrane domains (S1–S6), an S5–S6 pore-lining segment, and cytoplasmic N- and C-termini. The cytoplasmic N and C terminal domains that flank S1–S6 tend to be quite different between different TRP protein subfamilies, with the "TRP domain" (~25 aa immediately after



S6) being a notable exception. In some of the TRPM subfamily members, the most C-terminal region has acquired an enzymatic domain: TRPM2 has an ADP-ribose hydrolase domain [4], whereas TRPM6 [5, 6] and TRPM7 [7–9] have an alpha-kinase domain. These domains may play regulatory roles, but enzymatic activity per se is not required for channel activity [10–13].

The functions of different regions of TRP channels have been inferred through a variety of methods, including comparison with previously characterized protein motifs e.g., [4, 7, 14], sequencing of disease-causing alleles, e.g., [15–17], site-directed mutagenesis of candidate regulatory residues, e.g., [18–20], and *in vivo* selection for variants with altered activity, e.g., [21, 22]. Recently, high resolution structural data have been published for TRPV1 [23, 24] and TRPA1 [25], confirming the tetrameric structure prediction and highlighting the importance of the TRP domain for channel gating. The structural data also revealed additional sequences in TRPV1 and/or TRPA1 that are important for the regulation of channel activity, such as the "pre-S1 helix" and adjacent linker sequence, discussed further below. In the case of TRPM channels, relatively low resolution structural data are available for TRPM2, and these suggest extensive interactions between the N- and C-terminal cytoplasmic domains, similar to that reported for TRPA1 [26].

The genome of the nematode, *Caenorhabditis elegans*, contains three paralogous genes, *gon-2*, *gtl-1* and *gtl-2*, which encode cation channel proteins (GON-2, GTL-1 and GTL-2) that are similar to human TRPM6 and TRPM7, but lack the kinase domain. Like TRPM6 and TRPM7, the channels formed by GON-2, GTL-1 and GTL-2 are permeable to the divalent cations,  $\text{Ca}^{2+}$  and  $\text{Mg}^{2+}$ , and play a role in the systemic regulation of  $\text{Mg}^{2+}$  that is conserved in humans, *Drosophila* and nematodes [6, 27–31]. GON-2 and GTL-1 are both expressed in the intestine and act semi-redundantly to mediate the uptake of  $\text{Mg}^{2+}$  from the gut lumen. *gon-2(lf)*; *gtl-1(0)* (i.e., *gon-2* loss-of-function; *gtl-1* null) animals are unable to grow unless the medium is supplemented with high levels of  $\text{Mg}^{2+}$ . GON-2 probably also functions in the somatic gonad precursor cells, since these cells fail to proliferate in *gon-2(lf)* mutants [32]. GTL-2 is expressed in both the hypodermal cells and the excretory cell and is required for clearance of excess  $\text{Mg}^{2+}$  via the excretory system [31, 33]. *gtl-2(0)* mutants are unable to grow if the medium is supplemented with high levels of  $\text{Mg}^{2+}$ .

We have performed extensive genetic screens for mutations that suppress the gonadogenesis defect of *gon-2(q388ts)* mutants, and these resulted in the identification two new loci, *gem-1* [34] and *gem-4* [35]. During these screens, we also identified multiple intragenic suppressor mutations within *gon-2*, and these are described in this paper. We have also screened for mutations that suppress the  $\text{Mg}^{2+}$  sensitive phenotype of *gtl-2(0)* mutants, and this resulted in the identification multiple loss-of-function alleles of *gtl-1* [31], plus an unusual antimorphic allele of *gon-2*, which is described here. Together, these mutations in *gon-2* highlight a series of residues that are potentially important for TRPM channel regulation. In some cases, these are in regions of the protein that have been previously implicated in the regulation of TRP channel activity.

## Materials and Methods

### Nematode culture

*C. elegans* culture and genetic manipulations were performed essentially as described previously [31, 32, 34].

### Molecular biology

Standard methods were used to PCR amplify and sequence genomic DNA from *C. elegans*.

### Amino acid alignments

The software package CLC Main Workbench v. 6.6.5 ([www.clcbio.com](http://www.clcbio.com)) was used to perform amino acid alignments for graphical output.

### Strains

The following strains were used: CB4856 Wild type Hawaiian; LX929 *vsIs48[Punc-17::gfp]* X; EJ556 *gon-2(q388dx60) unc-29(e1072)* I; EJ557 *gon-2(q388dx65) unc-29(e1072)* I; EJ652 *unc-13(e51) gon-2(dx87)* I; EJ720 *gon-2(q388dx96) unc-29(e1072)* I; EJ922 *gon-2(q388dx116) unc-29(e1072)* I; EJ959 *gon-2(q388dx99) unc-29(e1072)* I; EJ1021 *gon-2(q388dx148)*; *gem-1(bc364)* I; EJ1110 *gon-2(q388)* I; EJ1173 *vsIs48[Punc-17::gfp]* N2/CB4856 hybrid X; EJ1190 *gon-2(q388)*; *vsIs48[Punc-17::gfp]*; EJ1191 *gon-2(q388dx146)*; *gem-1(bc364)* I; EJ1192 *unc-13(e51) gon-2(ok465)/unc-13(e51) lin-11(n566)* I; EJ1193 *gon-2(q388dx146)*; *gem-1(bc364)* I.

### Dosage testing

Strain LX929 *vsIs48[Punc-17::gfp]* X, which expresses GFP in all cholinergic neurons, was obtained from Michael Koelle (Yale University). LX929 (N2) males were mated with wild type CB4856 (Hawaiian) males, and *vsIs48* homozygous hermaphrodites were reisolated from the F2 to generate strain EJ1173. Males of this strain retain the vigorous mating ability of CB4856. EJ1173 males were crossed with *gon-2(q388)* hermaphrodites and *gon-2(q388); vsIs48* hermaphrodites were isolated from the F2 to generate strain EJ1190. These males are also vigorous maters and were used for the dosage experiments as follows. L4-stage hermaphrodites of genotype *gon-2(q388sup)* (i.e., intragenic revertant/suppressor alleles of *gon-2(q388)*) were incubated overnight at 23 C, then transferred to a cross plate containing multiple EJ1190 males. Incubation was continued at 23 C, and adults were transferred to a new plate after approximately 8 hrs, then removed 14 hours later. F1 hermaphrodite progeny were scored when they reached adulthood, with cross progeny uniquely identifiable due to the dominant *vsIs48* marker. Self progeny data were collected in parallel using GFP negative animals and/or plates where no cross was performed. All *gon-2(q388sup)* alleles except *dx116* were outcrossed once or more before testing suppression efficiency.

### Divalent cation depleted media (DCDM)

10 g of Agar (Carl Roth, Kobe I) was washed first with 500 ml of 20 mM EDTA, then three times with deionized water to remove most divalent cations. This was then used to prepare solid growth medium of the following final composition: 2% Agar, 4 mg/ml BactoTryptone (Difco), 25 mM HEPES pH7.4, 25 mM NaCl, 5 micrograms/ml cholesterol. 1M MgSO<sub>4</sub> and 1M CaCl<sub>2</sub> stock solutions were added in appropriate amounts for Mg<sup>2+</sup> and Ca<sup>2+</sup> supplementation experiments.

### Genetic characterization of *gon-2(dx87)* and comparison with *gon-2(ok465)*

Hermaphrodites of genotype *unc-13(e51) gon-2(ok465)/unc-13(e51) lin-11(n566)* were crossed with EJ1173 males and multiple non-Unc L4-stage hermaphrodites were transferred to DCDM plates and incubated at 23 C. *unc-13(e51) gon-2(ok465)* F2 hermaphrodites (distinguishable due to their sterility) were scored as adults. Essentially the same procedure was followed for *unc-13(e51) gon-2(dx87)/+ +* hermaphrodites, but F1s were not singled since all had the same genotype.

## Results and Discussion

### Reversion of *gon-2(q388)*

Although we isolated multiple loss-of-function alleles of *gon-2* during our initial characterization of this gene, most of our studies have utilized the *gon-2(q388)* allele [32]. This allele is advantageous, because all animals are fertile when raised at permissive temperature (15°–20°C), but nearly all (>90%) are gonadless (Gon)/sterile when raised at restrictive temperature (> 23°C). In dosage tests, *gon-2(q388)* exhibits very little activity at restrictive temperature. However, *gon-2(q388)* does evidently retain a low level of activity under restrictive conditions, because it can be suppressed by *gem-4(lf)* mutations, unlike the null/deletion allele, *gon-2(ok465)* [35]. *gon-2(q388)* converts a highly-conserved acidic residue (Glu) within the N-terminal cytoplasmic domain of GON-2 to a basic residue (Lys) (Fig 1) [36]. The results of reciprocal temperature shift experiments, suggest that *gon-2(q388)* probably affects a transient, irreversible process that is necessary for GON-2 stability, e.g., protein folding and/or channel assembly [32].

Intragenic revertants of *gon-2(q388ts)* were obtained by selecting for fertile derivatives at restrictive temperature after mutagenizing with EMS or 310 nm UV irradiation, essentially as described previously [34, 35]. Some screens included the *gem-1(bc364)* mutation, which enhances the penetrance of *gon-2(q388)* [34]. In the case of mutations that were found to be linked to *gon-2* during outcrossing, the *gon-2* coding sequence was PCR amplified and sequenced. The frequency of intragenic revertants was approximately  $5 \times 10^{-4}$  per mutagenized genome. We did not find any cases in which the *q388* mutation had directly reverted back to the wild type sequence. Possibly, this is because direct reversion would require a T → C transition mutation, which is not favored by either EMS or 310 nm UV treatment.

### Genetic characterization of intragenic revertants

The suppression efficiency of representative intragenic revertants was assessed by selfing homozygous *gon-2(q388sup)* hermaphrodites at restrictive temperature and scoring the gonadogenesis phenotype of the progeny. The efficiency of suppression ranges from 85% (*dx99*) to 100% (*dx146*) (Table 1). This group of intragenic revertant mutations was also tested for haplo-sufficiency by crossing homozygous *gon-2(q388sup)* hermaphrodites with *gon-2(q388)* males at restrictive temperature and scoring the offspring. *gon-2(q388)* has very little activity under these conditions, so this assay provides a good measure of dosage sensitivity of *gon-2(q388sup)* alleles. The strength of suppression among animals heterozygous for the suppressor alleles correlates well with the suppression efficiency measured for the homozygous strains (Table 1). In most cases, suppression efficiency is slightly lower when the intragenic revertant mutation is heterozygous, indicating that these alleles do not fully restore wild type gene function. However, *gon-2(q388dx146)* fully suppresses the gonadogenesis defect of *gon-2(q388)*, even when present in only a single dose.

### Molecular characterization of intragenic revertant mutations

The locations of mutant alleles of *gon-2* relative to the predicted protein topology are shown in Fig 1. Most sites were identified by only a single mutation, indicating that the screen is not near saturation. The codon for E996 appears to contain a mutational hotspot, since the identical C → T mutation was obtained independently as five different alleles, *dx115*, *dx116*, *dx129*, *dx130* and *dx147* (only *dx116* is indicated in Fig 1). Most of the revertant mutations are relatively near *gon-2(q388)* within the N-terminal cytoplasmic domain. Consistent with the idea that this area is preferentially affected, *dx148* (K991Q) and *dx65*(K991E) cause different alterations to a

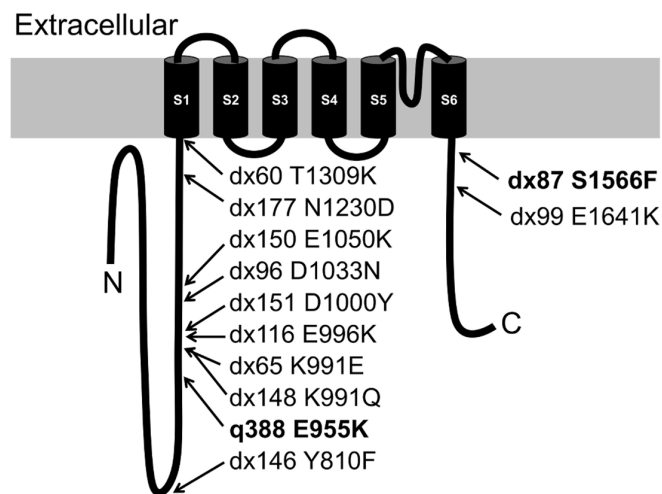


**Fig 1. Topology map of GON-2 (2032aa) with locations and aa changes of mutations.** The inactivating mutations, *q388* and *dx87*, are shown in bold.

doi:10.1371/journal.pone.0143445.g001

**Table 1. Dosage Testing of Intragenic Revertant Mutations.**

Allele Configuration	% Vul	% Evul	%WT	n
<i>gon-2(q388)/gon-2(q388)</i> <sup>1</sup>	93	5	2	553
<i>gon-2(q388dx60)/gon-2(q388dx60)</i> <sup>2</sup>	7	4	89	124
<i>gon-2(q388dx60)/gon-2(q388)</i>	11	8	81	132
<i>gon-2(q388dx99)/gon-2(q388dx99)</i> <sup>3</sup>	10	5	85	124
<i>gon-2(q388dx99)/gon-2(q388)</i>	24	15	51	164
<i>gon-2(q388dx116)/gon-2(q388dx116)</i> <sup>4</sup>	0	0	100	140
<i>gon-2(q388dx116)/gon-2(q388)</i>	0	5	95	153
<i>gon-2(q388dx146)/gon-2(q388dx146)</i> <sup>5</sup>	0	0	100	516
<i>gon-2(q388dx146)/gon-2(q388)</i>	0	0	100	583
<i>gon-2(q388dx65)/gon-2(q388dx65)</i> <sup>6</sup>	9	1	90	238
<i>gon-2(q388dx65)/gon-2(q388)</i>	23	8	69	159
<i>gon-2(q388dx148)/gon-2(q388dx148)</i> <sup>7</sup>	0	0.5	99	223
<i>gon-2(q388dx148)/gon-2(q388)</i>	0	1	99	257

Allele configuration is for animals derived from selfing or crosses, as described in Materials and Methods. Full genotypes of parental strains are listed in Materials and Methods. Vulvaless (Vul) animals have a severe gonadogenesis (Gon) phenotype, whereas Everted vulva (Evul) animals have a less severe defect in gonad development. Animals scored as wild type (WT) based on vulva morphology were also usually fertile.

<sup>1</sup> EJ1190

<sup>2</sup> EJ556

<sup>3</sup> EJ959

<sup>4</sup> EJ922

<sup>5</sup> EJ1193

<sup>6</sup> EJ557

<sup>7</sup> EJ1021

doi:10.1371/journal.pone.0143445.t001

single residue within this region. In each case, it is possible that the intragenic revertant mutation acts by somehow compensating for the effects of the *gon-2(q388)* mutation on protein folding/channel assembly. However, in the descriptions below, we focus on the potential significance of the mutations with regard to effects on channel activity that are independent of the effects *gon-2(q388)*.

**dx146.** This mutation alters a tyrosine residue that is also found in mammalian TRPM1,3,6,7 and *Drosophila* TRPM (DTRPM) (Fig 2). This is a candidate Src phosphorylation site YT [37] that could potentially affect channel localization, turnover, or inter-subunit interaction. Notably, the N-terminal cytoplasmic domain of TRPM6 contains multiple ankyrin-like domains that are likely to mediate interaction between channel subunits [38]. For example, the S141L mutation in human TRPM6 affects one of these ankyrin repeats and prevents channel subunit assembly, thus leading to hereditary  $Mg^{2+}$  deficiency [39].

**dx65, dx148.** These mutations both affect the same, highly conserved lysine residue (K991), relatively close to *gon-2(q388)* K955E (Fig 3). Lysines are candidate sumoylation sites, and sumoylation status is known to affect the activity of TRPM proteins [40]. However, this is probably not the basis for the effects of *dx65* and *dx148*, since they produce quantitatively different results (Table 1) even though each eliminates the candidate sumoylation site.

Additionally, of possible significance is the report by Stallmeyer et al. that in certain individuals with a putative gain-of-function mutation in TRPM4, a nearby conserved glycine is converted to serine (G582S; Fig 3) [41]. However, other amino acid alterations within TRPM4 were also present in these individuals, so it is uncertain whether G582S increases, decreases or has no effect on TRPM4 activity.

**dx116 and dx151.** These mutations affect residues immediately downstream of *dx65/dx148* (Fig 3), converting a moderately conserved glutamate to lysine (*dx116*, E996K) and a non-conserved aspartate to tyrosine (D1000Y).

**dx96 and dx150.** These affect a highly conserved acidic residue (*dx96* D1033N) and a non-conserved acidic residue (*dx150* E1050K) within a region that is important for TRPM6 activity (Fig 4). Jalkanen et al. identified the C707Y allele [42] and Lainez et al. identified the L708P allele [43] in patients with hypomagnesemia and secondary hypercalcemia (HSH). Lainez et al. found that the L7808P mutation severely impairs channel activity, but does not affect expression and trafficking, leading them to speculate that this region is required for proper interaction between channel subunits [43]. This region of TRPV1 forms a linker domain that is situated between the N-terminal ankyrin repeats and the pre-S1 helix [24]. Notably, G375 and G376 in TRPV1 mediate direct interaction between the linker domain and the N-terminal ankyrin repeats of adjacent subunits [24]. The sequence identity between TRPM and TRPV proteins is very low in this region; however, ankyrin-like repeats do exist in the N-terminal cytoplasmic domain of TRPM6 and 7 [38].

**dx177.** This mutation converts an asparagine to aspartate. No alignment is shown because the alteration occurs in a section of GON-2 that has similarity only to GTL-1.

**dx60.** This mutation converts an atypical threonine to lysine (Fig 5). Interestingly, this appears to represent a return to an ancestral state, since lysine is present at this position in GTL-2, as well as in the most closely related TRPM channels from mammals and *Drosophila*. *dx60* is situated at the end of the "pre-S1 helix" [24]. In TRPV1, this region interacts directly with the TRP domain, probably to maintain channel closure. Although this region of TRPM channels is not highly similar to TRPV1, it is predicted to have helical structure [44]. Therefore, *dx60* could potentially render the GON-2 channel more active by increasing its open probability. Of additional possible significance is that fact that pre-S1 helix region of GON-2 contains a sequence (QGTRKKIKMRRRFYEFYSAPI) that is predicted to bind to calmodulin (<http://calcium.uhnres.utoronto.ca/ctdb/ctdb/sequence.html>). Conceivably,



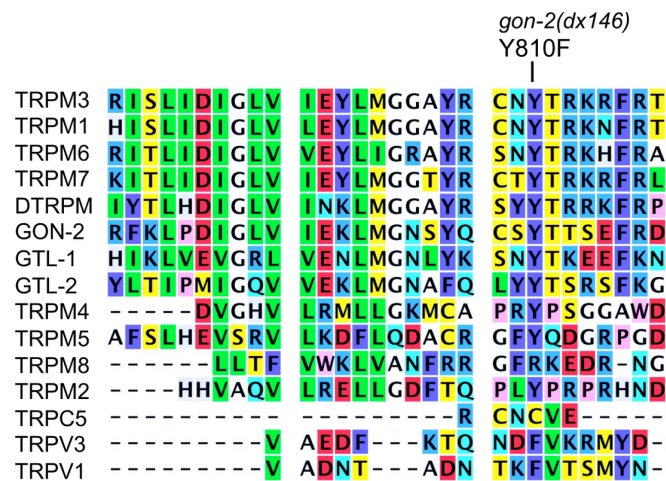


**Fig 2. Alignment of representative TRP channel protein sequences near the site of the *gon-2(dx146)* mutation.** The following GenBank accession numbers (or UniProt identifiers) were used to retrieve amino acid sequences of proteins shown in alignments. Human proteins: TRPV1 Q8NER1, TRPV3 Q8NET1, TRPC5 Q9UL62, TRPM1 NP\_001238949, TRPM2 XP\_011528036, TRPM3 NP\_060132, TRPM4 NP\_060106, TRPM5 NP\_055370, TRPM6 NP\_060132, TRPM7 NP\_060142, TRPM8 NP\_076985. *C. elegans* proteins: GON-2 CAB02303, GTL-1 CAA92726, GTL-2 CAB00861. *Drosophila melanogaster* protein: DTRPM A8DYE2.

doi:10.1371/journal.pone.0143445.g002

calmodulin could compete with the TRP domain for binding to the pre-S1 helix and this could explain the ability of low levels of cytoplasmic  $\text{Ca}^{2+}$  to activate GON-2 [45].

In the case of TRPM4, the pre-S1 helix interacts with phosphoinositides that modulate channel gating [46], so this is another protential regulatory mechanism that could be affected by *dx60*.

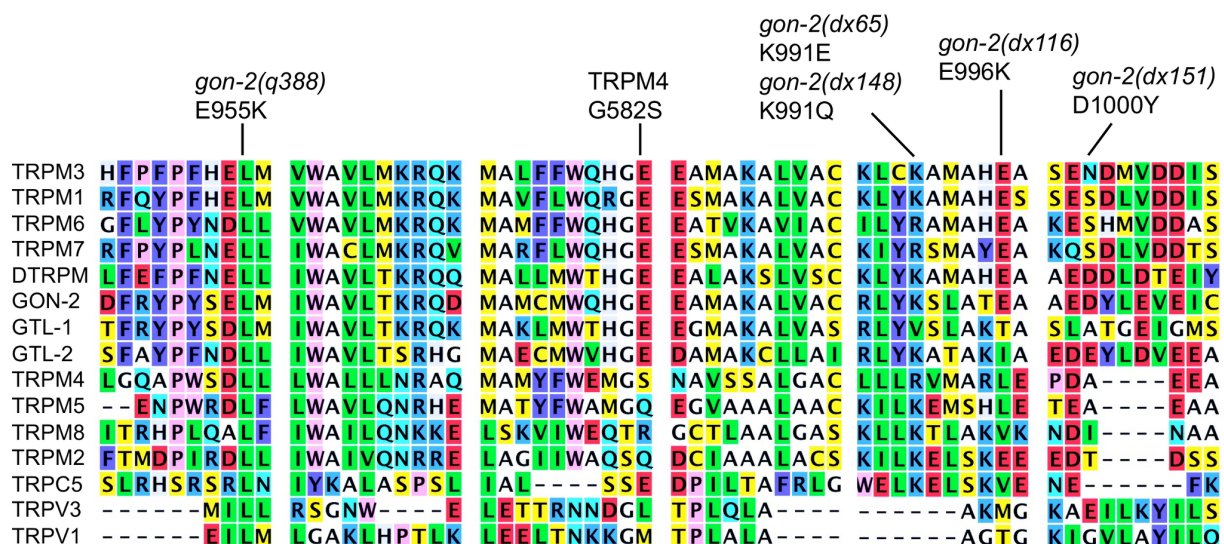


**Fig 3. TRP protein alignment from *gon-2(q388)* to *gon-2(dx151)*.**

doi:10.1371/journal.pone.0143445.g003

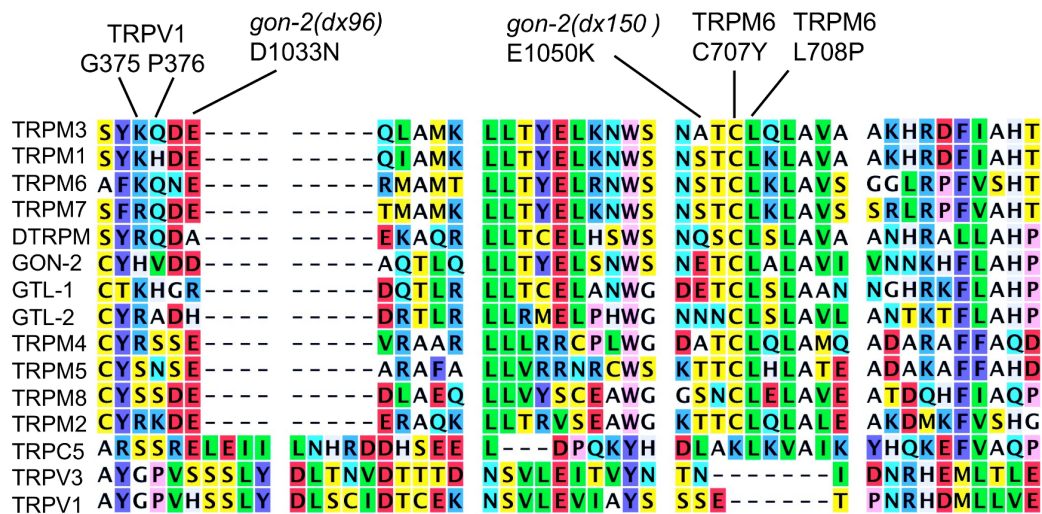


**Fig 4.** TRP protein alignment from *gon-2(dx96)*–*gon-2(dx150)*.

doi:10.1371/journal.pone.0143445.g004

Also of potential significance, Ubipred[47] predicts that 3 of the 8 high-confidence ubiquitylation sites in GON-2 (K1255, K1269 and K1272) are situated nearby. A decrease in ubiquitylation efficiency would be expected to result in increased channel expression on the plasma membrane [48–50].

**dx99.** This mutation converts a moderately conserved glutamate to lysine (Fig 6). This region of the protein is notable for multiple reasons. First, Lainez et al. identified the L1143P mutation of TRPM6 in a patient with HSH [43], and found that while the mutation severely impairs channel activity, it does not affect expression and/or trafficking. Second, two of the eight high-confidence candidate ubiquitylation sites within GON-2 are in this region, K1655 and K1659 [47]. Third, R721 of TRPV1 is required for channel activation by specific

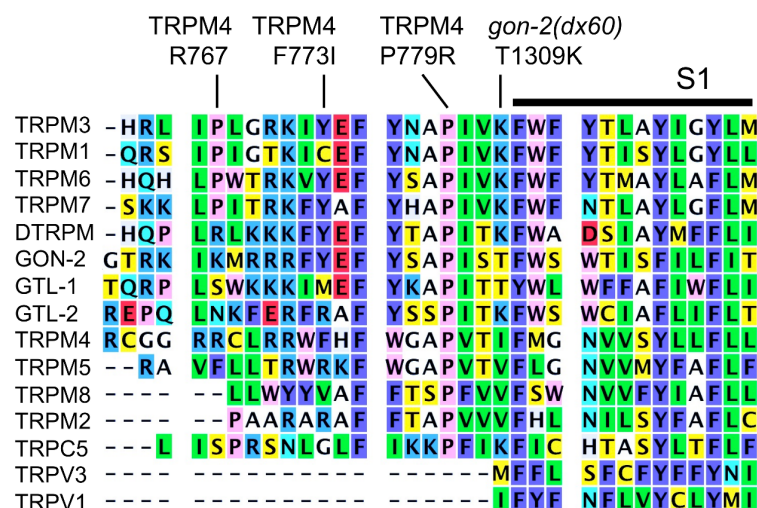


**Fig 5.** TRP protein alignment near *gon-2(dx60)*.

doi:10.1371/journal.pone.0143445.g005

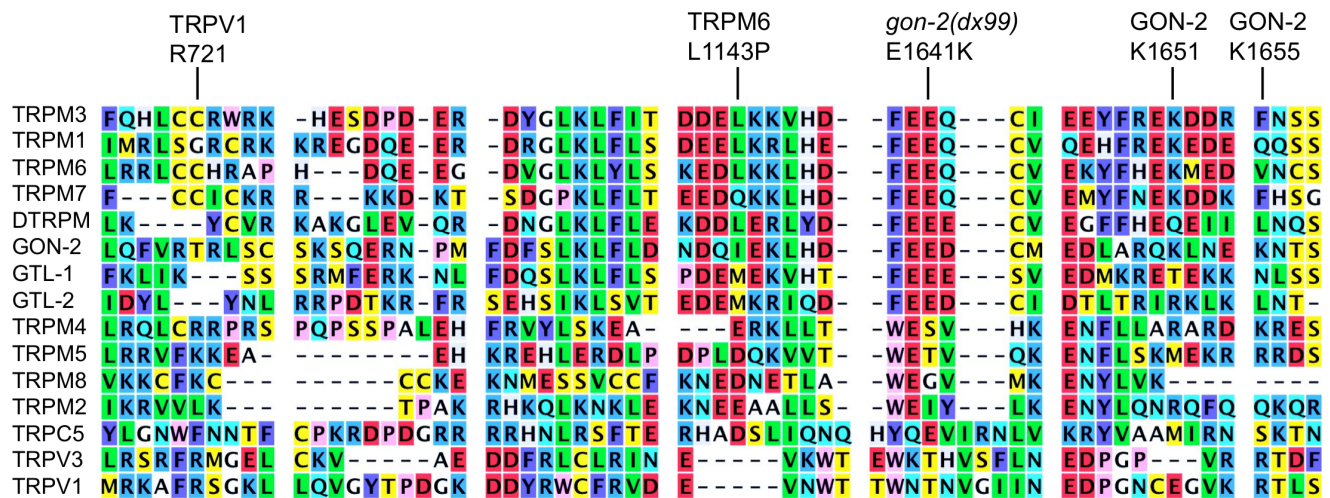


**Fig 6. TRP protein alignment near *gon-2(dx99)*.**

doi:10.1371/journal.pone.0143445.g006

phosphoinositides, probably via direct interaction [51]. The corresponding residue within GON-2 is situated within a high-confidence calmodulin binding sequence (LYHGVLILQFVR TRLSCKSKS; <http://calcium.uhnres.utoronto.ca/ctdb/ctdb/sequence.html>).

Several studies suggest that this region of GON-2 is likely to mediate direct interaction between channel subunits via the formation of coiled coils. Mei et al., showed that a predicted coiled-coil forming region of TRPM2 (beginning approximately 20 aa after the residue affected by *dx99*) is required for association between channel subunits [52, 53]. Fujiwara et al. [54] performed structural studies demonstrating that the corresponding region of TRPM7 can form anti-parallel coiled-coils. Finally, Paulsen et al. showed that an overlapping ~80 aa region of TRPA1 forms parallel coiled coils that mediate association between channel subunits [25]. When analyzed by JPRED4 [44], this region of TRPA1 is predicted to be mostly helical, but with multiple interruptions. Significantly, JPRED4 predicts that an 88 amino acid segment of GON-2 that includes the site of *dx99* (NDQIEKLHDFEEDCMEDLARQKLNEKNTSNEQRIL RADIRTDQILNRLIDLQAKESMGRDVINDVESRLASVEKAQNEILECVRALLN) is likely to be entirely helical except for a small gap (underlined residues). This is also true for TRPM6 and TRPM7, so this is likely to be a conserved structural feature that has the potential to mediate an extensive coiled-coil interaction between subunits. In summary, *dx99* could potentially affect *gon-2(q388)* activity by reducing ubiquitylation efficiency, altering affinity for regulatory phosphoinositides, or by potentiating successful channel assembly.

### Reversion of *gtl-2(0)*

*gtl-2(tm1463)* animals were mutagenized with EMS and then  $Mg^{2+}$ -resistant revertants were selected as described [31]. In the case of one of the revertant mutations, *dx154*, we observed Gon animals at high frequency during outcrossing. Through standard mapping and complementation testing we determined that *dx154* was an allele of *gon-2*. Upon sequencing the coding regions of *gon-2*, we found a single C->T mutation corresponding to *gon-2(dx154)*. This mutation is identical to *gon-2(dx87)*, which we identified in a previous screen for Gon mutants [36].

Two lines of evidence suggest that *gon-2(dx154)* is not a simple loss-of-function allele. First, the loss-of-function allele, *gon-2(q388)*, does not suppress the  $Mg^{2+}$  sensitivity of *gtl-2(tm1463)*



mutants. Second, we isolated only a single allele of *gon-2* in this screen, whereas we identified multiple loss-of-function alleles of *gtl-1*, a gene of similar size.

The ability of *gon-2(dx154)* to suppress *gtl-2(tm1463)* can be explained most simply if *gon-2(dx154)* produces an antimorphic protein that is capable of interfering with GTL-1 activity. This is consistent with the tetrameric structure of TRPM channels, and supports that idea that GON-2 and GTL-1 are able to form heterotetramers.

**Genetic characterization of *gon-2(dx87)*.** We used a stock carrying the *gon-2(dx87)* mutation (identical to *dx154*) to test whether this allele is able to interfere with the activity of *gon-2(+)*. In order to do this, we examined the *gon-2(dx87)* homozygous progeny of *gon-2(dx87)/+* heterozygous hermaphrodites, comparing these with *gon-2(0) (ok465)* homozygous progeny from *gon-2(0)/+* hermaphrodites (Table 2, lines 6 and 7). Due to maternally contributed *gon-2(+)* gene product, *gon-2(0)* homozygotes are almost always able to execute a sufficient number of gonadal cell divisions to generate an anchor cell, and thus induce the underlying hypodermal cells to produce a vulva. However, 100% of *gon-2(dx87)* homozygous progeny of a heterozygous mother are vulvaless. Therefore, *gon-2(dx87)* is able to interfere with *gon-2(+)* in addition to *gtl-1(+)*. *gon-2(dx87)* is not strongly antimorphic, because *gon-2(dx87)/gon-2(+)* progeny of a *gon-2(dx87)* homozygous mother always undergo normal development (Table 2, line 3).

One striking feature of *gon-2(dx87)* is that its effects on gonad development can be suppressed even by a low level of  $Mg^{2+}$  in the medium (1 mM; Table 2 lines 4–6). This is interesting, because it suggests that *gon-2(dx87)* homotetramers are able to permeate  $Mg^{2+}$  effectively into the gonad precursors. However, since *gon-2(dx154)* (= *dx87*) was isolated based on its ability to suppress the toxic hyperaccumulation of  $Mg^{2+}$  in *gtl-2(-)* animals that are grown on high  $Mg^{2+}$ , heterotetrameric complexes that contain both GON-2(dx87) and GTL-1 are probably significantly less active than heteromeric complexes that contain only wild type proteins.

**Possible mechanisms of action of *gon-2(dx87)*.** *dx87* converts a well-conserved serine within the TRP domain to a phenylalanine (Fig 7). Hofman et al. [55] showed that mutation of the corresponding serine residue of TRPM7 (S1107) to glutamate caused the channel to be constitutively active and insensitive to high concentrations (2 mM) of intracellular  $Mg^{2+}$ . Similarly, Luo et al. showed that changing E682 of TRPV3 to either glutamine or asparagine caused the channel to be significantly less sensitive to inhibition by intracellular  $Mg^{2+}$  [56]. Furthermore, Lin et al. identified the W692G of TRPV3 mutation in patients with Olmsted syndrome and showed that this mutation causes the channel to be constitutively active [57]. They suggested that, as in voltage-gated potassium channels, the region immediately C-terminal to S6 can interact with the S4–S5 cytoplasmic loop to maintain a closed channel state. In the case of TRPC5, Obhukov et al. [20], found that D633 and D636 mediate channel blockage by intracellular  $Mg^{2+}$  at positive voltages. Although these are not physiological conditions, these data again suggest that  $Mg^{2+}$  may interact directly with the TRP domain to maintain a closed channel state, possibly by promoting interactions between the TRP domain and one or more other cytoplasmic segments (S4–S5 loop, pre-S1 helix).

Additional factors are also likely to interact with the TRP domain. For example, Xie et al. [58] showed that R1088 of TRPM6 R1088 is required for full activation by PI(4,5)P<sub>2</sub>. Two other basic residues nearby are also important, but these are not conserved in GON-2. Furthermore, in the case of TRPV1, Poblete found that K694 interacts with phospho-head group of PI (4,5)P<sub>2</sub> [59].  $Ca^{2+}$  probably also interacts with the TRP domain; Yamaguchi et al. showed that mutation of either E1062 or D1039 reduced the activation of TRPM4 by intracellular  $Ca^{2+}$ , and argued that  $Ca^{2+}$  interacts directly with these residues [60]. It is also worth noting that Liu et al. found that the Brugada Syndrome L1075P allele of TRPM4 resulted in an increase in the amount of protein present on cell surface, suggesting a defect in endocytic trafficking [61].

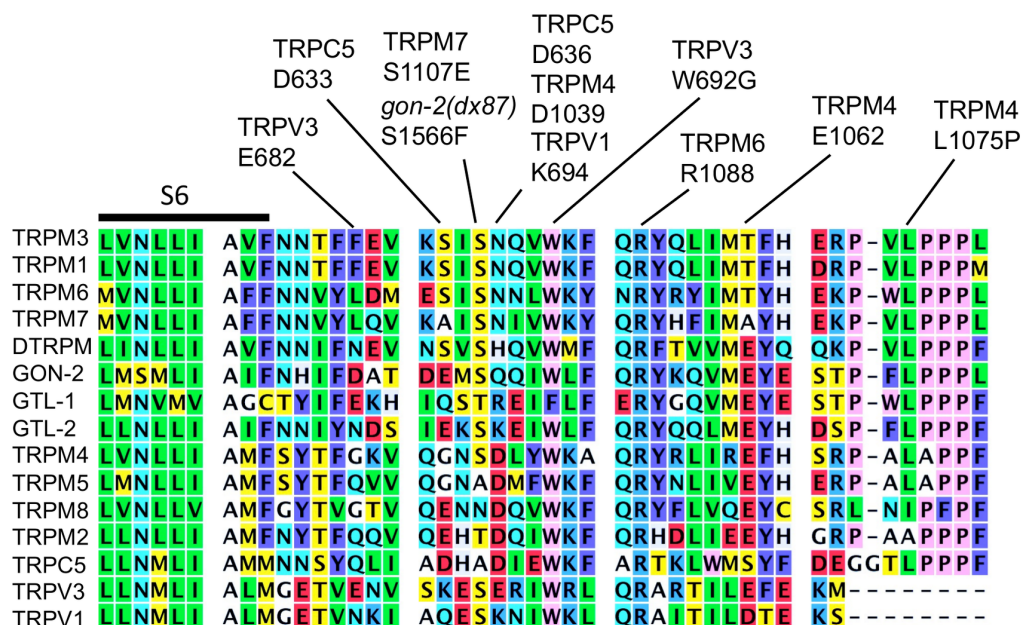
**Table 2. Effects of *gon-2(dx87)* on *gon-2(+)* Activity and in Response to Different Divalent Cation Concentrations.**

	Maternal Allele Configuration	Zygotic Allele Configuration	Mg <sup>2+</sup>	Ca <sup>2+</sup>	Gon	Evul	wt	n
1	<i>gon-2(dx87)/gon-2(+)</i>	<i>gon-2(dx87)/gon-2(dx87)</i>	0	0	95	4	1	81
2	<i>gon-2(ok465)/gon-2(+)</i>	<i>gon-2(ok465)/gon-2(ok465)</i>	0	0	3	12	85	103
3	<i>gon-2(dx87)/gon-2(dx87)</i>	<i>gon-2(dx87)/gon-2(+)</i>	0	0	0	0	100	151
4	<i>gon-2(dx87)/gon-2(dx87)</i>	<i>gon-2(dx87)/gon-2(dx87)</i>	0	0	100	0	0	253
5	<i>gon-2(dx87)/gon-2(dx87)</i>	<i>gon-2(dx87)/gon-2(dx87)</i>	1	0	0	3	97	177
6	<i>gon-2(dx87)/gon-2(dx87)</i>	<i>gon-2(dx87)/gon-2(dx87)</i>	10	0	0	0	100	425
7	<i>gon-2(dx87)/gon-2(dx87)</i>	<i>gon-2(dx87)/gon-2(dx87)</i>	1	10	89	5	5	340

Crossing schemes, full parental genotypes and culture conditions are described in Materials and Methods. Supplemental ion concentrations (in mM) are indicated. It should be noted that all strains were propagated on living *E. coli*, which contains at least trace amounts of Ca<sup>2+</sup> and Mg<sup>2+</sup>, even when grown on divalent cation depleted medium.

doi:10.1371/journal.pone.0143445.t002

Studies in *C. elegans*, indicate that GON-2 activity is regulated by each of the factors discussed above. Estevez et al. [45, 62] reported that outward currents through GON-2/GTL-1 (i.e., ORCa, [63]) are inhibited by submillimolar intracellular Mg<sup>2+</sup>, stimulated by relatively low intracellular Ca<sup>2+</sup> (11 nM), and inhibited by higher levels of intracellular Ca<sup>2+</sup> (250 nM). Based on steric considerations, they concluded that the likely site of inhibitory interaction with Ca<sup>2+</sup> is in close proximity to the plasma membrane/channel pore, i.e., possibly within the TRP domain. In a subsequent study from the same group, Xing et al., [64] showed that PLC gamma activates GON-2/GTL-1, and that this effect probably results from a decrease in the concentration of PI(4,5)P<sub>2</sub>. Their results also indicated that the inhibitory effects of PI(4,5)P<sub>2</sub> and Ca<sup>2+</sup> on GON-2/GTL-1 are independent, and thus probably mediated by separate sites on the channel. In a separate study, Teramoto et al. [30] performed electrophysiological characterization of

**Fig 7. TRP protein alignment near *gon-2(dx87)*.**

doi:10.1371/journal.pone.0143445.g007

cells isolated from *gon-2(-)* and *gtl-1(-)* animals, as well as physiological experiments with single and double mutant animals, and thus were able to ascribe specific properties to the individual GON-2 and GTL-1 channels. Their key findings were that the GON-2 channel is inhibited by intracellular  $Mg^{2+}$  levels above 1 mM, whereas GTL-1 is not inhibited even at 6 mM intracellular  $Mg^{2+}$ . *gon-2(-)* animals (which possess only GTL-1 activity) are relatively insensitive to growth inhibition by 10 mM  $Ca^{2+}$  in the medium, whereas *gtl-1(-)* mutants (which possess only GON-2 activity) grow very slowly under these conditions. Therefore, GON-2 is more sensitive than GTL-1 to inhibition by  $Ca^{2+}$ . Furthermore, the growth defect of *gtl-1(-)* mutants on 0 mM supplemental  $Mg^{2+}$  could be rescued by 5 mM EGTA, which preferentially chelates  $Ca^{2+}$ . It is unclear whether this inhibitory effect of  $Ca^{2+}$  is due to intracellular or extracellular effects on GON-2.

One simple explanation for the effects of *gon-2(dx87)* would be that it destroys a residue that facilitates intracellular exit of divalent cations from the channel pore. This would be a logical consequence of the removal of the polar serine residue and/or introduction of the bulky hydrophobic phenylalanine residue. Alternatively, *gon-2(dx87)* could increase the affinity of the TRP domain for binding by a negative regulator, e.g., PI(4,5)P<sub>2</sub>,  $Mg^{2+}$  or  $Ca^{2+}$ . Our data do not allow us to determine whether or not GON-2(dx87) is inhibited normally by intracellular  $Mg^{2+}$ . However, GON-2(dx87) is clearly sensitive to inhibition by  $Ca^{2+}$ , because the addition of 10 mM  $Ca^{2+}$  to medium that contains 1 mM  $Mg^{2+}$  causes an increase in the frequency of Gon animals from 0% to 89% (Table 2, line 7).

## Conclusions

In this study, we have identified seven evolutionarily conserved residues in the N-terminal cytoplasmic domain of GON-2, and one residue in the C-terminal cytoplasmic domain, as potentially important regulators of channel activity. Since each of these mutations was isolated as an intragenic revertant of the *gon-2(q388)* loss-of-function mutation, we do not know whether these mutations would affect channel activity when present in an otherwise wild type GON-2 protein. Furthermore, since our analyses are based on phenotypic output, we do not know the mechanism whereby these mutations affect channel activity, e.g., via altering protein folding, channel subunit trafficking, oligomeric assembly, or channel gating. We have also identified an unusual antimorphic allele of *gon-2* that converts a highly conserved serine residue within the TRP domain to phenylalanine. It is particularly intriguing that this Hofman et al. [55] showed that changing the corresponding residue of TRPM7 to glutamate resulted in a channel that was constitutively active, even in the presence of high intracellular  $Mg^{2+}$ . Therefore, this residue appears to be positioned at a key site involved in channel gating.

## Acknowledgments

The authors wish to thank Barbara Conradt for helpful discussions, plus use of laboratory equipment and space.

## Author Contributions

Conceived and designed the experiments: EJJ RDB JZ SNY. Performed the experiments: EJJ RDB JZ SNY. Analyzed the data: EJJ RDB JZ SNY. Contributed reagents/materials/analysis tools: EJJ RDB JZ SNY. Wrote the paper: EJJ JZ.

## References

1. Ramsey IS, Delling M, Clapham DE. An introduction to TRP channels. Annual review of physiology. 2006; 68:619–47. doi: [10.1146/annurev.physiol.68.040204.100431](https://doi.org/10.1146/annurev.physiol.68.040204.100431) PMID: [16460286](https://pubmed.ncbi.nlm.nih.gov/16460286/).

2. Venkatachalam K, Luo J, Montell C. Evolutionarily conserved, multitasking TRP channels: lessons from worms and flies. *Handbook of experimental pharmacology*. 2014; 223:937–62. doi: [10.1007/978-3-319-05161-1\\_9](https://doi.org/10.1007/978-3-319-05161-1_9) PMID: [24961975](https://pubmed.ncbi.nlm.nih.gov/24961975/); PubMed Central PMCID: PMC4340696.
3. Venkatachalam K, Montell C. TRP channels. *Annual review of biochemistry*. 2007; 76:387–417. doi: [10.1146/annurev.biochem.75.103004.142819](https://doi.org/10.1146/annurev.biochem.75.103004.142819) PMID: [17579562](https://pubmed.ncbi.nlm.nih.gov/17579562/); PubMed Central PMCID: PMC4196875.
4. Perraud AL, Fleig A, Dunn CA, Bagley LA, Launay P, Schmitz C, et al. ADP-ribose gating of the calcium-permeable LTRPC2 channel revealed by Nudix motif homology. *Nature*. 2001; 411(6837):595–9. doi: [10.1038/35079100](https://doi.org/10.1038/35079100) PMID: [11385575](https://pubmed.ncbi.nlm.nih.gov/11385575/).
5. Schlingmann KP, Weber S, Peters M, Niemann Nejsum L, Vitzthum H, Klingel K, et al. Hypomagnesemia with secondary hypocalcemia is caused by mutations in TRPM6, a new member of the TRPM gene family. *Nature genetics*. 2002; 31(2):166–70. doi: [10.1038/ng889](https://doi.org/10.1038/ng889) PMID: [12032568](https://pubmed.ncbi.nlm.nih.gov/12032568/).
6. Walder RY, Landau D, Meyer P, Shalev H, Tsolia M, Borochowitz Z, et al. Mutation of TRPM6 causes familial hypomagnesemia with secondary hypocalcemia. *Nature genetics*. 2002; 31(2):171–4. doi: [10.1038/ng901](https://doi.org/10.1038/ng901) PMID: [12032570](https://pubmed.ncbi.nlm.nih.gov/12032570/).
7. Runnels LW, Yue L, Clapham DE. TRP-PLIK, a bifunctional protein with kinase and ion channel activities. *Science*. 2001; 291(5506):1043–7. doi: [10.1126/science.1058519](https://doi.org/10.1126/science.1058519) PMID: [11161216](https://pubmed.ncbi.nlm.nih.gov/11161216/).
8. Montell-Zoller MK, Hermosura MC, Nadler MJ, Scharenberg AM, Penner R, Fleig A. TRPM7 provides an ion channel mechanism for cellular entry of trace metal ions. *The Journal of general physiology*. 2003; 121(1):49–60. PMID: [12508053](https://pubmed.ncbi.nlm.nih.gov/12508053/); PubMed Central PMCID: PMC2217320.
9. Ryazanova LV, Dorovkov MV, Ansari A, Ryazanov AG. Characterization of the protein kinase activity of TRPM7/ChaK1, a protein kinase fused to the transient receptor potential ion channel. *The Journal of biological chemistry*. 2004; 279(5):3708–16. doi: [10.1074/jbc.M308820200](https://doi.org/10.1074/jbc.M308820200) PMID: [14594813](https://pubmed.ncbi.nlm.nih.gov/14594813/).
10. Zhang Z, Yu H, Huang J, Faouzi M, Schmitz C, Penner R, et al. The TRPM6 kinase domain determines the Mg-ATP sensitivity of TRPM7/M6 heteromeric ion channels. *The Journal of biological chemistry*. 2014; 289(8):5217–27. doi: [10.1074/jbc.M113.512285](https://doi.org/10.1074/jbc.M113.512285) PMID: [24385424](https://pubmed.ncbi.nlm.nih.gov/24385424/); PubMed Central PMCID: PMC3931078.
11. Brandao K, Deason-Towne F, Zhao X, Perraud AL, Schmitz C. TRPM6 kinase activity regulates TRPM7 trafficking and inhibits cellular growth under hypomagnesian conditions. *Cellular and molecular life sciences: CMLS*. 2014; 71(24):4853–67. doi: [10.1007/s00018-014-1647-7](https://doi.org/10.1007/s00018-014-1647-7) PMID: [24858416](https://pubmed.ncbi.nlm.nih.gov/24858416/); PubMed Central PMCID: PMC4234683.
12. Knowles H, Li Y, Perraud AL. The TRPM2 ion channel, an oxidative stress and metabolic sensor regulating innate immunity and inflammation. *Immunologic research*. 2013; 55(1–3):241–8. doi: [10.1007/s12026-012-8373-8](https://doi.org/10.1007/s12026-012-8373-8) PMID: [22975787](https://pubmed.ncbi.nlm.nih.gov/22975787/).
13. Toth B, Iordanov I, Csanady L. Putative channel activity of TRPM2 cation channel is unrelated to pore gating. *Proceedings of the National Academy of Sciences of the United States of America*. 2014; 111(47):16949–54. doi: [10.1073/pnas.1412449111](https://doi.org/10.1073/pnas.1412449111) PMID: [25385633](https://pubmed.ncbi.nlm.nih.gov/25385633/); PubMed Central PMCID: PMC4250100.
14. Montell C, Rubin GM. Molecular characterization of the *Drosophila* trp locus: a putative integral membrane protein required for phototransduction. *Neuron*. 1989; 2(4):1313–23. PMID: [2516726](https://pubmed.ncbi.nlm.nih.gov/2516726/).
15. Reynolds DM, Hayashi T, Cai Y, Veldhuisen B, Watnick TJ, Lens XM, et al. Aberrant splicing in the PKD2 gene as a cause of polycystic kidney disease. *Journal of the American Society of Nephrology: JASN*. 1999; 10(11):2342–51. PMID: [10541293](https://pubmed.ncbi.nlm.nih.gov/10541293/).
16. Raychowdhury MK, Gonzalez-Perrett S, Montalbetti N, Timpanaro GA, Chasan B, Goldmann WH, et al. Molecular pathophysiology of mucopolipidosis type IV: pH dysregulation of the mucopolipin-1 cation channel. *Human molecular genetics*. 2004; 13(6):617–27. doi: [10.1093/hmg/ddh067](https://doi.org/10.1093/hmg/ddh067) PMID: [14749347](https://pubmed.ncbi.nlm.nih.gov/14749347/).
17. Schlingmann KP, Sassen MC, Weber S, Pechmann U, Kusch K, Pelken L, et al. Novel TRPM6 mutations in 21 families with primary hypomagnesemia and secondary hypocalcemia. *Journal of the American Society of Nephrology: JASN*. 2005; 16(10):3061–9. doi: [10.1681/ASN.2004110989](https://doi.org/10.1681/ASN.2004110989) PMID: [16107578](https://pubmed.ncbi.nlm.nih.gov/16107578/).
18. Li M, Du J, Jiang J, Ratzan W, Su LT, Runnels LW, et al. Molecular determinants of Mg<sup>2+</sup> and Ca<sup>2+</sup> permeability and pH sensitivity in TRPM6 and TRPM7. *The Journal of biological chemistry*. 2007; 282(35):25817–30. doi: [10.1074/jbc.M608972200](https://doi.org/10.1074/jbc.M608972200) PMID: [17599911](https://pubmed.ncbi.nlm.nih.gov/17599911/); PubMed Central PMCID: PMC3239414.
19. Brauchi S, Orta G, Mascayano C, Salazar M, Raddatz N, Urbina H, et al. Dissection of the components for PIP2 activation and thermosensation in TRP channels. *Proceedings of the National Academy of Sciences of the United States of America*. 2007; 104(24):10246–51. doi: [10.1073/pnas.0703420104](https://doi.org/10.1073/pnas.0703420104) PMID: [17548815](https://pubmed.ncbi.nlm.nih.gov/17548815/); PubMed Central PMCID: PMC1891241.
20. Obukhov AG, Nowicky MC. A cytosolic residue mediates Mg<sup>2+</sup> block and regulates inward current amplitude of a transient receptor potential channel. *The Journal of neuroscience: the official journal of*

- the Society for Neuroscience. 2005; 25(5):1234–9. doi: [10.1523/JNEUROSCI.4451-04.2005](https://doi.org/10.1523/JNEUROSCI.4451-04.2005) PMID: [15689561](https://pubmed.ncbi.nlm.nih.gov/15689561/).
21. Myers BR, Bohlen CJ, Julius D. A yeast genetic screen reveals a critical role for the pore helix domain in TRP channel gating. *Neuron*. 2008; 58(3):362–73. doi: [10.1016/j.neuron.2008.04.012](https://doi.org/10.1016/j.neuron.2008.04.012) PMID: [18466747](https://pubmed.ncbi.nlm.nih.gov/18466747/); PubMed Central PMCID: PMC2422846.
  22. Su Z, Zhou X, Haynes WJ, Loukin SH, Anishkin A, Saimi Y, et al. Yeast gain-of-function mutations reveal structure-function relationships conserved among different subfamilies of transient receptor potential channels. *Proceedings of the National Academy of Sciences of the United States of America*. 2007; 104(49):19607–12. doi: [10.1073/pnas.0708584104](https://doi.org/10.1073/pnas.0708584104) PMID: [18042709](https://pubmed.ncbi.nlm.nih.gov/18042709/); PubMed Central PMCID: PMC2148336.
  23. Cao E, Liao M, Cheng Y, Julius D. TRPV1 structures in distinct conformations reveal activation mechanisms. *Nature*. 2013; 504(7478):113–8. doi: [10.1038/nature12823](https://doi.org/10.1038/nature12823) PMID: [24305161](https://pubmed.ncbi.nlm.nih.gov/24305161/); PubMed Central PMCID: PMC4023639.
  24. Liao M, Cao E, Julius D, Cheng Y. Structure of the TRPV1 ion channel determined by electron cryo-microscopy. *Nature*. 2013; 504(7478):107–12. doi: [10.1038/nature12822](https://doi.org/10.1038/nature12822) PMID: [24305160](https://pubmed.ncbi.nlm.nih.gov/24305160/); PubMed Central PMCID: PMC4078027.
  25. Paulsen CE, Armache JP, Gao Y, Cheng Y, Julius D. Structure of the TRPA1 ion channel suggests regulatory mechanisms. *Nature*. 2015. doi: [10.1038/nature14871](https://doi.org/10.1038/nature14871) PMID: [26200340](https://pubmed.ncbi.nlm.nih.gov/26200340/).
  26. Maruyama Y, Ogura T, Mio K, Kiyonaka S, Kato K, Mori Y, et al. Three-dimensional reconstruction using transmission electron microscopy reveals a swollen, bell-shaped structure of transient receptor potential melastatin type 2 cation channel. *The Journal of biological chemistry*. 2007; 282(51):36961–70. doi: [10.1074/jbc.M705694200](https://doi.org/10.1074/jbc.M705694200) PMID: [17940282](https://pubmed.ncbi.nlm.nih.gov/17940282/).
  27. Alexander RT, Hoenderop JG, Bindels RJ. Molecular determinants of magnesium homeostasis: insights from human disease. *Journal of the American Society of Nephrology: JASN*. 2008; 19(8):1451–8. doi: [10.1681/ASN.2008010098](https://doi.org/10.1681/ASN.2008010098) PMID: [18562569](https://pubmed.ncbi.nlm.nih.gov/18562569/).
  28. Hofmann T, Chubanov V, Chen X, Dietz AS, Gudermann T, Montell C. Drosophila TRPM channel is essential for the control of extracellular magnesium levels. *PloS one*. 2010; 5(5):e10519. doi: [10.1371/journal.pone.0010519](https://doi.org/10.1371/journal.pone.0010519) PMID: [20463899](https://pubmed.ncbi.nlm.nih.gov/20463899/); PubMed Central PMCID: PMC2865541.
  29. Paravicini TM, Chubanov V, Gudermann T. TRPM7: a unique channel involved in magnesium homeostasis. *The international journal of biochemistry & cell biology*. 2012; 44(8):1381–4. doi: [10.1016/j.biocel.2012.05.010](https://doi.org/10.1016/j.biocel.2012.05.010) PMID: [22634382](https://pubmed.ncbi.nlm.nih.gov/22634382/).
  30. Teramoto T, Lambie EJ, Iwasaki K. Differential regulation of TRPM channels governs electrolyte homeostasis in the *C. elegans* intestine. *Cell metabolism*. 2005; 1(5):343–54. doi: [10.1016/j.cmet.2005.04.007](https://doi.org/10.1016/j.cmet.2005.04.007) PMID: [16054081](https://pubmed.ncbi.nlm.nih.gov/16054081/); PubMed Central PMCID: PMC2241660.
  31. Teramoto T, Sternick LA, Kage-Nakadai E, Sajjadi S, Siembida J, Mitani S, et al. Magnesium excretion in *C. elegans* requires the activity of the GTL-2 TRPM channel. *PloS one*. 2010; 5(3):e9589. doi: [10.1371/journal.pone.0009589](https://doi.org/10.1371/journal.pone.0009589) PMID: [20221407](https://pubmed.ncbi.nlm.nih.gov/20221407/); PubMed Central PMCID: PMC2833210.
  32. Sun AY, Lambie EJ. *gon-2*, a gene required for gonadogenesis in *Caenorhabditis elegans*. *Genetics*. 1997; 147(3):1077–89. PMID: [9383054](https://pubmed.ncbi.nlm.nih.gov/9383054/); PubMed Central PMCID: PMC1208235.
  33. Stawicki TM, Zhou K, Yochem J, Chen L, Jin Y. TRPM channels modulate epileptic-like convulsions via systemic ion homeostasis. *Current biology: CB*. 2011; 21(10):883–8. doi: [10.1016/j.cub.2011.03.070](https://doi.org/10.1016/j.cub.2011.03.070) PMID: [21549603](https://pubmed.ncbi.nlm.nih.gov/21549603/); PubMed Central PMCID: PMC4034270.
  34. Kemp BJ, Church DL, Hatzold J, Conradt B, Lambie EJ. *gem-1* encodes an SLC16 monocarboxylate transporter-related protein that functions in parallel to the *gon-2* TRPM channel during gonad development in *Caenorhabditis elegans*. *Genetics*. 2009; 181(2):581–91. doi: [10.1534/genetics.108.094870](https://doi.org/10.1534/genetics.108.094870) PMID: [19087963](https://pubmed.ncbi.nlm.nih.gov/19087963/); PubMed Central PMCID: PMC2644948.
  35. Church DL, Lambie EJ. The promotion of gonadal cell divisions by the *Caenorhabditis elegans* TRPM cation channel GON-2 is antagonized by GEM-4 copine. *Genetics*. 2003; 165(2):563–74. PMID: [14573470](https://pubmed.ncbi.nlm.nih.gov/14573470/); PubMed Central PMCID: PMC1462791.
  36. West RJ, Sun AY, Church DL, Lambie EJ. The *C. elegans gon-2* gene encodes a putative TRP cation channel protein required for mitotic cell cycle progression. *Gene*. 2001; 266(1–2):103–10. PMID: [11290424](https://pubmed.ncbi.nlm.nih.gov/11290424/).
  37. Prasad TS, Kandasamy K, Pandey A. Human Protein Reference Database and Human Proteinpedia as discovery tools for systems biology. *Methods in molecular biology*. 2009; 577:67–79. doi: [10.1007/978-1-60761-232-2\\_6](https://doi.org/10.1007/978-1-60761-232-2_6) PMID: [19718509](https://pubmed.ncbi.nlm.nih.gov/19718509/).
  38. Chubanov V, Gudermann T. Trpm6. *Handbook of experimental pharmacology*. 2014; 222:503–20. doi: [10.1007/978-3-642-54215-2\\_20](https://doi.org/10.1007/978-3-642-54215-2_20) PMID: [24756719](https://pubmed.ncbi.nlm.nih.gov/24756719/).
  39. Chubanov V, Waldegger S, Mederos y Schnitzler M, Vitzthum H, Sassen MC, Seyberth HW, et al. Disruption of TRPM6/TRPM7 complex formation by a mutation in the TRPM6 gene causes



- hypomagnesemia with secondary hypocalcemia. Proceedings of the National Academy of Sciences of the United States of America. 2004; 101(9):2894–9. doi: [10.1073/pnas.0305252101](https://doi.org/10.1073/pnas.0305252101) PMID: [14976260](https://pubmed.ncbi.nlm.nih.gov/14976260/); PubMed Central PMCID: PMC365716.
40. Kruse M, Schulze-Bahr E, Corfield V, Beckmann A, Stallmeyer B, Kurtbay G, et al. Impaired endocytosis of the ion channel TRPM4 is associated with human progressive familial heart block type I. The Journal of clinical investigation. 2009; 119(9):2737–44. doi: [10.1172/JCI38292](https://doi.org/10.1172/JCI38292) PMID: [19726882](https://pubmed.ncbi.nlm.nih.gov/19726882/); PubMed Central PMCID: PMC2735920.
  41. Stallmeyer B, Zumhagen S, Denjoy I, Duthoit G, Hebert JL, Ferrer X, et al. Mutational spectrum in the Ca(2+)-activated cation channel gene TRPM4 in patients with cardiac conduction disturbances. Human mutation. 2012; 33(1):109–17. doi: [10.1002/humu.21599](https://doi.org/10.1002/humu.21599) PMID: [21887725](https://pubmed.ncbi.nlm.nih.gov/21887725/).
  42. Jalkanen R, Pronicka E, Tynnismaa H, Hanauer A, Walder R, Alitalo T. Genetic background of HSH in three Polish families and a patient with an X;9 translocation. European journal of human genetics: EJHG. 2006; 14(1):55–62. doi: [10.1038/sj.ejhg.5201515](https://doi.org/10.1038/sj.ejhg.5201515) PMID: [16267500](https://pubmed.ncbi.nlm.nih.gov/16267500/).
  43. Lainez S, Schlingmann KP, van der Wijst J, Dworniczak B, van Zeeland F, Konrad M, et al. New TRPM6 missense mutations linked to hypomagnesemia with secondary hypocalcemia. European journal of human genetics: EJHG. 2014; 22(4):497–504. doi: [10.1038/ejhg.2013.178](https://doi.org/10.1038/ejhg.2013.178) PMID: [23942199](https://pubmed.ncbi.nlm.nih.gov/23942199/); PubMed Central PMCID: PMC3953905.
  44. Drozdetskiy A, Cole C, Procter J, Barton GJ. JPred4: a protein secondary structure prediction server. Nucleic acids research. 2015; 43(W1):W389–94. doi: [10.1093/nar/gkv332](https://doi.org/10.1093/nar/gkv332) PMID: [25883141](https://pubmed.ncbi.nlm.nih.gov/25883141/); PubMed Central PMCID: PMC4489285.
  45. Estevez AY, Strange K. Calcium feedback mechanisms regulate oscillatory activity of a TRP-like Ca<sup>2+</sup> conductance in *C. elegans* intestinal cells. The Journal of physiology. 2005; 567(Pt 1):239–51. doi: [10.1113/jphysiol.2005.091900](https://doi.org/10.1113/jphysiol.2005.091900) PMID: [15961418](https://pubmed.ncbi.nlm.nih.gov/15961418/); PubMed Central PMCID: PMC1474156.
  46. Bousova K, Jirku M, Bumba L, Bednarova L, Sulc M, Franek M, et al. PIP2 and PIP3 interact with N-terminus region of TRPM4 channel. Biophysical chemistry. 2015; 205:24–32. doi: [10.1016/j.bpc.2015.06.004](https://doi.org/10.1016/j.bpc.2015.06.004) PMID: [26071843](https://pubmed.ncbi.nlm.nih.gov/26071843/).
  47. Radivojac P, Vacic V, Haynes C, Cocklin RR, Mohan A, Heyen JW, et al. Identification, analysis, and prediction of protein ubiquitination sites. Proteins. 2010; 78(2):365–80. doi: [10.1002/prot.22555](https://doi.org/10.1002/prot.22555) PMID: [19722269](https://pubmed.ncbi.nlm.nih.gov/19722269/); PubMed Central PMCID: PMC3006176.
  48. Volland C, Galan JM, Urban-Grimal D, Devilliers G, Haguenaue-Tsapis R. Endocytosis and degradation of the uracil permease of *S. cerevisiae* under stress conditions: possible role of ubiquitin. Folia microbiologica. 1994; 39(6):554–7. PMID: [8550022](https://pubmed.ncbi.nlm.nih.gov/8550022/).
  49. Hicke L, Riezman H. Ubiquitination of a yeast plasma membrane receptor signals its ligand-stimulated endocytosis. Cell. 1996; 84(2):277–87. PMID: [8565073](https://pubmed.ncbi.nlm.nih.gov/8565073/).
  50. Hicke L, Dunn R. Regulation of membrane protein transport by ubiquitin and ubiquitin-binding proteins. Annual review of cell and developmental biology. 2003; 19:141–72. doi: [10.1146/annurev.cellbio.19.110701.154617](https://doi.org/10.1146/annurev.cellbio.19.110701.154617) PMID: [14570567](https://pubmed.ncbi.nlm.nih.gov/14570567/).
  51. Ufret-Vincenty CA, Klein RM, Collins MD, Rosasco MG, Martinez GQ, Gordon SE. Mechanism for phosphoinositide selectivity and activation of TRPV1 ion channels. The Journal of general physiology. 2015; 145(5):431–42. doi: [10.1085/jgp.201511354](https://doi.org/10.1085/jgp.201511354) PMID: [25918361](https://pubmed.ncbi.nlm.nih.gov/25918361/); PubMed Central PMCID: PMC4411251.
  52. Mei ZZ, Jiang LH. Requirement for the N-terminal coiled-coil domain for expression and function, but not subunit interaction of, the ADPR-activated TRPM2 channel. The Journal of membrane biology. 2009; 230(2):93–9. doi: [10.1007/s00232-009-9190-4](https://doi.org/10.1007/s00232-009-9190-4) PMID: [19652898](https://pubmed.ncbi.nlm.nih.gov/19652898/); PubMed Central PMCID: PMC2733183.
  53. Mei ZZ, Xia R, Beech DJ, Jiang LH. Intracellular coiled-coil domain engaged in subunit interaction and assembly of melastatin-related transient receptor potential channel 2. The Journal of biological chemistry. 2006; 281(50):38748–56. doi: [10.1074/jbc.M607591200](https://doi.org/10.1074/jbc.M607591200) PMID: [17060318](https://pubmed.ncbi.nlm.nih.gov/17060318/); PubMed Central PMCID: PMC1698503.
  54. Fujiwara Y, Minor DL Jr. X-ray crystal structure of a TRPM assembly domain reveals an antiparallel four-stranded coiled-coil. Journal of molecular biology. 2008; 383(4):854–70. doi: [10.1016/j.jmb.2008.08.059](https://doi.org/10.1016/j.jmb.2008.08.059) PMID: [18782578](https://pubmed.ncbi.nlm.nih.gov/18782578/); PubMed Central PMCID: PMC2630241.
  55. Hofmann T, Schafer S, Linseisen M, Sytik L, Gudermann T, Chubakov V. Activation of TRPM7 channels by small molecules under physiological conditions. Pflügers Archiv: European journal of physiology. 2014; 466(12):2177–89. doi: [10.1007/s00424-014-1488-0](https://doi.org/10.1007/s00424-014-1488-0) PMID: [24633576](https://pubmed.ncbi.nlm.nih.gov/24633576/).
  56. Luo J, Stewart R, Berdeaux R, Hu H. Tonic inhibition of TRPV3 by Mg<sup>2+</sup> in mouse epidermal keratinocytes. The Journal of investigative dermatology. 2012; 132(9):2158–65. doi: [10.1038/jid.2012.144](https://doi.org/10.1038/jid.2012.144) PMID: [22622423](https://pubmed.ncbi.nlm.nih.gov/22622423/); PubMed Central PMCID: PMC3423538.

57. Lin Z, Chen Q, Lee M, Cao X, Zhang J, Ma D, et al. Exome sequencing reveals mutations in TRPV3 as a cause of Olmsted syndrome. *American journal of human genetics*. 2012; 90(3):558–64. doi: [10.1016/j.ajhg.2012.02.006](https://doi.org/10.1016/j.ajhg.2012.02.006) PMID: [22405088](https://pubmed.ncbi.nlm.nih.gov/22405088/); PubMed Central PMCID: PMC3309189.
58. Xie J, Sun B, Du J, Yang W, Chen HC, Overton JD, et al. Phosphatidylinositol 4,5-bisphosphate (PIP (2)) controls magnesium gatekeeper TRPM6 activity. *Scientific reports*. 2011; 1:146. doi: [10.1038/srep00146](https://doi.org/10.1038/srep00146) PMID: [22180838](https://pubmed.ncbi.nlm.nih.gov/22180838/); PubMed Central PMCID: PMC3238349.
59. Poblete H, Oyarzun I, Olivero P, Comer J, Zuniga M, Sepulveda RV, et al. Molecular determinants of phosphatidylinositol 4,5-bisphosphate (PI(4,5)P2) binding to transient receptor potential V1 (TRPV1) channels. *The Journal of biological chemistry*. 2015; 290(4):2086–98. doi: [10.1074/jbc.M114.613620](https://doi.org/10.1074/jbc.M114.613620) PMID: [25425643](https://pubmed.ncbi.nlm.nih.gov/25425643/); PubMed Central PMCID: PMC4303662.
60. Yamaguchi S, Tanimoto A, Otsuguro K, Hibino H, Ito S. Negatively charged amino acids near and in transient receptor potential (TRP) domain of TRPM4 channel are one determinant of its Ca<sup>2+</sup> sensitivity. *The Journal of biological chemistry*. 2014; 289(51):35265–82. doi: [10.1074/jbc.M114.606087](https://doi.org/10.1074/jbc.M114.606087) PMID: [25378404](https://pubmed.ncbi.nlm.nih.gov/25378404/); PubMed Central PMCID: PMC4271215.
61. Liu H, Chatel S, Simard C, Syam N, Salle L, Probst V, et al. Molecular genetics and functional anomalies in a series of 248 Brugada cases with 11 mutations in the TRPM4 channel. *PloS one*. 2013; 8(1): e54131. doi: [10.1371/journal.pone.0054131](https://doi.org/10.1371/journal.pone.0054131) PMID: [23382873](https://pubmed.ncbi.nlm.nih.gov/23382873/); PubMed Central PMCID: PMC3559649.
62. Estevez AY, Roberts RK, Strange K. Identification of store-independent and store-operated Ca<sup>2+</sup> conductances in *Caenorhabditis elegans* intestinal epithelial cells. *The Journal of general physiology*. 2003; 122(2):207–23. doi: [10.1085/jgp.200308804](https://doi.org/10.1085/jgp.200308804) PMID: [12860924](https://pubmed.ncbi.nlm.nih.gov/12860924/); PubMed Central PMCID: PMC2229548.
63. Xing J, Yan X, Estevez A, Strange K. Highly Ca<sup>2+</sup>-selective TRPM channels regulate IP3-dependent oscillatory Ca<sup>2+</sup> signaling in the *C. elegans* intestine. *The Journal of general physiology*. 2008; 131(3):245–55. doi: [10.1085/jgp.200709914](https://doi.org/10.1085/jgp.200709914) PMID: [18299395](https://pubmed.ncbi.nlm.nih.gov/18299395/); PubMed Central PMCID: PMC2248719.
64. Xing J, Strange K. Phosphatidylinositol 4,5-bisphosphate and loss of PLCgamma activity inhibit TRPM channels required for oscillatory Ca<sup>2+</sup> signaling. *American journal of physiology Cell physiology*. 2010; 298(2):C274–82. doi: [10.1152/ajpcell.00394.2009](https://doi.org/10.1152/ajpcell.00394.2009) PMID: [19923421](https://pubmed.ncbi.nlm.nih.gov/19923421/); PubMed Central PMCID: PMC2822497.

### 3 General Discussion

The P5B ATPases are evolutionarily conserved transporters that function in humans to maintain normal neurological function. Animal genomes encode multiple P5B ATPases, which are likely to function redundantly in at least some contexts. This dissertation describes the use of the nematode *C. elegans* to investigate the functions of the full complement of paralogous P5B ATPases in a representative animal model. Chapter 1 aims to provide a basic characterization of the three paralogous *C. elegans* P5B ATPases with regard to phylogenetic relationship, tissue specific expression pattern, subcellular localization and phenotypic analyses of deficient animals. In Chapter 2, I describe the results of transgene complementation tests to rescue the corresponding phenotypes, assessment of whether the catalytic function is critical for biological function, and investigation of interchangeability. Chapter 3 describes novel alleles of *gon-2*, which encodes the *C. elegans* ortholog of the mammalian TRPM6 and TRPM7 cation channels. GON-2 protein interacts genetically with the P5B ATPase, CATP-6. Chapters 1 and 2 will be discussed together, followed by consideration of Chapter 3.

#### 3.1 Phylogenetic analysis of paralogous P5B ATPases

In Chapter 1, I described a phylogenetic analysis of paralogous P5B ATPases. The three *C. elegans* P5B ATPases display all of the signature motifs of P-type ATPases. The alignment shows a high degree of similarity within the putative substrate interaction region of M4, and a relatively high degree of similarity to human ATP13A2. In order to analyze the relationship of nematode P5B ATPases, I constructed a Maximum Likelihood (ML) tree of all corresponding orthologous aa sequences from *C. elegans*, five additional *Caenorhabditis* species (*C. japonica*, *C. brenneri*, *C. briggsae*, *C. latens* and *C. remanei*), more distant nematode species (*Pristionchus pacificus*, *Onchocerca flexuosa* and *Trichinella spiralis*) and *Drosophila melanogaster* as an outgroup. The ML tree shows that each *Caenorhabditis* species, except *C.*



*brenneri*, has one CATP-5-like, one CATP-6-like and one CATP-7-like P5B ATPase. The data suggest that *catp-6* and *catp-7* originated from the most recent gene duplication event, since CATP-6-like and CATP-7-like paralogs are more similar to each other than they are to the CATP-5-like paralogs. The close proximity of the *C. elegans catp-6* and *catp-7* genes on chromosome IV (0.52 cM distance) supports the idea of a relatively recent gene duplication event. The three paralogous P5B ATPases of *Pristionchus pacificus* do not group with the paralogous P5B ATPases of the Caenorhabditis clade, suggesting that the gene duplications are independent from each other. More distantly related nematodes, such as *Onchocerca flexuosa* and *Trichinella spiralis*, have only a single P5B ATPase. Therefore, I conclude that the Caenorhabditis P5B ATPases originated from a common ancestor and that the diversification occurred within the Caenorhabditis clade.

Recent phylogenetic data suggest that the invertebrate P5B ATPase clade is distinct from the vertebrate clade, indicating independent diversification events during evolution, supporting my findings (Sørensen *et al.* 2018). Remarkably, ATP13A2 appears to be more closely related to the invertebrate clade than to the ATP13A3 clade, prompting Sørensen *et al.* (2018) to hypothesize that ATP13A2 and ATP13A3 originated from a common ancestral gene early in the Deuterostomia clade. However, another explanation is that ATP13A2 and ATP13A3 were present in the last common ancestor of Deuterostomes and Protostomes, and that ATP13A3 was lost in the last common ancestor of the Protostomes.

### **3.2 Spatial and temporal expression patterns of *C. elegans* P5B ATPases**

By using CRISPR/Cas9 mediated recombination, I was able to tag each P5B ATPase of *C. elegans* at the endogenous locus with various fluorescent protein sequences. This enabled me to analyze the spatiotemporal expression patterns of native CATP-5, CATP-6 and CATP-7. I found that the *C. elegans* P5B ATPases are expressed in all major tissues. In some tissues, there are two P5B ATPases expressed, e.g., the excretory cell, the amphid neurons and the pharyngeal

muscles. In a few tissues, I found that all three paralogs are expressed, e.g. the intestinal cells, the DTCs and the spermatheca.

### 3.3 Subcellular localization of P5B ATPases

In human tissue culture cells ATP13A2 localizes to lysosomes, early and late endosomes/multi-vesicular bodies (MVBs) as well as recycling endosomes (Ramirez *et al.* 2006; Kong *et al.* 2014; Holemans *et al.* 2015; Sørensen *et al.* 2018). ATP13A3 was shown to localize to recycling endosomes, late endosomes and lysosomes (Sørensen *et al.* 2018). Ectopically expressed ATP13A4 was detected in association with the endoplasmic reticulum (ER) (Vallipuram and Grenville 2010). In contrast, endogenous ATP13A4 was detected in early and late endosomes (Sørensen *et al.* 2018).

In order to determine the vesicular compartment to which CATP-6 localizes in living nematodes, I used various subcellular markers and assayed for colocalization. When I drove expression of a C-terminal RFP-tagged version of LMP-1 (the *C. elegans* ortholog of LAMP1) in neurons, I observed strong colocalization with native CATP-6::GFP. However, in these cells, LMP-1::RFP and CATP-6::GFP were localized on the plasma membrane, rather than a vesicular compartment. The inappropriate localization of LMP-1 is likely due to masking of a lysosomal targeting signal by the C-terminal RFP tag. It is less obvious why overexpression of LMP-1::RFP caused incorrect localization of CATP-6::GFP. This could be due to direct physical interaction between the two proteins, or it could be due to a more general defect in membrane trafficking caused by high-level expression of the LMP-1 fusion protein. I did not observe substantial colocalization of CATP-6::GFP with the endosomal markers citrine::HGRS-1 and SS::GFP::CD4-HCIMPR, or the trans-Golgi network marker, TGN-38::GFP.

In the spermatheca I also observed colocalization between LMP-1::RFP (driven by the *sth-1* promoter) and native CATP-6::GFP, although in this case both proteins were localized on

vesicular membranes. These vesicles were obviously larger than the CATP-6::GFP positive vesicles in animals that do not express LMP-1::RFP, thus casting doubt on whether LMP-1 and CATP-6 are normally colocalized. Indeed, when I performed immunostainings for native CATP-6::GFP and native LMP-1 the two proteins were not colocalized in spermathecal cells. I did not observe substantial localization of CATP-6 to recycling endosomes marked by RME-1 or RAB-11, but CATP-6 localization does display obvious similarity to that of the early endosomal marker RFP::RAB-5. To establish whether RAB-5 and CATP-6 colocalize at the level of individual vesicles, higher resolution imaging will be necessary.

Based on their similarity to other P-type ATPases, it is likely that the P5Bs act as transporters that are crucial for the homeostasis of one or more substrates. The phylogenetic data and the partly distinct spatiotemporal expression patterns suggest that each P5B ATPase could potentially fulfill the same transporter function, but in different tissues or subcellular locations. This is consistent with the idea that the *C. elegans* P5B ATPases are currently in the process of functional diversification (Marques *et al.* 2008).

### **3.4 The transport substrate(s) of P5B ATPases**

The identity of the transport substrate(s) of the *C. elegans* P5B ATPases remains elusive. Various candidates for the transport substrate of P5B ATPases have been proposed based on biological evidence, but none of these has been definitively demonstrated. In the yeast, *Saccharomyces cerevisiae*, YPK9 was suggested to be involved in sequestering  $\text{Cd}^{2+}$ ,  $\text{Mn}^{2+}$ ,  $\text{Ni}^{2+}$  and  $\text{Se}^{2+}$  into the vacuole, therefore protecting against toxic effects in the cytosol (Schmidt *et al.* 2009). ATP13A2 deficient mice were shown to have an increased sensitivity towards supplemental  $\text{Mn}^{2+}$ , suggesting a role in  $\text{Mn}^{2+}$  homeostasis (Fleming *et al.* 2018). In mammalian tissue culture cells, loss of ATP13A2 function results in increased sensitivity to extracellular  $\text{Zn}^{2+}$  stress by and cytosolic  $\text{Zn}^{2+}$  concentrations are elevated, suggesting that this P5B might play a role in  $\text{Zn}^{2+}$  homeostasis (Tsunemi and Krainc 2014). Although it could be recently confirmed

that ectopically expressed ATP13A2 in mammalian tissue culture cells protects against the toxic effects of  $\text{Zn}^{2+}$  and  $\text{Mn}^{2+}$ , the authors did not find any evidence that either  $\text{Zn}^{2+}$  or  $\text{Mn}^{2+}$  is the direct transport substrate of ATP13A2 (Holemans *et al.* 2015; Martin *et al.* 2016). On the other hand, ATP13A2 and ATP13A3 have been suggested to be candidate polyamine transporters (de Tezanos Pinto *et al.* 2012; La Hera *et al.* 2013; Madan *et al.* 2016).

CATP-6 was originally implicated in  $\text{Mg}^{2+}$  homeostasis of the somatic gonad precursors, since proper CATP-6 function is critical for enabling *gem-1(gf)* to suppress *gon-2(lf)* (Lambie *et al.* 2013). In line with  $\text{Mg}^{2+}$  as a potential substrate, the amoebal P5B-ATPase, Kil2 of *Dictyostelium discoideum* is essential for  $\text{Mg}^{2+}$  dependent killing of ingested *Klebsiella pneumoniae* (Lelong *et al.* 2011).

With regard to the nematode P5Bs, the data of Heinick *et al.* (2010) suggest that polyamines are transported from the gut lumen into the intestinal cells via CATP-5 expressed on the apical brush boarder. I was able to reproduce the observation of Heinick *et al.* (2010) that norspermidine sensitivity can be restored to *catp-5(0)* mutant animals by expressing CATP-5::GFP. Furthermore, I found that catalytic activity of CATP-5 is critical for restoration of norspermidine sensitivity, indicating that transporter activity (or at least conformational change) is required for CATP-5 function.

### 3.5 P5B ATPase expression in the *C. elegans* reproductive system

I found that all of the *C. elegans* P5B ATPases are expressed in various tissues of the reproductive system in patterns that are both dynamic and overlapping. Each of the P5Bs is able to localize to internal membranous structures or to the plasma membrane in certain tissues and stages of development.

In the germ line, CATP-6::FP clearly localizes to the germ cell plasma membranes in the pachytene region, colocalizing with the membrane marker *ltIs44(P<sub>pit-1</sub>mCherry::ph<sup>PLC</sup><sup>δ</sup>)*. In spermatocytes, CATP-7 localizes to the plasma membrane and CATP-6 localizes to

tubular/vesicular structures close the rachis, suggesting that CATP-6 might be endocytosed in this area. The data show that CATP-6 and CATP-7 each can localize to the plasma membrane, indicating that CATP-5 is not unique among the P5B ATPases in this respect (Heinick *et al.* 2010). I also detected very weak germline expression of native GFP::CATP-5. This is consistent with RNA-seq data from the Kimble lab, which show that *catp-7* mRNA is 35-fold and *catp-6* is 370-fold higher expressed than *catp-5* mRNA in feminized gonads ((Ortiz *et al.* 2014); RNA isolated from somatic cells and germ cells).

All three P5B ATPases are expressed in the DTCs and the spermatheca. But only CATP-6 and CATP-7 are expressed on the plasma membrane of the gonadal sheath cells, which surround the bulk of the germ line. The strong expression of CATP-5, CATP-6 and CATP-7 in the reproductive system suggests that P5B ATPases play a crucial role in its development and function.

### **3.6 Overlapping functions of *catp-5*, *catp-6* and *catp-7* in fertility**

I analyzed the phenotypes of multiple genotypes of P5B ATPase deficient animals. Although each of the single mutants, *catp-5(0)*, *catp-6(0)* and *catp-7(0)* is viable and fertile, I observed distinct reproductive system defects and very low brood sizes in the *catp-6(0); catp-5(0)* and *catp-7(dx189) catp-6(0)* double mutants. This indicates that *catp-6* functions redundantly with each of the other P5Bs. However, the *catp-7(0); catp-5(0)* double mutant has normal fertility (and is overall very similar to wt) indicating that *catp-6* alone is sufficient for the majority of the functions performed by P5B ATPases in *C. elegans*. The *catp-7(dx189) catp-6(0); catp-5(0)* triple mutant is viable, but completely sterile.

#### **3.6.1 Redundancy of *catp-5* and *catp-6***

*catp-6(0); catp-5(0)* double mutants, have nearly normal somatic gonad development, but exhibit delayed germline proliferation and have very small brood sizes. This indicates that

CATP-7 alone is not sufficient to ensure fertility. On the other hand, since the somatic gonad appears to be nearly normal, CATP-7 appears to be largely sufficient for normal development of the somatic tissues.

The fertility defect of *catp-6(0); catp-5(0)* double mutants can be rescued by targeted expression of either *catp-5::gfp* or *catp-6::gfp* within either the germ line or the gonadal sheath cell. These results suggest that CATP-5 and CATP-6 perform the same biological functions and are consistent with the known physiological coupling between the gonadal sheath cells and the germ line (Starich *et al.* 2014). Interestingly, I also found that overexpression of CATP-7::GFP within the gonadal sheath cells is able to partially restore fertility in *catp-6(0); catp-5(0)* double mutants, supporting the idea that all three of the nematode P5Bs perform the same biological functions.

### 3.6.2 Redundancy of *catp-6* and *catp-7*

*catp-7(dx189) catp-6(0)* double mutants are usually sterile, exhibiting variably severe defects in somatic gonad development, with multiple tissues under-represented or absent. Gametogenesis and germline proliferation are also severely impaired. Consistent with a major defect in somatic gonadal tissues, the *catp-7(dx189) catp-6(0)* sterile phenotype can be rescued by expression of either *catp-6::mKate2* or *catp-7::gfp* from an extrachromosomal array. Furthermore, the sterile phenotype can be rescued by sheath cell specific expression of *catp-6::mKate2*, suggesting that the primary function of CATP-6 and CATP-7 is within the sheath cells.

Rescue requires catalytically active CATP-6::mKate2 or CATP-7::GFP which suggests that pumping activity (or at least conformational change) is necessary for each protein to function. On the other hand, I observe weak rescue (16% fertility; not statistically significant) if I express catalytically inactive CATP-7(D497N)::GFP in *catp-7(dx189) catp-6(0)* mutant animals. It is possible that there could be very weak transport substrate flux even without

phosphorylation of the transporter, as has been suggested for the SERCA pump (Sorenson 1983; Champeil 1996).

It is known that germline proliferation is dependent on the presence of somatic gonadal tissues. Laser ablation of the sheath/spermathecal precursor cells leads to reduced germline proliferation and to undifferentiated germ cells that arrest in the pachytene stage of meiosis. (McCarter *et al.* 1997). Thus, the absence of sheath cells would be sufficient to explain the sterile phenotype of *catp-7(dx189) catp-6(0)* double mutants. However, I observed impaired germline proliferation even in animals where multiple sheath cells were present, suggesting that sheath cell function itself is somehow defective in *catp-7(dx189) catp-6(0)* animals.

### **3.6.3 An integrated model for the functions of the *C. elegans* P5Bs within the hermaphrodite gonad**

Given the redundancy of CATP-5, CATP-6 and CATP-7 within the tissues of the reproductive system, it is likely that all three nematode P5B ATPases fulfill the same biological functions, but in somewhat different temporal and spatial contexts. Since gap junctions are formed between the gonadal sheath cells and the germ cells, there is continuity between the cytosol of the sheath cells and the germ line (and DTCs) (Starich *et al.* 2014). Thus, the simplest model would be that each P5B acts to pump some crucial factor into the cytosol from the extracellular fluid. Consequently, the germ line could obtain P5B transport substrates either by direct uptake or by transfer from the sheath cells.

I speculate that CATP-6 and CATP-7 function redundantly within the gonadal sheath cells to accumulate an unknown transport substrate from the pseudocoelomic fluid, and this substrate could be transferred to the germ line via gap junctions. Direct uptake of transport substrate from the pseudocoelomic fluid into the germ line can also be achieved via CATP-5 and/or CATP-6. Since my data support the idea that CATP-5 is a polyamine transporter, the simplest explanation for the functional overlap of CATP-5, CATP-6 and CATP-7 within the

germ line and the somatic sheath cells would be that they import polyamines into these cells. This would also imply that the sheath cells and the germ line are unable to autonomously produce sufficient quantities of polyamines to enable normal development and function of the reproductive system.

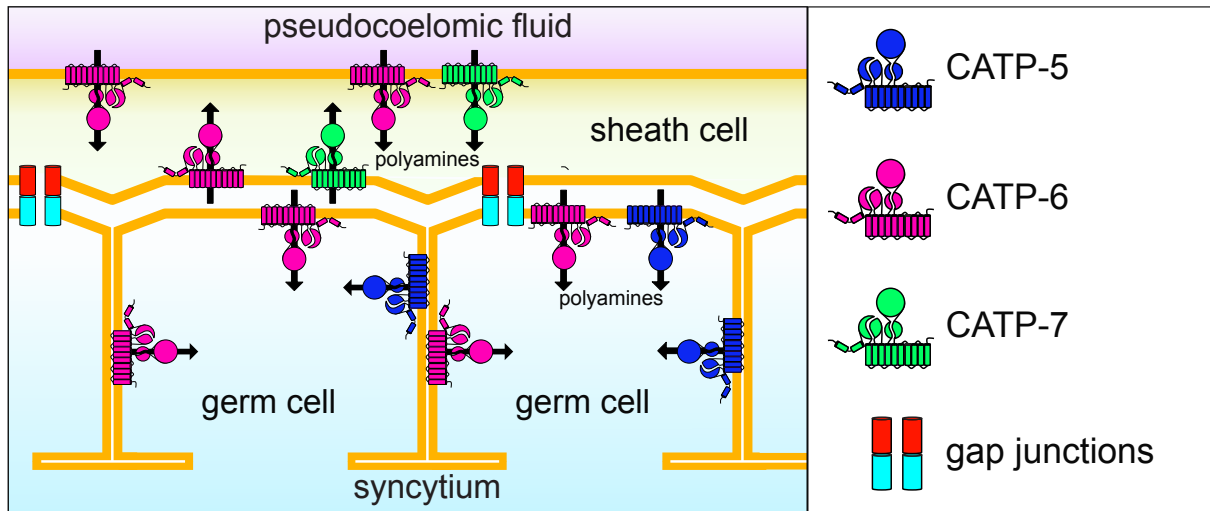


**Fig 13: Schematic model for the functions of the *C. elegans* P5Bs within the hermaphrodite gonad.** CATP-6 and CATP-7 function redundantly within the gonadal sheath cells to accumulate polyamines from the pseudocoelomic fluid. Direct uptake of polyamines from the pseudocoelomic fluid into the germ line could also be achieved via CATP-5 and/or CATP-6. Polyamines can be exchanged between both tissues via gap junctions.

### 3.7 Vulva development and DTC migration defects

#### 3.7.1 Vulva development defects in P5B mutants suggest possible impairment of Wnt signaling

The basis for the vulvaless (Vul) phenotype of *catp-7(dx189) catp-6(0)* animals remains unresolved. Since somatic gonad development is variably incomplete and/or delayed, the simplest explanation is that the anchor cell (AC) is not present, so no LIN-3 EGF (Epidermal Growth Factor) inductive signal is produced (Sulston and Horvitz 1977; Kimble and Hirsh 1979; Horvitz and Sulston 1980; Kimble 1981; Katz *et al.* 1995). However, CATP-6 and



CATP-7 are both expressed in the developing vulval epithelial cells, so it could also be that the vulval precursor cells (VPCs) are not fully competent to respond to inductive signal produced by the AC (Katz *et al.* 1995; Koga and Ohshima 1995). Failure of competence could result from inappropriate fate specification or (more likely) defective signal transduction via the RAS-MAPK or Wnt pathways (Horvitz and Sulston 1980; Hill and Sternberg 1992; Katz *et al.* 1995; Eisenmann and Kim 2000; Gleason *et al.* 2002; Green *et al.* 2008).

Defective Wnt signaling is also suggested by the unusual Multivulva (Muv) phenotype exhibited by some *catp-7(dx189) catp-6(0)* animals, in which a pseudovulva is formed posterior to the normal position of the vulva. This specific phenotype is also observed when the *lin-17* (Frizzled, Wnt receptor) is inactivated by mutation, leading to reversed orientation of the vulva precursor P7.p (Inoue *et al.* 2004; Deshpande *et al.* 2005). The same phenotype has also been observed in animals with altered CAN neuronal outgrowth (*vab-8* mutants) (Modzelewska *et al.* 2013). In the wt situation, these neurons express Ror/CAM-1 tyrosine kinase receptors that sequester posterior-secreted *egl-20* Wnt signals (WNT16), thus allowing *mom-2* Wnt signal (WNT4) secreted from the AC to correctly establish the polarity of the P7.p vulva precursor cell (Green *et al.* 2007; Modzelewska *et al.* 2013). Additionally, altered CAN neuronal outgrowth (and thus lack of posterior Wnt sequestering function) was found to trigger an ectopic vulva fate in the posterior P8.p vulva precursor, due to inappropriately high levels of posterior-derived *egl-20* signal, (Modzelewska *et al.* 2013). This is particularly notable, because in some of the Muv *catp-7(dx189) catp-6(0)* animals, the position of the pseudovulval protrusion is more consistent with origination from P8.p than P7.p.

### **3.7.2 Distal tip cell migration defects in nematode P5B mutants indicate perturbation of integrin function and Wnt signaling**

I observe distinct DTC migration phenotypes for *catp-6(0)*; *catp-5(0)* and *catp-7(dx189) catp-6(0)* double mutant animals. *catp-6(0)*; *catp-5(0)* double mutants have a perpetual DTC

## General Discussion

migration defect very similar to that observed in *vab-3(lf)* mutants (Nishiwaki 1999; Meighan and Schwarzbauer 2007). The VAB-3 transcription factor is crucial for downregulating  $\alpha$ -integrin *ina-1* and upregulating  $\alpha$ -integrin *pat-2*, which triggers the cessation of DTC migration (Meighan and Schwarzbauer 2007). Since P5B ATPase dysfunction leads to PD, it is notable that Pax6, the human ortholog of *vab-3*, has been shown to be important for dopaminergic neuron survival (Thomas *et al.* 2016), and  $\alpha 5 \beta 1$  integrin is known to be a direct target of Pax6 (Duncan *et al.* 2000). Furthermore, the expression of  $\alpha 5 \beta 1$  integrin is crucial for dopaminergic neurite outgrowth to the striatal cell region (Izumi *et al.* 2017).

In *catp-7(dx189) catp-6(0)* double mutant animals the DTCs often proceed in the wrong direction at the time of the second turn. This phenotype is very similar to that observed in mutants where either one of the integrin-associated proteins, SRC-1 or talin, is defective (Cram *et al.* 2003; Itoh *et al.* 2005). talin is a cytoskeletal-associated protein that binds to the cytoplasmic tail of  $\beta$ -integrin *pat-3* (Moulder *et al.* 1996; Calderwood *et al.* 1999; Cram *et al.* 2003). Interestingly, Cram *et al.* (2003) found that upon RNAi of *talin*, the sheath cells were severely impaired due to disorganized actin cytoskeleton, leading to sterility if both arms were affected. SRC-1 is a non-receptor protein tyrosine kinase (c-Src) that appears to function upstream of the CED-10 Rac pathway that controls actin cytoskeleton reorganization (Reddien and Horvitz 2000; Itoh *et al.* 2005). It was suggested that talin and SRC-1 might function together to mediate integrin signals to downstream targets that are specific to turning (Ming-Ching Wong 2012).

Cabello *et al.* (2010) observed a similar phenotype for multiple deficient Wnt proteins and suggested that in the context of DTC migration,  $\beta$ -Catenin independent non-canonical Wnt-signaling triggers the CED-10/Rac pathway through *gsk-3* (GSK-3 $\beta$ ) and *apr-1* (APC) in response to posterior *egl-20* signal. EGL-20 (WNT16) is secreted from the rectal epithelia cells and tail neurons, resulting in a posterior→anterior concentration gradient (Whangbo and

Kenyon 1999; Coudreuse 2006; Schwabiuk *et al.* 2009). Interestingly, it was shown that SRC-1 and Wnt-signaling act together in *C. elegans* early embryogenesis (Bei *et al.* 2002; Kim *et al.* 2013). However, in that context Wnt-signaling acts directly through  $\beta$ -Catenin to control CED-10-mediated actin cytoskeleton reorganization (Cabello *et al.* 2010; Gómez-Orte *et al.* 2013; Kim *et al.* 2013).

In line with Wnt signal transduction, 41% of *mig-14* mutant animals show the same phenotype as *catp-7(dx189) catp-6(0)* double mutant animals (Nishiwaki 1999; Shafaq-Zadah *et al.* 2015). *mig-14* encodes a Wnt cargo receptor in Wnt-secreting cells and is the *C. elegans* ortholog of human *gpr177* also known as *wntless* (Bänziger *et al.* 2006). This Wnt cargo receptor is a crucial for the secretion of Wnt molecules from Wnt-secreting cells and is recycled via endocytosis and retromer-mediated retrograde trafficking (Bänziger *et al.* 2006; Coudreuse and Korswagen 2007; Pan *et al.* 2008). The subunits APA-2, DPY-23, APB-1 and APS-2 (AP2, adaptor protein complex 2) are required for proper endocytosis of MIG-14 from the plasma membranous via retromer-dependent recycling of the cargo receptor. MIG-14 remains trapped in intracellular compartments if *vps-35* (VPS35, retromer complex) is deficient (Coudreuse and Korswagen 2007; Pan *et al.* 2008; Yang *et al.* 2008). The retromer complex was suggested to be involved in retrograde trafficking of the Wnt cargo receptor (MIG-14) from the endosome to the Golgi network (Coudreuse 2006). Consistent with the proposed link to the *catp-7(dx189) catp-6(0)* vulva defects, MIG-14 is expressed in the CAN neurons, the tail hypodermis, the developing vulva and in the same rectal epithelia cells that secrete posterior EGL-20 Wnt molecules (Whangbo and Kenyon 1999; Coudreuse 2006; Yang *et al.* 2008).

### 3.7.3 Integrated model for DTC migration and vulva development defects

How might the pleiotropic effects of the P5B mutants be explained? Since in the wt situation the Wnt cargo receptor MIG-14 (GPR177/Wntless) is crucial for the secretion of Wnt molecules from Wnt-secreting cells, impaired endocytosis or impaired retromer-mediated retrograde

trafficking would be sufficient to cause mislocalization of MIG-14, leading to either reduced EGL-20 (WNT16) secretion from posterior cells (causing altered DTC migration) and/or reduced MOM-2 (WNT4) secretion from the AC (causing altered vulva development).

Impairment of either endocytosis or retromer-mediated retrograde trafficking could also potentially cause mislocalization of the Wnt receptors (Frizzled), integrin receptors, Ror/CAM-1 Wnt sequestering receptors or the LET-23 EGF receptor. Defective function of one or more of these proteins could lead to the observed DTC migration and vulva induction defects.

Usenovic *et al.* (2012a) discovered a potential direct link between P5B function and Wnt signaling when they identified the Frizzled coreceptor, LRP6, in a yeast-two hybrid screen for ATP13A2 interactors (Tamai *et al.* 2000; Zeng *et al.* 2008; Usenovic *et al.* 2012a). However, there is no clear homolog for human LRP6 or LRP5 in the *C. elegans* genome (Eisenmann 2005). With regard to integrin function, it was shown that endocytosis of  $\beta 1$  integrins is clathrin dependent and that cell migration relies on retrograde transport (Arjonen *et al.* 2012; Shafaq-Zadah *et al.* 2015). Interestingly, clathrin-mediated endocytosis prolongs the duration of EGF signaling, since the endocytosed EGF receptors are recycled and not targeted for degradation (Sigismund *et al.* 2008). In contrast, non-clathrin-mediated endocytosed EGF receptors are targeted for lysosomal degradation (Sigismund *et al.* 2008).

It is significant that ATP13A2 was found to interact with candidates that primarily act in vesicular trafficking (Usenovic *et al.* 2012a). One of these candidates is AAK1 (AP2 associated kinase 1, *C. elegans sel-5*), an AP2 complex-associated kinase involved in the formation of clathrin-coated vesicles (Conner and Schmid 2002; Semerdjieva *et al.* 2008; Usenovic *et al.* 2012a). Another candidate is GAK, one of the major protein kinases in clathrin-coated vesicles (Korolchuk and Banting 2002; Usenovic *et al.* 2012a). Rab-5 was shown to be important for AP2 uncoating of endocytic clathrin-coated vesicles (Semerdjieva *et al.* 2008). In line with this, I found that CATP-6 localization shows obvious similarity to RFP::RAB-5 in spermathecal

cells. Moreover, native CATP-6::FP is strongly expressed in tail neurons, rectal epithelia cells, body wall muscles, DTCs and the developing vulva, all tissues which express MIG-14 Wnt cargo receptor, Ror/CAM-1 Wnt sequestering receptors, LIN-17 Wnt receptor, LET-23 EGF receptor or INA-1/PAT-2  $\alpha$ -integrin receptors. Since I observe each distinct phenotype at a relatively low frequency, nematode P5B ATPases might not be absolutely necessary for endocytosis or retromer-mediated retrograde trafficking, but deficiency of more than one P5B ATPase is sufficient to cause frequent DTC migration and vulva induction defects.

It is worth noting that mutations in human VPS35 that disrupt retrograde trafficking have been linked to PD as well (Vilariño-Güell *et al.* 2011; Zimprich *et al.* 2011). To my knowledge, GPR177 (MIG-14) has not been directly linked to PD, but as mentioned above, the expression of  $\alpha 5 \beta 1$  integrin is crucial for dopaminergic neurite outgrowth to the striatal cell region (Izumi *et al.* 2017). In addition, it was shown that Wnt molecule supplementation in cell culture media induces the proliferation of dopaminergic neuron precursor cells (Castelo-Branco *et al.* 2003).

Since aberrant function of P5B ATPases, integrins, VPS35 and Wnt-signaling are all associated with PD (Duncan *et al.* 2000; Ramirez *et al.* 2006; Vilariño-Güell *et al.* 2011; Zimprich *et al.* 2011; Berwick and Harvey 2012; Thomas *et al.* 2016; Izumi *et al.* 2017), and because ATP13A2 has been shown to cause endolysosomal trafficking defects (Usenovic *et al.* 2012a; Kett *et al.* 2015; Rinaldi *et al.* 2015), I speculate that nematode P5B ATPases regulate proper endocytosis/retrograde trafficking of integrins, EGF receptors, Wnt cargo receptors and/or Wnt receptors. Since the catalytic activity of nematode P5B ATPases is critical in order to rescue the mutant phenotypes, conformational change and/or substrate transport would probably be required for proper endocytosis or retrograde trafficking.

More experiments and observations could be performed to investigate these speculations. For example, the migration of neurons from the Q lineage should be altered if the posterior *egl-20* Wnt signal transduction is perturbed in *catp-7(dx189) catp-6(0)* double mutant animals. The

analysis of the EGL-20::GFP gradient in *catp-7(dx189) catp-6(0)* double mutants could provide greater insights into the relationship of nematode P5B ATPases and Wnt secretion or Wnt signal refining mechanisms. Moreover, immunocytochemistry to stain for APA-2 and CATP-6::GFP in combination with ultra-resolution microscopy could answer the question of whether CATP-6 localizes to clathrin-coated vesicles.

### 3.8 Common functions of *catp-6* and *catp-7* in the somatic gonad precursors

Multiple alleles of *catp-6*, but no alleles of *catp-7* were found via screening for mutations that block the ability of the *gem-1(gf)* mutations to suppress *gon-2(q388)* (Lambie *et al.* 2013). This suggests that *catp-6* is more important than *catp-7* for *gem-1* activity. In addition to the functional redundancy of CATP-6 and CATP-7 in context of the sheath cells, I found that overexpression of *catp-7* is able to compensate for the deficiency of *catp-6* in a *gon-2(lf); catp-6(lf); gem-1(gf)* background. Since I can detect both CATP-6 and CATP-7 in Z1 and Z4, but their subcellular localization patterns are non-identical, I speculate that the key site of action for P5B ATPases in Z1 and Z4 is the vesicular compartment to which CATP-6 localizes. The concentration of CATP-7 within this compartment might increase via endocytosis and membrane trafficking when the protein is overexpressed in the transformation rescue assays.

By taking into consideration my various observations for P5B ATPases in *C. elegans*, I propose the following model: In the wt situation, GON-2, GEM-1 and a fraction of CATP-7 are expressed on the plasma membrane of Z1 and Z4, while CATP-6, plus a minor fraction of CATP-7, are localized to cortical vesicles. GON-2 and GEM-1 mediate uptake of  $Mg^{2+}$  into the cytosol. In the absence of GON-2, GEM-1 is not able to mediate sufficient  $Mg^{2+}$  uptake to permit division of Z1 and Z4 unless its activity is augmented by a *gem-1(gf)* mutation. However, *gem-1(gf)* does not fully substitute for the absence of GON-2. Above a certain critical threshold,  $Mg^{2+}$  is able to activate the PI3K-AKT signaling cascade, leading to cell cycle progression

(Choudhury *et al.* 1997; Chang *et al.* 2003; Sahni and Scharenberg 2008; Wolf and Trapani 2012).

Since CATP-5 is a candidate polyamine transporter, it could be that CATP-6 (and CATP-7) could pump polyamines from cortical vesicles (which might act as a storage compartment) into the cytosol as a single transport substrate. Polyamines are known to be able to compensate for  $Mg^{2+}$  e.g. in DNA binding (Rowatt and Williams 1992) and are important for cell proliferation (Kihara and Snell 1957; Miller-Fleming *et al.* 2015).

Furthermore, it has recently been shown that when polyamine levels are artificially reduced via overexpression of SSAT, this leads to a decrease in the level of active phospho-AKT, resulting in reduced cell proliferation and migration; furthermore, these effects are reversible by supplementation with exogenous polyamines (Wang *et al.* 2017). Therefore, polyamines might play an important role in maintaining sufficient amounts of active phospho-AKT, so it is possible that *catp-6* (and *catp-7*) act in synergy with *gem-1(gf)* in order to compensate for *gon-2(lf)*.

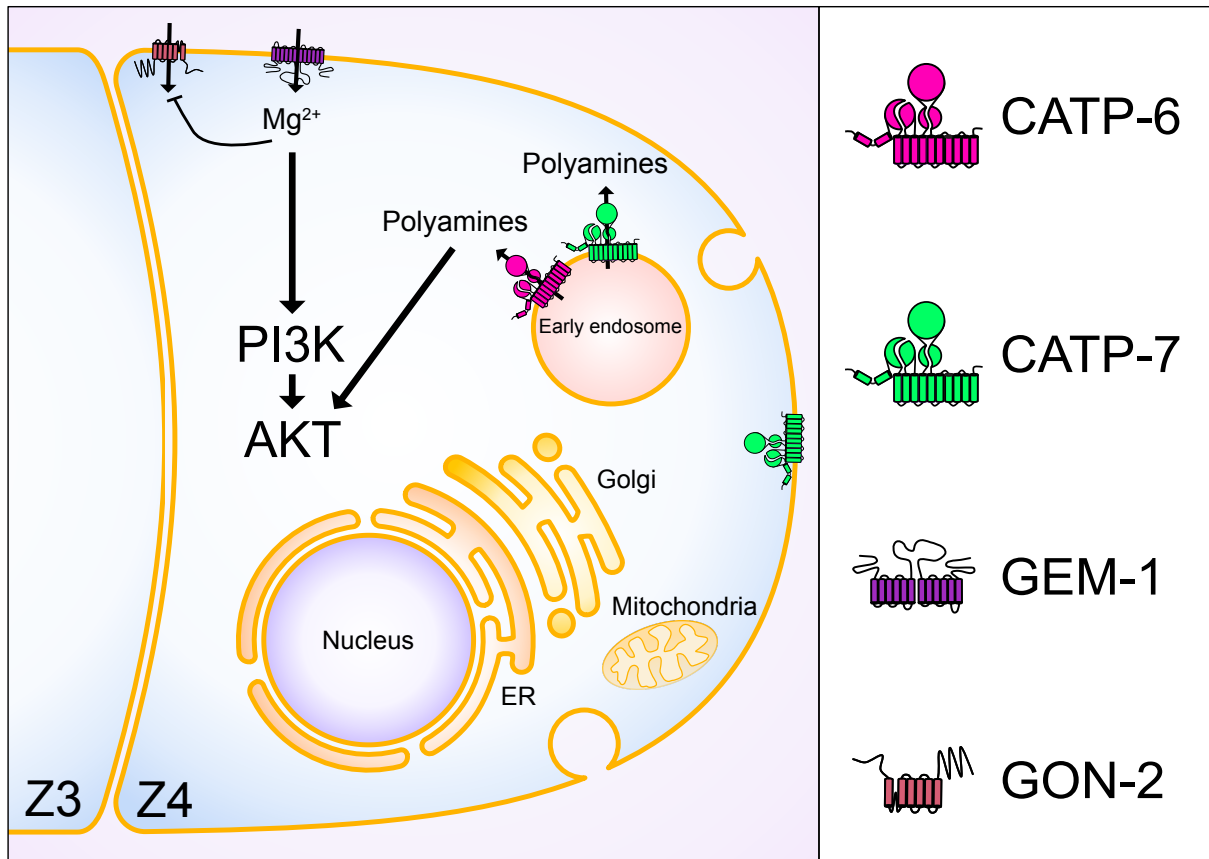


**Fig 14: Schematic model for the functions of CATP-6 and CATP-7 in Z1 and Z4.** GON-2, GEM-1 and CATP-7 localize to the plasma membrane of Z1 and Z4. CATP-6 and a minor fraction of CATP-7 localize to cortical vesicles. GON-2 and GEM-1 mediate uptake of  $Mg^{2+}$  into the cytosol.  $Mg^{2+}$  uptake activates the PI3K-AKT signaling cascade leading to cell cycle progression. GEM-1 activity needs to be augmented by a *gem-1(gf)* mutation in order to mediate sufficient  $Mg^{2+}$  uptake to permit division of Z1 and Z4 in the absence of GON-2. *gem-1(gf)* does not fully substitute for the absence of GON-2. On the plasma membrane, CATP-7 might not be able to pump sufficient amounts of polyamines into the cytosol from the pseudocoelomic fluid. The key site of action might be cortical vesicles that could store polyamines. CATP-6 (and CATP-7, when overexpressed) pump polyamines from cortical vesicles into the cytosol. These polyamines act in synergy with lower levels of  $Mg^{2+}$  (imported by *gem-1(gf)*) to phosphorylate and activate AKT.

### 3.9 GON-2 the TRPM6, TRPM7 ortholog

GON-2 is the *C. elegans* ortholog of mammalian TRPM6 and TRPM7 channels and is permeable to  $Mg^{2+}$  and  $Ca^{2+}$ , but lacks the kinase activity of the mammalian orthologs (Sun and Lambie 1997; West *et al.* 2001; Teramoto *et al.* 2005). GON-2 activity is critical for mitotic cell cycle progression of the somatic gonad precursors, Z1 and Z4 (West *et al.* 2001). *gon-2(lf)* mutant animals at restrictive temperature (23.5°C) are 100% Gonadless (Gon), without apparent defects in non-gonadal tissues (Sun and Lambie 1997; West *et al.* 2001).



## General Discussion

In Chapter 3, we describe 10 revertant mutations of *gon-2(lf)* (*gon-2(q388)*) that affect 9 different residues within GON-2. I tested 6 representative revertant mutations of *gon-2(lf)* via scoring the phenotypes of sergeants from homozygous as well as haploinsufficient animals. The efficiency of suppression of the Gon phenotype by the revertant mutations ranges from 85% (*dx99*) to 100% (*dx146*). Suppression of *gon-2(lf)* is slightly lower in heterozygous animals. Only *dx146* is able to suppress *gon-2(lf)* to 100% even if only a single copy of this allele is present. 9 of the revertant mutations of *gon-2(lf)* are located relatively near *gon-2(q388)* in the N-terminal cytosolic segment and one mutation is located in the cytosolic C-terminal domain. Notably, 8 of the 9 residues affected by the revertant mutations are potentially critical for channel regulation and formation. Further experiments would need to be done to explore whether these sites alter processes such protein folding, channel assembly, subunit trafficking, post-translational modification or gating of the channel by small molecules.

Moreover, we analyzed a single mutant allele, *gon-2(dx87)*, that reverts the  $Mg^{2+}$ -hypersensitive phenotype of *gtl-2(0)* mutant animals. *gon-2(dx87)* mutant animals are 100% Gon. This mutation is located in the cytosolic C-terminal TRP-domain. We find that *gon-2(dx87)* acts as an antimorphic protein, probably by forming heterotetramers with GON-2(+) and GTL-1(+). The Gon phenotype of *gon-2(dx87)* mutant animals can be rescued even with low levels of extracellular  $Mg^{2+}$  (1 mM), but not if the medium is supplemented with 10 mM  $Ca^{2+}$ . This suggests that the GON-2(dx87) mutant protein might be hypersensitive to inhibition by  $Ca^{2+}$ . Estevez *et al.* (2005) showed that GON-2/GTL-1 channels (ORCa) are feedback-inhibited when intracellular  $Ca^{2+}$  concentrations reach ~250 nM and that the binding site for  $Ca^{2+}$  is likely to be very close to the plasma membrane. Therefore, we speculate that the *gon-2(dx87)* mutation causes the TRP domain to have an increased affinity/accessibility for negative regulation by  $Ca^{2+}$ .

## General Discussion

With regard to the cell cycle progression defect of Z1 and Z4 observed in *gon-2(lf)* mutant animals (Hong *et al.* 1998), it is notable that lymphocytes lacking TRPM7 showed decreased phosphorylation of AKT, and are unable to proliferate unless the medium is supplemented with 10-15 mM  $Mg^{2+}$  (Sahni and Scharenberg 2008). Sahni *et al.* (2008) showed that constitutive activation of phosphoinositide 3-kinase (PI3K) bypasses the requirement for TRPM7 in cell cycle progression, supporting the idea of TRPM7-dependent activation of PI3K signaling. In cancer cells, it has been shown that reduction of TRPM7 activity leads to a decrease in phospho-AKT and phospho-Src, concomitant with inhibition of cell proliferation and cell migration (Wang *et al.* 2014; Chen *et al.* 2015). It has been proposed that  $Mg^{2+}$  import through TRPM7 activates the PI3K-AKT signaling cascade, possibly directly as a limiting cofactor for mTOR ( $Mg^{2+}$  complexed with ATP) (Rubin 2005; Wolf and Trapani 2012). Activated AKT has also been shown to phosphorylate  $\beta$ -Catenin and increase its transcriptional activity (Fang *et al.* 2007; Wang *et al.* 2017), which raises the question of whether GON-2 might potentiate Wnt signaling in the gonadal precursors. However, any such effect is likely to be minor, because impairment of canonical Wnt signaling in Z1 and Z4 leads to defects in their asymmetric divisions, whereas *gon-2(lf)* simply reduces division frequency, without obvious effects on cell polarity (Sun and Lambie 1997; Miskowski *et al.* 2001; Siegfried and Kimble 2002).

## 4 References

- Al-Din A. S., Wriekat A., Mubaidin A., Dasouki M., Hiari M., 1994 Pallido-pyramidal degeneration, supranuclear upgaze paresis and dementia: Kufor-Rakeb syndrome. *Acta Neurologica Scandinavica* **89**: 347–352.
- Albers R. W., 2003 Biochemical Aspects of Active Transport. <http://dx.doi.org/10.1146/annurev.bi.36.070167.003455> **36**: 727–756.
- Arjonen A., Alanko J., Veltel S., Ivaska J., 2012 Distinct Recycling of Active and Inactive  $\beta$ 1 Integrins. *Traffic* **13**: 610–625.
- Austin J., Kimble J., 1987 *glp-1* Is required in the germ line for regulation of the decision between mitosis and meiosis in *C. elegans*. *Cell* **51**: 589–599.
- Austin J., Kimble J., 1989 Transcript analysis of *glp-1* and *lin-12*, homologous genes required for cell interactions during development of *C. elegans*. *Cell* **58**: 565–571.
- Axelsen K. B., Palmgren M. G., 1998 Evolution of Substrate Specificities in the P-Type ATPase Superfamily. *J Mol Evol* **46**: 84–101.
- Bando T., Ikeda T., Kagawa H., 2005 The Homeoproteins MAB-18 and CEH-14 Insulate the Dauer Collagen Gene *col-43* from Activation by the Adjacent Promoter of the Spermatheca Gene *sth-1* in *Caenorhabditis elegans*. *J. Mol. Biol.* **348**: 101–112.
- Bastide F., Meissner G., Fleischer S., Post R. L., 1973 Similarity of the active site of phosphorylation of the adenosine triphosphatase from transport of sodium and potassium ions in kidney to that for transport of calcium ions in the sarcoplasmic reticulum of muscle. *J. Biol. Chem.* **248**: 8385–8391.
- Bänziger C., Soldini D., Schütt C., Zipperlen P., Hausmann G., Basler K., 2006 Wntless, a Conserved Membrane Protein Dedicated to the Secretion of Wnt Proteins from Signaling Cells. *Cell* **125**: 509–522.
- Bei Y. Y., Hogan J. J., Berkowitz L. A. L., Soto M. M., Rocheleau C. E. C., Pang K. M. K., Collins J. J., Mello C. C. C., 2002 SRC-1 and Wnt Signaling Act Together to Specify Endoderm and to Control Cleavage Orientation in Early *C. elegans* Embryos. *Dev. Cell* **3**: 13–13.
- Bento C. F., Ashkenazi A., Jimenez-Sanchez M., Rubinsztein D. C., 2016 The Parkinson's disease-associated genes *ATP13A2* and *SYT11* regulate autophagy via a common pathway. *Nature Communications* **7**: 11803.
- Berridge M. J., 1995 Calcium signalling and cell proliferation. *Bioessays* **17**: 491–500.
- Berry L. W., Westlund B., Schedl T., 1997 Germ-line tumor formation caused by activation of *glp-1*, a *Caenorhabditis elegans* member of the Notch family of receptors. *Development* **124**: 925–936.

## References

- Berwick D. C., Harvey K., 2012 The importance of Wnt signalling for neurodegeneration in Parkinson's disease. *Biochim. Soc. Trans.* **40**: 1123–1128.
- Biamino E., Di Gregorio E., Belligni E. F., Keller R., Riberi E., Gandione M., Calcia A., Mancini C., Giorgio E., Cavalieri S., Pappi P., Talarico F., Fea A. M., De Rubeis S., Cirillo Silengo M., Ferrero G. B., Brusco A., 2016 A novel 3q29 deletion associated with autism, intellectual disability, psychiatric disorders, and obesity. *Am. J. Med. Genet. B Neuropsychiatr. Genet.* **171B**: 290–299.
- Bras J., Verloes A., Schneider S. A., Mole S. E., Guerreiro R. J., 2012 Mutation of the parkinsonism gene *ATP13A2* causes neuronal ceroid-lipofuscinosis. *Hum. Mol. Genet.* **21**: 2646–2650.
- Brenner S., 1974 The genetics of *Caenorhabditis elegans*. *Genetics* **77**: 71–94.
- Bublitz M., Morth J. P., Nissen P., 2011 P-type ATPases at a glance. *Journal of Cell Science* **124**: 2515–2519.
- Bublitz M., Poulsen H., Morth J. P., Nissen P., 2010 In and out of the cation pumps: P-type ATPase structure revisited. *Curr Opin Struct Biol* **20**: 431–439.
- Buechner M., Hall D. H., Bhatt H., Hedgecock E. M., 1999 Cystic Canal Mutants in *Caenorhabditis elegans* Are Defective in the Apical Membrane Domain of the Renal (Excretory) Cell. *Dev. Biol.* **214**: 227–241.
- Cabello J., Neukomm L. J., Günesdogan U., Burkart K., Charette S. J., Lochnit G., Hengartner M. O., Schnabel R., 2010 The Wnt Pathway Controls Cell Death Engulfment, Spindle Orientation, and Migration through CED-10/Rac (B Conradt, Ed.). *PLoS Biol.* **8**: e1000297.
- Calderwood D. A., Zent R., Grant R., Rees D. J., Hynes R. O., Ginsberg M. H., 1999 The Talin head domain binds to integrin beta subunit cytoplasmic tails and regulates integrin activation. *J. Biol. Chem.* **274**: 28071–28074.
- Casadaban M. J., Martinez-Arias A., Shapira S. K., Chou J., 1983 Beta-galactosidase gene fusions for analyzing gene expression in *Escherichia coli* and yeast. *Meth. Enzymol.* **100**: 293–308.
- Castelo-Branco G., Wagner J., Rodriguez F. J., Kele J., Sousa K., Rawal N., Pasolli H. A., Fuchs E., Kitajewski J., Arenas E., 2003 Differential regulation of midbrain dopaminergic neuron development by Wnt-1, Wnt-3a, and Wnt-5a. *Proc. Natl. Acad. Sci. U.S.A.* **100**: 12747–12752.
- Champeil P., 1996 Kinetic characterization of sarcoplasmic reticulum Ca<sup>2+</sup>-ATPase. In: *ATPases, Biomembranes: A Multi-Volume Treatise*. Elsevier, pp. 43–76.
- Chang F., Lee J. T., Navolanic P. M., Steelman L. S., Shelton J. G., Blalock W. L., Franklin R. A., McCubrey J. A., 2003 Involvement of PI3K/Akt pathway in cell cycle progression, apoptosis, and neoplastic transformation: a target for cancer chemotherapy. *Leukemia* **2003** **17**: 590–603.

## References

- Chen C., Fenk L. A., de Bono M., 2013 Efficient genome editing in *Caenorhabditis elegans* by CRISPR-targeted homologous recombination. *Nucleic Acids Res* **41**: e193–e193.
- Chen W.-L., Turlova E., Sun C., Kim J.-S., Huang S., Zhong X., Guan Y.-Y., Wang G.-L., Rutka J., Feng Z.-P., Sun H.-S., 2015 Xyloketal B Suppresses Glioblastoma Cell Proliferation and Migration in Vitro through Inhibiting TRPM7-Regulated PI3K/Akt and MEK/ERK Signaling Pathways. *Marine Drugs* 2015, Vol. 13, Pages 2505-2525 **13**: 2505–2525.
- Choudhury G. G., Karamitsos C., Hernandez J., Gentilini A., Bardgett J., Abboud H. E., 1997 PI-3-kinase and MAPK regulate mesangial cell proliferation and migration in response to PDGF. *Am. J. Physiol.* **273**: F931–8.
- Christensen M., Estevez A., Yin X., Fox R., Morrison R., McDonnell M., Gleason C., Miller D. M., Strange K., 2002 A primary culture system for functional analysis of *C. elegans* neurons and muscle cells. *Neuron* **33**: 503–514.
- Chubanov V., Waldegger S., Schnitzler M. M. Y., Vitzthum H., Sassen M. C., Seyberth H. W., Konrad M., Gudermann T., 2004 Disruption of TRPM6/TRPM7 complex formation by a mutation in the TRPM6 gene causes hypomagnesemia with secondary hypocalcemia. *Proc. Natl. Acad. Sci. U.S.A.* **101**: 2894–2899.
- Church D. L., Guan K. L., Lambie E. J., 1995 Three genes of the MAP kinase cascade, *mek-2*, *mpk-1/sur-1* and *let-60* ras, are required for meiotic cell cycle progression in *Caenorhabditis elegans*. *Development* **121**: 2525–2535.
- Clausen J. D., McIntosh D. B., Vilsen B., Woolley D. G., Andersen J. P., 2003 Importance of Conserved N-domain Residues Thr 441, Glu 442, Lys 515, Arg 560, and Leu 562 of Sarcoplasmic Reticulum Ca<sup>2+</sup>-ATPase for MgATP Binding and Subsequent Catalytic Steps. *J. Biol. Chem.* **278**: 20245–20258.
- Conner S. D., Schmid S. L., 2002 Identification of an adaptor-associated kinase, AAK1, as a regulator of clathrin-mediated endocytosis. *J. Cell Biol.* **156**: 921–929.
- Consortium T. C. E. D. M., 2012 Large-Scale Screening for Targeted Knockouts in the *Caenorhabditis elegans* Genome. *G3&#58; Genes|Genomes|Genetics* **2**: 1415–1425.
- Coudreuse D., Korswagen H. C., 2007 The making of Wnt: new insights into Wnt maturation, sorting and secretion. *Development* **134**: 3–12.
- Coudreuse D. Y. M., 2006 Wnt Gradient Formation Requires Retromer Function in Wnt-Producing Cells. *Science* **312**: 921–924.
- Cram E. J., Clark S. G., Schwarzbauer J. E., 2003 Talin loss-of-function uncovers roles in cell contractility and migration in *C. elegans*. *Journal of Cell Science* **116**: 3871–3878.
- Crossgrove J., Zheng W., 2004 Manganese toxicity upon overexposure. *NMR Biomed.* **17**: 544–553.
- de Tezanos Pinto F., Corradi G. R., la Hera de D. P., Adamo H. P., 2012 CHO cells expressing the human P5-ATPase ATP13A2 are more sensitive to the toxic effects of herbicide Paraquat. *Neurochemistry International* **60**: 243–248.

## References

- Dehay B., Ramirez A., Martinez-Vicente M., Perier C., Canron M.-H., Doudnikoff E., Vital A., Vila M., Klein C., Bezard E., 2012 Loss of P-type ATPase ATP13A2/PARK9 function induces general lysosomal deficiency and leads to Parkinson disease neurodegeneration. *Proceedings of the National Academy of Sciences* **109**: 9611–9616.
- Demirsoy S., Martin S., Motamedi S., van Veen S., Holemans T., Van den Haute C., Jordanova A., Baekelandt V., Vangheluwe P., Agostinis P., 2017 ATP13A2/PARK9 regulates endo-/lysosomal cargo sorting and proteostasis through a novel PI(3, 5)P2-mediated scaffolding function. *Hum. Mol. Genet.* **26**: 1656–1669.
- Deshpande R., Inoue T., Priess J. R., Hill R. J., 2005 *lin-17/Frizzled* and *lin-18* regulate POP-1/TCF-1 localization and cell type specification during *C. elegans* vulval development. *Dev. Biol.* **278**: 118–129.
- Dickinson D. J., Goldstein B., 2016 CRISPR-Based Methods for *Caenorhabditis elegans* Genome Engineering. *Genetics* **202**: 885–901.
- Dirr E. R., Ekhatov O. R., Blackwood R., Holden J. G., Masliah E., Schultheis P. J., Fleming S. M., 2018 Exacerbation of sensorimotor dysfunction in mice deficient in *Atp13a2* and overexpressing human wildtype alpha-synuclein. *Behav. Brain Res.* **343**: 41–49.
- Duncan M. K., Kozmik Z., Cveklova K., Piatigorsky J., Cvekl A., 2000 Overexpression of PAX6(5a) in lens fiber cells results in cataract and upregulation of (alpha)5(beta)1 integrin expression. *Journal of Cell Science* **113** ( Pt 18): 3173–3185.
- Eisenmann D. M., 2005 Wnt signaling. *WormBook*: 1–17.
- Eisenmann D. M., Kim S. K., 2000 Protruding Vulva Mutants Identify Novel Loci and Wnt Signaling Factors That Function During *Caenorhabditis elegans* Vulva Development. *Genetics* **156**: 1097–1116.
- Estes K. A., Hanna-Rose W., 2009 The anchor cell initiates dorsal lumen formation during *C. elegans* vulval tubulogenesis. *Dev. Biol.* **328**: 297–304.
- Estevez A. Y., Strange K., 2005 Calcium feedback mechanisms regulate oscillatory activity of a TRP-like Ca<sup>2+</sup>-conductance in *C. elegans* intestinal cells. *The Journal of Physiology* **567**: 239–251.
- Estrada-Cuzcano A., Martin S., Chamova T., Synofzik M., Timmann D., Holemans T., Andreeva A., Reichbauer J., De Rycke R., Chang D.-I., van Veen S., Samuel J., Schöls L., Pöppel T., Møllerup Sørensen D., Asselbergh B., Klein C., Zuchner S., Jordanova A., Vangheluwe P., Tournev I., Schüle R., 2017 Loss-of-function mutations in the *ATP13A2/PARK9* gene cause complicated hereditary spastic paraplegia (SPG78). *Brain* **140**: 287–305.
- Fang D., Hawke D., Zheng Y., Xia Y., Meisenhelder J., Nika H., Mills G. B., Kobayashi R., Hunter T., Lu Z., 2007 Phosphorylation of beta-catenin by AKT promotes beta-catenin transcriptional activity. *J. Biol. Chem.* **282**: 11221–11229.
- Fire A., Xu S., Montgomery M. K., Kostas S. A., Driver S. E., Mello C. C., 1998 Potent and specific genetic interference by double-stranded RNA in *Caenorhabditis elegans*. *Nature* **391**: 806–811.

## References

- Fleming S. M., Santiago N. A., Mullin E. J., Pamphile S., Karkare S., Lemkuhl A., Ekhaton O. R., Linn S. C., Holden J. G., Aga D. S., Roth J. A., Liou B., Sun Y., Shull G. E., Schultheis P. J., 2018 The effect of manganese exposure in *Atp13a2*-deficient mice. *NeuroToxicology* **64**: 256–266.
- Frøkjaer-Jensen C., Davis M. W., Hopkins C. E., Newman B. J., Thummel J. M., Olesen S.-P., Grunnet M., Jorgensen E. M., 2008 Single-copy insertion of transgenes in *Caenorhabditis elegans*. *Nat. Genet.* **40**: 1375–1383.
- Frøkjaer-Jensen C., Davis M. W., Sarov M., Taylor J., Flibotte S., LaBella M., Pozniakovsky A., Moerman D. G., Jorgensen E. M., 2014 Random and targeted transgene insertion in *Caenorhabditis elegans* using a modified *Mos1* transposon. *Nature Methods* **11**: 529–534.
- Gitler A. D., Chesi A., Geddie M. L., Strathearn K. E., Hamamichi S., Hill K. J., Caldwell K. A., Caldwell G. A., Cooper A. A., Rochet J.-C., Lindquist S., 2009 Alpha-synuclein is part of a diverse and highly conserved interaction network that includes PARK9 and manganese toxicity. *Nat. Genet.* **41**: 308–315.
- Gleason J. E., Korswagen H. C., Eisenmann D. M., 2002 Activation of Wnt signaling bypasses the requirement for RTK/Ras signaling during *C. elegans* vulval induction. *Genes Dev.* **16**: 1281–1290.
- Gómez-Orte E., Sáenz-Narciso B., Moreno S., Cabello J., 2013 Multiple functions of the noncanonical Wnt pathway. *Trends Genet.* **29**: 545–553.
- Green J. L., Inoue T., Sternberg P. W., 2007 The *C. elegans* ROR receptor tyrosine kinase, CAM-1, non-autonomously inhibits the Wnt pathway. *Development* **134**: 4053–4062.
- Green J. L., Inoue T., Sternberg P. W., 2008 Opposing Wnt pathways orient cell polarity during organogenesis. *Cell* **134**: 646–656.
- Groenestege W. M. T., Hoenderop J. G., van den Heuvel L., Knoers N., Bindels R. J., 2006 The epithelial Mg<sup>2+</sup> channel transient receptor potential melastatin 6 is regulated by dietary Mg<sup>2+</sup> content and estrogens. *J. Am. Soc. Nephrol.* **17**: 1035–1043.
- Grünewald A., Arns B., Seibler P., Rakovic A., Münchau A., Ramirez A., Sue C. M., Klein C., 2012 ATP13A2 mutations impair mitochondrial function in fibroblasts from patients with Kufor-Rakeb syndrome. *Neurobiology of Aging* **33**: 1843.e1–1843.e7.
- Guida V., Sinibaldi L., Pagnoni M., Bernardini L., Loddo S., Margiotti K., Digilio M. C., Fadda M. T., Dallapiccola B., Iannetti G., Alessandro D. L., 2015 A de novo proximal 3q29 chromosome microduplication in a patient with oculo auriculo vertebral spectrum. *Am. J. Med. Genet. A* **167A**: 797–801.
- Habtemichael N., Kovacs G., 2002 Cloning the *AFURSI* gene which is up-regulated in senescent human parenchymal kidney cells. *Gene* **283**: 271–275.
- Hall D. H., Winfrey V. P., Blaeuer G., Hoffman L. H., Furuta T., Rose K. L., Hobert O., Greenstein D., 1999 Ultrastructural Features of the Adult Hermaphrodite Gonad of *Caenorhabditis elegans*: Relations between the Germ Line and Soma. *Dev. Biol.* **212**: 101–123.

## References

- Hampshire D. J., Roberts E., Crow Y., Bond J., Mubaidin A., Wriekat A. L., Al-Din A., Woods C. G., 2001 Kufor-Rakeb syndrome, pallido-pyramidal degeneration with supranuclear upgaze paresis and dementia, maps to 1p36. *J. Med. Genet.* **38**: 680–682.
- Harteneck C., Plant T. D., Schultz G., 2000 From worm to man: three subfamilies of TRP channels. *Trends in Neurosciences* **23**: 159–166.
- Heinick A., Urban K., Roth S., Spies D., Nunes F., Phanstiel O., Liebau E., Luersen K., 2010 *Caenorhabditis elegans* P5B-type ATPase CATP-5 operates in polyamine transport and is crucial for norspermidine-mediated suppression of RNA interference. *FASEB J* **24**: 206–217.
- Henderson S. T., Gao D., Lambie E. J., Kimble J., 1994 *lag-2* may encode a signaling ligand for the GLP-1 and LIN-12 receptors of *C. elegans*. *Development* **120**: 2913–2924.
- Higgins C. F., 1992 ABC Transporters: From Microorganisms to Man. *Annu. Rev. Cell. Biol.* **8**: 67–113.
- Hill R. J., Sternberg P. W., 1992 The gene *lin-3* encodes an inductive signal for vulval development in *C. elegans*. *Nature* **358**: 470–476.
- Hirsh D., Oppenheim D., Klass M., 1976 Development of the reproductive system of *Caenorhabditis elegans*. *Dev. Biol.* **49**: 200–219.
- Holemans T., Sørensen D. M., van Veen S., Martin S., Hermans D., Kemmer G. C., Van den Haute C., Baekelandt V., Günther Pomorski T., Agostinis P., Wuytack F., Palmgren M., Eggermont J., Vangheluwe P., 2015 A lipid switch unlocks Parkinson's disease-associated ATP13A2. *Proc. Natl. Acad. Sci. U.S.A.* **112**: 9040–9045.
- Hong Y., Roy R., Ambros V., 1998 Developmental regulation of a cyclin-dependent kinase inhibitor controls postembryonic cell cycle progression in *Caenorhabditis elegans*. *Development* **125**: 3585–3597.
- Horvitz H. R., Sulston J. E., 1980 Isolation and genetic characterization of cell-lineage mutants of the nematode *Caenorhabditis elegans*. *Genetics* **96**: 435–454.
- Humeau J., Bravo-San Pedro J. M., Vitale I., Nuñez L., Villalobos C., Kroemer G., Senovilla L., 2018 Calcium signaling and cell cycle: Progression or death. *Cell Calcium* **70**: 3–15.
- Inoue T., Oz H. S., Wiland D., Gharib S., Deshpande R., Hill R. J., Katz W. S., Sternberg P. W., 2004 *C. elegans* LIN-18 is a Ryk ortholog and functions in parallel to LIN-17/Frizzled in Wnt signaling. *Cell* **118**: 795–806.
- Itoh B., Hirose T., Takata N., Nishiwaki K., Koga M., Ohshima Y., Okada M., 2005 SRC-1, a non-receptor type of protein tyrosine kinase, controls the direction of cell and growth cone migration in *C. elegans*. *Development* **132**: 5161–5172.
- Izumi Y., Wakita S., Kanbara C., Nakai T., Akaike A., Kume T., 2017 Integrin  $\alpha 5 \beta 1$  expression on dopaminergic neurons is involved in dopaminergic neurite outgrowth on striatal neurons. *Sci Rep* **7**: 42111.
- Jardetzky O., 1966 Simple Allosteric Model for Membrane Pumps. *Nature* **211**: 969–970.



## References

- Katz W. S., Hill R. J., Clandinin T. R., Sternberg P. W., 1995 Different levels of the *C. elegans* growth factor LIN-3 promote distinct vulval precursor fates. *Cell* **82**: 297–307.
- Kelly W. G., Xu S., Montgomery M. K., Fire A., 1997 Distinct requirements for somatic and germline expression of a generally expressed *Caenorhabditis elegans* gene. *Genetics* **146**: 227–238.
- Kemp B. J., Church D. L., Hatzold J., Conradt B., Lambie E. J., 2009 *gem-1* encodes an SLC16 monocarboxylate transporter-related protein that functions in parallel to the *gon-2* TRPM channel during gonad development in *Caenorhabditis elegans*. *Genetics* **181**: 581–591.
- Kemp B. J., Hatzold J., Sternick L. A., Cornman-Homonoff J., Whitaker J. M., Tieu P. J., Lambie E. J., 2007 In vivo construction of recombinant molecules within the *Caenorhabditis elegans* germ line using short regions of terminal homology. *Nucleic Acids Res* **35**: e133–e133.
- Kett L. R., Stiller B., Bernath M. M., Tasset I., Blesa J., Jackson-Lewis V., Chan R. B., Zhou B., Di Paolo G., Przedborski S., Cuervo A. M., Dauer W. T., 2015  $\alpha$ -Synuclein-independent histopathological and motor deficits in mice lacking the endolysosomal Parkinsonism protein Atp13a2. *J. Neurosci.* **35**: 5724–5742.
- Kihara H., Snell E. E., 1957 Spermine and related polyamines as growth stimulants for lactobacillus casei. *Proc. Natl. Acad. Sci. U.S.A.* **43**: 867–871.
- Kim S., Ishidate T., Sharma R., Soto M. C., Conte D., Mello C. C., Shirayama M., 2013 Wnt and CDK-1 regulate cortical release of WRM-1/ $\beta$ -catenin to control cell division orientation in early *Caenorhabditis elegans* embryos. *Proceedings of the National Academy of Sciences* **110**: E918–27.
- Kimble J., 1981 Alterations in cell lineage following laser ablation of cells in the somatic gonad of *Caenorhabditis elegans*. *Dev. Biol.* **87**: 286–300.
- Kimble J., Hirsh D., 1979 The postembryonic cell lineages of the hermaphrodite and male gonads in *Caenorhabditis elegans*. *Dev. Biol.* **70**: 396–417.
- Kimble J. E., White J. G., 1981 On the control of germ cell development in *Caenorhabditis elegans*. *Dev. Biol.* **81**: 208–219.
- Kitada T., Asakawa S., Hattori N., Matsumine H., Yamamura Y., Minoshima S., Yokochi M., Mizuno Y., Shimizu N., 1998 Mutations in the parkin gene cause autosomal recessive juvenile parkinsonism. *Nature* **392**: 605–608.
- Koga M., Ohshima Y., 1995 Mosaic analysis of the let-23 gene function in vulval induction of *Caenorhabditis elegans*. *Development* **121**: 2655–2666.
- Kong S. M. Y., Chan B. K. K., Park J.-S., Hill K. J., Aitken J. B., Cottle L., Farghaian H., Cole A. R., Lay P. A., Sue C. M., Cooper A. A., 2014 Parkinson's disease-linked human PARK9/ATP13A2 maintains zinc homeostasis and promotes  $\alpha$ -Synuclein externalization via exosomes. *Hum. Mol. Genet.* **23**: 2816–2833.

## References

- Korolchuk V. I., Banting G., 2002 CK2 and GAK/auxilin2 Are Major Protein Kinases in Clathrin-Coated Vesicles. *Traffic* **3**: 428–439.
- Kostich M., Fire A., Fambrough D. M., 2000 Identification and molecular-genetic characterization of a LAMP/CD68-like protein from *Caenorhabditis elegans*. *Journal of Cell Science* **113** ( Pt **14**): 2595–2606.
- Kühlbrandt W., 2004 Biology, structure and mechanism of P-type ATPases. *Nat Rev Mol Cell Biol* **5**: 282–295.
- Kwasnicka-Crawford D. A., Carson A. R., Roberts W., Summers A. M., Rehnström K., Järvelä I., Scherer S. W., 2005 Characterization of a novel cation transporter ATPase gene (ATP13A4) interrupted by 3q25-q29 inversion in an individual with language delay. *Genomics* **86**: 182–194.
- La Hera De D. P., Corradi G. R., Adamo H. P., de Tezanos Pinto F., 2013 Parkinson's disease-associated human P5B-ATPase ATP13A2 increases spermidine uptake. *Biochem. J.* **450**: 47–53.
- Lambie E. J., Bruce R. D., Zielich J., Yuen S. N., 2015 Novel Alleles of *gon-2*, a *C. elegans* Ortholog of Mammalian TRPM6 and TRPM7, Obtained by Genetic Reversion Screens. (S-Z Xu, Ed.). *PLoS ONE* **10**: e0143445.
- Lambie E. J., Tieu P. J., Lebedeva N., Church D. L., Conradt B., 2013 CATP-6, a *C. elegans* Ortholog of ATP13A2 PARK9, Positively Regulates GEM-1, an SLC16A Transporter (S Ahmed, Ed.). *PLoS ONE* **8**: e77202.
- Lancaster C. R. D., 2004 Ion pump in the movies. *Nature* **432**: 286–287.
- Lelong E., Marchetti A., Guého A., Lima W. C., Sattler N., Molmeret M., Hagedorn M., Soldati T., Cosson P., 2011 Role of magnesium and a phagosomal P-type ATPase in intracellular bacterial killing. *Cell. Microbiol.* **13**: 246–258.
- Lynch-Day M. A., Mao K., Wang K., Zhao M., Klionsky D. J., 2012 The role of autophagy in Parkinson's disease. *Cold Spring Harbor Perspectives in Medicine* **2**: a009357–a009357.
- MacDonald R. S., 2000 The role of zinc in growth and cell proliferation. *J. Nutr.* **130**: 1500S–8S.
- Madan M., Patel A., Skrubber K., Geerts D., Altomare D. A., Iv O. P., 2016 ATP13A3 and caveolin-1 as potential biomarkers for difluoromethylornithine-based therapies in pancreatic cancers. *Am J Cancer Res* **6**: 1231–1252.
- Marques A. C., Vinckenbosch N., Brawand D., Kaessmann H., 2008 Functional diversification of duplicate genes through subcellular adaptation of encoded proteins. *Genome Biol.* **9**: R54.
- Martin S., van Veen S., Holemans T., Demirsoy S., Van den Haute C., Baekelandt V., Agostinis P., Eggermont J., Vangheluwe P., 2016 Protection against Mitochondrial and Metal Toxicity Depends on Functional Lipid Binding Sites in ATP13A2. *Parkinson's Disease* **2016**: 1–11.

## References

- Matsumine H., Saito M., Shimoda-Matsubayashi S., Tanaka H., Ishikawa A., Nakagawa-Hattori Y., Yokochi M., Kobayashi T., Igarashi S., Takano H., Sanpei K., Koike R., Mori H., Kondo T., Mizutani Y., Schäffer A. A., Yamamura Y., Nakamura S., Kuzuhara S., Tsuji S., Mizuno Y., 1997 Localization of a gene for an autosomal recessive form of juvenile Parkinsonism to chromosome 6q25.2-27. *The American Journal of Human Genetics* **60**: 588–596.
- McCarter J., Bartlett B., Dang T., Schedl T., 1997 Soma–Germ Cell Interactions in *Caenorhabditis elegans*: Multiple Events of Hermaphrodite Germline Development Require the Somatic Sheath and Spermathecal Lineages. *Dev. Biol.* **181**: 121–143.
- McCarter J., Bartlett B., Dang T., Schedl T., 1999 On the Control of Oocyte Meiotic Maturation and Ovulation in *Caenorhabditis elegans*. *Dev. Biol.* **205**: 111–128.
- Meighan C. M., Schwarzbauer J. E., 2007 Control of *C. elegans* hermaphrodite gonad size and shape by *vab-3/Pax6*-mediated regulation of integrin receptors. *Genes Dev.* **21**: 1615–1620.
- Mello C. C., Kramer J. M., Stinchcomb D., Ambros V., 1991 Efficient gene transfer in *C. elegans*: extrachromosomal maintenance and integration of transforming sequences. *EMBO J.* **10**: 3959–3970.
- Miller-Fleming L., Olin-Sandoval V., Campbell K., Ralser M., 2015 Remaining Mysteries of Molecular Biology: The Role of Polyamines in the Cell. *J. Mol. Biol.* **427**: 3389–3406.
- Ming-Ching Wong J. E. S., 2012 Gonad morphogenesis and distal tip cell migration in the *Caenorhabditis elegans* hermaphrodite. *Wiley interdisciplinary reviews. Developmental biology* **1**: 519–531.
- Miskowski J., Li Y., Kimble J., 2001 The *sys-1* Gene and Sexual Dimorphism during Gonadogenesis in *Caenorhabditis elegans*. *Dev. Biol.* **230**: 61–73.
- Modzelewska K., Lauritzen A., Hasenoeder S., Brown L., Georgiou J., Moghal N., 2013 Neurons Refine the *Caenorhabditis elegans* Body Plan by Directing Axial Patterning by Wnts (J Ahringer, Ed.). *PLoS Biol.* **11**: e1001465.
- Morth J. P., Pedersen B. P., Buch-Pedersen M. J., Andersen J. P., Vilsen B., Palmgren M. G., Nissen P., 2011 A structural overview of the plasma membrane Na<sup>+</sup>, K<sup>+</sup>-ATPase and H<sup>+</sup>-ATPase ion pumps. *Nat Rev Mol Cell Biol* **12**: 60–70.
- Morth J. P., Pedersen B. P., Toustrup-Jensen M. S., Sørensen T. L.-M., Petersen J., Andersen J. P., Vilsen B., Nissen P., 2007 Crystal structure of the sodium-potassium pump. *Nature Publishing Group* **450**: 1043–1049.
- Moulder G. L., Huang M. M., Waterston R. H., Barstead R. J., 1996 Talin requires beta-integrin, but not vinculin, for its assembly into focal adhesion-like structures in the nematode *Caenorhabditis elegans*. *Mol Biol Cell* **7**: 1181–1193.
- Møller A. B., Asp T., Holm P. B., Palmgren M. G., 2008 Phylogenetic analysis of P5 P-type ATPases, a eukaryotic lineage of secretory pathway pumps. *Mol Phylogenet Evol* **46**: 619–634.

## References

- Møller J. V., Juul B., le Maire M., 1996 Structural organization, ion transport, and energy transduction of P-type ATPases. *Biochim Biophys Acta* **1286**: 1–51.
- Møller J. V., Olesen C., Winther A.-M. L., Nissen P., 2010 The sarcoplasmic Ca<sup>2+</sup>-ATPase: design of a perfect chemi-osmotic pump. *Quart. Rev. Biophys.* **43**: 501–566.
- Nelson F. K., Riddle D. L., 1984 Functional study of the *Caenorhabditis elegans* secretory-excretory system using laser microsurgery. - PubMed - NCBI. *J. Exp. Zool.* **231**: 45–56.
- Newman A. P., White J. G., Sternberg P. W., 1996 Morphogenesis of the *C. elegans* hermaphrodite uterus. *Development* **122**: 3617–3626.
- Nishiwaki K., 1999 Mutations affecting symmetrical migration of distal tip cells in *Caenorhabditis elegans*. *Genetics* **152**: 985–997.
- Olesen C., 2004 Dephosphorylation of the Calcium Pump Coupled to Counterion Occlusion. *Science* **306**: 2251–2255.
- Ortiz M. A., Noble D., Sorokin E. P., Kimble J., 2014 A New Dataset of Spermatogenic vs. Oogenic Transcriptomes in the Nematode *Caenorhabditis elegans*. *Genes/Genomes/Genetics* **4**: 1765–1772.
- Palmgren M. G., Nissen P., 2011 P-type ATPases. *Annu Rev Biophys* **40**: 243–266.
- Pan C.-L., Baum P. D., Gu M., Jorgensen E. M., Clark S. G., Garriga G., 2008 *C. elegans* AP-2 and Retromer Control Wnt Signaling by Regulating MIG-14/Wntless. *Dev. Cell* **14**: 132–139.
- Park J.-S., Koentjoro B., Veivers D., Mackay-Sim A., Sue C. M., 2014 Parkinson's disease-associated human ATP13A2 (PARK9) deficiency causes zinc dyshomeostasis and mitochondrial dysfunction. *Hum. Mol. Genet.* **23**: 2802–2815.
- Park S. K., Choi V. N., Hwang A. B. J., 2013 LIN-12/Notch Regulates *lag-1* and *lin-12* Expression during Anchor Cell/Ventral Uterine Precursor Cell Fate Specification. *Molecules and Cells* **35**: 249–254.
- Pedersen P. L., Carafoli E., 1986 Ion motive ATPases. I. Ubiquity, properties, and significance to cell function. *Trends Biochem Sci* **12**: 146–150.
- Perraud A. L., Fleig A., Dunn C. A., Bagley L. A., Launay P., Schmitz C., Stokes A. J., Zhu Q., Bessman M. J., Penner R., Kinet J. P., Scharenberg A. M., 2001 ADP-ribose gating of the calcium-permeable LTRPC2 channel revealed by Nudix motif homology. *Nature* **411**: 595–599.
- Pickrell A. M., Youle R. J., 2015 The Roles of PINK1, Parkin, and Mitochondrial Fidelity in Parkinson's Disease. *Neuron* **85**: 257–273.
- Polymeropoulos M. H., Lavedan C., Leroy E., Ide S. E., Dehejia A., Dutra A., Pike B., Root H., Rubenstein J., Boyer R., Stenroos E. S., Chandrasekharappa S., Athanassiadou A., Papapetropoulos T., Johnson W. G., Lazzarini A. M., Duvoisin R. C., Di Iorio G., Golbe L. I., Nussbaum R. L., 1997 Mutation in the *alpha-synuclein* gene identified in families with Parkinson's disease. *Science* **276**: 2045–2047.

## References

- Post R. L., 1969 Flexibility of an Active Center in Sodium-Plus-Potassium Adenosine Triphosphatase. *The Journal of General Physiology* **54**: 306–326.
- Priess J. R., Schnabel H., Schnabel R., 1987 The *glp-1* locus and cellular interactions in early *C. elegans* embryos. *Cell* **51**: 601–611.
- Ramirez A., Heimbach A., Gründemann J., Stiller B., Hampshire D., Cid L. P., Goebel I., Mubaidin A. F., Wriekat A.-L., Roeper J., Al-Din A., Hillmer A. M., Karsak M., Liss B., Woods C. G., Behrens M. I., Kubisch C., 2006 Hereditary parkinsonism with dementia is caused by mutations in *ATP13A2*, encoding a lysosomal type 5 P-type ATPase. *Nat. Genet.* **38**: 1184–1191.
- Ramonet D., Podhajski A., Stafa K., Sonnay S., Trancikova A., Tsika E., Pletnikova O., Troncoso J. C., Glauser L., Moore D. J., 2012 PARK9-associated ATP13A2 localizes to intracellular acidic vesicles and regulates cation homeostasis and neuronal integrity. *Hum. Mol. Genet.* **21**: 1725–1743.
- Ramsey I. S., Delling M., Clapham D. E., 2006 An introduction to trp channels. <http://dx.doi.org/10.1146/annurev.physiol.68.040204.100431> **68**: 619–647.
- Rayaprolu S., Seven Y. B., Howard J., Duffy C., Altshuler M., Moloney C., Giasson B. I., Lewis J., 2018 Partial loss of ATP13A2 causes selective gliosis independent of robust lipofuscinosis. *Molecular and Cellular Neuroscience* **92**: 17–26.
- Reddien P. W., Horvitz H. R., 2000 CED-2/CrkII and CED-10/Rac control phagocytosis and cell migration in *Caenorhabditis elegans*. *Nat. Cell Biol.* **2**: 131–136.
- Rinaldi D. E., Corradi G. R., Cuesta L. M., Adamo H. P., de Tezanos Pinto F., 2015 The Parkinson-associated human P5B-ATPase ATP13A2 protects against the iron-induced cytotoxicity. *Biochim Biophys Acta* **1848**: 1646–1655.
- Rose K. L., Winfrey V. P., Hoffman L. H., Hall D. H., Furuta T., Greenstein D., 1997 The POU gene *ceh-18* promotes gonadal sheath cell differentiation and function required for meiotic maturation and ovulation in *Caenorhabditis elegans*. *Dev. Biol.* **192**: 59–77.
- Rowatt E., Williams R. J., 1992 The binding of polyamines and magnesium to DNA. *J. Inorg. Biochem.* **46**: 87–97.
- Ruaud A.-F., Bessereau J.-L., 2007 The P-type ATPase CATP-1 is a novel regulator of *C. elegans* developmental timing that acts independently of its predicted pump function. *Development* **134**: 867–879.
- Rubin H., 2005 The membrane, magnesium, mitosis (MMM) model of cell proliferation control. *Magnes Res* **18**: 268–274.
- Ryazanova L. V., Dorovkov M. V., Ansari A., Ryazanov A. G., 2004 Characterization of the protein kinase activity of TRPM7/ChaK1, a protein kinase fused to the transient receptor potential ion channel. *J. Biol. Chem.* **279**: 3708–3716.
- Sahni J., Scharenberg A. M., 2008 TRPM7 Ion Channels Are Required for Sustained Phosphoinositide 3-Kinase Signaling in Lymphocytes. *Cell Metabolism* **8**: 84–93.

## References

- Schindelin J., Arganda-Carreras I., Frise E., Kaynig V., Longair M., Pietzsch T., Preibisch S., Rueden C., Saalfeld S., Schmid B., Tinevez J.-Y., White D. J., Hartenstein V., Eliceiri K., Tomancak P., Cardona A., 2012 Fiji: an open-source platform for biological-image analysis. *Nature Methods* **9**: 676–682.
- Schlingmann K. P., Waldegger S., Konrad M., Chubanov V., Gudermann T., 2007 TRPM6 and TRPM7—Gatekeepers of human magnesium metabolism. *Biochimica et Biophysica Acta (BBA) - Molecular Basis of Disease* **1772**: 813–821.
- Schlingmann K. P., Weber S., Peters M., Niemann Nejsum L., Vitzthum H., Klingel K., Kratz M., Haddad E., Ristoff E., Dinour D., Syrrou M., Nielsen S., Sassen M., Waldegger S., Seyberth H. W., Konrad M., 2002 Hypomagnesemia with secondary hypocalcemia is caused by mutations in TRPM6, a new member of the TRPM gene family. *Nat. Genet.* **31**: 166–170.
- Schmidt K., Wolfe D. M., Stiller B., Pearce D. A., 2009 Cd<sup>2+</sup>, Mn<sup>2+</sup>, Ni<sup>2+</sup> and Se<sup>2+</sup> toxicity to *Saccharomyces cerevisiae* lacking YPK9p the orthologue of human ATP13A2. *Biochem. Biophys. Res. Commun.* **383**: 198–202.
- Schwabiuk M., Coudiere L., Merz D. C., 2009 SDN-1/syndecan regulates growth factor signaling in distal tip cell migrations in *C. elegans*. *Dev. Biol.* **334**: 235–242.
- Semerdjieva S., Shortt B., Maxwell E., Singh S., Fonarev P., Hansen J., Schiavo G., Grant B. D., Smythe E., 2008 Coordinated regulation of AP2 uncoating from clathrin-coated vesicles by *rab5* and hRME-6. *J. Cell Biol.* **183**: 499–511.
- Seydoux G., Greenwald I., 1989 Cell autonomy of *lin-12* function in a cell fate decision in *C. elegans*. *Cell* **57**: 1237–1245.
- Shafaq-Zadah M., Gomes-Santos C. S., Bardin S., Maiuri P., Maurin M., Iranzo J., Gautreau A., Lamaze C., Caswell P., Goud B., Johannes L., 2015 Persistent cell migration and adhesion rely on retrograde transport of  $\beta 1$  integrin. *Nat. Cell Biol.* **18**: 54–64.
- Siegfried K. R., Kimble J., 2002 POP-1 controls axis formation during early gonadogenesis in *C. elegans*. *Development* **129**: 443–453.
- Sigismund S., Argenzio E., Tosoni D., Cavallaro E., Polo S., Di Fiore P. P., 2008 Clathrin-mediated internalization is essential for sustained EGFR signaling but dispensable for degradation. *Dev. Cell* **15**: 209–219.
- Sorensen T. L. M., 2004 Phosphoryl Transfer and Calcium Ion Occlusion in the Calcium Pump. *Science* **304**: 1672–1675.
- Sorenson M. M., 1983 Calcium control of passive permeability to calcium in sarcoplasmic reticulum vesicles. *J. Biol. Chem.* **258**: 7684–7690.
- Starich T. A., Hall D. H., Greenstein D., 2014 Two Classes of Gap Junction Channels Mediate Soma-Germline Interactions Essential for Germline Proliferation and Gametogenesis in *Caenorhabditis elegans*. *Genetics* **198**: 1127–1153.
- Stawicki T. M., Zhou K., Yochem J., Chen L., Jin Y., 2011 TRPM Channels Modulate Epileptic-like Convulsions via Systemic Ion Homeostasis. *Current Biology* **21**: 883–888.

## References

- Stinchcomb D. T., Shaw J. E., Carr S. H., Hirsh D., 1985 Extrachromosomal DNA transformation of *Caenorhabditis elegans*. *Mol. Cell. Biol.* **5**: 3484–3496.
- Sulston J. E., 1988 5 Cell Lineage. In: *The Nematode Caenorhabditis Elegans*, Cold Spring Harbor Laboratory Press.
- Sulston J. E., Horvitz H. R., 1977 Post-embryonic cell lineages of the nematode, *Caenorhabditis elegans*. *Dev. Biol.* **56**: 110–156.
- Sulston J. E., Schierenberg E., White J. G., Thomson J. N., 1983 The embryonic cell lineage of the nematode *Caenorhabditis elegans*. *Dev. Biol.* **100**: 64–119.
- Sun A. Y., Lambie E. J., 1997 *gon-2*, a gene required for gonadogenesis in *Caenorhabditis elegans*. *Genetics* **147**: 1077–1089.
- Sørensen D. M., Buch-Pedersen M. J., Palmgren M. G., 2010 Structural divergence between the two subgroups of P5 ATPases. *Biochim Biophys Acta* **1797**: 846–855.
- Sørensen D. M., Holemans T., van Veen S., Martin S., Arslan T., Haagendahl I. W., Holen H. W., Hamouda N. N., Eggermont J., Palmgren M., Vangheluwe P., 2018 Parkinson disease related ATP13A2 evolved early in animal evolution (DJ Moore, Ed.). *PLoS ONE* **13**: e0193228.
- Tamai K., Semenov M., Kato Y., Spokony R., Liu C., Katsuyama Y., Hess F., Saint-Jeannet J. P., He X., 2000 LDL-receptor-related proteins in Wnt signal transduction. *Nature* **407**: 530–535.
- Tan J., Zhang T., Jiang L., Chi J., Hu D., Pan Q., Wang D., Zhang Z., 2011 Regulation of Intracellular Manganese Homeostasis by Kufor-Rakeb Syndrome-associated ATP13A2 Protein. *J. Biol. Chem.* **286**: 29654–29662.
- Teramoto T., Lambie E. J., Iwasaki K., 2005 Differential regulation of TRPM channels governs electrolyte homeostasis in the *C. elegans* intestine. *Cell Metabolism* **1**: 343–354.
- Teramoto T., Sternick L. A., Kage-Nakadai E., Sajjadi S., Siembida J., Mitani S., Iwasaki K., Lambie E. J., 2010 Magnesium Excretion in *C. elegans* Requires the Activity of the GTL-2 TRPM Channel (AC Hart, Ed.). *PLoS ONE* **5**: e9589.
- Thomas M. G., Stone L., Allan P., Barker A. R., White B. R., 2016 PAX6 expression may be protective against dopaminergic cell loss in Parkinson's disease. *CNS & Neurological Disorders - Drug Targets* **15**: 73–79.
- Toustrup-Jensen M. S., Holm R., Einholm A. P., Schack V. R., Morth J. P., Nissen P., Andersen J. P., Vilsen B., 2009 The C terminus of Na<sup>+</sup>,K<sup>+</sup>-ATPase controls Na<sup>+</sup> affinity on both sides of the membrane through Arg935. *J. Biol. Chem.* **284**: 18715–18725.
- Toyoshima C., Inesi G., 2004 Structural Basis of Ion Pumping by Ca<sup>2+</sup>-ATPase of the Sarcoplasmic Reticulum. *Annu. Rev. Biochem.* **73**: 269–292.
- Toyoshima C., Nakasako M., Nomura H., Ogawa H., 2000 Crystal structure of the calcium pump of sarcoplasmic reticulum at 2.6 Å resolution. *Nature* **405**: 647–655.

## References

- Tsunemi T., Krainc D., 2014 Zn<sup>2+</sup> dyshomeostasis caused by loss of ATP13A2/PARK9 leads to lysosomal dysfunction and alpha-synuclein accumulation. *Hum. Mol. Genet.* **23**: 2791–2801.
- Usenovic M., Knight A. L., Ray A., Wong V., Brown K. R., Caldwell G. A., Caldwell K. A., Stagljar I., Krainc D., 2012a Identification of novel ATP13A2 interactors and their role in  $\alpha$ -synuclein misfolding and toxicity. *Hum. Mol. Genet.* **21**: 3785–3794.
- Usenovic M., Tresse E., Mazzulli J. R., Taylor J. P., Krainc D., 2012b Deficiency of ATP13A2 Leads to Lysosomal Dysfunction,  $\alpha$ -Synuclein Accumulation, and Neurotoxicity. *Journal of Neuroscience* **32**: 4240–4246.
- Valente E. M., Bentivoglio A. R., Dixon P. H., Ferraris A., Ialongo T., Frontali M., Albanese A., Wood N. W., 2001 Localization of a novel locus for autosomal recessive early-onset parkinsonism, *PARK6*, on human chromosome 1p35-p36. *The American Journal of Human Genetics* **68**: 895–900.
- Vallipuram J., Grenville J., 2010 The E646D-ATP13A4 Mutation Associated with Autism Reveals a Defect in Calcium Regulation. *Cell Mol Neurobiol* **30**: 233–246.
- van Beek N., Patsatsi A., Gupta Y., Möller S., Freitag M., Lemcke S., Recke A., Zillikens D., Schmidt E., Ibrahim S., 2015 A family with atypical Hailey Hailey disease--is there more to the underlying genetics than ATP2C1? (AE Toland, Ed.). *PLoS ONE* **10**: e0121253.
- van Veen S., Sorensen D. M., Holemans T., Holen H. W., Palmgren M. G., Vangheluwe P., 2014 Cellular function and pathological role of ATP13A2 and related P-type transport ATPases in Parkinson's disease and other neurological disorders. *Front Mol Neurosci* **7**.
- Vilariño-Güell C., Wider C., Ross O. A., Dachsel J. C., Kachergus J. M., Lincoln S. J., Soto-Ortolaza A. I., Cobb S. A., Wilhoite G. J., Bacon J. A., Behrouz B., Melrose H. L., Hentati E., Puschmann A., Evans D. M., Conibear E., Wasserman W. W., Aasly J. O., Burkhard P. R., Djaldetti R., Ghika J., Hentati F., Krygowska-Wajs A., Lynch T., Melamed E., Rajput A., Rajput A. H., Solida A., Wu R.-M., Uitti R. J., Wszolek Z. K., Vingerhoets F., Farrer M. J., 2011 VPS35 Mutations in Parkinson Disease. *The American Journal of Human Genetics* **89**: 162–167.
- Walderhaug M. O., Post R. L., Saccomani G., Leonard R. T., Briskin D. P., 1985 Structural relatedness of three ion-transport adenosine triphosphatases around their active sites of phosphorylation. *J. Biol. Chem.* **260**: 3852–3859.
- Wang C., Ruan P., Zhao Y., Li X., Wang J., Wu X., Liu T., Wang S., Hou J., Li W., Li Q., Li J., Dai F., Fang D., Wang C., Xie S., 2017 Spermidine/spermine N1-acetyltransferase regulates cell growth and metastasis via AKT/ $\beta$ -catenin signaling pathways in hepatocellular and colorectal carcinoma cells. *Oncotarget* **8**: 1092–1109.
- Wang J., Liao Q.-J., Zhang Y., Zhou H., Luo C.-H., Tang J., Wang Y., Tang Y., Zhao M., Zhao X.-H., Zhang Q.-Y., Xiao L., 2014 TRPM7 is required for ovarian cancer cell growth, migration and invasion. *Biochem. Biophys. Res. Commun.* **454**: 547–553.
- Ward S., Carrel J. S., 1979 Fertilization and sperm competition in the nematode *Caenorhabditis elegans*. *Dev. Biol.* **73**: 304–321.



## References

- West R. J., Sun A. Y., Church D. L., Lambie E. J., 2001 The *C. elegans gon-2* gene encodes a putative TRP cation channel protein required for mitotic cell cycle progression. *Gene* **266**: 103–110.
- Whangbo J., Kenyon C., 1999 A Wnt signaling system that specifies two patterns of cell migration in *C. elegans*. *Molecular Cell* **4**: 851–858.
- Wilkinson H. A., Fitzgerald K., Greenwald I., 1994 Reciprocal changes in expression of the receptor *lin-12* and its ligand *lag-2* prior to commitment in a *C. elegans* cell fate decision. *Cell* **79**: 1187–1198.
- Winklhofer K. F., Haass C., 2010 Mitochondrial dysfunction in Parkinson's disease. *Biochimica et Biophysica Acta (BBA) - Molecular Basis of Disease* **1802**: 29–44.
- Wolf F. I., Trapani V., 2012 Magnesium and its transporters in cancer: a novel paradigm in tumour development. *Clinical Science* **123**: 417–427.
- Wolf F. I., Trapani V., Cittadini A., 2008 Magnesium and the control of cell proliferation: looking for a needle in a haystack. *Magnes Res* **21**: 83–91.
- Wöhlke A., Philipp U., Bock P., Beineke A., Lichtner P., Meitinger T., Distl O., 2011 A One Base Pair Deletion in the Canine *ATP13A2* Gene Causes Exon Skipping and Late-Onset Neuronal Ceroid Lipofuscinosis in the Tibetan Terrier (GS Barsh, Ed.). *PLoS Genet* **7**: e1002304.
- Xing J., Yan X., Estevez A., Strange K., 2008 Highly Ca<sup>2+</sup>-selective TRPM Channels Regulate IP<sub>3</sub>-dependent Oscillatory Ca<sup>2+</sup> Signaling in the *C. elegans* Intestine. *The Journal of General Physiology* **131**: 245–255.
- Yamaguchi H., Matsushita M., Nairn A. C., Kuriyan J., 2001 Crystal Structure of the Atypical Protein Kinase Domain of a TRP Channel with Phosphotransferase Activity. *Molecular Cell* **7**: 1047–1057.
- Yamasaki K., Daiho T., Danko S., Suzuki H., 2010 Ca<sup>2+</sup> release to lumen from ADP-sensitive phosphoenzyme E1PCa<sup>2+</sup> without bound K<sup>+</sup> of sarcoplasmic reticulum Ca<sup>2+</sup>-ATPase. *J. Biol. Chem.* **285**: 38674–38683.
- Yang P.-T., Lorenowicz M. J., Silhankova M., Coudreuse D. Y. M., Betist M. C., Korswagen H. C., 2008 Wnt Signaling Requires Retromer-Dependent Recycling of MIG-14/Wntless in Wnt-Producing Cells. *Dev. Cell* **14**: 140–147.
- Zeng X., Huang H., Tamai K., Zhang X., Harada Y., Yokota C., Almeida K., Wang J., Doble B., Woodgett J., Wynshaw-Boris A., Hsieh J.-C., He X., 2008 Initiation of Wnt signaling: control of Wnt coreceptor Lrp6 phosphorylation/activation via frizzled, dishevelled and axin functions. *Development* **135**: 367–375.
- Zielich J., Tzima E., Schröder E. A., Jemel F., Conradt B., Lambie E. J., 2018 Overlapping expression patterns and functions of three paralogous P5B ATPases in *Caenorhabditis elegans* (M-H Lee, Ed.). *PLoS ONE* **13**: e0194451.

## References

Zimprich A., Benet-Pagès A., Struhal W., Graf E., Eck S. H., Offman M. N., Haubenberger D., Spielberger S., Schulte E. C., Lichtner P., Rossle S. C., Klopp N., Wolf E., Seppi K., Pirker W., Presslauer S., Mollenhauer B., Katzenschlager R., Foki T., Hotzy C., Reinthaler E., Harutyunyan A., Kralovics R., Peters A., Zimprich F., Brücke T., Poewe W., Auff E., Trenkwalder C., Rost B., Ransmayr G., Winkelmann J., Meitinger T., Strom T. M., 2011 A Mutation in *VPS35*, Encoding a Subunit of the Retromer Complex, Causes Late-Onset Parkinson Disease. *The American Journal of Human Genetics* **89**: 168–175.

## **Acknowledgment**

I would like to express my sincere gratitude and appreciation to my mentor, friend and surf buddy PD Dr. Eric John Lambie for the excellent supervision during my doctoral research. Thank you for your immense scientific input and for teaching me all the great laboratory skills. I would also like to thank you for motivating me in times of frustration and creating such a great working atmosphere.

I would like to thank Prof. Dr. Barbara Conradt for the excellent scientific contribution and for giving me the opportunity to work in the research group of Cell and Developmental Biology at the LMU (Ludwig-Maximilians-University) Munich. It has been a great scientific and personal experience.

Many thanks to all the members of the Conradt lab, especially to Laura, Sebastian, Simon, Ryan, Sriyash, Nadin, Stephane, Jennifer, Christian, Fabs, Fabian, Hai, Anna, Marion, Elisabeth, Nadja and Melanie for creating such a friendly atmosphere and helping me with the different techniques.

I would also like to express my sincere gratitude and appreciation to my parents for their endless support and for helping me in every situation. This dissertation would not be possible without you.

Last but not least, I would like to express my sincere gratitude to my girlfriend Irena for her endless patience and for keeping me happy and motivated throughout my studies. This is already the third time that I express my appreciation to you in a thesis but this will be the last thesis, I promise.

## **Appendices**

---

## **Establishment of a CRISPR/Cas9-based strategy for inducible protein dimerization**

Jeffrey Zielich, Sriyash Mangal, Esther Zanin, Eric J. Lambie

**Published: April 17, 2018. microPublication: Biology**

---

04/17/2018 – Open Access

# Establishment of a CRISPR/Cas9-based strategy for inducible protein dimerization

Jeffrey Zielich, Sriyash Mangal, Esther Zanin and Eric J. Lambie

Department of Cell and Developmental Biology, Ludwig-Maximilians-University, Munich, Planegg-Martinsried, Germany.

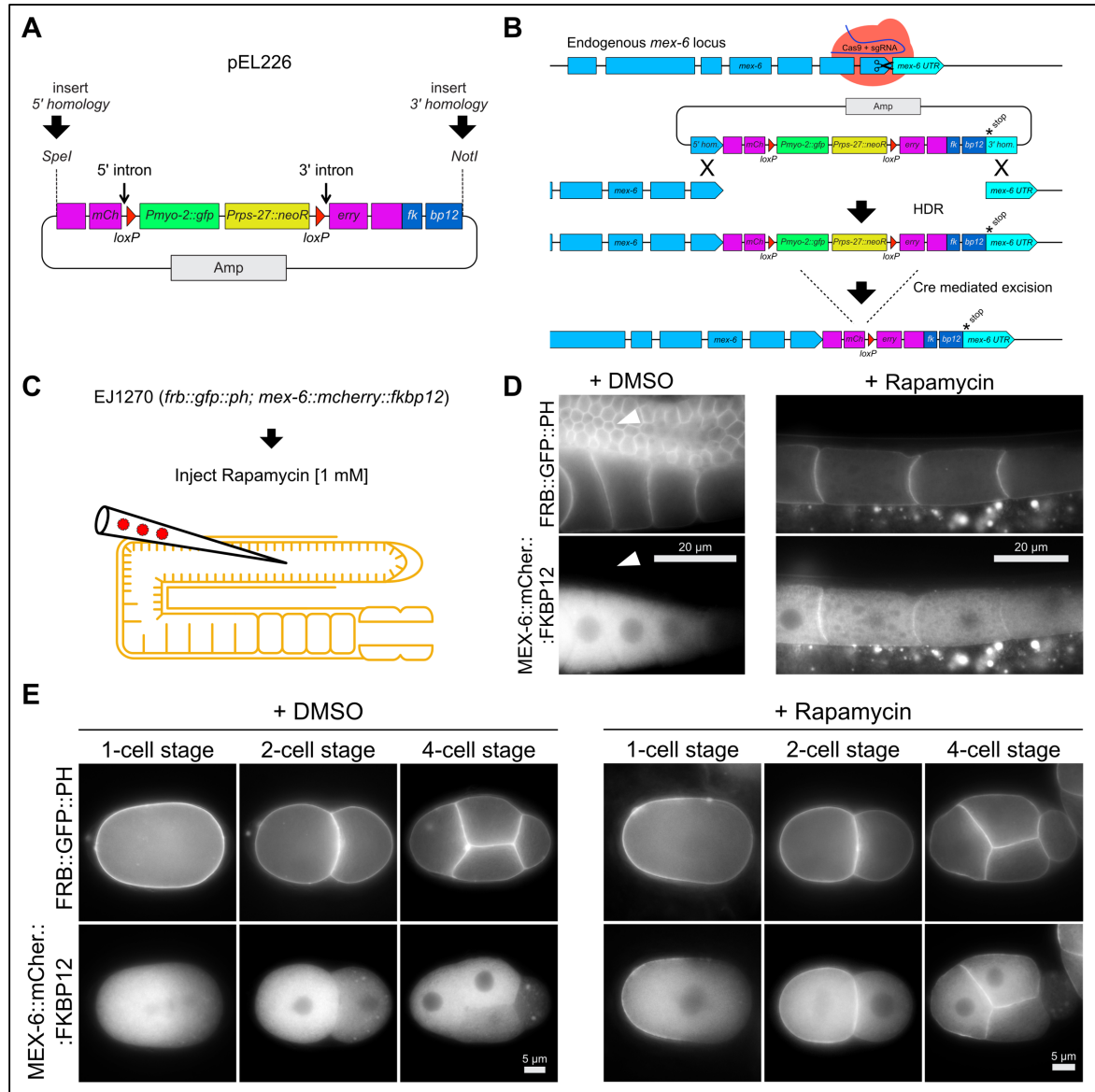


**Figure 1: CRISPR-based dual-marker selection cassette for rapamycin-induced protein dimerization in *C. elegans*.** (A) The codon-optimized *fkbp12* sequence together with a *NotI* site for 3' homology region insertion was introduced in the *mCherry*-tag repair donor vector (Norris *et al.* 2015) to generate vector pEL226. (B) Schematic overview of CRISPR/Cas9 mediated *mCherry::fkbp12* tag of endogenous *mex-6*, including Cre-mediated excision of the dual marker selection cassette, resulting in strain EJ1269. (C) Injection of 1 mM rapamycin into adult stage gonads (Mangal *et al.* 2018) of strain EJ1270 expressing FRB::GFP::PH and MEX-6::mCherry::FKBP12 (obtained by crossing EJ1269 into ZAN87,

Table 2). (D) Epifluorescence microscopy images of adult stage proximal gonads imaged ~ 6 hours after the gonads were injected with DMSO (*n* = 4) or 1 mM rapamycin (*n* = 5). MEX-6::mCherry::FKBP12 signal increases in later stage oocytes and remains cytosolic if 10 % DMSO is injected into the gonad. Arrowheads point to the pachytene region of the gonad where MEX-

04/17/2018 – Open Access

6::mCherry::FKBP12 is not detectable. Injection of rapamycin induces the binding of the FRB and FKBP12 domains and thereby translocates MEX-6::mCherry::FKBP12 to the plasma membrane of diakinesis-stage oocytes. (E) Epifluorescence microscopy images of 1-cell, 2-cell and 4-cell stage embryos imaged ~ 6 hours after the gonads were injected with DMSO (1-cell stage  $n = 5$ ; 2-cell stage  $n = 4$ ; 4-cell stage  $n = 7$ ) or 1 mM rapamycin (1-cell stage  $n = 10$ ; 2-cell stage  $n = 16$ ; 4-cell stage  $n = 10$ ). 1-cell stage embryos showing a cytosolic anterior gradient and 2-cell / 4-cell stage embryos showing strong expression in the AB lineage (DMSO). Upon rapamycin injection, MEX-6::mCherry::FKBP12 translocates to the plasma membrane in the anterior region (1-cell stage) and the anterior blastomeres (2-cell and 4-cell stage).

## Description:

Induced protein dimerization is a useful tool to study protein function. A well-established method takes advantage of the binding between the FKBP12 protein (FK506 binding protein 12 kDa) and the FRB domain of the mTOR kinase upon interaction with rapamycin (Putyrski and Schultz 2012). Recently we established a rapamycin-inducible dimerization system for the germ line and early embryos of *C. elegans* (Mangal *et al.* 2018). We demonstrated the translocation of mCherry::FKBP12 to the plasma membrane via rapamycin induced binding to FRB::GFP::PH (anchored to the plasma membrane). In order to study the function of a native protein upon rapamycin induced translocation it would be advantageous to tag the genomic region of the gene of interest (GOI) with *mCherry::fkbp12* to ensure that the fusion protein is controlled by its native environment.

The CRISPR/Cas9 system has revolutionized genome engineering in *C. elegans* (Chen *et al.* 2013; Arribere *et al.* 2014; Paix *et al.* 2015; Dickinson *et al.* 2015; Norris *et al.* 2015; Schwartz and Jorgensen 2016). DNA double-stranded breaks are generated by the endonuclease Cas9, which is guided to its target by a single guide RNA (sgRNA) (Jinek *et al.* 2012). If a repair donor vector is provided carrying a transgenic sequence flanked by 5' and 3' homology regions, the cell can repair these double-stranded breaks via homology directed repair (HDR) by incorporating the transgenic sequence into the cleaved locus. This enables *e.g.* N- or C-terminal fluorescent protein fusions of the GOI. Drug-selection based screening methods to tag native proteins have been developed (Dickinson *et al.* 2015; Norris *et al.* 2015; Schwartz and Jorgensen 2016). One of these streamlined methods uses a dual marker selection cassette (Norris *et al.* 2015).

Herein, we describe a modification of the dual-marker selection cassette plasmid of Norris *et al.* (2015) that can be used in conjunction with CRISPR/Cas9, TALEN or Zinc Finger Nucleases to tag endogenous proteins for inducible translocation to the plasma membrane during early embryogenesis or in the germ line.

We modified Norris's *mCherry*-tag repair donor vector by fusing a *C. elegans* codon-optimized *fkbp12* sequence 3' to *mCherry* (Mangal *et al.* 2018) and re-establishing the critical *NotI* site for 3' homology region insertion (Figure 1 A; pEL226). This vector can be used to C-terminally tag any GOI by following the protocol of Norris *et al.* (2015), including subsequent Cre-mediated excision of the dual marker selection cassette (Figure 1 B). As proof of principle we C-terminally tagged the locus of *mex-6* on chromosome II with *mCherry::fkbp12* (Figure 1 B). We observed increasing cytoplasmic mCherry signal in late-stage oocytes, and anterior enrichment in early-stage embryos (Figure 1 D and E; DMSO control). We did not detect any mCherry signal in the pachytene region of adult stage gonads (Figure 1 D arrowheads; DMSO control). These observations confirm previous localization studies for *mex-6(ax2065[mex-6::gfp])* II transgenic animals (Paix *et al.* 2014), and mirror those for observed for the paralogous protein, MEX-5 (Schubert *et al.* 2000; Griffin *et al.* 2011). We crossed the MEX-6::mCherry::FKBP12 expressing strain (EJ1269,

Table 2) with a strain that expresses FRB::GFP::PH (ZAN87; Mangal *et al.*, 2018), which localizes to the plasma membrane in the germ line and early embryos (Figure 1 D and E), and then singled F2 hermaphrodites to obtain a strain that is homozygous for both insertions (EJ1270,

Table 2). Animals from this strain were injected with 1 mM rapamycin into the pachytene region of the germ line to induce binding between the FRB and FKBP12 domains. As expected, we observed strong accumulation of MEX-6::mCherry::FKBP12 signal at the plasma membrane of late-stage oocytes and anterior blastomeres of early embryos, 6 h after injection (Figure 1 D and E). Importantly, the MEX-6::mCherry::FKBP12 remains cytoplasmic if DMSO is injected into the germ line as a control (Figure 1 D and E).

Our repair donor vector can be easily modified to tag any GOI with *mCherry::fkbp12* in a well-established and streamlined manner (Norris *et al.* 2015) and it expands the *C. elegans* CRISPR/Cas9 toolbox for the rapamycin-

04/17/2018 – Open Access

inducible dimerization system. By crossing into the strain that expresses FRB::GFP::PH (ZAN87) (Mangal *et al.* 2018) it becomes possible to translocate an endogenously tagged mCherry::FKBP12 protein to the plasma membrane of early embryos or the germ line. Additionally, MEX-6::mCherry::FKBP12 could be used to enrich a protein-of-interest that is tagged with FRB::GFP within the anterior region of early embryos.

### Reagents:

Standard methods for DNA amplification, analysis and manipulation were used. PCR products were amplified by using Phusion® High-Fidelity DNA Polymerase (New England Biolabs), according to the manufacturer's protocol. DNA sequences were obtained by Sanger sequencing.

We inserted a *C. elegans* codon optimized sequence of *fkbp12* (plus a flexible linker 5' of *fkbp12*, gcaggtggaggtact) into the unique *NotI* site of loxP\_myo2\_neoR\_mCherry\_intron (Norris *et al.* 2015) via Gibson assembly (Gibson *et al.* 2009) by creating a new unique *NotI* site 3' of *fkbp12*. The resulting vector pEL226 is a universal repair donor vector to tag any locus with *mCherry::fkbp12*. We digested pEL226 with *SpeI* and *NotI* and subsequently column purified the DNA. We amplified ~575 bp 5' and 3' homology region of the C-terminus of *mex-6* from genomic DNA (3' homology region includes the stop codon of *mex-6* exon7, PAM(*mex-6.1*) was mutated to NCA) with primers carrying homology tails (Table 1) to the unique *SpeI* and *NotI* sites of pEL226. PCR products were subsequently column purified. All four fragments (PCR products plus pEL226 fragments) were fused together via Gibson assembly (pEL228).

We designed sgRNA(*mex-6.1*) via the online sgRNA design tool <http://crispr.cos.uni-heidelberg.de/index.html> (Stemmer *et al.* 2015). sgRNA(*mex-6.1*) is almost identical to sgRNA18 (Paix *et al.* 2014) but shifted by 1 nt 3' and therefore using another PAM. sgRNA(*mex-6.1*) expression plasmid (pEL227) was cloned by using pRB1017 following the protocol of (Arribere *et al.* 2014). All plasmids were purified by using PureLink™ HQ Mini Plasmid DNA Purification Kit (Invitrogen) and eluted with Ultrapure Water for Molecular Biology (Merck / EMD MilliporeSigma). We used the following injection-mix concentrations (Norris *et al.* 2015): Peft-3::Cas9\_SV40-NLS::tbb-2\_UTR (*P<sub>cas9</sub>* expression plasmid) at 50 ng/μl, sgRNA(*mex-6.1*) plasmid (pEL227, based on pRB1017) at 100 ng/μl, repair donor vector (pEL228) at 50 ng/μl (based on pEL226), pCFJ90 (Frøkjær-Jensen *et al.* 2014) at 2.5 ng/μl (*P<sub>mex-6</sub>*), pCFJ104 (Frøkjær-Jensen *et al.* 2014) at 5ng/μl (*P<sub>mex-6</sub>*). Ultrapure Water for Molecular Biology (Merck / EMD MilliporeSigma) was added to a total volume of 10 μl.

We injected 62 young adults (N2) and obtained 7 independent lines. We proceeded with one line and injected a Cre recombinase expression vector (pDD104). We used the following injection-mix concentrations: pDD104 (Dickinson *et al.* 2013) at 50 ng/μl and pCFJ90 at 2.5 ng/μl. After successful Cre-mediated excision of the dual marker selection cassette (Norris *et al.* 2015), we obtained the strain EJ1269 (Table 2) showing mCherry signal consistent with GFP signal observed in *mex-6(ax2065[mex-6::gfp])* II (Paix *et al.* 2014). Finally we crossed EJ1269 into ZAN87 (Mangal *et al.* 2018) resulting in EJ1270 (Table 2).

The rapamycin-induced dimerization was performed according to (Mangal *et al.* 2018). Microscopy was performed 6 h after injection. Worms were dissected with 20 gauge hypodermic needles in M9 to release embryos. Whole worms were immobilized with 10 mM levamisole. Whole worms or embryos and were mounted on 4% agarose pads. Animals were imaged by using Zeiss Axioskop 2 and MetaMorph software (Molecular Devices). Image processing was performed in Fiji/imageJ 2.0.0 (Schindelin *et al.* 2012), brightness and contrast were adjusted either in Fiji/imageJ 2.0.0 or Affinity Designer 1.6.1 (Serif).

**Table 1: Primer homology tail sequences for cloning homology arms into pEL226**

Primer homology tails	homology tail sequence
forward primer 5' homology ( <i>SpeI</i> )	aaacgacggccagtgaattca
reverse primer 5' homology ( <i>SpeI</i> , introducing an alanine 5' of <i>mCherry</i> )	cttctcacccttgagaccatagc
forward primer 3' homology ( <i>NotI</i> , introducing an alanine 3' of <i>fkbp12</i> , [optional stop codon])	cgagctcctcaagctcgaggct[tag]
reverse primer 3' homology ( <i>NotI</i> )	tgattacgccaagcttgccg



**Table 2: Used *C. elegans* strains**

Strain name	Genotype	Reference
<b>ZAN87</b>	<i>estSi50[pEZ156;pmex-5::frb::gfp::ph::tbb2; cb-unc-119(+)]I; unc-119(ed3) III</i>	(Mangal <i>et al.</i> 2018)
<b>EJ1269</b>	<i>mex-6(dx203[mex-6::mcherry::fkbp12 + loxP]) II</i>	This study
<b>EJ1270</b>	<i>estSi50[pEZ156;pmex-5::frb::gfp::ph::tbb2; cb-unc-119(+)]I; mex-6(dx203[mex-6::mcherry::fkbp12 + loxP]) II</i>	This study

## Acknowledgments:

We thank John Calarco for providing repair donor vector loxP\_myo2\_neoR\_mCherry\_intron (Norris *et al.* 2015).

## References:

- Arribere J. A., Bell R. T., Fu B. X. H., Artiles K. L., Hartman P. S., Fire A. Z., 2014 Efficient marker-free recovery of custom genetic modifications with CRISPR/Cas9 in *Caenorhabditis elegans*. *Genetics* **198**: 837–846.
- Chen C., Fenk L. A., de Bono M., 2013 Efficient genome editing in *Caenorhabditis elegans* by CRISPR-targeted homologous recombination. *Nucleic Acids Res* **41**: e193–e193.
- Dickinson D. J., Pani A. M., Heppert J. K., Higgins C. D., Goldstein B., 2015 Streamlined Genome Engineering with a Self-Excising Drug Selection Cassette. *Genetics* **200**: 1035–1049.
- Dickinson D. J., Ward J. D., Reiner D. J., Goldstein B., 2013 Engineering the *Caenorhabditis elegans* genome using Cas9-triggered homologous recombination. *Nature Methods* **10**: 1028–1034.
- Frøkjær-Jensen C., Davis M. W., Sarov M., Taylor J., Flibotte S., LaBella M., Pozniakovsky A., Moerman D. G., Jorgensen E. M., 2014 Random and targeted transgene insertion in *Caenorhabditis elegans* using a modified Mos1 transposon. *Nature Methods* **11**: 529–534.
- Gibson D. G., Young L., Chuang R.-Y., Venter J. C., Hutchison C. A., Smith H. O., 2009 Enzymatic assembly of DNA molecules up to several hundred kilobases. *Nature Methods* **6**: 343–345.
- Griffin E. E., Odde D. J., Seydoux G., 2011 Regulation of the MEX-5 gradient by a spatially segregated kinase/phosphatase cycle. *Cell* **146**: 955–968.
- Jinek M., Chylinski K., Fonfara I., Hauer M., Doudna J. A., Charpentier E., 2012 A programmable dual-RNA-guided DNA endonuclease in adaptive bacterial immunity. *Science* **337**: 816–821.
- Mangal S., Zielich J., Lambie E. J., Zanin E., 2018 Rapamycin-induced protein dimerization as a tool for *C. elegans* research. *Micropublication: biology Dataset*.
- Norris A. D., Kim H.-M., Colaiácovo M. P., Calarco J. A., 2015 Efficient Genome Editing in *Caenorhabditis elegans* with a Toolkit of Dual-Marker Selection Cassettes. *Genetics* **201**: 449–458.
- Paix A., Folkmann A., Rasoloson D., Seydoux G., 2015 High Efficiency, Homology-Directed Genome Editing in *Caenorhabditis elegans* Using CRISPR/Cas9 Ribonucleoprotein Complexes. *Genetics* **201**: genetics.115.179382–54.
- Paix A., Wang Y., Smith H. E., Lee C.-Y. S., Calidas D., Lu T., Smith J., Schmidt H., Krause M. W., Seydoux G., 2014 Scalable and Versatile Genome Editing Using Linear DNAs with Micro-Homology to Cas9 Sites in *Caenorhabditis elegans*. *Genetics* **198**: genetics.114.170423–1356.

04/17/2018 – *Open Access*

Putyrski M., Schultz C., 2012 Protein translocation as a tool: The current rapamycin story. *FEBS Letters* **586**: 2097–2105.

Schindelin J., Arganda-Carreras I., Frise E., Kaynig V., Longair M., Pietzsch T., Preibisch S., Rueden C., Saalfeld S., Schmid B., Tinevez J.-Y., White D. J., Hartenstein V., Eliceiri K., Tomancak P., Cardona A., 2012 Fiji: an open-source platform for biological-image analysis. *Nature Methods* **9**: 676–682.

Schubert C. M., Lin R., de Vries C. J., Plasterk R. H., Priess J. R., 2000 MEX-5 and MEX-6 function to establish soma/germline asymmetry in early *C. elegans* embryos. *Molecular Cell* **5**: 671–682.

Schwartz M. L., Jorgensen E. M., 2016 SapTrap, a Toolkit for High-Throughput CRISPR/Cas9 Gene Modification in *Caenorhabditis elegans*. *Genetics*: genetics.115.184275.

Stemmer M., Thumberger T., del Sol Keyer M., Wittbrodt J., Mateo J. L., 2015 CCTop: An Intuitive, Flexible and Reliable CRISPR/Cas9 Target Prediction Tool (S Maas, Ed.). *PLoS ONE* **10**: e0124633.

## Funding

E.J.L. was supported by DFG grant LA3380/2, and this work was also supported by the Emmy-Noether-Program (ZA619/3-1) from the DFG to E.Z.

**Reviewed by** Adam Norris

**Received** 04/12/2018, **Accepted** 04/16/2018. **Available** starting WormBase release WS266, **Published Online** 04/17/2018.

**Copyright:** © 2018. This is an open-access article distributed under the terms of the Creative Commons Attribution License, which permits unrestricted use, distribution, and reproduction in any medium, provided the original author and source are credited.

**Citation:** Zielich, J; Mangal, S; Zanin, E; Lambie, EJ (2018): Establishment of a CRISPR/Cas9-based strategy for inducible protein dimerization. *Micropublication: biology. Dataset*. <https://doi.org/10.17912/W2208R>

---

**Rapamycin-induced protein dimerization as a tool for *C. elegans* research**

Sriyash Mangal, Jeffrey Zielich, Eric J. Lambie, Esther Zanin

**Published: March 20, 2018. microPublication: Biology**

---

## Rapamycin-induced protein dimerization as a tool for *C. elegans* research

Sriyash Mangal, Jeffrey Zielich, Eric J. Lambie and Esther Zanin

Department of Cell and Developmental Biology, Ludwig-Maximilians-University, Munich, Planegg-Martinsried, Germany.

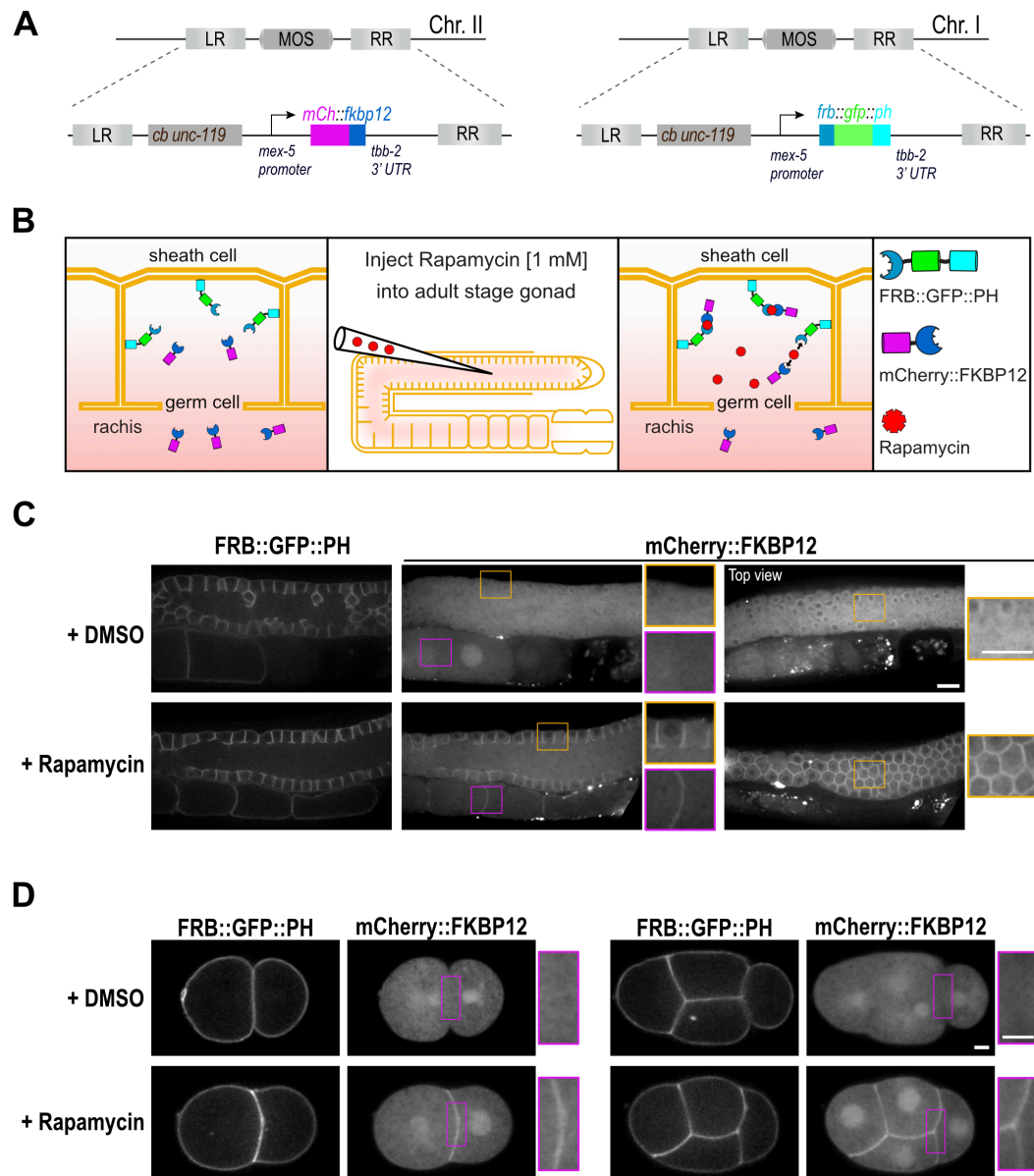


**Figure 1.** After injection of rapamycin, cytosolic mCherry::FKBP12 dimerizes with FRB::GFP::PH and translocates to the plasma membrane. (A) The mCherry-tagged FKBP12 and GFP-PH-tagged FRB transgenes under control of the *mex-5* promoter and *tbb-2* 3' UTR were integrated into chromosome II and chromosome I, respectively. (B) Schematic representation of rapamycin-induced heterodimerization of FRB and FKBP12 fusion proteins in the *C. elegans* gonad. The GFP-tagged FRB domain is tethered to the plasma membrane by the PH domain and the mCherry-tagged FKBP12 is present in the cytoplasm.

03/20/2018 – Open Access

After injection of 1 mM rapamycin into the gonad, heterodimers of FRB and FKBP12 fusion proteins form and mCherry::FKBP12 translocates to the plasma membrane. **(C)** Confocal images of germ line of an adult worm expressing FRB::GFP::PH and mCherry::FKBP12 2-3 hours after injection with DMSO ( $n = 19$ ) or 1 mM rapamycin ( $n = 29$ ) into the gonad.  $n$  = number of gonads. Yellow insets highlight the plasma membrane of gonadal germ cells and magenta insets highlight the plasma membrane of oocytes. Scale bar 10  $\mu$ m. **(D)** Confocal images of two-cell and four-cell embryos imaged approximately 2-3 hours after the gonads were injected with DMSO (2-cell embryo  $n = 10$ ; 4-cell embryo  $n = 9$ ) or 1 mM rapamycin (2-cell embryo  $n = 8$ ; 4-cell embryo  $n = 9$ ). Insets highlight the plasma membrane between the blastomeres. Scale bar 5  $\mu$ m.

## Description:

Induced protein dimerization is an invaluable tool in cellular biology to study protein function. Induced dimerization has been widely used to modulate enzymatic activity as well as expression and localization of proteins (Voß *et al.*, 2015; DeRose *et al.*, 2013). A popular method employs the chemical dimerizer rapamycin to induce binding between the FRB domain of the mTOR kinase and the FKBP12 protein (FK506 binding protein 12 kDa) (Putyrski and Schultz, 2012). Rapamycin-induced protein dimerization has been extensively used in cell culture systems and yeast to control RhoA GTPases signaling (Inoue *et al.*, 2005), protein stability (Janse *et al.*, 2004) or phosphoinositide composition of the plasma membrane (Ueno *et al.*, 2011). The small nematode *C. elegans* is a popular model system for cell biology, however to our knowledge, rapamycin-induced protein dimerization has not been successfully used in this organism. To establish the rapamycin-induced protein dimerization technique in *C. elegans* we codon-optimized the human FRB and FKBP12 domains and introduced one intron to ensure high expression of the transgenes. The FRB domain was fused to GFP and the plekstrin homology domain (PH) (Audhya *et al.*, 2005) at the C-terminus to anchor it at the plasma membrane and the FKBP12 domain was fused to mCherry (Figure 1A, B). Both transgenes are controlled by the *mex-5* promoter and *tbb-2* 3'UTR to ensure high and ubiquitous expression of the fusion proteins. After we generated single-copy integrations using MosSCI (Frøkjær-Jensen *et al.*, 2008) both strains were crossed together. As expected FRB::GFP::PH localizes to the plasma membrane in the germ line and early embryos and mCherry::FKBP12 is present in the cytoplasm and the nucleus (Figure 1C, D). To induce binding of the FRB and FKBP12 domains and thereby translocation of the mCherry::FKBP12 to the plasma membrane, we injected 1 mM rapamycin into the pachytene region of the germ line. Upon rapamycin injection, mCherry::FKBP12 translocated from the cytoplasm to the plasma membrane in all germ lines (Figure 1C) and early embryos analyzed (Figure 1D). In control worms injected with DMSO, translocation of mCherry::FKBP12 to the plasma membrane was not observed (Figure 1C, D). As expected in rapamycin-injected worms expressing only the mCherry::FKBP12 transgene, no translocation of mCherry::FKBP12 to the plasma membrane was visible ( $n = 7$  gonads). Importantly after rapamycin injection we did not observe alterations in gonad morphology ( $n = 29$  gonads) and early embryonic divisions ( $n = 17$  embryos) or embryonic lethality (+DMSO 281/0; +rapamycin 302/0; number of viable/dead progeny) validating applicability of our system for future cell biological studies. mCherry::FKBP12 localizes to the nucleus and the cytoplasm and therefore dimerization can be induced in both compartments. In case dimerization will be used to selectively target proteins to the nucleus or cytoplasm additional modifications of the presented system will be required. In summary, we establish a rapamycin-inducible dimerization system in *C. elegans* and demonstrate that it can be used to target a protein of interest to a specific subcellular region in the germ line and in early embryos. Our system can be directly used to target any protein to the plasma membrane of germ cells or early embryos by fusing it to the FKBP12 domain. Moreover, it can be easily modified to target proteins to different subcellular locations and to control protein activity or stability.

## Reagents

### Generation of *C. elegans* strains

*C. elegans* strains were grown at 20°C on NGM agar plates according to standard procedures (Stiernagle, 2006). Gibson cloning (E2611; NEB) was used to construct transgenes encoding FRB::GFP::PH and mCherry::FKBP12 in pCFJ350. cDNA sequences of human FRB (NM\_004958) and FKBP12 (CR542168) were codon-optimized (Redemann *et al.*, 2011) for expression in *C. elegans* and introns were introduced between amino acids 25(K)-26(G) and amino acids 35(K)-36(K), respectively and DNA was synthesized by Eurofins Genomics. In the FRB domain 'threonine' 2098 was mutated to 'leucine' which allows the binding to rapamycin derivatives that do not interact with mTOR kinase (Bayle *et al.*, 2006). Single-copy insertions of FRB::GFP::PH and mCherry::FKBP12 were generated on chromosomes I and II, respectively, using the MosSCI method (Frøkjær-Jensen *et al.*, 2008; 2014). Expression of the transgenes was controlled by the *mex-5* promoter and the *tbb-2* 3' UTR (Zeiser *et al.*, 2011).

03/20/2018 – Open Access

Finally, the two *C. elegans* strains *frb::gfp::ph* and *mCherry::fkbp12* were crossed together to obtain expression of both transgenes in one strain.

**Table 1 Used *C. elegans* strains**

Strain Name	Genotype	Reference
EG6699	<i>ttTi5605</i> II; <i>unc-119(ed3)</i> III; <i>oxEx1578</i>	Frøkjær-Jensen <i>et al.</i> , 2008
EG8078	<i>oxTi185</i> I; <i>unc-119(ed3)</i> III	Frøkjær-Jensen <i>et al.</i> , 2014
ZAN87	<i>estSi50[pEZ156;pmex-5::frb::gfp::ph::tbb2; cb-unc-119(+)]I</i> ; <i>unc-119(ed3)</i> III	This study.
ZAN98	<i>estSi54[pEZ159;pmex-5::mCherry::fkbp12::tbb2; cb-unc-119(+)]II</i> ; <i>unc-119(ed3)</i> III	This study.
ZAN101	<i>estSi50[pEZ156;pmex-5::frb::gfp::ph::tbb2; cb-unc-119(+)]I</i> ; <i>estSi54[pEZ159;pmex-5::mCherry::fkbp12::tbb2; cb-unc-119(+)]II</i> ; <i>unc-119(ed3)</i> III	This study.

## Rapamycin injection

10 mM stock of rapamycin (Cayman Chemical, 13346) was prepared in DMSO and stored at -20°C. The two gonad arms of adult worms were injected with 1 mM rapamycin or 10% DMSO (control) diluted to their final concentration in water.

## Fluorescence Microscopy

For imaging *C. elegans* embryos, adult worms were dissected 1.5 to 2 hours after injection in a 4-μl drop of M9 buffer on an 18 × 18-mm coverslip, and the coverslip was inverted onto a 2% agarose pad. For imaging adult *C. elegans* worms, a few animals were mounted on a 10% agarose pad (prepared in 0.6x M9 buffer) with 1 ul of immobilizing 0.10 micron beads (00876, Polysciences) (Kim *et al.*, 2013). An 18 × 18-mm coverslip was placed on top and the surrounding region of the agarose pad was filled with mineral oil to prevent shrinking of the agarose pad. All images were acquired at 25°C on an eclipse Ti spinning disk confocal (Nikon), which was controlled by NIS Elements 4.51 and equipped with a 100x 1.45-NA Plan-Apo-chromat oil immersion objective, a 488-nm and 561-nm laser line, and an Andor DU-888 X-11056 camera.

## References

- Audhya, A., F. Hyndman, I.X. McLeod, A.S. Maddox, J.R. Yates, A. Desai, and K. Oegema. 2005. A complex containing the Sm protein CAR-1 and the RNA helicase CGH-1 is required for embryonic cytokinesis in *Caenorhabditis elegans*. *The Journal of Cell Biology*. 171:267–279. doi:10.1083/jcb.200506124.
- Bayle, J.H., J.S. Grimley, K. Stankunas, J.E. Gestwicki, T.J. Wandless, and G.R. Crabtree. 2006. Rapamycin Analogs with Differential Binding Specificity Permit Orthogonal Control of Protein Activity. *Chemistry & Biology*. 13:99–107. doi:10.1016/j.chembiol.2005.10.017.
- DeRose, R., T. Miyamoto, and T. Inoue. 2013. Manipulating signaling at will: chemically-inducible dimerization (CID) techniques resolve problems in cell biology. *Pflugers Arch - Eur J Physiol*. 465:409–417. doi:10.1007/s00424-012-1208-6.
- Frøkjær-Jensen, C., M. Wayne Davis, C.E. Hopkins, B.J. Newman, J.M. Thummel, S.-P. Olesen, M. Grunnet, and E.M. Jorgensen. 2008. Single-copy insertion of transgenes in *Caenorhabditis elegans*. *Nat Genet*. 40:1375–1383. doi:10.1038/ng.248.

03/20/2018 – Open Access

Frøkjær-Jensen, C., M.W. Davis, M. Sarov, J. Taylor, S. Flibotte, M. LaBella, A. Pozniakovsky, D.G. Moerman, and E.M. Jorgensen. 2014. Random and targeted transgene insertion in *Caenorhabditis elegans* using a modified Mos1 transposon. *Nature Methods*. 11:529–534. doi:10.1038/nmeth.2889.

Inoue, T., W.D. Heo, J.S. Grimley, T.J. Wandless, and T. Meyer. 2005. An inducible translocation strategy to rapidly activate and inhibit small GTPase signaling pathways. *Nature Methods*. 2:415–418. doi:10.1038/nmeth763.

Janse, D.M., B. Crosas, D. Finley, and G.M. Church. 2004. Localization to the proteasome is sufficient for degradation. *Journal of Biological Chemistry*. 279:21415–21420. doi:10.1074/jbc.M402954200.

Kim, E., L. Sun, C.V. Gabel, and C. Fang-Yen. 2013. Long-Term Imaging of *Caenorhabditis elegans* Using Nanoparticle-Mediated Immobilization. *PLoS ONE*. 8:e53419–6. doi:10.1371/journal.pone.0053419.

Putyrski, M., and C. Schultz. 2012. Protein translocation as a tool: The current rapamycin story. *FEBS Letters*. 586:2097–2105. doi:10.1016/j.febslet.2012.04.061.

Redemann, S., S. Schloissnig, S. Ernst, A. Pozniakowsky, S. Ayloo, A.A. Hyman, and H. Bringmann. 2011. Codon adaptation–based control of protein expression in *C. elegans*. *Nature Methods*. 8:250–252. doi:10.1038/nmeth.1565.

Stiernagle, T. 2006. Maintenance of *C. elegans*. *WormBook*. 1–11. doi:10.1895/wormbook.1.101.1.

Ueno, T., B.H. Falkenburger, C. Pohlmeier, and T. Inoue. 2011. Triggering actin comets versus membrane ruffles: distinctive effects of phosphoinositides on actin reorganization. *Science Signaling*. 4:ra87–ra87. doi:10.1126/scisignal.2002033.

Voß, S., L. Klewer, and Y.-W. Wu. 2015. Chemically induced dimerization: reversible and spatiotemporal control of protein function in cells. *Curr Opin Chem Biol*. 28:194–201. doi:10.1016/j.cbpa.2015.09.003.

Zeiser, E., C. Frøkjær-Jensen, E. Jorgensen, and J. Ahringer. 2011. MosSCI and Gateway Compatible Plasmid Toolkit for Constitutive and Inducible Expression of Transgenes in the *C. elegans* Germline. *PLoS ONE*. 6:e20082–6. doi:10.1371/journal.pone.0020082.

## Acknowledgments:

We thank the Center for Advanced Light Microscopy (CALM) and especially H. Harz for outstanding microscopy support.

## Funding:

E.Z. was supported by the Emmy-Noether-Program (ZA619/3-1) from the DFG, and this work was also supported by DFG grant LA3380/2 to E.J.L.

**Reviewed by** Ann Wehman

**Received** 02/28/2018, **Accepted** 03/19/2018. **Available** starting WormBase release WS266, **Published Online** 03/20/2018.

**Copyright:** © 2018. This is an open-access article distributed under the terms of the Creative Commons Attribution License, which permits unrestricted use, distribution, and reproduction in any medium, provided the original author and source are credited.

**Citation:** Mangal, S; Zielich, J; Lambie, EJ; Zanin E. (2018): Rapamycin-induced protein dimerization as a tool for *C. elegans* research. Micropublication: biology. Dataset. <https://doi.org/10.17912/W2BH3H>

## **Jeffrey Zielich CV**



# Jeffrey Zielich

Department of Biology II  
Ludwig-Maximilians-University of Munich (LMU)  
Cell and Developmental Biology  
Großhaderner Str. 2  
82152 Planegg-Martinsried  
zielich@bio.lmu.de

## Academic career

- 11/2014 to 08/2018 Ludwig-Maximilians-University of Munich  
Department: Cell and Developmental Biology  
**PhD candidate** (Dr. rer .nat)  
"Functional characterization of the three *C. elegans* orthologs of the human Parkinson's disease-associated gene *PARK9/ATP13A2*"
- 10/2012 to 09/2014 Ludwig-Maximilians-University of Munich  
**Degree: Master of Science** (Evolution, Ecology and Systematics)  
"Functional analysis of *cis*-regulatory elements in the *TotA-TotC* intergenic region of *Drosophila melanogaster*"
- 03/2009 to 08/2012 Ruprecht-Karls-University of Heidelberg  
**Degree: Bachelor of Science** (Bioscience)  
"Analysis of ROSA26-Evi gain-of-function mice skin after TPA induced acute inflammation" (**at the German Cancer Research Center DKFZ in Heidelberg**)
- 02/2006 to 01/2009 Bergisches Kolleg in Wuppertal  
**Degree: General qualification for university entrance**
- 08/2001 to 07/2004 Berufskolleg Barmen Europaschule in Wuppertal  
**Degree: Management assistant in wholesale and foreign trade**

## Professional experience

- Since 11/2014 Ludwig-Maximilians-University of Munich  
**PhD candidate in Cell and Developmental Biology**
  - Extensive hands-on experience in CRISPR/Cas9
  - Project planning, troubleshooting and development of molecular tools
  - Data analysis by using the coding language R and MS-Excel
  - Poster presentations and talks at international conferences / meetings
  - Supervision of Master and Bachelor students
- 07/2013 to 07/2014 Ludwig-Maximilians-University of Munich  
**Tutor: Courses for undergraduate students**
  - Evolutionary Biology 1 and 2
  - Molecular Biology and Biochemistry for Bioinformaticians**Tutor: "Studi-forscht" projects**
- 07/2011 to 08/2012 German Cancer Research Center DKFZ in Heidelberg  
Department: Signaling and Functional Genomics  
**Student research assistant**

- 09/2004 to 05/2005 St. Josef Krankenhaus für Orthopädie und Rheumatologie in Wuppertal  
**Community service**  
Technical supply service
- 08/2001 bis 07/2004 Rich. Schulz Söhne Nachf. GmbH in Wuppertal  
Industrial supply company / electrical wholesale  
**Management assistant in wholesale and foreign trade**

## International conferences & awards

- 11/2017 ENABLE conference, European Academy for Biomedical Science in Barcelona  
**1<sup>st</sup> European PhD and Postdoc symposium**  
Poster presentation  
**ENABLE travel grant (250 €)**
- 06/2015 University of California UCLA in Los Angeles  
**20<sup>th</sup> International *C. elegans* Meeting**  
Scientific participant

## Scientific publications

- Zielich, J., Tzima, E., Schröder, E.A., Jemel, F., Conradt, B., Lambie, E.J., 2018 Overlapping expression patterns and functions of three paralogous P5B ATPases in *Caenorhabditis elegans*. PLoS ONE 13, e0194451. doi:10.1371/journal.pone.0194451
- Zielich J., Mangal S., Zanin E., Lambie E. J., 2018 Establishment of a CRISPR/Cas9-based strategy for inducible protein dimerization. microPublication: Biology. Dataset. doi:10.17912/W2208R
- Mangal, S., Zielich, J., Lambie, E.J., Zanin, E., 2018 Rapamycin-induced protein dimerization as a tool for *C. elegans* research. microPublication: Biology. Dataset. doi:10.17912/W2BH3H
- Lambie, E.J., Bruce, R.D., Zielich, J., Yuen, S.N., 2015 Novel Alleles of *gon-2*, a *C. elegans* Ortholog of Mammalian TRPM6 and TRPM7, Obtained by Genetic Reversion Screens. PLoS ONE 10, e0143445. doi:10.1371/journal.pone.0143445
- Submitted for publication:  
Herzig, V., Nixon, S., Salim, A., Verma, S., Abongwa, M., Zielich, J., Rios, L.R., Bais, S., Greenberg, R., Chubanov, V., Lambie, E.J., Capon, R., Robertson, A., Kotze, A.C., King, G.F., Discovery and characterization of a spider-venom polyamine with selective toxicity against the human filarial parasite *Brugia malayi* and other nematodes.